

# Quadrupolar Ordering in Two-Dimensional Spin-One Systems

THÈSE N° 5037 (2011)

PRÉSENTÉE LE 29 AVRIL 2011  
À LA FACULTÉ SCIENCES DE BASE  
CHAIRE DE THÉORIE DE LA MATIÈRE CONDENSÉE  
PROGRAMME DOCTORAL EN PHYSIQUE

ÉCOLE POLYTECHNIQUE FÉDÉRALE DE LAUSANNE

POUR L'OBTENTION DU GRADE DE DOCTEUR ÈS SCIENCES

PAR

Tamás András TÓTH

acceptée sur proposition du jury:

Prof. N. Baluc, présidente du jury  
Prof. F. Mila, Dr K. Penc, directeurs de thèse  
Prof. D. Ivanov, rapporteur  
Prof. A. Kolezhuk, rapporteur  
Prof. C. Lhuillier, rapporteur



ÉCOLE POLYTECHNIQUE  
FÉDÉRALE DE LAUSANNE

Suisse  
2011



# Résumé

Le but principal de ce travail de thèse est d’approfondir notre connaissance de la compétition entre degrés de liberté magnétiques et quadrupolaires sur des réseaux à deux dimensions.

Des études récentes du matériau  $\text{NiGa}_2\text{S}_4$  ont révélé plusieurs propriétés anormales qui pourraient être expliquées par la présence d’un ordre quadrupolaire. Comme le modèle de Heisenberg bilinéaire-biquadratique pour des spins  $S = 1$  donne lieu aux phases ferroquadrupolaire et antiferroquadrupolaire, c’est un bon candidat pour la description du système à basse température. Dans ce travail, nous proposons un modèle plus réaliste qui tient compte de l’anisotropie sur site. Nous avons réalisé une étude détaillée du diagramme de phase variationnel de ce modèle et nous avons montré qu’il donne lieu à nombre de phases non-conventionnelles. Nous avons déduit le spectre d’excitations des phases quadrupolaires de ce diagramme de phase et nous avons mis en évidence que l’ordre ferroquadrupolaire est particulièrement sensible à la nature de l’anisotropie. Finalement, nous avons étudié perturbativement les effets quantiques dans la limite d’une grande anisotropie et nous avons montré que la dégénérescence non-triviale de la solution en champ moyen est levée par l’émergence d’une phase supersolide. Nous avons aussi discuté les conséquences expérimentales de nos résultats dans le contexte de l’étude de  $\text{NiGa}_2\text{S}_4$ .

Dans la deuxième partie de la thèse, nous tentons d’approfondir la compréhension de l’influence mutuelle entre la frustration géométrique et les degrés de liberté quadrupolaires en décrivant le diagramme de phase du modèle bilinéaire-biquadratique pour des spins 1 sur un réseau carré. Notre approche variationnelle révèle un remarquable plateau d’aimantation  $1/2$  de caractère à la fois quadrupolaire et magnétique, au-dessus de la phase “semi-ordonnée” classiquement dégénérée, et ce résultat est confirmé par des diagonalisations exactes sur des réseaux de taille finie. Au-dessous du plateau, le phénomène d’“ordre-par-le-désordre” donne lieu à un état antiferroquadrupolaire ordonné sur trois sous-réseaux, état réellement surprenant étant donné la nature bipartite du réseau carré. Nous avons pris un soin particulier à

---

étudier les propriétés du modèle de Heisenberg  $SU(3)$ , pour lequel il y a une compétition subtile entre fluctuations thermiques et quantiques. Nos résultats suggèrent la disparition de l'ordre de Néel à deux sous-réseaux sur un intervalle fini au-dessous du point  $SU(3)$ . Nous avons aussi discuté les conséquences expérimentales pour les états isolants de Mott d'atomes fermioniques à trois saveurs dans des réseaux optiques.

**Mots-clés:** ordre quadrupolaire/nématique, interactions biquadratiques, systèmes frustrés, anisotropie sur site,  $NiGa_2S_4$ , supersolide, plateau d'aimantation, modèle de Heisenberg  $SU(3)$ , approximation de champ moyen, théorie d'ondes de saveur, "ordre-par-le-désordre", diagonalisations exactes

# Abstract

The principal aim of this thesis is to gain a better understanding of the competition between magnetic and quadrupolar degrees of freedom on two-dimensional lattices.

Recent experimental investigations of the material  $\text{NiGa}_2\text{S}_4$  revealed several anomalous properties that might be accounted for within the framework of quadrupolar ordering. Exhibiting both a ferroquadrupolar and an antiferroquadrupolar phase, the  $S = 1$  bilinear-biquadratic Heisenberg model on the triangular lattice is a possible candidate for describing the low-temperature behaviour of the system. In this work, we put forward a more realistic model that includes single-ion anisotropy. We perform a thorough investigation of the variational phase diagram of this model and we show that it exhibits a variety of unconventional phases. We derive the excitation spectrum of the quadrupolar phases in the phase diagram and we point out that ferroquadrupolar order is particularly sensitive to the nature of anisotropy. Finally, we study quantum effects in the perturbative limit of large anisotropy and we argue that the non-trivial degeneracy of the mean-field solution is lifted by an emergent supersolid phase. We also discuss our results in the context of  $\text{NiGa}_2\text{S}_4$ .

In the second part of the thesis, we aim at gaining an insight into the interplay between geometrical frustration and quadrupolar degrees of freedom by mapping out the phase diagram of the spin-one bilinear-biquadratic model on the square lattice. Our variational approach reveals a remarkable  $1/2$ -magnetization plateau of mixed quadrupolar and magnetic character above the classically degenerate “semi-ordered” phase, and this finding is corroborated by exact diagonalization of finite clusters. “Order-by-disorder” phenomenon gives rise to a state featuring three-sublattice antiferroquadrupolar order below the plateau, which is truly surprising given the bipartite nature of the square lattice. We place particular emphasis on investigating the properties of the  $\text{SU}(3)$  Heisenberg model, which is shown to feature a subtle competition between quantum and thermal fluctuations. Our results suggest a suppression of two-sublattice Néel order in a finite window below

---

the  $SU(3)$  point. Experimental implications for the Mott-insulating states of three-flavour fermionic atoms in optical lattices are discussed.

**Keywords:** quadrupolar/nematic order, biquadratic interactions, frustrated systems, single-ion anisotropy,  $NiGa_2S_4$ , supersolid, magnetization plateau,  $SU(3)$  Heisenberg model, mean-field approximation, flavour-wave theory, “order-by-disorder”, exact diagonalizations

# Acknowledgements

I would like to express my sincere gratitude to both of my supervisors, the support of whom has been essential for the completion of this doctoral thesis. Frédéric Mila provided me with a research-friendly environment in which I had the opportunity to collaborate on a daily basis with an excellent group of people, who lacked neither scientific prowess, nor the human touch. It was a pleasure to be associated with this person of remarkable leadership qualities, who nonetheless had the patience required to teach students at a high level, and I particularly enjoyed our one-on-one collaboration on the semi-classical theory of magnetization plateaus. Karlo Penc never hesitated to offer his kind help in times of need, and he also had a rare knack for appearing in my bleaker moments to demonstrate the actual simplicity of seemingly insurmountable problems. It feels appropriate to remember Patrik Fazekas at this point: he not only played a crucial role in my choice of research topic via his course on magnetism and his highly reputable book, but also kindly encouraged me to start a Ph. D. in Lausanne. It is all too sad that I have never had the opportunity to pay back some of the debt that I owe him.

I consider myself very fortunate to have been surrounded by colleagues who made me feel good about coming to the office and with whom it felt natural to spend time together beyond (their) working hours as well. I would like to thank in particular the people I had the largest overlap with: Andreas Läuchli, who was my main point of reference for the first two years of my doctoral studies and who has remained an invaluable collaborator ever since; Kai Schmidt, for his kind support both at the beginning and at the end; Ioannis Rouschatzakis, for his great attitude to life and his vast reserves of energy; Salvatore Manmana, for our time spent together both at and away from the office; Jean-David Picon, who is one of the kindest and most helpful people I have ever had the pleasure to know, and with whom every discussion was worthwhile; and Julien Sudan, for being simply “génial” in every aspect. I am grateful to all the other members of the group - Andreas Lüscher, Julien Dorier, Sandro Wenzel, Laura Messio and the “twins”: Frédéric Michaud

---

and Tommaso Coletta - for maintaining a good atmosphere and contributing to the supportive environment. Amongst the various visitors we had over the past four years, I particularly enjoyed discussing with Bruce Normand, François Vernay and Sergey Korshunov.

All throughout my doctoral studies, teaching remained a very pleasurable activity for me, and I am indebted to Mikhail Shaposhnikov for starting me on the road. He encouraged a real partnership in teaching, and his door was always open for my questions. I also had the opportunity of working together with a fine group of assistants, and I particularly cherish the memory of entering the ring alongside Julien Sudan, Julian Piatek and Bastien Dalla Piazza.

During my four years in Switzerland, I made many friends who I hold in high esteem and the support of whom I gratefully acknowledge. While I find the task of listing them one by one far too intimidating - I hope that they will forgive me for this -, I feel absolutely obliged to thank two in particular: Balázs Sipos, a master of all trades, for taking me under his wing right from the start; and Gøran Nilsen, a man with an exquisite taste and a brilliant sense of humour, who introduced me to many fine things in life. I thank the open-space community for literally making me feel at home in the Cubotron, and I am particularly indebted to Claude Becker and Daniel Zenhäusern, my fellow travellers on the long road, whose friendship I hold very dear.

I would like to give a very special thanks to Alessandra, who brought sunshine into the last two years of my Ph. D. and who provided me with a healthy touch of reality whenever I wandered dangerously deep into the realm of theoretical physics.

I am indebted to my family - Apu, Marci, Betty, Nagyi, Klári, Antoine, Danó and Kriszti - for their ongoing and unconditional support. This thesis is dedicated to Anyu and Pali, who can unfortunately not share in this moment of rejoicing. Their memory fills me with inspiration and their company is sorely missed at every step in life that I take.

# Contents

<b>1</b>	<b>Preface</b>	<b>1</b>
<b>2</b>	<b>Introduction to quadrupoles</b>	<b>5</b>
2.1	Quadrupolar nature of a single spin one . . . . .	5
2.1.1	SU(3)-bosonic representation of an $\mathbf{S} = \mathbf{1}$ spin . . . . .	8
2.1.2	Coherent spin states vs quadrupolar states . . . . .	12
2.1.3	Parametrization of spin-one states . . . . .	15
2.1.4	Orientating quadrupoles with a field . . . . .	18
2.2	The biquadratic interaction . . . . .	21
2.2.1	SU(3) symmetry of the bilinear-biquadratic Hamiltonian . . . . .	23
2.2.2	The bond and the triangle . . . . .	26
2.2.3	Variational approach for spin-one systems . . . . .	29
2.2.4	Origins of the biquadratic coupling . . . . .	36
<b>3</b>	<b>Quadrupolar ordering on the triangular lattice</b>	<b>45</b>
3.1	Phase diagram of the bilinear-biquadratic model . . . . .	46
3.1.1	Isotropic case: $D = 0$ . . . . .	48
3.1.2	Easy-plane anisotropy field: $D > 0$ . . . . .	52
3.1.3	Easy-axis anisotropy field: $D < 0$ . . . . .	56
3.2	Excitation spectrum of quadrupolar phases . . . . .	62
3.2.1	Ferroquadrupolar phase . . . . .	63
3.2.2	Quadrupolar umbrella phase . . . . .	68
3.3	Perturbative analysis in the limit of large anisotropy . . . . .	74
3.3.1	Easy-plane anisotropy: finite- $J$ corrections to the gap . . . . .	75
3.3.2	Easy-axis anisotropy: emergence of supersolidity . . . . .	80
3.4	Conclusions . . . . .	83
<b>4</b>	<b>Three-sublattice ordering on the square lattice</b>	<b>85</b>
4.1	Three-sublattice ordering in the “semi-ordered” phase . . . . .	87
4.1.1	Lift of degeneracy via a magnetic field . . . . .	88
4.1.2	A numerical analysis of quantum effects . . . . .	92

---

4.1.3	“Order-by-disorder” . . . . .	97
4.1.4	The role of helical states . . . . .	107
4.2	Three-sublattice ordering of the SU(3) Heisenberg model . . .	109
4.2.1	Semi-classical approach . . . . .	109
4.2.2	Numerical approach . . . . .	112
4.2.3	Thermal fluctuations and dimensionality . . . . .	113
4.3	Instability of the Néel state below the SU(3) point . . . . .	115
4.4	Conclusions . . . . .	121
<b>A</b>	<b>Stability analysis in the variational approach</b>	<b>125</b>
<b>B</b>	<b>Classical XXZ model on the triangular lattice</b>	<b>129</b>
B.1	Stationary “non-planar” configurations . . . . .	131
B.2	Stationary “planar” configurations . . . . .	133
B.3	Ground-state configurations . . . . .	137
B.4	Quantum effects in the XXZ model . . . . .	139
	<b>Bibliography</b>	<b>143</b>

# Chapter 1

## Preface

The term "magnetic" conventionally refers to systems that exhibit ordering of atomic dipoles due to quantum-mechanical exchange: as liquids crystallize into solids on cooling, spins in magnets generally develop a long-range periodic order. However, quantum fluctuations enhanced by frustration and low dimensionality may suppress the ordering process and lead to the appearance of qualitatively new quantum phases: these are called spin liquids. The exploration of such novel phases represents one of the central themes of contemporary condensed matter physics.

The relevant effects produced by low dimensionality may be demonstrated by considering the isotropic antiferromagnetic (AFM) nearest-neighbour Heisenberg model of spins one-half on a bipartite lattice. In the case of the cubic lattice, the ground state shows magnetic long-range order with an effective spin shortening of less than 20%, and even though the value is greater on a square lattice (it is approximately 40%), long-range magnetic order is still preserved in two dimensions. In the case of the chain however, the ground state retains the full spin-rotational symmetry of the Hamiltonian, and the staggered magnetization vanishes.

While low dimensionality generally enhances quantum fluctuations and may thus either reduce or completely suppress the order parameter of a classically stable ordered phase, frustrated interactions on the square lattice may lead to a variety of qualitatively different behaviours already at the classical level. In the limit of the triangular lattice, which is achieved by introducing couplings along one of the diagonal directions, we find that whatever spin arrangement we try, we cannot minimize simultaneously all single-bond energies. The classical ground state of the isotropic AFM Heisenberg model on a triangular lattice will feature a 120-degree ordering of the spins, and since the AFM interactions are doomed to be less effective in a non-collinear structure than a collinear one, fluctuation effects become more spectacular in the

quantum limit: for a system consisting of spins one-half, the effective spin shortening exceeds 50%, which is quite a bit larger than what is found for the square lattice. However, instead of yielding an ordered state as a compromise, frustrated interactions may also induce disorder via a large degeneracy, as it happens for the  $J_1$ - $J_2$  model on the square lattice for  $J_2/J_1 \geq 1/2$ , and the quantum limit may then give rise to a number of interesting phenomena, such as the promotion of an ordered state within the classically degenerate manifold via the so-called “order-by-disorder” mechanism.

Considerable effort has been dedicated to the investigation of spin-one systems in the above context, and results have shown in a number of cases the emergence of phases which both lack a classical analogue and are qualitatively different from phases that appear in the extreme quantum case of spins one-half: the most noteworthy example is perhaps the celebrated Haldane phase of the antiferromagnetic spin-one chain. In the current study, we will concentrate on the quadrupolar degrees of freedom that are associated with spin-one systems. A quadrupolar state is a type of non-magnetic state that breaks  $SU(2)$  symmetry by exhibiting a long-range order of quadrupolar operators: instead of the usual vector that is representative of dipolar order, the order parameter in a quadrupolar phase becomes a tensor of rank two. A local example of a quadrupole is the  $S_z = 0$  state of an  $S = 1$  spin: even though the expectation value of the spin components vanishes in such a time-reversal-invariant state, anisotropic spin fluctuations nevertheless break  $SU(2)$  symmetry. The fluctuations occur mostly in the directions perpendicular to an axis (in our example: the  $z$  axis) that is referred to as the director. The aim of the present work is to gain an insight into the nature of quadrupolar ordering within the conceptual frameworks of low dimensionality and frustration.

The thesis is organized as follows. In the first half of chapter 2, we give a general introduction into the quadrupolar character of spin-one wavefunctions, and we draw a comparison between the quadrupolar states of spins one and the qualitatively different coherent spin states of spins one-half. The second half of the chapter is devoted to a study of the bilinear-biquadratic Hamiltonian, which is the minimal model for describing the competition between magnetic and quadrupolar degrees of freedom in spin-one systems. We begin chapter 3 by reviewing the phase diagram of the bilinear-biquadratic Hamiltonian on the triangular lattice, which has recently been explored in an attempt to provide a phenomenological explanation for the low-temperature behaviour of the material  $NiGa_2S_4$ . Motivated both by theoretical curiosity and the possible experimental relevance, we map out the phase diagram of the model in the presence of single-ion anisotropy, placing particular emphasis on quadrupolar phases. Finally, having thoroughly investigated the effect

of biquadratic interactions on the triangular lattice, we work our way towards a better understanding of the interplay between geometrical frustration and quadrupolar behaviour in chapter 4 by studying the bilinear-biquadratic Hamiltonian on the square lattice.



# Chapter 2

## Introduction to quadrupoles

In this introductory chapter, we discuss the basic elements of quadrupolar physics in spin-one systems. We will show that a spin-one wavefunction contains quadrupolar degrees of freedom, which can be accessed via a set of operators that are quadratic in the conventional spin operators, and as a result, it may describe a state that is invariant under time reversal and has no magnetic moment. We will parametrize these so-called quadrupolar states and we will investigate their behaviour in the presence of a magnetic field and an anisotropy field. We will also introduce an  $SU(3)$ -bosonic representation of  $S = 1$  spins that lies at the heart of the semi-classical theory of quadrupolar phases. We will begin the second half of the chapter by presenting the bilinear-biquadratic Hamiltonian that describes the most general isotropic interaction between neighbouring spins one on a lattice, and after discussing its symmetry properties, we will investigate its spectrum for elementary systems. We will introduce furthermore a variational ansatz that may render this Hamiltonian tractable on two- and three-dimensional lattices by allowing for a mean-field description of quadrupolar phases. Finally, we will review a set of mechanisms that may give rise to an effective biquadratic coupling in realistic spin systems.

### 2.1 Quadrupolar nature of a single spin one

A common way of introducing a basis in the Hilbert space of a local  $S = 1$  spin is by choosing the  $z$  axis as a quantization axis for the spin operator and selecting the three eigenstates of  $S^z$ . However, in order to describe

quadrupolar physics, we find it more convenient to define the following basis:

$$\begin{aligned} |x\rangle &= \frac{i}{\sqrt{2}} (|1\rangle - |\bar{1}\rangle), \\ |y\rangle &= \frac{1}{\sqrt{2}} (|1\rangle + |\bar{1}\rangle), \\ |z\rangle &= -i|0\rangle. \end{aligned} \tag{2.1}$$

A general normalized wavefunction with a fixed phase may then be characterized by four real parameters:

$$|\psi\rangle = e^{i\alpha} \sin \vartheta \cos \varphi |x\rangle + e^{i\beta} \sin \vartheta \sin \varphi |y\rangle + \cos \vartheta |z\rangle, \tag{2.2}$$

where  $\{\vartheta, \varphi\} \in [0, \pi/2]$  and  $\{\alpha, \beta\} \in [0, 2\pi[$ . A particularly attractive feature of the basis (2.1) is that the time-reversal operator  $\tau$  leaves it invariant: this can be easily verified by recalling<sup>1</sup> that time reversal changes the sign of  $|0\rangle$ , while it interchanges  $|1\rangle$  and  $|\bar{1}\rangle$ , i. e.  $\tau|0\rangle = -|0\rangle$ ,  $\tau|1\rangle = |\bar{1}\rangle$  and  $\tau|\bar{1}\rangle = |1\rangle$ . Another interesting property of the basis (2.1) is that its elements are zero-eigenvalue eigenstates of the corresponding spin operators,

$$S^x|x\rangle = S^y|y\rangle = S^z|z\rangle = 0, \tag{2.3}$$

and in fact, the action of the spin operators on the basis (2.1) can be written in a concise form:

$$S^\alpha|\beta\rangle = i \sum_{\gamma=x,y,z} \varepsilon_{\alpha\beta\gamma} |\gamma\rangle. \tag{2.4}$$

Any hermitian operator  $\hat{O}$  acting in the Hilbert space of a spin one can be decomposed into a sum of the form

$$\hat{O} = \sum_{\alpha,\beta=1}^3 A_{\alpha\beta} |\alpha\rangle\langle\beta|, \tag{2.5}$$

where the  $|1\rangle$ ,  $|2\rangle$  and  $|3\rangle$  states form a basis of the Hilbert space and  $A_{\alpha\beta}^* = A_{\beta\alpha}$ . Since a three-dimensional self-adjoint matrix is characterized by nine real parameters, we may introduce eight non-trivial independent physical

<sup>1</sup>Alternatively, one may envisage  $|0\rangle$ ,  $|1\rangle$  and  $|\bar{1}\rangle$  as the triplet states of two spins one-half:  $|0\rangle = \frac{1}{\sqrt{2}} (|\uparrow\downarrow\rangle + |\downarrow\uparrow\rangle)$ ,  $|1\rangle = |\uparrow\uparrow\rangle$  and  $|\bar{1}\rangle = |\downarrow\downarrow\rangle$ . A general  $S = 1/2$  wavefunction of the form  $|\psi\rangle = \exp(-i\varphi/2) \cos(\vartheta/2) |\uparrow\rangle + \exp(i\varphi/2) \sin(\vartheta/2) |\downarrow\rangle$  describes a spin pointing in the  $\{\vartheta, \varphi\}$  direction, and  $\tau$  reverses all spin components by definition, thus we may deduce that, neglecting an overall phase factor,  $\tau\alpha|\uparrow\rangle = \alpha^*|\downarrow\rangle$  and  $\tau\alpha|\downarrow\rangle = -\alpha^*|\uparrow\rangle$ .

operators<sup>2</sup> that are possible on-site order parameters for a system consisting of spins one. Obviously, three such candidates are the components of the spin operator, while the remaining five will contain these to a higher order. Generally speaking, the  $2k + 1$  components of a rank- $k$  tensor operator  $\mathbf{T}^{(k)}$  satisfy the following commutation relations [1]:

$$\begin{aligned} [S^z, T_q^{(k)}] &= qT_q^{(k)}, \\ [S^\pm, T_q^{(k)}] &= \sqrt{k(k+1) - q(q \pm 1)}T_{q\pm 1}^{(k)}. \end{aligned} \quad (2.6)$$

Using (2.6), we may systematically construct  $T_q^{(k)}$  for all  $q \in [-k, k]$ . The  $k = 1$  case reproduces  $S^+$ ,  $S^z$  and  $S^-$ , whereas for  $k = 2$  we find

$$\begin{aligned} T_2^{(2)} &= S^+S^+, \\ T_1^{(2)} &= -(S^+S^z + S^zS^+), \\ T_0^{(2)} &= \sqrt{\frac{2}{3}}(3(S^z)^2 - S(S+1)), \\ T_{-1}^{(2)} &= (S^-S^z + S^zS^-), \\ T_{-2}^{(2)} &= S^-S^-. \end{aligned} \quad (2.7)$$

Suitable linear combinations of the five  $T_q^{(2)}$  operators result in five hermitian operators that we may arrange conveniently in a vectorial form:

$$\mathbf{Q} = \begin{pmatrix} Q^{x^2-y^2} \\ Q^{3z^2-r^2} \\ Q^{xy} \\ Q^{yz} \\ Q^{zx} \end{pmatrix} = \begin{pmatrix} (S^x)^2 - (S^y)^2 \\ \frac{1}{\sqrt{3}}(2(S^z)^2 - (S^x)^2 - (S^y)^2) \\ S^xS^y + S^yS^x \\ S^yS^z + S^zS^y \\ S^zS^x + S^xS^z \end{pmatrix}. \quad (2.8)$$

We call the components of  $\mathbf{Q}$  quadrupolar order parameters. An alternative way of introducing them is by decomposing the  $S^\alpha S^\beta$  quadratic form<sup>3</sup> into a scalar  $S(S+1)\delta^{\alpha\beta}/3$  representing the spin length, a three-component vector  $(S^{\alpha\beta} - S^{\beta\alpha})/2$  (dipolar operators) and a symmetric, traceless, rank-two tensor  $(S^{\alpha\beta} + S^{\beta\alpha})/2 - S(S+1)\delta^{\alpha\beta}/3$  (quadrupolar operators). It is worth noting at this point that even though  $T_q^{(k)} = 0$  for  $k > 2$  in the case of a spin one<sup>4</sup>, one may envisage more possible on-site order parameters for higher spins:

<sup>2</sup>A trivial operator is the identity operator  $\hat{I} = \sum_\alpha |\alpha\rangle\langle\alpha|$ .

<sup>3</sup>Note that any operator having a non-vanishing expectation value in a time-reversal-invariant state (such as the elements of the basis (2.1)) has to contain products of an even number of spin operators.

<sup>4</sup>However,  $T_q^{(k)} = 0$  already for  $k = 2$  in the case of a spin one-half.

indeed, a spin of size  $S$  will feature multipolar states of degrees  $k$  up to  $2S$ , the order parameters being rank- $k$  tensor operators.

In conclusion, apart from spin ordering, a system of local spins one is inherently capable of showing quadrupolar order. The competition of the two vectorial order parameters  $\mathbf{S}$  and  $\mathbf{Q}$  is reflected in the following equality that is valid for an arbitrary spin-one wavefunction:

$$\langle \mathbf{S} \rangle^2 + \langle \mathbf{Q} \rangle^2 = \frac{4}{3}. \quad (2.9)$$

One may show that  $|S, S^z\rangle$  is an eigenstate of  $\mathbf{Q}^2$  for any spin  $S$ :

$$\mathbf{Q}^2 |S, S^z\rangle = \frac{4}{3} S(S+1) \left( S(S+1) - \frac{3}{4} \right) |S, S^z\rangle, \quad (2.10)$$

and consequently

$$(\mathbf{Q}^2 + \mathbf{S}^2) |S, S^z\rangle = \frac{4}{3} S^2 (S+1)^2 |S, S^z\rangle, \quad (2.11)$$

we may therefore view (2.9) as a sum rule for the standard deviations of the possible on-site order parameters of a spin one. We would assume that similar sum rules can be constructed for higher spins, involving all their multipolar degrees of freedom.

### 2.1.1 SU(3)-bosonic representation of an $S = 1$ spin

We will now present the basic ingredients of an SU(3)-bosonic representation of spin-one states and operators. The notions introduced here will prove essential in later sections, when we wish to treat elementary excitations of quadrupolar phases.

A standard construction of the SU(3) generators is based on three independent pairs of annihilation and creation operators (often referred to as three “flavours”),  $\{(a_i, a_i^\dagger), i = 1, 2, 3\}$ , that obey the following commutation relations:

$$[a_i, a_j^\dagger] = \delta_{ij}, \quad [a_i, a_j] = 0, \quad [a_i^\dagger, a_j^\dagger] = 0. \quad (2.12)$$

Let us define the operators

$$Q_\alpha = \frac{1}{2} \hat{a}^\dagger \lambda_\alpha \hat{a}, \quad \alpha = 1, 2 \dots 8, \quad (2.13)$$

where  $\hat{a}^\dagger = (a_1^\dagger, a_2^\dagger, a_3^\dagger)$  and  $\lambda_\alpha$  are the Gell-Mann matrices that satisfy the commutation relations<sup>5</sup>

$$[\lambda_\alpha, \lambda_\beta] = 2if_{\alpha\beta\gamma}\lambda_\gamma, \quad \alpha, \beta, \gamma = 1, 2, \dots, 8 \quad (2.14)$$

with well-known real structure constants  $f_{\alpha\beta\gamma}$ . The  $Q_\alpha$  operators are hermitian and one can show that they obey SU(3) Lie-algebra commutation relations: indeed,

$$\begin{aligned} [Q_\alpha, Q_\beta] &= \frac{1}{4}a_i^\dagger a_j a_k^\dagger a_l (\lambda_{\alpha,ij}\lambda_{\beta,kl} - \lambda_{\beta,ij}\lambda_{\alpha,kl}) = \\ &= \frac{1}{4}a_i^\dagger (a_k^\dagger a_j + \delta_{kj}) a_l (\lambda_{\alpha,ij}\lambda_{\beta,kl} - \lambda_{\beta,ij}\lambda_{\alpha,kl}) = \\ &= \frac{1}{4}a_i^\dagger a_k^\dagger a_j a_l (\lambda_{\alpha,ij}\lambda_{\beta,kl} - \lambda_{\beta,ij}\lambda_{\alpha,kl}) + \\ &\quad + \frac{1}{4}a_i^\dagger a_l (\lambda_{\alpha,ik}\lambda_{\beta,kl} - \lambda_{\beta,ik}\lambda_{\alpha,kl}) = \\ &= \frac{1}{4}a_i^\dagger a_k^\dagger a_j a_l (\lambda_{\alpha,ij}\lambda_{\beta,kl} - \lambda_{\beta,ij}\lambda_{\alpha,kl}) + \frac{1}{4}a_i^\dagger a_l 2if_{\alpha\beta\gamma}\lambda_{\gamma,il}, \end{aligned} \quad (2.15)$$

and since the four-operator term gives zero as a result of bosonic commutation relations,

$$\begin{aligned} \frac{1}{4}a_i^\dagger a_k^\dagger a_j a_l (\lambda_{\alpha,ij}\lambda_{\beta,kl} - \lambda_{\beta,ij}\lambda_{\alpha,kl}) &= \frac{1}{4}a_k^\dagger a_i^\dagger a_l a_j (\lambda_{\alpha,kl}\lambda_{\beta,ij} - \lambda_{\beta,kl}\lambda_{\alpha,ij}) = \\ &= -\frac{1}{4}a_k^\dagger a_i^\dagger a_l a_j (\lambda_{\alpha,ij}\lambda_{\beta,kl} - \lambda_{\beta,ij}\lambda_{\alpha,kl}) = \\ &= -\frac{1}{4}a_i^\dagger a_k^\dagger a_j a_l (\lambda_{\alpha,ij}\lambda_{\beta,kl} - \lambda_{\beta,ij}\lambda_{\alpha,kl}), \end{aligned} \quad (2.16)$$

we end up with

$$[Q_\alpha, Q_\beta] = if_{\alpha\beta\gamma}Q_\gamma. \quad (2.17)$$

In addition to the above property, each  $Q_\alpha$  conserves the total number of bosons:

$$[Q_\alpha, \hat{N}] = 0, \quad (2.18)$$

where  $\hat{N} = \hat{a}^\dagger \hat{a}$ , it is therefore convenient to restrict ourselves to a subspace of the complete Hilbert space in which the total number of bosons is a fixed

---

<sup>5</sup>Note that from now on, we use the convention of summing over any index that appears twice in an expression.

number  $N$ . This way, one may systematically generate all “triangular” irreducible representations of  $SU(3)$ , as they are in one-to-one correspondence with integer numbers [2]. A basis of the selected subspace is given by the states  $|n_1, n_2, n_3\rangle$ , where  $n_i$  denote bosonic occupation numbers that satisfy the constraint

$$n_1 + n_2 + n_3 = N. \quad (2.19)$$

It can be shown that  $|n_1, n_2, n_3\rangle$  is an eigenstate of the operator  $Q_\alpha Q_\alpha$ :

$$Q_\alpha Q_\alpha |n_1, n_2, n_3\rangle = \frac{N}{3}(N+3)|n_1, n_2, n_3\rangle. \quad (2.20)$$

In order to represent a local  $S = 1$  spin, we may set  $N = 1$  (the Hilbert space has dimensionality three) and choose the spin operators in the following manner:

$$\mathbf{S} = \begin{pmatrix} S^x \\ S^y \\ S^z \end{pmatrix} = \begin{pmatrix} 2Q_5 \\ -2Q_7 \\ -2Q_2 \end{pmatrix}. \quad (2.21)$$

One may easily verify that the spin commutation relations

$$[S^\alpha, S^\beta] = i\varepsilon_{\alpha\beta\gamma}S^\gamma \quad (2.22)$$

are indeed satisfied. The quadrupolar operators defined in (2.8) are the following<sup>6</sup>:

$$\mathbf{Q} = \begin{pmatrix} Q^{x^2-y^2} \\ Q^{3z^2-r^2} \\ Q^{xy} \\ Q^{yz} \\ Q^{zx} \end{pmatrix} = \begin{pmatrix} 2Q_3 \\ 2Q_8 \\ -2Q_1 \\ -2Q_4 \\ -2Q_6 \end{pmatrix}. \quad (2.23)$$

Via use of the operator-identity

$$(\mathbf{Q}^2 + \mathbf{S}^2) = 4Q_\alpha Q_\alpha, \quad (2.24)$$

equation (2.20), and by showing that

$$\mathbf{S}^2 |n_1, n_2, n_3\rangle = 2|n_1, n_2, n_3\rangle, \quad (2.25)$$

one can verify that equations (2.10) and (2.11) are indeed satisfied for our case of  $S = 1$ . Let us however turn our attention now to the physical interpretation of the bosonic operators  $\{a_1, a_2, a_3\}$  and the basis states they

---

<sup>6</sup>This is a direct consequence of setting  $N = 1$ . Note that choosing spin operators according to (2.21) is possible for any value of  $N$ .

represent:  $|1, 0, 0\rangle$ ,  $|0, 1, 0\rangle$  and  $|0, 0, 1\rangle$ . Based on (2.4), we may deduce a bosonic form for the spin operators, and comparing it to (2.21), we find that the three flavours correspond in fact to the basis (2.1). From now on, we shall therefore refer to the bosonic operators  $\{a_1, a_2, a_3\}$  as  $\{a_y, a_x, a_z\}$ . The explicit bosonic form of the spin operators is given by

$$\mathbf{S} = \begin{pmatrix} S^x \\ S^y \\ S^z \end{pmatrix} = \begin{pmatrix} i(a_z^\dagger a_y - a_y^\dagger a_z) \\ i(a_x^\dagger a_z - a_z^\dagger a_x) \\ i(a_y^\dagger a_x - a_x^\dagger a_y) \end{pmatrix}, \quad (2.26)$$

while that of the quadrupolar operators is written as

$$\mathbf{Q} = \begin{pmatrix} Q^{x^2-y^2} \\ Q^{3z^2-r^2} \\ Q^{xy} \\ Q^{yz} \\ Q^{zx} \end{pmatrix} = \begin{pmatrix} a_y^\dagger a_y - a_x^\dagger a_x \\ \frac{1}{\sqrt{3}}(a_x^\dagger a_x + a_y^\dagger a_y - 2a_z^\dagger a_z) \\ -(a_y^\dagger a_x + a_x^\dagger a_y) \\ -(a_z^\dagger a_y + a_y^\dagger a_z) \\ -(a_z^\dagger a_x + a_x^\dagger a_z) \end{pmatrix}. \quad (2.27)$$

Before concluding this subsection, we would like to draw the reader's attention to a few more mathematical observations that bear physical relevance.

In particular for our study of spin-one systems, it will prove useful to emphasize that the representation of the  $SU(3)$  Lie algebra that was generated by the  $Q_\alpha$  operators defined in (2.13) has a complex conjugate representation, the generators of which are given by

$$-Q_\alpha^* = \frac{1}{2}\hat{a}^\dagger(-\lambda_\alpha^*)\hat{a}, \quad \alpha = 1, 2 \dots 8. \quad (2.28)$$

It follows from the structure constants  $f_{\alpha\beta\gamma}$  being real that the  $-Q_\alpha^*$  operators satisfy the same commutation relations as the  $Q_\alpha$  operators. In order to see this, it suffices to take the complex conjugate of (2.17):

$$\begin{aligned} [Q_\alpha^*, Q_\beta^*] &= -if_{\alpha\beta\gamma}Q_\gamma^*, \\ [-Q_\alpha^*, -Q_\beta^*] &= if_{\alpha\beta\gamma}(-Q_\gamma^*). \end{aligned} \quad (2.29)$$

As the three Gell-Mann matrices corresponding to the spin components defined in (2.21) are purely imaginary, while all the other Gell-Mann matrices are purely real, we may simply replace  $Q_\alpha$  by  $-Q_\alpha^*$  on the right-hand side of (2.21), whereas the same replacement on the right-hand side of (2.23) induces a minus sign. In other words, the two representations are not equivalent.

In order to draw a parallel with the well-known Schwinger-boson construction, we point out that one may also define  $SU(2)$  generators via the method

described above, namely by introducing only two pairs of bosonic creation and annihilation operators that obey (2.12), and consequently replacing the definition of the generators (2.13) by

$$S^\alpha = \frac{1}{2} \hat{a}^\dagger \sigma^\alpha \hat{a}, \quad \alpha = x, y, z, \quad (2.30)$$

where  $\hat{a}^\dagger = (a_1^\dagger, a_2^\dagger)$  and  $\sigma^\alpha$  are the Pauli matrices satisfying the commutation relations

$$[\sigma^\alpha, \sigma^\beta] = 2i\varepsilon_{\alpha\beta\gamma} \sigma^\gamma, \quad \alpha, \beta, \gamma = x, y, z. \quad (2.31)$$

An important difference from the case of SU(3)-bosons is that one is in fact able to generate all irreducible representations of the SU(2) Lie algebra this way: different representations correspond to a different total number of bosons, i.e. to different spin lengths.

As a closing remark, we add that introducing  $N$  bosonic flavours allows for the construction of the  $N^2$  generators of the SU( $N$ ) Lie algebra<sup>7</sup>:

$$S_{mm'} = a_m^\dagger a_{m'}, \quad m, m' = 1, 2 \dots N. \quad (2.32)$$

It is easily checked that the operators above indeed satisfy SU( $N$ ) commutation relations<sup>8</sup>:

$$[S_{mm'}, S_{nn'}] = \delta_{m'n} S_{mm'} - \delta_{mn'} S_{nm'}. \quad (2.33)$$

This property paves the way to a straightforward generalization of the concepts introduced in this subsection, which eventually allows for a systematic treatment of bosonic excitations of general multipolar phases of high ( $S > 1$ ) spins.

### 2.1.2 Coherent spin states vs quadrupolar states

A coherent spin state  $|\mathbf{\Omega}\rangle$  is a state in which the spin length is maximal, i.e.  $(\langle \mathbf{\Omega} | \mathbf{S} | \mathbf{\Omega} \rangle)^2 = 1$  in the case of a spin one<sup>9</sup>. Such a state describes a spin pointing in the direction of the unit vector  $\mathbf{\Omega}$  and is fully characterized by the polar angles  $\{\vartheta, \varphi\}$ :

$$\langle \mathbf{\Omega} | \mathbf{S} | \mathbf{\Omega} \rangle = S \mathbf{\Omega} = S \begin{pmatrix} \sin \vartheta \cos \varphi \\ \sin \vartheta \sin \varphi \\ \cos \vartheta \end{pmatrix}, \quad (2.34)$$

<sup>7</sup>Note that the number of non-trivial generators is  $N^2 - 1$ .

<sup>8</sup>One may also check that the commutation relations remain intact even if the operators  $a_i$  are fermionic instead of being bosonic.

<sup>9</sup>It is useful to note right from the outset that the Hilbert space of a spin one-half consists only of coherent spin states.

where  $\vartheta \in [0, \pi]$  and  $\varphi \in [0, 2\pi[$ . The coherent spin state  $|\mathbf{\Omega}\rangle$  is furthermore an eigenstate of the spin component parallel to the vector  $\mathbf{\Omega}$ :

$$(\mathbf{\Omega} \cdot \mathbf{S}) |\mathbf{\Omega}\rangle = S |\mathbf{\Omega}\rangle. \quad (2.35)$$

For the case of a spin one, the coherent spin states may conveniently be written in the form

$$|\mathbf{\Omega}\rangle = \frac{1 + \cos \vartheta}{2} e^{-i\varphi} |1\rangle + \frac{\sin \vartheta}{\sqrt{2}} |0\rangle + \frac{1 - \cos \vartheta}{2} e^{i\varphi} |\bar{1}\rangle, \quad (2.36)$$

and they obey the completeness relation

$$\hat{I} = \frac{3}{4\pi} \int_{\vartheta=0}^{\pi} \int_{\varphi=0}^{2\pi} d\vartheta d\varphi \sin \vartheta |\mathbf{\Omega}\rangle \langle \mathbf{\Omega}|. \quad (2.37)$$

Applying the identity operator  $\hat{I}$  in the form (2.37) to an arbitrary spin-one state  $|\psi\rangle$ , one finds

$$|\psi\rangle = \hat{I} |\psi\rangle = \frac{3}{4\pi} \int_{\vartheta=0}^{\pi} \int_{\varphi=0}^{2\pi} d\vartheta d\varphi \sin \vartheta \langle \mathbf{\Omega} | \psi \rangle |\mathbf{\Omega}\rangle, \quad (2.38)$$

i.e.  $|\psi\rangle$  may be expressed as a superposition of coherent spin states with amplitudes  $\langle \mathbf{\Omega} | \psi \rangle$ . This result allows for a pictorial representation of spin-one wavefunctions that we will make use of later on.

A quadrupolar state  $|\mathbf{d}\rangle$  of a spin one is a state in which the spin length is zero:  $(\langle \mathbf{d} | \mathbf{S} | \mathbf{d} \rangle)^2 = 0$ . However, spin fluctuations are anisotropic in such a time-reversal-invariant state, as they occur only in a plane perpendicular to an axis that is referred to as the *director*. As an example, one may verify that the state  $|0\rangle$  is a quadrupolar state with the axis  $z$  as the director: indeed, spin components vanish (time-reversal invariance up to a phase factor), furthermore  $(S^x)^2 |0\rangle = |0\rangle$  and  $(S^y)^2 |0\rangle = |0\rangle$ , while  $(S^z)^2 |0\rangle = 0$ . A quadrupolar state is fully characterized by the polar angles  $\{\vartheta, \varphi\}$  defining the unit vector

$$\mathbf{d} = \begin{pmatrix} \sin \vartheta \cos \varphi \\ \sin \vartheta \sin \varphi \\ \cos \vartheta \end{pmatrix} \quad (2.39)$$

that points along the director axis. Quadrupolar states may be written in a convenient form using the basis (2.1):

$$|\mathbf{d}\rangle = d_x |x\rangle + d_y |y\rangle + d_z |z\rangle, \quad (2.40)$$

where  $d_i$  are the components of the vector  $\mathbf{d}$ . This form reveals the nematic nature of a quadrupolar state:  $|-\mathbf{d}\rangle = -|\mathbf{d}\rangle$ , i.e. the quadrupolar states

characterized by  $\mathbf{d}$  and  $-\mathbf{d}$  are physically equivalent. Bearing that in mind, we shall nonetheless often refer to the vector  $\mathbf{d}$  as the director, rather than to the axis along which it points. The quadrupolar state  $|\mathbf{d}\rangle$  is an eigenstate of the spin component parallel to the director  $\mathbf{d}$ :

$$(\mathbf{d} \cdot \mathbf{S}) |\mathbf{d}\rangle = 0. \quad (2.41)$$

We have shown that while a single  $S = 1/2$  spin is always in a coherent spin state (or dipolar state), an  $S = 1$  spin may also be a quadrupole, which might lead us to expect that a further increase of the dimensionality of the local Hilbert space would yield even more exotic multipolar states. This is indeed the case, as we will briefly demonstrate for  $S = 3/2$  wavefunctions. Let us compose a basis  $|S^z\rangle$  with the help of three spins one-half:

$$\left|\frac{3}{2}\right\rangle = |\uparrow\uparrow\uparrow\rangle, \quad \left|\frac{1}{2}\right\rangle = \frac{1}{\sqrt{3}} (|\downarrow\uparrow\uparrow\rangle + |\uparrow\downarrow\uparrow\rangle + |\uparrow\uparrow\downarrow\rangle), \quad (2.42)$$

$$\left|-\frac{3}{2}\right\rangle = |\downarrow\downarrow\downarrow\rangle, \quad \left|-\frac{1}{2}\right\rangle = \frac{1}{\sqrt{3}} (|\uparrow\downarrow\downarrow\rangle + |\downarrow\uparrow\downarrow\rangle + |\downarrow\downarrow\uparrow\rangle). \quad (2.43)$$

Since  $\tau|\uparrow\rangle = |\downarrow\rangle$  and  $\tau|\downarrow\rangle = -|\uparrow\rangle$ , it follows that

$$\tau\left|\frac{3}{2}\right\rangle = \left|-\frac{3}{2}\right\rangle, \quad \tau\left|\frac{1}{2}\right\rangle = -\left|-\frac{1}{2}\right\rangle, \quad (2.44)$$

$$\tau\left|-\frac{3}{2}\right\rangle = -\left|\frac{3}{2}\right\rangle, \quad \tau\left|-\frac{1}{2}\right\rangle = \left|\frac{1}{2}\right\rangle, \quad (2.45)$$

which makes it clear that it is impossible to construct a time-reversal-invariant state for an  $S = 3/2$  spin, for essentially the same reason as it is for a spin one-half. As a matter of fact, this conclusion can be reached for half-integer-spins in general, as they can be composed of an odd number of spins one-half, and therefore, according to the celebrated Kramers-theorem, an arbitrary half-integer-spin wavefunction  $|\psi\rangle$  will be orthogonal to  $\tau|\psi\rangle$ . On the other hand, it is quite easy to write down a spin-three-half state in which the spin length is zero: take as an example the state

$$|O\rangle = \frac{1}{\sqrt{2}} \left( \left|\frac{3}{2}\right\rangle + \left|-\frac{3}{2}\right\rangle \right). \quad (2.46)$$

Having seen that  $|O\rangle$  is neither a dipole nor a quadrupole (in the sense that it is not time-reversal-invariant), we conclude that we have found a state of octupolar character. Now, based on [3], we may write the coherent spin states of a general spin  $S$  in the form

$$e^{i\varphi}|\Omega\rangle = \left(\cos\frac{\vartheta}{2}\right)^{2S} \exp\left\{\tan\frac{\vartheta}{2}e^{i\varphi}S^-\right\}|S^z = S\rangle, \quad (2.47)$$

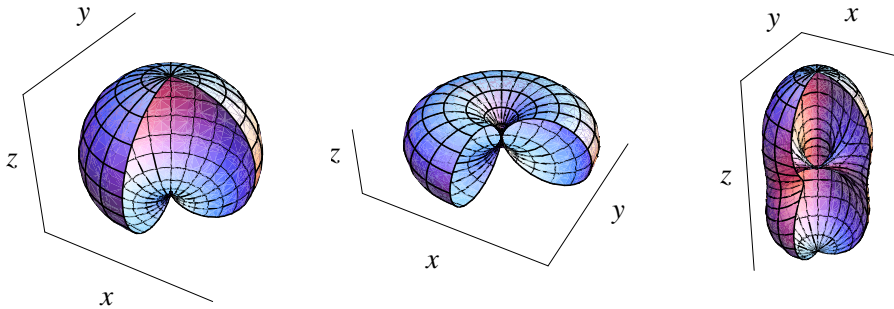


Figure 2.1: Spherical plots of the amplitudes  $|\langle \Omega | \psi \rangle|^2$  for (from left to right) an  $S = 1/2$  dipole ( $|\psi\rangle = |\uparrow\rangle$ ), an  $S = 1$  quadrupole ( $|\psi\rangle = |0\rangle$ ) and an  $S = 3/2$  state of octupolar character ( $|\psi\rangle = |O\rangle$ ).

where we have introduced the phase factor on the left-hand side in order to remain consistent with the expression (2.36), and we note furthermore that the completeness relation (2.37) can be easily extended to the case of an arbitrary spin by replacing the prefactor  $3/4\pi$  by  $(2S+1)/4\pi$ . With the help of these results, we have created spherical plots of the amplitudes  $|\langle \Omega | \psi \rangle|^2$  for a spin-one-half dipole, a spin-one quadrupole and a spin-three-half octupole: these are shown in figure 2.1.

### 2.1.3 Parametrization of spin-one states

Coherent spin states and quadrupolar states are only the two “extreme” types of states that a spin one may assume. A general spin-one state will reveal both spin and quadrupolar character (see (2.9)), and its physically relevant properties will in fact be fully determined by four independent real parameters (see (2.2)). It follows that fixing the length and the direction of the spin vector does not lead to a unique physical state, as three parameters are sufficient to account for these properties<sup>10</sup>. While one may think of a variety of ways of characterizing spin-one wavefunctions, we will often prefer to adopt the parametrization of [4] that introduces a pair of three-dimensional vectors. In this subsection, we explain the details of this parametrization.

We shall write a general spin-one state  $|\psi\rangle$  in the form

$$|\psi\rangle = (u_x + iv_x)|x\rangle + (u_y + iv_y)|y\rangle + (u_z + iv_z)|z\rangle, \quad (2.48)$$

<sup>10</sup>For spins one-half, however, the polar angles  $\{\vartheta, \varphi\}$  of the spin vector already define a wavefunction that is unique up to a phase factor.

where the real vectors  $\mathbf{u}$  and  $\mathbf{v}$  satisfy the normalization constraint

$$\mathbf{u}^2 + \mathbf{v}^2 = 1, \quad (2.49)$$

and the overall phase of  $|\psi\rangle$  is adjusted so that the following condition holds:

$$\mathbf{u} \cdot \mathbf{v} = 0. \quad (2.50)$$

The expectation value of the spin operator in the state  $|\psi\rangle$  is

$$\langle\psi|\mathbf{S}|\psi\rangle = 2\mathbf{u} \times \mathbf{v}, \quad (2.51)$$

and the spin length is given by

$$(\langle\psi|\mathbf{S}|\psi\rangle)^2 = 4\mathbf{u}^2\mathbf{v}^2. \quad (2.52)$$

Coherent spin states correspond to  $\mathbf{u}^2 = \mathbf{v}^2 = 1/2$ , while a quadrupolar state will have either  $\mathbf{u}^2 = 0$  or  $\mathbf{v}^2 = 0$ , with the non-vanishing vector defining the director. One may in fact refer to the larger of the two vectors as the director in the case  $0 < (\langle\psi|\mathbf{S}|\psi\rangle)^2 < 1$  as well: it will become apparent in the next paragraph why this extended concept of a director holds no ambiguity.

Let us assume first that an arbitrary normalized spin-one state may indeed be written in the form (2.48) with the conditions (2.49) and (2.50) satisfied, and take a look at what different  $\{\mathbf{u}, \mathbf{v}\}$  choices are equivalent in the sense that the corresponding wavefunctions are related to each other by a phase transformation. Let us define a restricted phase transformation of the state  $|\psi\rangle$  so that the resulting state

$$|\psi'\rangle = e^{i\gamma}|\psi\rangle \quad (2.53)$$

can also be characterized by vectors  $\mathbf{u}'$  and  $\mathbf{v}'$  satisfying conditions (2.49) and (2.50). The vectors  $\mathbf{u}'$  and  $\mathbf{v}'$  can be written as

$$\begin{aligned} \mathbf{u}' &= \cos \gamma \mathbf{u} - \sin \gamma \mathbf{v}, \\ \mathbf{v}' &= \cos \gamma \mathbf{v} + \sin \gamma \mathbf{u}, \end{aligned} \quad (2.54)$$

which makes it clear that they automatically satisfy (2.49). Their scalar product is

$$\mathbf{u}' \cdot \mathbf{v}' = (\cos^2 \gamma - \sin^2 \gamma) \mathbf{u} \cdot \mathbf{v} + \cos \gamma \sin \gamma (\mathbf{u}^2 - \mathbf{v}^2), \quad (2.55)$$

so we can deduce that an equivalent formulation of condition (2.50) is

$$\sin(2\gamma) (\mathbf{u}^2 - \mathbf{v}^2) = 0. \quad (2.56)$$

If  $\mathbf{u}^2 = \mathbf{v}^2$ , (2.56) is satisfied for an arbitrary  $\gamma$ , and a phase transformation becomes equivalent to a simultaneous rotation of  $\mathbf{u}$  and  $\mathbf{v}$  around a common axis perpendicular to their plane<sup>11</sup>. However, if  $\mathbf{u}^2 \neq \mathbf{v}^2$ , we have to restrict  $\gamma$ : the case  $\gamma = 0$  is the identity,  $\gamma = \pi$  corresponds to taking the opposite of both  $\mathbf{u}$  and  $\mathbf{v}$ , while  $\gamma = \pi/2$  and  $\gamma = -\pi/2$  correspond to taking the opposite of one of the vectors and changing their order, i.e to the cases  $\{-\mathbf{v}, \mathbf{u}\}$  and  $\{\mathbf{v}, -\mathbf{u}\}$ . Therefore, without loss of generality, we may adopt the convention of choosing the pair of vectors  $\{\mathbf{u}, \mathbf{v}\}$  in such a way that  $\mathbf{u}^2 > \mathbf{v}^2$ , and we may refer to  $\mathbf{u}$  as the director<sup>12</sup>.

We will now verify the initial assumption of the previous paragraph. Let us take a normalized spin-one wavefunction of the form (2.48) with the vectors  $\{\mathbf{u}, \mathbf{v}\}$  satisfying condition (2.49), but not condition (2.50): we will show that a suitable phase transformation of the form (2.53) will result in a state  $|\psi'\rangle$  that is characterized by vectors that satisfy both conditions. The vectors  $\mathbf{u}'$  and  $\mathbf{v}'$  are given by (2.54), and they automatically satisfy (2.49). However, their scalar product (2.55) vanishes if and only if the following equation holds:

$$\cos(2\gamma) 2\mathbf{u} \cdot \mathbf{v} + \sin(2\gamma) (\mathbf{u}^2 - \mathbf{v}^2) = 0. \quad (2.57)$$

If  $\mathbf{u}^2 \neq \mathbf{v}^2$ , the phase  $\gamma$  is well-defined by

$$\tan 2\gamma = \frac{2\mathbf{u} \cdot \mathbf{v}}{\mathbf{v}^2 - \mathbf{u}^2}, \quad (2.58)$$

where  $\gamma \in ]-\pi/4, \pi/4[$ . Note that choices of  $\gamma$  outside of this interval would simply correspond to choosing between equivalent sets of  $\{\mathbf{u}', \mathbf{v}'\}$ , as discussed in the previous paragraph. If  $\mathbf{u}^2 = \mathbf{v}^2$ , one may choose  $\gamma = \pi/4$ , for instance.

Finally, we wish to illustrate the practical use of this parametrization in distinguishing between physically different wavefunctions that feature the same spin vector  $\langle \mathbf{S} \rangle$ , with a spin length lower than one (in other words, the spin is not “fully developed”). It is evident from (2.51) that the director  $\mathbf{u}$  has to lie in the plane perpendicular to the spin vector, and combining equations (2.49) and (2.52), we find that its length is completely determined by the spin length:

$$\mathbf{u}^2 = \frac{1}{2} \left( 1 + \sqrt{1 - (\langle \psi | \mathbf{S} | \psi \rangle)^2} \right). \quad (2.59)$$

Nonetheless, the director may still freely rotate around in the plane, and each

<sup>11</sup>In this particular case, the vectors  $\mathbf{u}'$ ,  $\mathbf{v}'$ ,  $\mathbf{u}$  and  $\mathbf{v}$  all have the same length  $1/\sqrt{2}$ .

<sup>12</sup>Note that coherent spin states do not have a director.

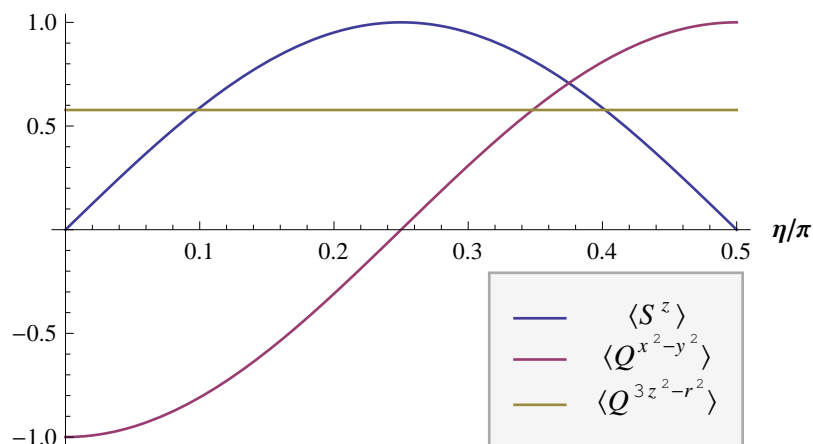


Figure 2.2: Plot of every non-vanishing spin and quadrupole component of the wavefunction  $|\psi\rangle = \cos \eta|x\rangle + i \sin \eta|y\rangle$ . While  $\langle S^z \rangle$  is symmetric,  $\langle Q^{x^2-y^2} \rangle$  is antisymmetric around  $\eta = \pi/4$ .

resulting configuration will correspond to a different quadrupole moment<sup>13</sup>. Let us exemplify this statement with the help of a simple trial wavefunction:

$$|\psi\rangle = \cos \eta|x\rangle + i \sin \eta|y\rangle, \quad (2.60)$$

where  $\eta \in ]0, \pi/2[$ . The wavefunction  $|\psi\rangle$  describes a dipole moment  $\langle \mathbf{S} \rangle = (0, 0, \sin 2\eta)$  that is symmetric around  $\eta = \pi/4$ , the director however, while being undefined for  $\eta = \pi/4$ , is either the  $x$  axis or the  $y$  axis, depending on whether  $\eta < \pi/4$  or  $\eta > \pi/4$ . This indicates that the quadrupole moment will not show the same symmetry as the dipole moment, and indeed,  $\langle \mathbf{Q} \rangle = (-\cos 2\eta, 1/\sqrt{3}, 0, 0, 0)$ . In figure 2.2, we plot all non-vanishing components of  $\langle \mathbf{S} \rangle$  and  $\langle \mathbf{Q} \rangle$ .

### 2.1.4 Orientating quadrupoles with a field

Let us investigate the effect of a magnetic field on quadrupolar states. We will assume as a starting point that we have a lattice structure comprising spins one, and due to local isotropic interactions, the system is in a so-called *ferro-quadrupolar* phase: every site features a quadrupolar state and the directors are parallel to each other, however, global SU(2) symmetry implies that this common director may point anywhere<sup>14</sup>. The question we ask ourselves now

<sup>13</sup>Note however that configurations that are related to each other by a rotation of  $\pi$  are physically equivalent.

<sup>14</sup>We will encounter such phases later on in this work.

is the following: what happens if we turn on a small uniform magnetic field of the form  $-hS^z$ ? Since the dipole moment vanishes in a quadrupolar state, there is no first-order selection within the degenerate manifold, and therefore in order to find the answer, we have to take into account the deformation of the local wavefunctions. Since the model retains rotational symmetry around the  $z$  axis, we may assume without loss of generality that the directors lie in the  $zx$  plane in the  $h \rightarrow 0$  limit. The lowest-order deformation of such a state

$$|\psi_0\rangle = \sin \vartheta |x\rangle + \cos \vartheta |z\rangle \quad (2.61)$$

may be described by the wavefunction

$$|\psi\rangle = |\psi_0\rangle + \delta (\cos \eta e^{i\alpha} |\psi_1\rangle + \sin \eta e^{i\beta} |\psi_2\rangle), \quad (2.62)$$

where  $\delta \ll 1$  and

$$\begin{aligned} |\psi_1\rangle &= -\cos \vartheta |x\rangle + \sin \vartheta |z\rangle, \\ |\psi_2\rangle &= |y\rangle \end{aligned} \quad (2.63)$$

define a basis together with  $|\psi_0\rangle$ . With the help of (2.4), we find

$$\begin{aligned} S^z |\psi\rangle &= -i\delta \sin \vartheta \sin \eta e^{i\beta} |\psi_0\rangle + i\delta \cos \vartheta \sin \eta e^{i\beta} |\psi_1\rangle + \\ &+ i (\sin \vartheta - \delta \cos \vartheta \cos \eta e^{i\alpha}) |\psi_2\rangle, \end{aligned} \quad (2.64)$$

and therefore the first non-vanishing correction to the energy is given by

$$-h \frac{\langle \psi | S^z | \psi \rangle}{\langle \psi | \psi \rangle} = -2h\delta \sin \vartheta \sin \eta \sin \beta. \quad (2.65)$$

The energy may be minimized by taking either  $\{\vartheta = \pi/2, \eta = \beta = \pm\pi/2\}$  or  $\{\vartheta = -\pi/2, \eta = -\beta = \pm\pi/2\}$ , and we end up with

$$|\psi\rangle = \pm (|x\rangle + i\delta |y\rangle). \quad (2.66)$$

In conclusion, the director turns perpendicular to the magnetic field, and the quadrupole starts developing a dipole moment parallel to the field [4, 5].

If the ferroquadrupolar phase is submitted to a uniform field that corresponds to a quadrupolar operator, the directors may be orientated without a deformation of the local wavefunctions. Perhaps the simplest example of this kind of mechanism is evoked by a single-ion anisotropy field of the form  $D(S^z)^2$ . Taking the same wavefunction  $|\psi_0\rangle$  as in the preceding paragraph, we find

$$D \langle \psi_0 | (S^z)^2 | \psi_0 \rangle = D \sin^2 \vartheta, \quad (2.67)$$

i. e. the non-vanishing expectation value of the anisotropy field leads to a lift of the ground-state degeneracy. An easy-plane field ( $D > 0$ ) will pin the director to the  $z$  axis, while an easy-axis field ( $D < 0$ ) will only confine it to the  $xy$  plane. We mention that in real materials, single-ion anisotropy generally arises due to a combined effect of the crystal field and the spin-orbit coupling. In particular, let us briefly consider a lattice featuring  $\text{Ni}^{2+}$  ions in an octahedral environment. In this case, the crystal field splits  $d$ -orbitals into two groups, corresponding to a lower  $t_{2g}$  level and a higher  $e_g$  level, and the resulting electronic configuration  $t_{2g}^6 e_g^2$  will have a total spin  $S = 1$ . Since the orbital moment is completely quenched, spin-orbit coupling may be treated in higher-order perturbation theory, and it is reasonable to expect the emergence of single-ion anisotropy in such a calculation, as this is the simplest magnetic-field-independent term that a single-ion effective spin Hamiltonian may feature for  $S > 1/2$  spins<sup>15</sup>. The fact that the crystal field does not make a distinction between the positive and the negative  $z$  axis is nicely encapsulated in the time-reversal invariance of single-ion anisotropy, furthermore, in contrast to Dzyaloshinsky-Moriya interactions [6, 7], which are also quadratic in spin operators, single-ion anisotropy is compatible with the inversion symmetry of a lattice. For a more detailed discussion on this topic, we refer the reader to the excellent book by Patrik Fazekas [8].

Finally, let us discuss the magnetization process of a spin one that is prepared in a quadrupolar state via an easy-plane anisotropy field. We write the Hamiltonian as

$$H = D(S^z)^2 - \mathbf{h} \cdot \mathbf{S}, \quad (2.68)$$

however, we will only treat the cases where the magnetic field is either parallel or perpendicular to the director. A magnetic field applied along the director ( $\mathbf{h} = h\mathbf{e}_z$ ) leaves the ground state unharmed below the critical value  $h_c = D$ , at which there is a level-crossing with the state  $|1\rangle$ : considering a system of decoupled spins, one would find a jump in the magnetization per site from zero to one at the critical magnetic field, which is the hallmark of a first-order phase transition. On the other hand, if the applied magnetic field is perpendicular to the director ( $\mathbf{h} = h\mathbf{e}_x$ ), a quite different behaviour is observed. As the magnetic field is increased, the ground state evolves continuously from the non-magnetic state to the fully polarized one:

$$|\psi\rangle = \cos \eta |z\rangle - i \sin \eta |y\rangle, \quad (2.69)$$

where

$$\tan \eta = \frac{\sqrt{D^2 + 4h^2} - D}{2h}. \quad (2.70)$$

---

<sup>15</sup>Single-ion anisotropy is forbidden for spin-one-half ions, which is perhaps most easily seen by noting that the square of any Pauli matrix is the identity operator.

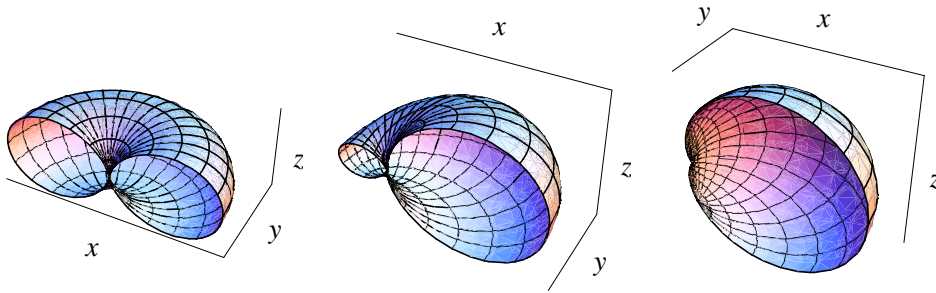


Figure 2.3: Spherical plots of the amplitudes  $|\langle \mathbf{\Omega} | \psi \rangle|^2$  for three states of the form (2.69): (from left to right) a pure quadrupole ( $\eta = 0$ ), a state with magnetization  $1/2$ , and a fully polarized state ( $\eta = \pi/4$ ).

The intermediate state  $\eta \in ]0, \pi/4[$  has a director along the  $z$  axis and a dipole moment of length  $\sin 2\eta$  pointing in the  $x$  direction. Consequently, for a system of independent spins, one would expect to observe a smooth magnetization curve as a function of the magnetic field. We present spherical plots of the amplitudes  $|\langle \mathbf{\Omega} | \psi \rangle|^2$  at three different stages of the magnetization process in figure 2.3.

## 2.2 The biquadratic interaction

The general form of an isotropic coupling between two spins one is given by the bilinear-biquadratic Hamiltonian:

$$H = J \cos \vartheta \mathbf{S}_1 \mathbf{S}_2 + J \sin \vartheta (\mathbf{S}_1 \mathbf{S}_2)^2, \quad (2.71)$$

where  $J > 0$  sets an energy scale and  $\vartheta \in [0, 2\pi[$  controls the sign and the relative strength of the two independent terms. Introducing higher powers of the scalar product  $\mathbf{S}_1 \mathbf{S}_2$ , or any other scalar operator<sup>16</sup> in fact, does not change the form of (2.71), since these extra terms can be rewritten as a linear combination of bilinear and biquadratic terms. One may verify this statement by using the well-known formula

$$D^{(j_1)} \otimes D^{(j_2)} = \sum_{\oplus j=|j_1-j_2|}^{j_1+j_2} D^{(j)}, \quad (2.72)$$

where  $D^{(j)}$  denotes the spin- $j$  representation of  $SU(2)$ . Indeed, a pair of  $S = 1$  spins may form a singlet, a triplet and a quintuplet, therefore the independent

<sup>16</sup>Scalar operators are  $SU(2)$ -invariant, i.e. they commute with the total spin.

operators acting in the Hilbert space may be classified according to

$$\begin{aligned} (D^{(0)} \oplus D^{(1)} \oplus D^{(2)}) \otimes (D^{(0)} \oplus D^{(1)} \oplus D^{(2)}) &= \\ &= 3D^{(0)} \oplus 6D^{(1)} \oplus 6D^{(2)} \oplus 3D^{(3)} \oplus D^{(4)}, \end{aligned} \quad (2.73)$$

i.e. we find two non-trivial scalar operators, six dipolar operators, six quadrupolar operators, three octupolar operators and one hexadecupolar operator. It is interesting to contrast this result to the case of a bond of spins one-half [9], where one would find only one non-trivial scalar operator  $\mathbf{S}_1\mathbf{S}_2$ , three vectorial operators  $\mathbf{S}_1 + \mathbf{S}_2$ ,  $\mathbf{S}_1 - \mathbf{S}_2$  and  $\mathbf{S}_1 \times \mathbf{S}_2$ , as well as a quadrupolar operator<sup>17</sup>. We may conclude that (2.71) is indeed the most general SU(2)-invariant Hamiltonian for a pair of spins one<sup>18</sup>.

A closer look at the formula (2.73) suggests that one may systematically construct all independent scalar operators for a pair of spins  $S$  by taking the scalar products of each on-site order parameter. This implies that it should be possible to reexpress the biquadratic term  $(\mathbf{S}_1\mathbf{S}_2)^2$  as a linear combination of  $\mathbf{S}_1\mathbf{S}_2$  and  $\mathbf{Q}_1\mathbf{Q}_2$ , and indeed, a straightforward calculation reveals that

$$\mathbf{Q}_1\mathbf{Q}_2 = \frac{4}{3}(\mathbf{S}_1\mathbf{S}_2)^2 - \frac{2}{3}(\mathbf{S}_1 \times \mathbf{S}_2)^2 + \frac{1}{3}\mathbf{S}_1\mathbf{S}_2, \quad (2.75)$$

which, combined with

$$\begin{aligned} (\mathbf{S}_1 \times \mathbf{S}_2)^2 &= \varepsilon_{\alpha\beta\gamma}\varepsilon_{\alpha\tau\nu}S_1^\beta S_2^\gamma S_1^\tau S_2^\nu = \\ &= (\delta_{\beta\tau}\delta_{\gamma\nu} - \delta_{\beta\nu}\delta_{\gamma\tau}) S_1^\beta S_2^\gamma S_1^\tau S_2^\nu = \\ &= S_1^\beta S_1^\beta S_2^\gamma S_2^\gamma - S_1^\beta S_1^\gamma S_2^\gamma S_2^\beta = \\ &= S^2(S+1)^2 - S_1^\beta S_1^\gamma (S_2^\beta S_2^\gamma + i\varepsilon_{\gamma\beta\alpha}S_2^\alpha) = \\ &= S^2(S+1)^2 - (\mathbf{S}_1\mathbf{S}_2)^2 + i\varepsilon_{\alpha\beta\gamma}S_1^\beta S_1^\gamma S_2^\alpha = \\ &= S^2(S+1)^2 - (\mathbf{S}_1\mathbf{S}_2)^2 - \mathbf{S}_1\mathbf{S}_2, \end{aligned} \quad (2.76)$$

<sup>17</sup>Note that SU(2) symmetry and the  $Z_2$  geometrical symmetry of the bond are independent from each other, therefore each order parameter will either stay invariant or change sign if the indices 1 and 2 are interchanged. Remembering that triplet (singlet) states are symmetric (antisymmetric) in spin space and denoting by  $A_1$  ( $A_2$ ) the symmetric (antisymmetric) representation of  $Z_2$ , one finds

$$\begin{aligned} (D^{(1)} \otimes A_1 \oplus D^{(0)} \otimes A_2) \otimes (D^{(1)} \otimes A_1 \oplus D^{(0)} \otimes A_2) &= \\ &= 2D^{(0)} \otimes A_1 \oplus 2D^{(1)} \otimes A_2 \oplus D^{(1)} \otimes A_1 \oplus D^{(2)} \otimes A_2. \end{aligned} \quad (2.74)$$

<sup>18</sup>For a pair of spins  $S$ , one would find  $2S$  non-trivial scalar operators, thus a general isotropic Hamiltonian may contain powers of the scalar product  $\mathbf{S}_1\mathbf{S}_2$  up to  $2S$ .

leads eventually to

$$\mathbf{Q}_1 \mathbf{Q}_2 = 2 (\mathbf{S}_1 \mathbf{S}_2)^2 + \mathbf{S}_1 \mathbf{S}_2 - \frac{2}{3} S^2 (S + 1)^2. \quad (2.77)$$

Substituting (2.77) into (2.71) and setting the spin length to one yields a new form of the bilinear-biquadratic Hamiltonian:

$$H = J \left( \cos \vartheta - \frac{\sin \vartheta}{2} \right) \mathbf{S}_1 \mathbf{S}_2 + J \frac{\sin \vartheta}{2} \mathbf{Q}_1 \mathbf{Q}_2 + J \frac{4 \sin \vartheta}{3}. \quad (2.78)$$

### 2.2.1 SU(3) symmetry of the bilinear-biquadratic Hamiltonian

We shall now discuss the symmetry properties of the bilinear-biquadratic pair-Hamiltonian (2.71) of spins one. Let us introduce three bosonic flavours satisfying (2.12) on each site, with the condition that operators belonging to different sites are independent. Denoting by  $a_i$  and  $b_i$  ( $i = 1, 2, 3$ ) the flavours on site 1 and 2, respectively, we may thus write

$$[a_i, b_j] = [a_i, b_j^\dagger] = 0, \quad i, j = 1, 2, 3. \quad (2.79)$$

Using the SU(3) generators  $Q_\alpha^{(1)}$  and  $Q_\alpha^{(2)}$  constructed on each site according to (2.13), one may define the operators

$$Q_\alpha^T = Q_\alpha^{(1)} + Q_\alpha^{(2)}, \quad \alpha = 1, 2 \dots 8, \quad (2.80)$$

which are easily shown to be hermitian and to obey the SU(3) Lie-algebra commutation relations (2.17). The generators  $Q_\alpha^T$  provide a means of verifying that the coupling  $Q_\alpha^{(1)} Q_\alpha^{(2)}$  is SU(3)-invariant: indeed,

$$\begin{aligned} [Q_\alpha^{(1)} Q_\alpha^{(2)}, Q_\beta^T] &= [Q_\alpha^{(1)} Q_\alpha^{(2)}, Q_\beta^{(1)} + Q_\beta^{(2)}] = \\ &= [Q_\alpha^{(1)}, Q_\beta^{(1)}] Q_\alpha^{(2)} + Q_\alpha^{(1)} [Q_\alpha^{(2)}, Q_\beta^{(2)}] = \\ &= i f_{\alpha\beta\gamma} (Q_\gamma^{(1)} Q_\alpha^{(2)} + Q_\alpha^{(1)} Q_\gamma^{(2)}) = \\ &= 0, \end{aligned} \quad (2.81)$$

since the structure constants  $f_{\alpha\beta\gamma}$  are completely antisymmetric. Using (2.21) and (2.23), and thereby restricting the Hilbert space to that of local spins one, we may express  $Q_\alpha^{(1)} Q_\alpha^{(2)}$  in terms of spin and quadrupolar operators,

$$Q_\alpha^{(1)} Q_\alpha^{(2)} = \frac{1}{4} (\mathbf{S}_1 \mathbf{S}_2 + \mathbf{Q}_1 \mathbf{Q}_2), \quad (2.82)$$

and a glance at (2.78) tells us therefore that the bilinear-biquadratic Hamiltonian (2.71) is SU(3)-invariant at the points  $\vartheta = \pi/4$  and  $\vartheta = 5\pi/4$ , where it assumes the form of an isotropic SU(3) Heisenberg model. For this reason, we shall refer to the points  $\vartheta = \pi/4$  and  $\vartheta = 5\pi/4$  as antiferro and ferro SU(3) points, respectively. Actually, it can be shown via use of the complex conjugate representation (2.28) on one of the sites (take site 2 for instance) that there exist two additional points of SU(3) symmetry: indeed, the coupling  $-Q_\alpha^{(1)}Q_\alpha^{*(2)}$  commutes with the SU(3) generators  $\{Q_\alpha^{(1)} - Q_\alpha^{*(2)}, \alpha = 1, 2 \dots 8\}$ , and it can be rewritten for spins one as

$$-Q_\alpha^{(1)}Q_\alpha^{*(2)} = \frac{1}{4}(\mathbf{S}_1\mathbf{S}_2 - \mathbf{Q}_1\mathbf{Q}_2), \quad (2.83)$$

hence the Hamiltonian (2.71) is SU(3)-invariant at the points  $\vartheta = \pi/2$  and  $\vartheta = 3\pi/2$  as well.

Introducing single-ion anisotropy of the form

$$H_D = D((S_1^z)^2 + (S_2^z)^2) \quad (2.84)$$

generally reduces the SU(2) symmetry of the Hamiltonian (2.71) to  $U(1) \times \mathbb{Z}_2$ , however, the case of the SU(3)-symmetric points is somewhat special. Rewriting the anisotropy term as

$$H_D = 4D(Q_2^{(1)}Q_2^{(1)} + Q_2^{(2)}Q_2^{(2)}), \quad (2.85)$$

one may verify that it commutes with the first three components of  $Q^T$  defined in (2.80). Let us take the first component  $Q_1^T$  as an example:

$$\begin{aligned} & [Q_2^{(1)}Q_2^{(1)} + Q_2^{(2)}Q_2^{(2)}, Q_1^T] = \\ & = [Q_2^{(1)}Q_2^{(1)} + Q_2^{(2)}Q_2^{(2)}, Q_1^{(1)} + Q_1^{(2)}] = \\ & = Q_2^{(1)}[Q_2^{(1)}, Q_1^{(1)}] + [Q_2^{(1)}, Q_1^{(1)}]Q_2^{(1)} + \\ & \quad + Q_2^{(2)}[Q_2^{(2)}, Q_1^{(2)}] + [Q_2^{(2)}, Q_1^{(2)}]Q_2^{(2)} = \\ & = if_{21\gamma} \left( Q_2^{(1)}Q_\gamma^{(1)} + Q_\gamma^{(1)}Q_2^{(1)} + Q_2^{(2)}Q_\gamma^{(2)} + Q_\gamma^{(2)}Q_2^{(2)} \right) = \\ & = if_{213} \left( Q_2^{(1)}Q_3^{(1)} + Q_3^{(1)}Q_2^{(1)} + Q_2^{(2)}Q_3^{(2)} + Q_3^{(2)}Q_2^{(2)} \right), \end{aligned} \quad (2.86)$$

where we have used the fact that the only non-zero structure constant  $f_{\alpha\beta\gamma}$  that has two of the indices  $\{1, 2, 3\}$  has the third one as well. The anticommutators can be rewritten with the help of the bosonic expressions (2.13),

and following steps similar to those in (2.15), we indeed find

$$\begin{aligned} \{Q_2, Q_3\} &= \frac{1}{4} a_i^\dagger a_k^\dagger a_j a_l (\lambda_{2,ij} \lambda_{3,kl} + \lambda_{3,ij} \lambda_{2,kl}) + \\ &\quad + \frac{1}{4} a_i^\dagger a_l (\lambda_{2,ik} \lambda_{3,kl} + \lambda_{3,ik} \lambda_{2,kl}) = \\ &= 0, \end{aligned} \quad (2.87)$$

since the first three Gell-Mann matrices are of the form

$$\lambda_i = \begin{pmatrix} \sigma^i & 0 \\ 0 & 0 \end{pmatrix}, \quad (2.88)$$

i. e. they anticommute with each other, and the four-operator term vanishes for a local spin one. The first three components of  $Q^T$  form an  $SU(2)$  subalgebra of  $SU(3)$ , and therefore the result

$$[H_D, Q_\alpha^T] = 0, \quad \alpha = 1, 2, 3 \quad (2.89)$$

unveils the remaining  $SU(2) \times Z_2$  symmetry of the complete Hamiltonian  $H + H_D$  at the ferro and antiferro  $SU(3)$  points. Let us note that these symmetry considerations are valid for the  $SU(3)$  points  $\vartheta = \pi/2$  and  $\vartheta = 3\pi/2$  as well, as one may demonstrate by using the complex conjugate representation (2.28) on one of the two sites.

Finally, let us take another look at the form of the Hamiltonian (2.71) at the ferro and antiferro  $SU(3)$  points. Denoting the total number of bosons on each site by  $N_i$  ( $i = 1, 2$ ), we may rewrite the operator  $Q_\alpha^{(1)} Q_\alpha^{(2)}$  in a bosonic form as

$$Q_\alpha^{(1)} Q_\alpha^{(2)} = \frac{1}{2} \sum_{ij} a_i^\dagger a_j b_j^\dagger b_i - \frac{1}{6} N_1 N_2, \quad (2.90)$$

and setting the spin length to one ( $N_1 = N_2 = 1$ ), we find the identity

$$\mathbf{S}_1 \mathbf{S}_2 + \mathbf{Q}_1 \mathbf{Q}_2 = 2P_{12} - \frac{2}{3}, \quad (2.91)$$

where the so-called transposition operator

$$P_{12} = \sum_{ij} a_i^\dagger a_j b_j^\dagger b_i \quad (2.92)$$

exchanges the states of the two sites<sup>19</sup>. Injecting (2.91) into (2.78), we derive yet another expression for the bilinear-biquadratic Hamiltonian:

$$H = J (\cos \vartheta - \sin \vartheta) \mathbf{S}_1 \mathbf{S}_2 + J \sin \vartheta (1 + P_{12}). \quad (2.93)$$

<sup>19</sup>The Schwinger-bosonic construction of the  $SU(2)$  algebra (2.30) allows for a similar identity: setting the spin length to one-half, one finds  $2\mathbf{S}_1 \mathbf{S}_2 + 1/2 = P_{12}$ .

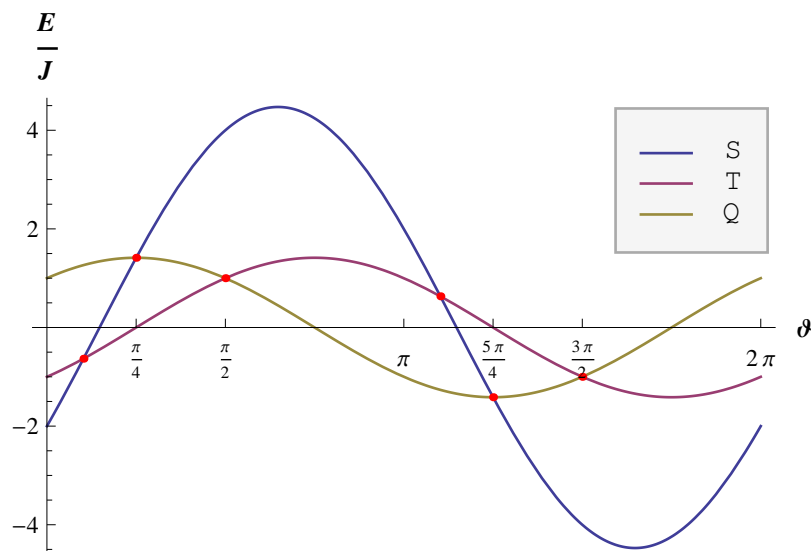


Figure 2.4: Singlet (S), triplet (T) and quintuplet (Q) energy levels of the Hamiltonian (2.71) of a spin-one bond. We find level-crossings at the four  $SU(3)$ -symmetric points, as well as at two extra points satisfying  $\tan \vartheta = 1/3$ .

### 2.2.2 The bond and the triangle

We have shown earlier that (2.71) is the most general spin-rotationally invariant Hamiltonian for a bond of spins one. In order to derive its spectrum, it is sufficient to notice that it can be rewritten as

$$H = \frac{J_2}{4} (\mathbf{S}_1 + \mathbf{S}_2)^4 + \left( \frac{J_1}{2} - 2J_2 \right) (\mathbf{S}_1 + \mathbf{S}_2)^2 + (4J_2 - 2J_1), \quad (2.94)$$

where we have used the notation  $J_1 = J \cos \vartheta$  and  $J_2 = J \sin \vartheta$  for brevity. The energy levels can be divided into a non-degenerate singlet level, a three-fold degenerate triplet level and a five-fold degenerate quintuplet level, and the corresponding eigenvalues are

$$\begin{aligned} E_S &= 4J_2 - 2J_1, \\ E_T &= J_2 - J_1, \\ E_Q &= J_2 + J_1. \end{aligned} \quad (2.95)$$

A plot of the energy levels is presented in figure 2.4. The crossing of the singlet and quintuplet levels at  $\vartheta = \pi/4$  and  $\vartheta = 5\pi/4$  is due to the fact that the Hamiltonian (2.71) becomes an  $SU(3)$  Heisenberg model at these points, and therefore it only gives rise to an energy difference between  $SU(3)$  multiplets. The corresponding eigenstates of (2.92) are easily derived with

the help of the bosonic representation: denoting the three flavours defined on each site by  $a$ ,  $b$  and  $c$ , we find that the symmetric states  $|aa\rangle$ ,  $|bb\rangle$ ,  $|cc\rangle$ ,  $|ab\rangle + |ba\rangle$ ,  $|ac\rangle + |ca\rangle$  and  $|bc\rangle + |cb\rangle$  belong to the eigenvalue  $2J_2$ , while the antisymmetric states  $|ab\rangle - |ba\rangle$ ,  $|ac\rangle - |ca\rangle$  and  $|bc\rangle - |cb\rangle$  belong to the eigenvalue 0. We note that, using a common shorthand-notation for irreducible SU(3) representations (for reference, see [10]), the transformation properties of these states under the SU(3) algebra can be summed up in a concise manner as  $3 \otimes 3 = 6 \oplus \bar{3}$ . Similarly, the crossing of the triplet and quintuplet levels at the SU(3) points  $\vartheta = \pi/2$  and  $\vartheta = 3\pi/2$  may be interpreted as  $3 \otimes \bar{3} = 8 \oplus 1$ . Finally, we note that a degeneracy of the singlet and triplet levels occurs for  $\tan \vartheta = 1/3$ , where the Hamiltonian (2.71) becomes equivalent to a projector to the quintuplet subspace:

$$H = 2J_1 P_{S=2} - \frac{2J_1}{3}, \quad (2.96)$$

with

$$P_{S=2} = \frac{1}{24} ((\mathbf{S}_1 + \mathbf{S}_2)^2 - 2) (\mathbf{S}_1 + \mathbf{S}_2)^2. \quad (2.97)$$

If we extend such a coupling with  $J_1 > 0$  over a chain of spins one and impose periodic boundary conditions, we end up with a unique ground state, the so-called valence-bond solid state [11].

While we do not wish to enter a thorough discussion on this subject, we nonetheless deem it worthwhile to mention that the spin-one bilinear-biquadratic chain exhibits a particularly rich phase diagram that includes the famous Haldane phase with a homogeneous ground state, a gapped spectrum and an exponential decay of correlations. The gap collapses at  $\vartheta = -\pi/4$ , where an exact solution is provided by the Bethe ansatz (see references in [11]), and the decay of correlations follows a power law. This critical point marks the boundary of the Haldane phase with another singlet phase, the so-called dimerized phase, in which the spectrum of excitations is gapped and spin correlations are short-ranged again, however, the ground state breaks translational symmetry and becomes two-fold degenerate. The dimerized phase spans the whole  $-\pi/4 < \vartheta < -3\pi/4$  region [12], which includes the integrable point  $\vartheta = -\pi/2$  [13]. The ferro SU(3) point separates the dimerized phase from a ferromagnetic phase, and it has the particular property of allowing for long-range ferroquadrupolar correlations, despite the system being one-dimensional, owing to the fact that the ferroquadrupolar order parameter commutes with the Hamiltonian at this point [14]. Finally, we note that the exactly-solvable Lai-Sutherland point  $\vartheta = \pi/4$  [15, 16] separates the Haldane phase from a critical phase with three soft modes at  $k = 0$  and  $k = \pm 2\pi/3$  [17]. Interestingly enough, the dominant correlations in the critical phase are antiferroquadrupolar, and they have a period of three lattice

spacings. For further references and a discussion on recent developments, see [18]. Reference [8] contains an instructive comparison of the properties of the spin-one-half chain and the spin-one chain.

Finally, let us add some remarks on the spin-one triangle. One may construct fourteen independent  $SU(2)$ -invariant physical operators in this case, but restricting ourselves to two-spin interactions leaves us with only six, namely the bilinear and the biquadratic terms defined on each bond<sup>20</sup>: using (2.93), the Hamiltonian can thus be written as

$$H = J (\cos \vartheta - \sin \vartheta) (\mathbf{S}_1 \mathbf{S}_2 + \mathbf{S}_2 \mathbf{S}_3 + \mathbf{S}_3 \mathbf{S}_1) + J \sin \vartheta (3 + P_{12} + P_{23} + P_{31}). \quad (2.98)$$

Even though the Hamiltonian (2.98) can not be expressed simply in terms of the total spin operator, unlike the Hamiltonian (2.71) of a bond, one may nonetheless carry out a useful decomposition<sup>21</sup> with the help of the following hermitian  $SU(3)$  generators that are defined analogously to (2.80):

$$Q_\alpha^T = Q_\alpha^{(1)} + Q_\alpha^{(2)} + Q_\alpha^{(3)}, \quad \alpha = 1, 2 \dots 8. \quad (2.99)$$

Using (2.91) and (2.82), we rewrite the Hamiltonian (2.98) as

$$H = J (\cos \vartheta - \sin \vartheta) \left( \frac{1}{2} (\mathbf{S}_1 + \mathbf{S}_2 + \mathbf{S}_3)^2 - 3 \right) + J \sin \vartheta (4 + 2 (Q_\alpha^{(1)} Q_\alpha^{(2)} + Q_\alpha^{(2)} Q_\alpha^{(3)} + Q_\alpha^{(3)} Q_\alpha^{(1)})), \quad (2.100)$$

and finally, using the definition of the spin operators (2.21), as well as the  $N = 1$  case of (2.20), we derive the expression

$$H = J (\cos \vartheta - \sin \vartheta) (2 (Q_5^T Q_5^T + Q_2^T Q_2^T + Q_7^T Q_7^T) - 3) + J \sin \vartheta Q_\alpha^T Q_\alpha^T. \quad (2.101)$$

We note the appearance of the Casimir operator  $Q_\alpha^T Q_\alpha^T$ , which commutes with all of the generators<sup>22</sup>, i. e.

$$\begin{aligned} [Q_\alpha^T Q_\alpha^T, Q_\beta^T] &= Q_\alpha^T [Q_\alpha^T, Q_\beta^T] + [Q_\alpha^T, Q_\beta^T] Q_\alpha^T = \\ &= i f_{\alpha\beta\gamma} (Q_\alpha^T Q_\gamma^T + Q_\gamma^T Q_\alpha^T) = \\ &= 0, \end{aligned} \quad (2.102)$$

<sup>20</sup>In the case of a spin-one-half triangle however, there are only four independent scalars: apart from the bilinear interactions, one may also define a scalar chirality of the form  $\mathbf{S}_1 (\mathbf{S}_2 \times \mathbf{S}_3)$ , which is easily shown to be hermitian, as well as to commute with the total spin.

<sup>21</sup>This decomposition is available for all geometries where each site is connected to all other ones. The bond, the triangle and the tetrahedron are examples of such ‘‘complete graphs’’.

<sup>22</sup>An analogous Casimir operator in  $SU(2)$  Lie algebras is the operator  $\mathbf{S}^2$ .

hence we find that the total spin  $S_T$  and the pair of Dynkin coefficients  $(q_1, q_2)$  representing  $SU(3)$  multiplets<sup>23</sup> are all good quantum numbers and can be used to label eigenstates of the Hamiltonian (2.98). Without entering into further details (for the complete spectrum, see [18]), we note that  $3 \otimes 3 \otimes 3 = 10 \oplus 8 \oplus 8 \oplus 1$ . At the ferro  $SU(3)$  point, the ground state is ten-fold degenerate, and it belongs to the  $A_1$  (completely symmetric) representation of the  $D_3$  point group of the triangle, while at the antiferro  $SU(3)$  point (and in its vicinity), it is a non-degenerate  $SU(3)$  singlet belonging to the  $A_2$  representation of  $D_3$ . The points  $\vartheta = \pi/2$  and  $\vartheta = 3\pi/2$  lose their  $SU(3)$ -symmetric character due to the presence of frustration. Let us conclude by highlighting an important difference between the spin-one bond and the spin-one triangle: for  $\vartheta \in [\pi/4, \pi/2[$ , the former has a triplet ground state, while the lowest-lying level of the latter is a singlet, which means that the bond is more easily magnetized than the triangle in this particular region. Interestingly enough, this simple observation remains quite relevant when one applies a variational treatment to the square and the triangular lattices.

### 2.2.3 Variational approach for spin-one systems

In this subsection, we will introduce the basic elements of a variational scheme that will be used extensively throughout the present work. The key approximation of the method lies in neglecting quantum entanglement between the  $S = 1$  spins that are defined on different sites, however, all on-site quantum-mechanical degrees of freedom are treated accurately, including those of quadrupolar nature. Mathematically speaking, we approximate the ground state of a lattice of  $L$  sites with a site-factorized wavefunction of the form

$$|\psi\rangle = \prod_{j=1}^n \prod_{i \in \lambda_j} |\psi_j(i)\rangle, \quad (2.103)$$

where the normalized spin-one wavefunction  $|\psi_j(i)\rangle$  is defined on site  $i$ , while the index  $j$  accounts for the fact that one may allow for different wavefunctions on different sites: the number of different single-site wavefunctions is  $n$ , and  $\lambda_j$  denotes the ensemble of sites featuring the same wavefunction. As the phase of  $|\psi_j(i)\rangle$  may be chosen arbitrarily<sup>24</sup>,  $|\psi\rangle$  is determined by  $4n$  real parameters, where  $n \leq L$ . Our aim is to minimize the expectation value  $\langle \psi | H | \psi \rangle$ , where  $H$  is the Hamiltonian of the lattice.

<sup>23</sup>Dynkin coefficients provide a unique labeling, in contrast to our earlier notation, which is only used for small representations. Expressions such as  $3 \otimes 3 = 6 \oplus \bar{3}$  can thus be rewritten as  $(1, 0) \otimes (1, 0) = (2, 0) \oplus (0, 1)$ .

<sup>24</sup>Changing the phase of any  $|\psi_j(i)\rangle$  corresponds to an overall phase transformation of  $|\psi\rangle$  and thus leaves expectation values invariant.

It has to be emphasized that while such a variational approach may give a useful insight into the physics of two- or higher-dimensional systems [19], where at zero temperature one often encounters a symmetry-breaking long-range-ordered state that can be characterized by a relevant on-site order parameter, it is generally of limited use in the study of one-dimensional systems, where, unless the order parameter is a conserved quantity, quantum fluctuations are expected to restore the continuous symmetry of the Hamiltonian. One may think of the spin-one bilinear-biquadratic chain for instance, where out of the four phases, the ferromagnetic one is the only one that features long-range order, and it is not possible to describe the other three phases in terms of a site-factorized wavefunction of the form (2.103). On the other hand, when it is applicable, the variational ansatz (2.103) may not only give a good approximation of the ground state in terms of its dominant correlations, but it also serves as a natural starting point for studying the excitation spectrum and the effect of quantum fluctuations by means of a flavour-wave expansion. We will discuss these issues in detail further on, but it might already be useful to quote an analogy with spin-one-half systems, where on-site wavefunctions describe classical dipole moments in essence, and quantum fluctuations may be induced systematically via a  $1/S$ -expansion. The underlying concepts can be extended in a straightforward manner to systems of higher spins, however, the on-site wavefunctions may quickly develop a considerable complexity, and consequently, the minimization problem becomes more complicated as well. We also mention that several attempts have been made to render the variational treatment suitable for the study of one-dimensional systems [19, 20].

In order to provide a simple but rather instructive demonstration, we will now apply the variational method to a spin-one bilinear-biquadratic bond: this is a problem that was first studied in the excellent paper by Papanicolaou [19]. While one may be tempted to overlook the importance of investigating elementary systems within the variational framework, the results we derive here will actually prove to be essential when we attempt to construct the variational ground state of realistic two-dimensional lattices. One finds that the minimization is greatly simplified for some selected values of  $\vartheta$ , namely at the antiferromagnetic (AFM) and ferromagnetic (FM) points that feature a pure bilinear coupling, and at the so-called antiferroquadrupolar (AFQ) and ferroquadrupolar (FQ) points, where only quadrupole moments are coupled (with a positive and a negative coefficient, respectively). We present the result of the minimization at these particular points first.

**AFM point** ( $\vartheta = 0$ ) : Both sites feature coherent spin states with the spin vectors pointing in opposite directions.

**FM point** ( $\vartheta = \pi$ ) : Coherent spin states with coinciding spin vectors.

**AFQ point** ( $\vartheta = \arctan 2 \approx 0.35\pi$ ) : A glance at (2.78) tells us that we have to minimize  $\langle \mathbf{Q}_1 \mathbf{Q}_2 \rangle$ , which can be rewritten as

$$\langle \mathbf{Q}_1 \mathbf{Q}_2 \rangle = |\mathbf{d}_1^* \cdot \mathbf{d}_2|^2 + |\mathbf{d}_1 \cdot \mathbf{d}_2|^2 - \frac{2}{3}, \quad (2.104)$$

where the components of the vector  $\mathbf{d}_i$  give the projection of  $|\psi_i\rangle$  to the states of the basis (2.1). We see that  $\langle \mathbf{Q}_1 \mathbf{Q}_2 \rangle$  is minimized if  $|\psi_2\rangle$  is orthogonal both to  $|\psi_1\rangle$  and its time-reversal transform: it follows that one of the sites has to have a pure quadrupole with a director  $\mathbf{d}$ , while the other one will feature either a quadrupole with its director perpendicular to  $\mathbf{d}$ , or a spin vector of arbitrary length pointing along  $\mathbf{d}$ .

**FQ point** ( $\vartheta = \arctan 2 + \pi \approx 1.35\pi$ ) :  $\langle \mathbf{Q}_1 \mathbf{Q}_2 \rangle$  is maximized by two quadrupolar states with parallel directors<sup>25</sup>.

A numerical minimization reveals that each of the above solutions extends over a finite  $\vartheta$ -interval, and the four resulting regions are separated from each other by SU(3)-symmetric points<sup>26</sup>: this is perhaps most visible on the plot of the energy-minimum as a function of  $\vartheta$  that we show in figure 2.5. It is important to emphasize that the AFQ solution is peculiar in the sense that fixing the state on the first site as a quadrupole with a well-defined director does not completely determine the state on the second site. In fact, as we show in figure 2.6, the state on the second site may interpolate continuously between a pure quadrupole and a coherent spin state: the director may rotate around that of the first site, and the spin length may also be chosen arbitrarily. The degeneracy of the bond-solution has a remarkable consequence, when one extends the AFQ coupling to a spin-one triangle. While a dipole moment is no longer admitted in this case, the energy of every bond can be minimized simultaneously via three quadrupolar states with mutually perpendicular directors, hence the frustration effect is lifted (see figure 2.7). At the same time, since the variational solution is unique up to global SU(2)

<sup>25</sup>We note that for two quadrupolar states,  $\langle \mathbf{Q}_1 \mathbf{Q}_2 \rangle = 2(\mathbf{d}_1 \cdot \mathbf{d}_2)^2 - \frac{2}{3}$  is maximized (minimized) by a parallel (perpendicular) arrangement of directors, therefore we say that a negative (positive) quadrupolar exchange favours a ferroquadrupolar (antiferroquadrupolar) state.

<sup>26</sup>This finding is easily verified analytically [19]. In fact, in analogy with (2.104), we may rewrite the bilinear coupling as  $\langle \mathbf{S}_1 \mathbf{S}_2 \rangle = |\mathbf{d}_1^* \cdot \mathbf{d}_2|^2 - |\mathbf{d}_1 \cdot \mathbf{d}_2|^2$ , and we may deduce that the total energy can only be minimized by configurations in which  $|\mathbf{d}_1^* \cdot \mathbf{d}_2|^2$  and  $|\mathbf{d}_1 \cdot \mathbf{d}_2|^2$  both attain extreme values.

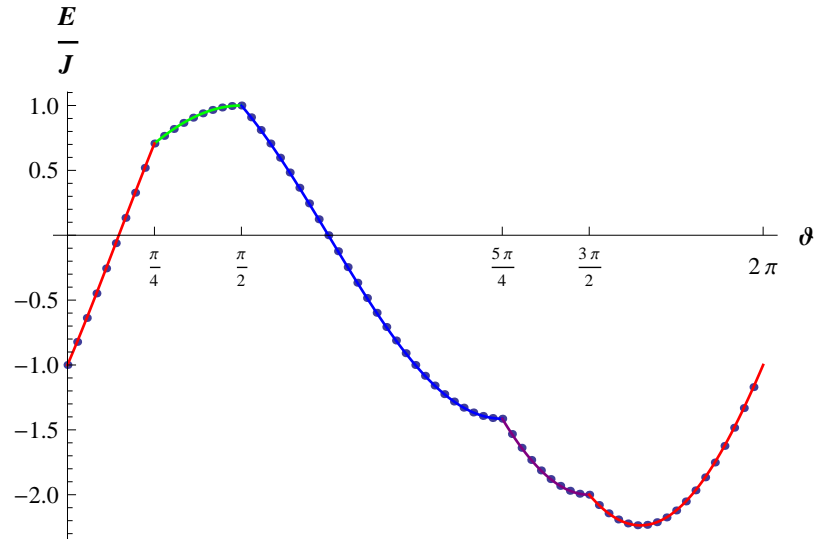


Figure 2.5: Variational energy of the spin-one bilinear-biquadratic bond. The dots are the results of a numerical minimization, while the curves come from conjecturing particular types of solutions: AFM (red curve), AFQ (green curve), FM (blue curve) and FQ (purple curve). The four distinct regions are separated by the SU(3)-symmetric points.

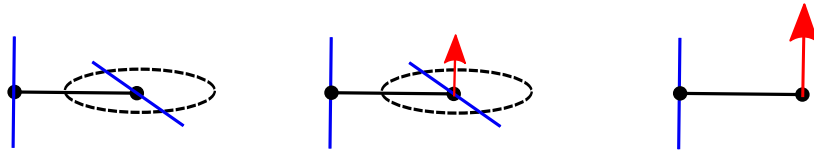


Figure 2.6: Degeneracy of the AFQ solution for a bond. Keeping one of the sites in a quadrupolar state, one may find either a quadrupole (left), a partially developed dipole (middle) or a fully polarized state (right) on the second site. Directors and dipole moments are represented by blue lines and red arrows, respectively.

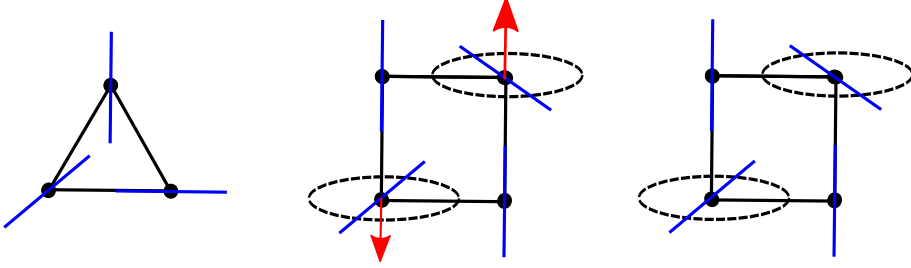


Figure 2.7: Interplay of frustrated geometry and antiferroquadrupolar coupling. While the variational solution for a triangle is unique up to global  $SU(2)$  rotations (left), the square admits a number of possible configurations (two examples are shown in the middle and on the right). Directors and dipole moments are represented by blue lines and red arrows, respectively.

rotations, non-trivial degeneracies are eliminated. The importance of frustrated geometries in this aspect is further exemplified by the case of a single square, where it can be shown that a configuration with minimum energy will feature two quadrupoles with parallel directors along one of the diagonals of the square, but the states on the other two sites can be varied independently from each other, and even if both states are magnetic, they might feature different spin lengths or the dipoles might point in opposite directions (although they will have to align themselves with the common director of the quadrupoles). We depict two examples in figure 2.7.

Let us now treat the  $SU(3)$ -symmetric points separately.

**antiferro  $SU(3)$  point** ( $\vartheta = \pi/4$ ) : With the help of (2.93), we may deduce that the quantity to minimize is  $\langle P_{12} \rangle = |\langle \psi_1 | \psi_2 \rangle|^2$ , i. e. the states on the two sites have to be orthogonal to each other. A wide range of possibilities includes the solutions for the AFM point and the AFQ point, and one finds that a peculiar type of antiferromagnetic state is also satisfactory: it features two spin vectors of the same length pointing in opposite directions, and the directors of the two states are perpendicular to each other.

**ferro  $SU(3)$  point** ( $\vartheta = 5\pi/4$ ) : The two sites must feature the same states.

$\vartheta = \pi/2$  : A variety of solutions includes those of the AFQ point and the FM point, as well as a peculiar type of ferromagnetic state which features the same spin vector on both sites, while the directors of the two states are perpendicular to each other.

$\vartheta = 3\pi/2$  : The minimum is given by the solutions of the AFM point and

the FQ point, and by an intermediate type of state which features two spin vectors of the same length pointing in opposite directions, while the directors remain the same on both sites (in other words, the two states are connected via time reversal).

It turns out that these points of higher symmetry do not only admit the solutions of the two regions that they separate from each other, but also allow for configurations that interpolate continuously between these solutions. Simple examples of such intermediate states could be

$$\begin{aligned} |\psi_1\rangle &= \cos \eta |x\rangle + i \sin \eta |y\rangle, \\ |\psi_2\rangle &= \cos \eta |y\rangle + i \sin \eta |x\rangle \end{aligned} \quad (2.105)$$

for  $\vartheta = \pi/4$ ,

$$\begin{aligned} |\psi_1\rangle &= \cos \eta |x\rangle + i \sin \eta |y\rangle, \\ |\psi_2\rangle &= \cos \eta |x\rangle + i \sin \eta |y\rangle \end{aligned} \quad (2.106)$$

for  $\vartheta = 5\pi/4$ ,

$$\begin{aligned} |\psi_1\rangle &= \cos \eta |x\rangle + i \sin \eta |y\rangle, \\ |\psi_2\rangle &= \cos \eta |y\rangle - i \sin \eta |x\rangle \end{aligned} \quad (2.107)$$

for  $\vartheta = \pi/2$ , and

$$\begin{aligned} |\psi_1\rangle &= \cos \eta |x\rangle + i \sin \eta |y\rangle, \\ |\psi_2\rangle &= \cos \eta |x\rangle - i \sin \eta |y\rangle \end{aligned} \quad (2.108)$$

for  $\vartheta = 3\pi/2$ , with  $\eta \in [0, \pi/4]$ : these configurations are depicted in figure 2.8. It is interesting to notice a particular difference between the SU(3) points  $\vartheta = \pi/2$  and  $\vartheta = 3\pi/2$ : while the earlier possesses a number of exotic variational ground states that are different from the ones we mentioned explicitly, the latter does not admit other configurations but the ones that interpolate between the AFM and the FQ solutions<sup>27</sup>. As a consequence, if we consider a spin-one triangle with pure biquadratic couplings<sup>28</sup>, we get very different types of behaviour depending on the sign of the coupling. For a negative sign, the variational ansatz yields a simple ferroquadrupolar configuration,

<sup>27</sup>The exact spectrum of the bond may provide an explanation for this difference: since the triplet and quintuplet levels cross at these points, the ground state is eight-fold degenerate for  $\vartheta = \pi/2$ , while it is non-degenerate for  $\vartheta = 3\pi/2$  (see figure 2.4), therefore practically any state written up at random has a good chance of belonging to the ground-state manifold for  $\vartheta = \pi/2$ .

<sup>28</sup>We remind the reader that this model does not possess SU(3) symmetry.

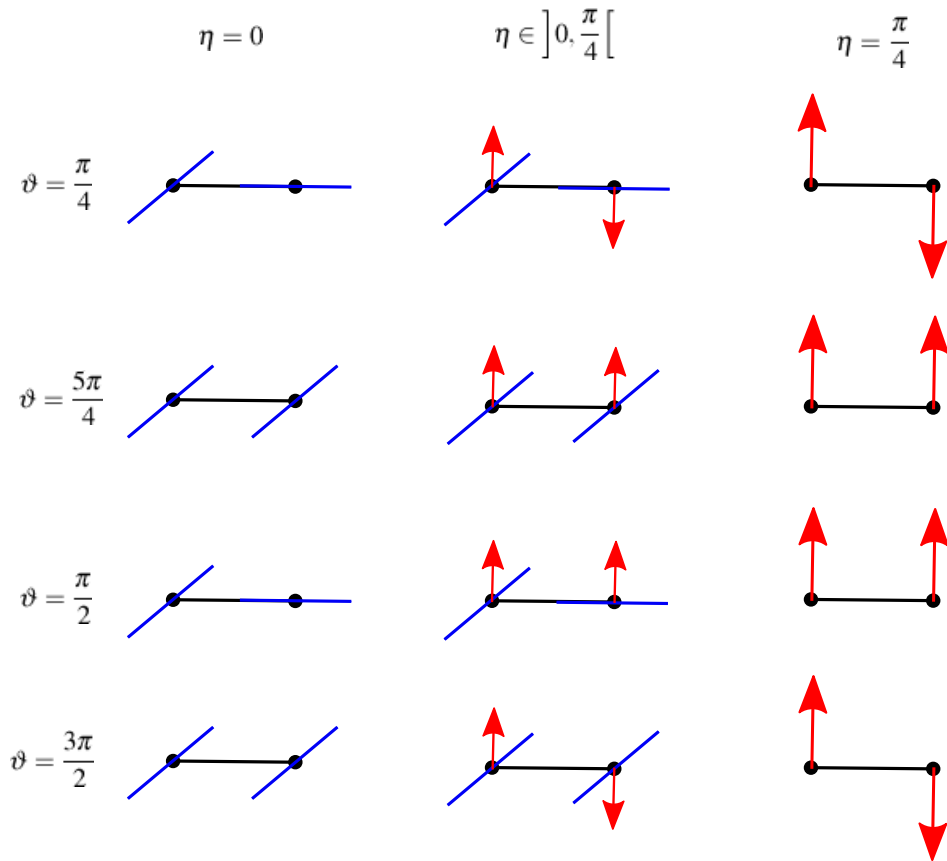


Figure 2.8: Interpolating configurations at the SU(3) points. In each row from top to bottom, we represent pictorially the wavefunction (2.105), (2.106), (2.107) and (2.108), respectively. Blue lines symbolize directors, while red arrows symbolize dipole moments.

however, for a positive sign, we still end up with an extensive degeneracy<sup>29</sup>. These observations suggest that the ferroquadrupolar region of the bilinear-biquadratic model extends further for the triangle than for the bond (i. e. it penetrates the  $\vartheta > 3\pi/2$  domain), moreover, the point  $\vartheta = \pi/2$  remains a separating point between the ferromagnetic and the antiferroquadrupolar regions for the triangle as well. Finally, we add that the interpolating state found for the bond at  $\vartheta = \pi/2$  allows for a particular configuration on the triangle, in which one of the sites is quadrupolar, the other two feature identical spin vectors that are parallel to the director of the quadrupole, and the directors of the two magnetic states are perpendicular to each other<sup>30</sup>.

### 2.2.4 Origins of the biquadratic coupling

Classical spin systems with frustrated antiferromagnetic interactions often possess a high degeneracy in the ground-state manifold, and are therefore particularly susceptible to perturbations. Several cases are known where the introduction of a physically-motivated extra term induces a selection mechanism that favours a *collinear* configuration of the spins, and this effect can be conveniently modeled with the help of a phenomenological biquadratic interaction. As an example, one might think of the coupling between spin and lattice degrees of freedom that originates in the dependence of the exchange integrals on the atomic positions in a crystal [21]. Since the exchange integrals are linear functions of the displacement coordinates, while the elastic energy of the deformation shows quadratic behaviour, a frustrated system may gain energy by distorting the lattice: naturally, the lattice distortion and the associated energy gain depend on the particular spin configuration, and this leads to a lift of degeneracy in the ground-state manifold. This phenomenon is discussed in detail for the case of a single tetrahedral molecule with four spins in [22], and one indeed finds that collinear states are selected. If we assume that the exchange integral for a pair of spins  $i$  and  $j$  depends only on the inter-atomic distance (a reasonable assumption for direct exchange), furthermore that the elastic energy associated with a bond distortion can be written as  $\kappa(\delta r_{ij})^2/2$ , where  $\delta r_{ij}$  is the variation of the bond length and  $\kappa$  is the elastic constant, we end up with the so-called bond-phonon model:

$$H^{\text{bp}} = \sum_{\langle i,j \rangle} \left\{ J(1 - \alpha \delta r_{ij}) \mathbf{S}_i \mathbf{S}_j + \frac{\kappa}{2} (\delta r_{ij})^2 \right\}, \quad (2.109)$$

<sup>29</sup>Naturally, the solutions include the fully polarized ferromagnetic configuration, as well as the antiferroquadrupolar state with three mutually perpendicular directors.

<sup>30</sup>We only mention in a footnote that this result explains the emergence of an exotic 2/3-magnetization plateau in the vicinity of  $\vartheta = \pi/2$  for the triangular lattice bilinear-biquadratic model [5].

where  $\alpha$  is the spin-lattice coupling constant. Considering  $\delta r_{ij}$  as independent parameters, we may integrate them out<sup>31</sup> and find an effective spin Hamiltonian:

$$H_{\text{eff}}^{\text{bp}} = J \sum_{\langle i,j \rangle} \{ \mathbf{S}_i \mathbf{S}_j - b (\mathbf{S}_i \mathbf{S}_j)^2 \}, \quad (2.110)$$

where  $b = J\alpha^2/2\kappa$  is a dimensionless constant. We may conclude that due to the emergent biquadratic term, a collinear arrangement of spins will become favourable. It was suggested on the basis of the bond-phonon model, as well as the improved site-phonon model which induces an effective coupling between different bond variables, that lattice distortion may play a crucial role in the stabilization of the robust half-magnetization plateau phase that was found in some spinel oxides [24, 25]. Let us point out however that the introduction of extra coupling terms is not the only way of lifting the ground-state degeneracy in classical frustrated systems. It was shown on a quite general basis that both quantum and thermal fluctuations tend to favour collinear spin configurations, and they may eventually give rise to long-range order in a vast variety of systems [26, 27, 28, 29]: this is the so-called “order-by-disorder” phenomenon [30]. The associated ground-state selection may often be modeled by introducing an effective biquadratic exchange term: the case of the anisotropic Heisenberg model (or XXZ model) will be discussed in detail in appendix B.

Having motivated the study of biquadratic terms in classical spin systems, we will abandon this topic for the remainder of the present work. In fact, these classical biquadratic terms are not only conceptually very different from the quantum-mechanical biquadratic interaction that addresses the quadrupolar nature of spins one, but the physical intuition gained from the study of the earlier might also be misleading in the study of the latter<sup>32</sup>. One must emphasize that the variational approach based on site-factorized wavefunctions is not quite the same as the classical treatment where the spins become unit vectors, and this remains true even if we restrict the Hilbert space to coherent spin states. This is easily demonstrated already for a single biquadratic bond: considering a pair of coherent spin states,  $\langle (\mathbf{S}_1 \mathbf{S}_2)^2 \rangle \sim \langle P_{12} \rangle - \langle \mathbf{S}_1 \mathbf{S}_2 \rangle$  is minimized only by a ferromagnetic configuration, a classical biquadratic term however gives the same for parallel and antiparallel spins, and it is minimized only by a pair of perpendicular spins. Even though the difference in this particular case might simply be attributed to the apparent presence

<sup>31</sup>Note that this step breaks down for quantum spins due to non-commutativity [23].

<sup>32</sup>The 1/3-magnetization plateau on the triangular lattice, however, can be seen as a counterexample, as it may be stabilized either via an effective biquadratic term modeling quantum fluctuations around the classical limit [28], or via the introduction of a true quantum-mechanical biquadratic term in a spin-one system [5].

of quadrupolar components in the coupling, one might wonder about the possibility of frustrating a spin-one system with pure bilinear couplings to such an extent that it starts accessing the quadrupolar degrees of freedom in the on-site wavefunctions. This certainly does not happen yet for a spin-one triangle, as the variational approach yields 120-degree order with fully developed spins in this case. Bearing these remarks in mind, we will nonetheless often refer to the variational treatment as “classical” for two reasons: firstly, because even though on-site wavefunctions describe quantum-mechanical degrees of freedom, there is no entanglement between wavefunctions belonging to different sites<sup>33</sup>, and secondly, because site-factorized wavefunctions provide a starting point for the flavour-wave expansion that is analogous to the semi-classical spin-wave expansion.

In the upcoming chapters, we will consider the biquadratic interaction as a true quantum-mechanical term stemming from virtual fermionic transitions that are associated with the Hubbard model in the limit of strong repulsion. Having electrons in mind, one may not expect the emergence of biquadratic terms in the non-degenerate Hubbard model, since it accounts for the physics of Mott insulators with localized spins one-half, however, the presence of orbital degeneracy may quite naturally give rise to an effective biquadratic coupling. In order to demonstrate this, we present the case of the simple  $e_g$  molecule, following the discussion in [8]. Let us consider two sites, each with a two-fold degenerate orbital: the electronic operators corresponding to the one-particle states can be written as  $c_{ja\sigma}^\dagger$  and  $c_{jb\sigma}$ , where  $j \in \{1, 2\}$  is the site index,  $a$  and  $b$  represent the orbitals, and  $\sigma \in \{\uparrow, \downarrow\}$  stands for the spin variable. Assuming that the hopping does not mix the orbitals, furthermore that all hopping processes have an equal amplitude  $t$ , we may write the one-particle hopping term as

$$H_{\text{hop}} = -t \sum_{\sigma} \left( c_{1a\sigma}^\dagger c_{2a\sigma} + c_{2a\sigma}^\dagger c_{1a\sigma} + c_{1b\sigma}^\dagger c_{2b\sigma} + c_{2b\sigma}^\dagger c_{1b\sigma} \right). \quad (2.111)$$

We will denote the on-site Hubbard repulsion for electrons in the same orbital by  $U$ , and for electrons in different orbitals by  $U_{ab}$ , and we introduce an exchange constant  $J > 0$  that ensures that if two electrons occupy different orbitals on the same site, they form a spin triplet. The two-particle

---

<sup>33</sup>For this reason, the variational ansatz may also be called a mean-field ansatz.

interaction can then be written as

$$\begin{aligned}
H_{\text{int}} = & U \sum_j (n_{ja\uparrow}n_{ja\downarrow} + n_{jb\uparrow}n_{jb\downarrow}) + U_{ab} \sum_j \sum_{\sigma,\sigma'} n_{ja\sigma}n_{jb\sigma'} - \\
& - 2J \sum_j \frac{n_{ja\uparrow} - n_{ja\downarrow}}{2} \frac{n_{jb\uparrow} - n_{jb\downarrow}}{2} - \\
& - J \sum_j \left( c_{ja\uparrow}^\dagger c_{ja\downarrow} c_{jb\downarrow}^\dagger c_{jb\uparrow} + c_{ja\downarrow}^\dagger c_{ja\uparrow} c_{jb\uparrow}^\dagger c_{jb\downarrow} \right),
\end{aligned} \tag{2.112}$$

where the last term, the spin-flip term, is the only non-diagonal one. Let us consider the system at half-filling (four electrons), in the limit of strong interaction defined by  $U, U_{ab}, J \gg t$ . In the absence of the hopping terms ( $t = 0$ ), the ground-state manifold is spanned by configurations featuring two electrons on each site, one in each orbital, and the two electrons of a given site form a triplet. Since the local triplets are independent, the ground state is nine-fold degenerate. However, if charge fluctuations are not entirely suppressed but still remain relatively small, they introduce an effective coupling between the spin degrees of freedom of the on-site triplets, in the spirit of perturbation theory. Naturally, since  $H_{\text{hop}} + H_{\text{int}}$  is isotropic with respect to the spin variables, the effective Hamiltonian  $H_{\text{eff}}$  will be an SU(2)-invariant spin-one model: in order to find  $H_{\text{eff}}$ , it is therefore sufficient to calculate the energy of the  $|S = 2, S^z = 2\rangle$  quintuplet state, the  $|S = 1, S^z = 1\rangle$  triplet state and the  $|S = 0, S^z = 0\rangle$  singlet state. Elementary spin algebra reveals the form of these states:

$$\begin{aligned}
|S = 2, S^z = 2\rangle &= |1\rangle \otimes |1\rangle, \\
|S = 1, S^z = 1\rangle &= \frac{1}{\sqrt{2}} (|0\rangle \otimes |1\rangle - |1\rangle \otimes |0\rangle), \\
|S = 0, S^z = 0\rangle &= \frac{1}{\sqrt{3}} (|1\rangle \otimes |\bar{1}\rangle + |\bar{1}\rangle \otimes |1\rangle - |0\rangle \otimes |0\rangle),
\end{aligned} \tag{2.113}$$

where  $|0\rangle$ ,  $|1\rangle$  and  $|\bar{1}\rangle$  represent the on-site triplet states. Let us denote the three states on the left-hand side of (2.113) by  $|Q\rangle$ ,  $|T\rangle$  and  $|S\rangle$  for brevity,

and express them with the help of the fermionic operators:

$$\begin{aligned}
|Q\rangle &= c_{1a\uparrow}^\dagger c_{1b\uparrow}^\dagger c_{2a\uparrow}^\dagger c_{2b\uparrow}^\dagger |\text{vac}\rangle, \\
|T\rangle &= \frac{1}{2} \left[ \left( c_{1a\downarrow}^\dagger c_{1b\uparrow}^\dagger + c_{1a\uparrow}^\dagger c_{1b\downarrow}^\dagger \right) c_{2a\uparrow}^\dagger c_{2b\uparrow}^\dagger - \right. \\
&\quad \left. - c_{1a\uparrow}^\dagger c_{1b\uparrow}^\dagger \left( c_{2a\downarrow}^\dagger c_{2b\uparrow}^\dagger + c_{2a\uparrow}^\dagger c_{2b\downarrow}^\dagger \right) \right] |\text{vac}\rangle, \\
|S\rangle &= \frac{1}{\sqrt{3}} \left[ c_{1a\uparrow}^\dagger c_{1b\uparrow}^\dagger c_{2a\downarrow}^\dagger c_{2b\downarrow}^\dagger + c_{1a\downarrow}^\dagger c_{1b\downarrow}^\dagger c_{2a\uparrow}^\dagger c_{2b\uparrow}^\dagger - \right. \\
&\quad \left. - \frac{1}{2} \left( c_{1a\downarrow}^\dagger c_{1b\uparrow}^\dagger + c_{1a\uparrow}^\dagger c_{1b\downarrow}^\dagger \right) \left( c_{2a\downarrow}^\dagger c_{2b\uparrow}^\dagger + c_{2a\uparrow}^\dagger c_{2b\downarrow}^\dagger \right) \right] |\text{vac}\rangle,
\end{aligned} \tag{2.114}$$

where  $|\text{vac}\rangle$  is the electronic vacuum. The energy of the quintuplet level is easy to find, since neither hopping, nor spin-flip events may occur in the state  $|Q\rangle$ , i. e. it is an eigenstate of the Hamiltonian. The associated energy-eigenvalue is

$$E_Q = 2U_{ab} - J. \tag{2.115}$$

Acting with the Hamiltonian on the triplet state, we find an ionized state:

$$(H_{\text{hop}} + H_{\text{int}}) |T\rangle = (2U_{ab} - J) |T\rangle - 2t |T_{\text{exc}}\rangle, \tag{2.116}$$

where

$$\begin{aligned}
|T_{\text{exc}}\rangle &= \frac{1}{2} \left[ c_{1a\uparrow}^\dagger c_{2a\uparrow}^\dagger \left( c_{1b\uparrow}^\dagger c_{1b\downarrow}^\dagger + c_{2b\uparrow}^\dagger c_{2b\downarrow}^\dagger \right) + \right. \\
&\quad \left. + c_{1b\uparrow}^\dagger c_{2b\uparrow}^\dagger \left( c_{1a\uparrow}^\dagger c_{1a\downarrow}^\dagger + c_{2a\uparrow}^\dagger c_{2a\downarrow}^\dagger \right) \right] |\text{vac}\rangle,
\end{aligned} \tag{2.117}$$

however, since

$$(H_{\text{hop}} + H_{\text{int}}) |T_{\text{exc}}\rangle = (2U_{ab} + U) |T_{\text{exc}}\rangle - 2t |T\rangle, \tag{2.118}$$

the states  $|T\rangle$  and  $|T_{\text{exc}}\rangle$  span a two-dimensional subspace of the Hamiltonian. Subtracting the constant  $E_Q$  from the energy of both states, we may find the triplet-quintuplet splitting by solving the equation

$$\begin{vmatrix} -\lambda & -2t \\ -2t & -\lambda + U + J \end{vmatrix} = 0 \tag{2.119}$$

and picking the solution  $\lambda$  that vanishes in the  $t \rightarrow 0$  limit. The result is

$$E_T - E_Q = \frac{U + J}{2} \left( 1 - \sqrt{1 + \frac{16t^2}{(U + J)^2}} \right), \tag{2.120}$$

which may be expanded to quartic order in  $t$  as

$$E_T - E_Q \approx -\frac{4t^2}{U+J} + \frac{16t^4}{(U+J)^3}. \quad (2.121)$$

The energy of the singlet level can be found in a similar way, however, the calculation is a bit more tedious, therefore we will only quote the result from [8]:

$$E_S - E_Q \approx -\frac{6t^2}{U+J} + \frac{12t^4}{(U+J)^2} \left( \frac{3}{U+J} - \frac{2}{2(U+U_{ab})+J} - \frac{2}{2(U-U_{ab})+J} \right). \quad (2.122)$$

The lowest-order term is easily verified with the help of second-order perturbation theory: indeed,

$$H_{\text{hop}}|S\rangle = \sqrt{6}t|S_{\text{exc}}\rangle, \quad (2.123)$$

where the excited state

$$|S_{\text{exc}}\rangle = \frac{1}{\sqrt{8}} \left[ \left( c_{1a\uparrow}^\dagger c_{2a\downarrow}^\dagger - c_{1a\downarrow}^\dagger c_{2a\uparrow}^\dagger \right) \left( c_{1b\uparrow}^\dagger c_{1b\downarrow}^\dagger + c_{2b\uparrow}^\dagger c_{2b\downarrow}^\dagger \right) + \left( c_{1b\uparrow}^\dagger c_{2b\downarrow}^\dagger - c_{1b\downarrow}^\dagger c_{2b\uparrow}^\dagger \right) \left( c_{1a\uparrow}^\dagger c_{1a\downarrow}^\dagger + c_{2a\uparrow}^\dagger c_{2a\downarrow}^\dagger \right) \right] |\text{vac}\rangle \quad (2.124)$$

is connected to  $|S\rangle$  via a matrix element  $\sqrt{6}t$ , and the excitation energy is  $U+J$ . Let us compare the energy levels we obtained to those of a spin-one bilinear-biquadratic Hamiltonian: a glance at (2.95) reveals that we need to satisfy

$$\begin{aligned} E_T - E_Q &= -2J_1, \\ E_S - E_Q &= 3(J_2 - J_1), \end{aligned} \quad (2.125)$$

which gives

$$\begin{aligned} J_1 &= \frac{2t^2}{U+J} - \frac{8t^4}{(U+J)^3}, \\ J_2 &= \frac{4t^4}{(U+J)^2} \left( \frac{1}{U+J} - \frac{2}{2(U+U_{ab})+J} - \frac{2}{2(U-U_{ab})+J} \right), \end{aligned} \quad (2.126)$$

up to fourth order in  $t$ . Considering only second-order virtual hopping processes, we recover a pure antiferromagnetic Heisenberg coupling, which should not come as a surprise, since these processes only involve the exchange

of a single electron of spin one-half. However, starting from fourth order in  $t$ , the bilinear interaction alone is insufficient to account for the splitting of the energy levels, and we find an effective biquadratic term which, assuming that  $U - U_{ab} \ll U$ , has a negative coefficient. Since the bilinear-biquadratic Hamiltonian is the most general spin-rotationally invariant Hamiltonian for a pair of spins one, virtual hopping processes of higher order will only renormalize the coupling coefficients  $J_1$  and  $J_2$  in the present case. If our molecule had higher on-site spins, further terms would emerge in subsequent orders of  $t$ , however, the biquadratic interaction would still be the dominant correction to the Heisenberg Hamiltonian: in fact, this coupling was first found experimentally for  $\text{Mn}^{2+}$  ions with an  $S = 5/2$  spin [31, 32]. On the other hand, if one considers a molecule comprising several spin-one sites, terms such as  $(\mathbf{S}_1\mathbf{S}_2)(\mathbf{S}_2\mathbf{S}_3)$  might appear already at the fourth order in  $t$ , in addition to plaquette exchange and further-neighbour pair exchange that are present in spin-one-half systems as well [33].

Our study of the  $e_g$  molecule might lead us to think that the effective biquadratic interaction will generally have a small negative coefficient. While this is certainly a reasonable expectation in most cases, we have to keep in mind that we have completely neglected the role of higher-lying states in the preceding discussion. In fact, if we introduce a low-lying third orbital  $c$  that is separated by a small crystal-field splitting from the orbitals  $a$  and  $b$ , we will allow for additional second-order hopping processes that favour a ferromagnetic alignment of spins<sup>34</sup>, and this may eventually reduce the value of  $J_1$  quite considerably, perhaps even push it in the negative regime. Cancellation effects in the leading order of perturbation theory enhance the role of higher-order contributions, and a dominant biquadratic term with  $J_2 < 0$  was shown to emerge in several situations of orbital quasi-degeneracy [34, 35]. We mention that the underlying mechanism seems to be experimentally realized in the spin-one chain system  $\text{LiVGe}_2\text{O}_6$  [36]. While a sizeable biquadratic interaction with  $J_2 > 0$  still remains to be found within the framework of the electronic Hubbard model, an effective spin-one model with  $J_1 = J_2 > 0$  is easily recovered if we consider *three-flavour fermions* in the limit of strong interaction. Let us take a simplified  $\text{SU}(3)$ -symmetric Hubbard model with a single orbital:

$$H = -t \sum_{\langle i,j \rangle, \alpha} (c_{i\alpha}^\dagger c_{j\alpha} + c_{j\alpha}^\dagger c_{i\alpha}) + U \sum_{i, \alpha < \beta} n_{i\alpha} n_{i\beta}, \quad (2.127)$$

<sup>34</sup>Starting out from the state  $|Q\rangle$  for instance, an electron now has the opportunity to hop back and forth via the  $c$  orbital of the neighbouring site, and the intermediate state will have a relatively low energy due to Hund's coupling that favours parallel spins on a given site. As a result, the quintuplet configuration will gain energy.

where  $c_{i\alpha}^\dagger$  and  $c_{i\alpha}$  create and annihilate a fermion at site  $i$  with flavour  $\alpha$ , respectively, and  $n_{i\alpha} = c_{i\alpha}^\dagger c_{i\alpha}$ . Considering  $L/3$  fermions on a lattice of  $L$  sites (1/3-filling), the ground-state manifold has a degeneracy of  $3^L$  in the absence of hopping: each particle occupies a different site with an arbitrary flavour. Virtual hopping processes will induce an effective interaction between the flavour degrees of freedom, and to second order in  $t/U$ , the low-energy physics is captured by the SU(3) antiferromagnetic Heisenberg model with a coupling constant  $J = 2t^2/U$ :

$$H_{\text{eff}} = J \sum_{\langle i,j \rangle} P_{ij}, \quad (2.128)$$

where  $P_{ij}$  is the familiar transposition operator that exchanges the states of sites  $i$  and  $j$ , i. e.  $P_{ij}|\alpha_i\beta_j\rangle = |\beta_i\alpha_j\rangle$ . The effective model  $H_{\text{eff}}$  can be seen as a spin-one bilinear-biquadratic model at the antiferro SU(3) point  $\vartheta = \pi/4$ .



## Chapter 3

# Quadrupolar ordering on the triangular lattice in the presence of single-ion anisotropy

In recent years, considerable effort has been dedicated to the exploration of the phase diagram of the spin-one bilinear-biquadratic model on the triangular lattice. These extensive studies have been partly motivated by experimental investigations of the material  $\text{NiGa}_2\text{S}_4$  (see figure 3.1) that revealed anomalous low-temperature properties indicating the emergence of a spin-liquid state [37]. Extending the Heisenberg model with a phenomenological biquadratic term, Tsunetsugu and Arikawa have shown that several of these properties, in particular the absence of magnetic Bragg peaks, the finite value of the susceptibility at zero temperature and the characteristic  $T^2$ -behaviour of the specific heat, might be accounted for within the framework of antiferroquadrupolar ordering [38]. Läuchli, Mila and Penc mapped out the complete phase diagram of the model in a magnetic field: having compared the two emergent quadrupolar phases, they pointed out experimentally relevant properties that depended on the sign of the biquadratic coupling and they emphasized that the occurrence of ferroquadrupolar order in the material remained a possibility as well [5]. A parallel study by Bhattacharjee, Shenoy and Senthil highlighted the role of anisotropy in the context of distinguishing between the two different types of nematic order [39]. We should mention that the unambiguous identification of such elusive states of matter remains quite a challenge from the experimental point of view [40, 41, 42], and alternative theoretical attempts were also made to explain the measurements [43, 44], however, the recent finite-temperature results of Stoudenmire,

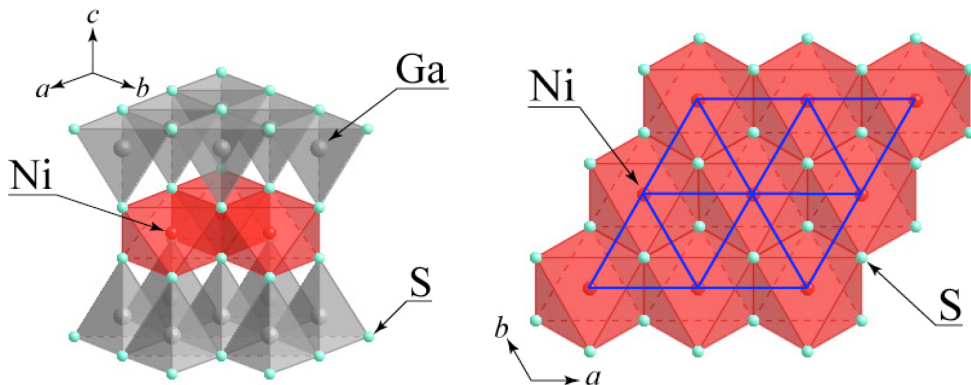


Figure 3.1: Crystal structure of  $\text{NiGa}_2\text{S}_4$ . The material is a Mott insulator featuring a highly two-dimensional structure with triangular layers of  $\text{NiS}_2$ . Magnetism is associated with the  $S = 1$  spin of the  $\text{Ni}^{2+}$  ions. The figures are taken from [37].

Trebst and Balents reasserted the possible relevance of quadrupolar physics to  $\text{NiGa}_2\text{S}_4$  [45].

In this chapter, we are aiming to enter the above discussion via a detailed study of the effect of single-ion anisotropy on quadrupolar phases. More specifically, we will consider spins one on a triangular lattice with nearest-neighbour bilinear-biquadratic interactions in the presence of a uniform anisotropy field:

$$H = J \sum_{\langle i,j \rangle} [\cos \vartheta \mathbf{S}_i \mathbf{S}_j + \sin \vartheta (\mathbf{S}_i \mathbf{S}_j)^2] + D \sum_i (S_i^z)^2. \quad (3.1)$$

We will perform a thorough investigation of the variational phase diagram of the model (3.1), employ flavour-wave theory to derive the excitation spectrum of the emergent quadrupolar phases, and carry out a perturbative analysis of the effect of quantum fluctuations in the limit of large (easy-plane or easy-axis) anisotropy. We will conclude the chapter by discussing our results in the context of  $\text{NiGa}_2\text{S}_4$ .

### 3.1 Phase diagram of the bilinear-biquadratic model with an anisotropy field

Let us calculate the ground-state phase diagram of the model (3.1) within the framework of the variational ansatz (2.103) that was introduced in the

previous chapter<sup>1</sup>. The following considerations reveal that one may assume three-sublattice order in the minimization of  $\langle \psi | H | \psi \rangle$ , i. e. the wavefunction (2.103) can be chosen to be of the form

$$\prod_{i \in \Lambda_A} |\psi_A(i)\rangle \prod_{i \in \Lambda_B} |\psi_B(i)\rangle \prod_{i \in \Lambda_C} |\psi_C(i)\rangle, \quad (3.2)$$

where  $\Lambda_j$  denotes the ensemble of sites belonging to sublattice  $j$ . Let us rewrite the Hamiltonian (3.1) as a sum of triangular plaquette terms:

$$H = \sum_{\alpha=1}^{2L} H_{\alpha}, \quad (3.3)$$

where  $L$  is the total number of sites. Denoting the spins of plaquette  $\alpha$  by  $\{\mathbf{S}_{i,\alpha}, i = 1, 2, 3\}$  and using the convention  $\mathbf{S}_{4,\alpha} \equiv \mathbf{S}_{1,\alpha}$ , we may write the plaquette Hamiltonian as

$$H_{\alpha} = \frac{J}{2} \sum_{i=1}^3 [\cos \vartheta \mathbf{S}_{i,\alpha} \mathbf{S}_{i+1,\alpha} + \sin \vartheta (\mathbf{S}_{i,\alpha} \mathbf{S}_{i+1,\alpha})^2] + \frac{D}{6} \sum_{i=1}^3 (S_{i,\alpha}^z)^2, \quad (3.4)$$

where the factors  $1/2$  and  $1/6$  account for the fact that every spin belongs to six different plaquettes and every bond has two neighbouring plaquettes. A priori, the plaquette energies may not be minimized independently from each other, and thus, denoting the ground-state energy of  $H_{\alpha}$  by  $E_{\alpha}$ , one may only state that  $2LE_{\alpha}$  is a lower bound of the ground-state energy of the total Hamiltonian. Nonetheless, there is an essentially unique way of constructing spin configurations that minimize all plaquette energies, and thus the energy of the total Hamiltonian as well. Indeed, let us select a plaquette of the triangular lattice and choose a configuration that minimizes its energy: this arrangement of spins can then be extended in an unambiguous way over the whole lattice, leading to a three-sublattice ordered state of the form (3.2) that minimizes  $\langle \psi | H | \psi \rangle$ . Choosing a plaquette configuration that does not minimize the energy of the selected plaquette, or deviating from the prescribed way of extending the plaquette solution over the whole lattice both lead to states of higher energy<sup>2</sup>. We may conclude therefore that it

<sup>1</sup>We will often refer to the resulting phase diagram as the mean-field or classical phase diagram.

<sup>2</sup>On the other hand, one may envisage a case where the plaquette solution is such that fixing two of the spins does not determine the third spin completely, thus there are several different ways of constructing ground states over the whole lattice, starting from a single plaquette. The triangular lattice Ising antiferromagnet could serve as an example of such a case.

is sufficient to minimize the energy of three spins on a triangle in order to minimize  $\langle \psi | H | \psi \rangle$ . The energy per site of a three-sublattice ordered state is given by

$$\varepsilon = \langle \psi_\Delta | H_\Delta | \psi_\Delta \rangle, \quad (3.5)$$

where

$$\begin{aligned} H_\Delta = & J \cos \vartheta [\mathbf{S}_1 \mathbf{S}_2 + \mathbf{S}_2 \mathbf{S}_3 + \mathbf{S}_3 \mathbf{S}_1] + \\ & + J \sin \vartheta [(\mathbf{S}_1 \mathbf{S}_2)^2 + (\mathbf{S}_2 \mathbf{S}_3)^2 + (\mathbf{S}_3 \mathbf{S}_1)^2] + \\ & + \frac{D}{3} [(S_1^z)^2 + (S_2^z)^2 + (S_3^z)^2] \end{aligned} \quad (3.6)$$

and

$$|\psi_\Delta\rangle = |\psi_1\rangle |\psi_2\rangle |\psi_3\rangle. \quad (3.7)$$

In some simple cases, the ground state may be found analytically, however, for a general set of parameters  $\{\vartheta, D/J\}$ , the minimization has to be carried out numerically<sup>3</sup>. In appendix A, we present the principal elements of a stability analysis that may complement these numerical investigations.

### 3.1.1 Isotropic case: $D = 0$

We should emphasize that familiarity with the variational solution for a single bilinear-biquadratic bond proves invaluable in the swift determination of the phase diagram of the model (3.1) in the isotropic case  $D = 0$ . In fact, with the help of the results of subsection 2.2.3, an interested reader may immediately deduce five-eighth of the complete phase diagram. However, since the present problem has already been investigated [38, 5], we prefer to skip a discussion on technicalities that are associated with exploring the ground-state manifold of the model, and state the final results straightaway instead. We find four distinct phases: an antiferroquadrupolar (AFQ) phase for  $\pi/4 < \vartheta < \pi/2$ , a ferromagnetic (FM) phase in the region  $\pi/2 < \vartheta < 5\pi/4$ , a ferroquadrupolar (FQ) phase in the interval  $5\pi/4 < \vartheta \leq \theta$ , and finally, an antiferromagnetic (AFM) phase in the parameter ranges  $\theta < \vartheta \leq 2\pi$  and  $0 \leq \vartheta < \pi/4$ , where we have denoted by  $\theta = 2\pi - \arctan 2 \approx 1.65\pi$  a second-order phase boundary between the FQ and AFM phases. A plot of the energy of a bond is shown as a function of  $\vartheta$  in figure 3.2. In the FM phase, the same coherent spin state is found on every site, while the FQ and AFQ phases feature pure quadrupolar

<sup>3</sup>We have optimized the Random Search method of Mathematica 5.2 for this task. In our experience, this method is far more efficient in finding global minima of  $\varepsilon$  than other built-in direct search methods of Mathematica such as Nelder-Mead, Differential Evolution or Simulated Annealing.

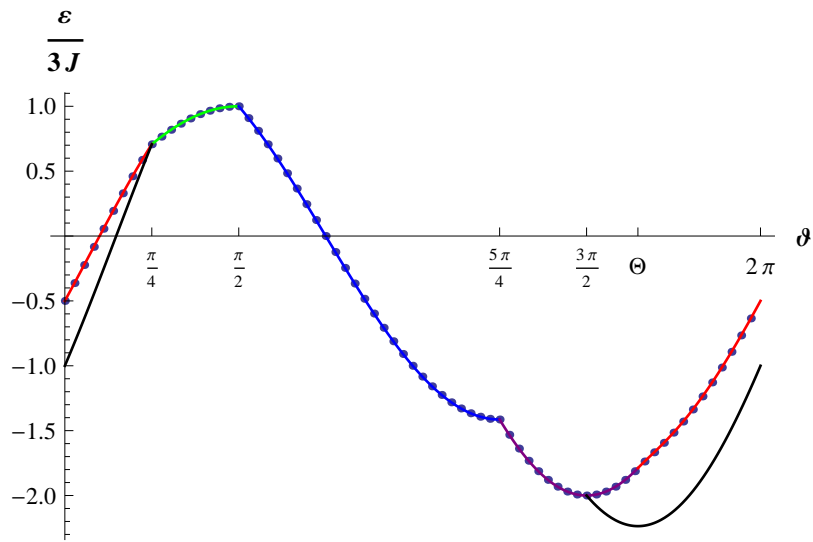


Figure 3.2: Energy of a bond in the three-sublattice ordered state on the triangular lattice. The dots are the results of a numerical minimization, while the curves come from conjecturing particular types of phases: AFM (red curve), AFQ (green curve), FM (blue curve) and FQ (purple curve). The point  $\theta \approx 1.65\pi$  denotes a second-order phase transition. The variational energy of an isolated spin-one bond is also shown for comparison (black curve) in the region where the bonds of the triangular lattice are frustrated.

states: in the earlier, the quadrupoles are identical, while in the latter, a three-sublattice order is formed via three different quadrupolar states with mutually perpendicular directors. None of the bonds are frustrated in the region  $\pi/4 \leq \vartheta \leq 3\pi/2$ , however, the shift in the boundary of the FQ phase to the  $\vartheta > 3\pi/2$  region is a manifest sign of frustration at work: eventually, the FQ phase becomes locally unstable at  $\vartheta = \theta$ , and the ensuing continuous transition gives rise to a peculiar AFM phase. This latter features three dipole moments of equal length forming 120-degree order: the directors of the three states are collinear for  $\vartheta < 0$ , they are undefined for  $\vartheta = 0$  as the spin vectors become fully developed, and they subtend an angle of 120 degrees with each other for  $\vartheta > 0$ . In order to provide a full description of the AFM phase, we introduce the single-site wavefunctions

$$\begin{aligned} |\psi_1\rangle &= \cos \eta |z\rangle - i \sin \eta |y\rangle, \\ |\psi_2\rangle &= \cos \eta |z\rangle + i \sin \eta \left( \frac{\sqrt{3}}{2} |x\rangle + \frac{1}{2} |y\rangle \right), \\ |\psi_3\rangle &= \cos \eta |z\rangle + i \sin \eta \left( -\frac{\sqrt{3}}{2} |x\rangle + \frac{1}{2} |y\rangle \right), \end{aligned} \quad (3.8)$$

where  $\eta \in ]0, \pi/2[$ . The set (3.8) corresponds to three spins in the  $xy$  plane with an angle of 120 degrees between each pair of them: the spin length is  $\sin(2\eta)$ , the quadrupolar exchange between any two states is given by  $\langle \mathbf{Q}_i \mathbf{Q}_j \rangle = \frac{4}{3} - 4 \sin^2 \eta + \frac{10}{4} \sin^4 \eta$ , and the directors of the three states are parallel to the  $z$  axis for  $\eta < \pi/4$ , whereas they form 120-degree order in the  $xy$  plane for  $\eta > \pi/4$ . A minimization of  $\varepsilon$  with respect to  $\eta$  gives

$$\begin{aligned} \sin^2 \eta &= \frac{3 \sin \vartheta + 6 \cos \vartheta}{\frac{3}{2} \sin \vartheta + 12 \cos \vartheta}, \\ \frac{\varepsilon}{J} &= 6 \sin \vartheta - \frac{(3 \sin \vartheta + 6 \cos \vartheta)^2}{3 \sin \vartheta + 24 \cos \vartheta}. \end{aligned} \quad (3.9)$$

We see that the expressions (3.9) are consistent with the properties of the AFM phase that we mentioned earlier. At the antiferro SU(3) point, we find  $\sin \eta = \sqrt{2/3}$ , which ensures the orthogonality of the set (3.8). In the  $\vartheta \rightarrow \theta$  limit, we recover a ferroquadrupolar state with directors parallel to the  $z$  axis. Finally, let us say a few words about the three phase boundaries that were not shifted by the presence of frustration. We should not feel surprised to find that both the ferro and the antiferro SU(3) points admit the configurations that are representative of the neighbouring phases, however, the same property holds for the  $\vartheta = \pi/2$  point, despite the fact that its

SU(3)-symmetric character is lost due to frustration. All three points possess a variety of variational solutions, and while this degeneracy is easily captured for the SU(3)-symmetric points<sup>4</sup>, it is quite difficult to characterize at the point  $\vartheta = \pi/2$ . Nonetheless, it is interesting to note that, as follows from our earlier discussion on interpolating states (see figure 2.8, for instance), a peculiar deformation of the antiferroquadrupolar arrangement is allowed both for  $\vartheta = \pi/2$  and  $\vartheta = \pi/4$ . Two of the quadrupoles may develop dipole moments along the director of the third quadrupole, while the directors of the three states remain mutually perpendicular: for  $\vartheta = \pi/2$ , the two dipole moments are identical, while for  $\vartheta = \pi/4$ , they add up to zero.

Before moving on to the case of finite anisotropy, let us give an overview of the effect of quantum fluctuations on the phase diagram of the isotropic model [5]. It is clear that the symmetry-breaking long-range ordered states that stem from the variational approach may only be stabilized in the thermodynamic limit, however, exact diagonalization of small clusters provides nonetheless a useful numerical insight into the physics of the quantum system. Different phases may be identified by calculating the correlation functions and by investigating the low-energy spectrum: should a long-range ordered state emerge in the thermodynamic limit, finite-size scaling will reveal its dominant correlations, furthermore, a particular set of eigenstates, the so-called Anderson tower, is expected to gradually collapse on the ground state upon an increase of the system size [46]. We should emphasize that the symmetry properties of the states that form the tower are intimately linked to those of the proposed long-range ordered state [47]. An introduction to the related concept of symmetry-breaking is given in [48], and the Anderson towers that were obtained for the present problem may be found in [18]. It turns out that the mean-field description of the phase diagram is basically correct on qualitative grounds, which is certainly an important motivating factor for the variational study of the model (3.1) in the  $D \neq 0$  case. However, quantum fluctuations give rise to a further shift in the boundary of the FQ phase towards the  $\vartheta = 0$  point, and this change is quite considerable, as the numerical analysis indicates  $\theta^{\text{ED}} \approx 1.9\pi$ . The proximity of this quantum phase transition to the Heisenberg point, together with the finding that long-range ferroquadrupolar order may coexist with short-range helical magnetic order, are among the principal arguments in support of the idea that the elusive properties of NiGa<sub>2</sub>S<sub>4</sub> may be attributed to the presence of strong ferroquadrupolar correlations in this material.

---

<sup>4</sup>For  $\vartheta = 5\pi/4$ , all sites feature the same state, whereas at the point  $\vartheta = \pi/4$ , the requirement is that the three states that are representative of the three sublattices form a basis in the Hilbert space of a spin one.

### 3.1.2 Easy-plane anisotropy field: $D > 0$

Let us begin by highlighting two observations that will prove particularly helpful in understanding the variational phase diagram of the model (3.1) in the  $D > 0$  case. Firstly, we should point out that the quantum-mechanical model possesses a unique ferroquadrupolar ground state with all directors aligned parallel to the  $z$  axis in the  $D/J \rightarrow \infty$  limit, and in the variational approach, one should recover this solution at a sufficiently large but finite  $D/J$  ratio for an arbitrary fixed value of  $\vartheta$ . We note that the variational energy of the configuration is  $\varepsilon/J = 6 \sin \vartheta$ . Secondly, all four phases that are present for the isotropic model feature a high level of degeneracy, therefore it is natural to expect that the behaviour of the system in the  $D/J \rightarrow 0$  limit will be governed by a lift of degeneracy that is associated with the symmetry-reducing character of the anisotropy field.

The phase diagram features six distinct phases, and it is shown in figure 3.3. The ferroquadrupolar phase mentioned earlier occupies the region  $5\pi/4 \leq \vartheta \leq \theta$  down to arbitrarily small values of the anisotropy field, however, lowering  $D$  for other values of  $\vartheta$  may give rise to three different phases via a second-order phase transition.

$\theta - 2\pi < \vartheta < \pi/4$  : Three-sublattice order emerges at  $D/J = 3 \sin \vartheta + 6 \cos \vartheta$ .

We enter a phase where we find three spin vectors of equal length in the  $xy$  plane with an angle of 120 degrees between them, and the three states feature coinciding directors that are parallel to the  $z$  axis. The phase is described by the wavefunctions (3.8), and a minimization with respect to  $\eta$  yields

$$\begin{aligned} \sin^2 \eta &= \frac{3 \sin \vartheta + 6 \cos \vartheta - \frac{D}{J}}{\frac{3}{2} \sin \vartheta + 12 \cos \vartheta}, \\ \frac{\varepsilon}{J} &= 6 \sin \vartheta - \frac{\left(3 \sin \vartheta + 6 \cos \vartheta - \frac{D}{J}\right)^2}{3 \sin \vartheta + 24 \cos \vartheta}. \end{aligned} \tag{3.10}$$

Decreasing  $D$  leads to an increase in the spin length, and if  $\vartheta > 0$ , we eventually end up with coherent spin states at  $D/J = 9 \sin \vartheta/4$  (dashed line in figure 3.3): below this value of the anisotropy, the parameter  $\eta$  in the wavefunctions (3.8) becomes greater than  $\pi/4$ , i. e. the directors show 120-degree order in the  $xy$  plane. In the  $D \rightarrow 0$  limit, we recover the AFM phase.

$\pi/4 < \vartheta \leq \arctan 4 \approx 0.4\pi$  : At  $D/J = 9 \sin \vartheta$ , the directors of the three sublattices open up to form an umbrella configuration, however, the states remain purely quadrupolar. The three directors have the same  $z$

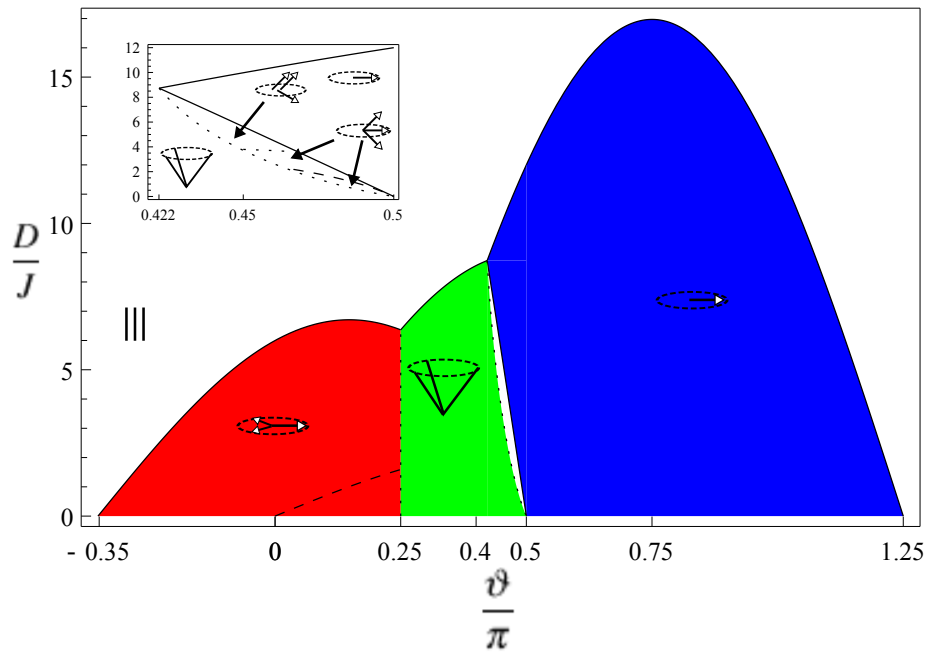


Figure 3.3: Variational phase diagram of the spin-one bilinear-biquadratic model with an easy-plane anisotropy field on the triangular lattice. Solid (dotted) lines denote second-order (first-order) phase boundaries. The arrows represent partially polarized magnetic moments: along the dashed lines, at least one of the spins is in a coherent spin state. Solid black lines represent quadrupolar directors. Inset: a magnified view of the phases with fan-like spin configurations.

component, and they subtend an angle of 120 degrees with each other in the  $xy$  plane. The phase is described by the wavefunctions

$$\begin{aligned} |\psi_1\rangle &= \cos \eta |z\rangle + \sin \eta |x\rangle, \\ |\psi_2\rangle &= \cos \eta |z\rangle + \sin \eta \left( -\frac{1}{2}|x\rangle + \frac{\sqrt{3}}{2}|y\rangle \right), \\ |\psi_3\rangle &= \cos \eta |z\rangle + \sin \eta \left( -\frac{1}{2}|x\rangle - \frac{\sqrt{3}}{2}|y\rangle \right), \end{aligned} \quad (3.11)$$

and a minimization with respect to  $\eta$  leads to

$$\begin{aligned} \sin^2 \eta &= \frac{9 \sin \vartheta - \frac{D}{J}}{\frac{27}{2} \sin \vartheta}, \\ \frac{\varepsilon}{J} &= 6 \sin \vartheta - \frac{(9 \sin \vartheta - \frac{D}{J})^2}{27 \sin \vartheta}. \end{aligned} \quad (3.12)$$

The overlap between the wavefunctions of nearest-neighbour sites is given by  $1 - 3 \sin^2 \eta/2$ , and it vanishes in the  $D \rightarrow 0$  limit, where we recover the usual AFQ phase.

$\arctan 4 < \vartheta < 5\pi/4$  : The quadrupoles start developing identical dipole moments in the  $xy$  plane at  $D/J = 12(\sin \vartheta - \cos \vartheta)$ , but the directors remain pinned to the  $z$  axis. The wavefunctions are given by

$$|\psi_1\rangle = |\psi_2\rangle = |\psi_3\rangle = \cos \eta |z\rangle - i \sin \eta |y\rangle, \quad (3.13)$$

and a minimization with respect to  $\eta$  yields

$$\begin{aligned} \sin^2 \eta &= \frac{12(\sin \vartheta - \cos \vartheta) - \frac{D}{J}}{24(\sin \vartheta - \cos \vartheta)}, \\ \frac{\varepsilon}{J} &= 6 \sin \vartheta - \frac{(12(\sin \vartheta - \cos \vartheta) - \frac{D}{J})^2}{48(\sin \vartheta - \cos \vartheta)}. \end{aligned} \quad (3.14)$$

Lowering the anisotropy leads to an increase in the spin length, and if  $\vartheta \geq \pi/2$ , we recover the FM phase with fully developed dipole moments in the  $D \rightarrow 0$  limit. However, if  $\vartheta < \pi/2$ , a second-order transition occurs at  $D = 36 \cos \vartheta$ , which will be discussed in detail further on.

The case of  $\vartheta = \pi/4$  is somewhat special, due to the remaining SU(2) symmetry of the model (3.1) along this line. The general variational solution can

be written in the form

$$\begin{aligned} |\psi_1\rangle &= \cos \eta |z\rangle + \sin \eta |i\rangle, \\ |\psi_2\rangle &= \cos \eta |z\rangle + \sin \eta |j\rangle, \\ |\psi_3\rangle &= \cos \eta |z\rangle + \sin \eta |k\rangle, \end{aligned} \quad (3.15)$$

where  $\eta \in ]0, \pi/2[$ , and the wavefunctions  $|i\rangle$ ,  $|j\rangle$  and  $|k\rangle$  are linear combinations of  $|x\rangle$  and  $|y\rangle$  that satisfy the constraint

$$\langle i|j\rangle = \langle j|k\rangle = \langle k|i\rangle = -\frac{1}{2}. \quad (3.16)$$

A minimization with respect to  $\eta$  results in the same expression as (3.12), and it is easily seen that the variational solution admits the configurations of the two phases that are separated from each other by the  $\vartheta = \pi/4$  line.

The inset of figure 3.3 reveals that the phase diagram is rather exotic in the  $\arctan 4 < \vartheta < \pi/2$  region. Here, an instability of the large- $D$  ferroquadrupolar phase gives rise to a phase with spontaneous magnetization in the  $xy$  plane, however, the directors remain parallel to the  $z$  axis and the ordering wavevector is still  $\mathbf{k} = 0$ . This phase is different in almost every aspect from the three-sublattice ordered quadrupolar umbrella phase that retains time-reversal invariance, and which is expected to be stable for  $D \ll J$ , however, a partial resolution of this discrepancy is achieved by a tilting of the directors from the  $z$  axis at  $D/J = 36 \cos \vartheta$ . The concomitant second-order transition leads to the appearance of two fan-like spin configurations: the arrangement of spins found for smaller (larger) values of  $\vartheta$  features a non-vanishing (vanishing) magnetization component along the  $z$  axis.

**$m_z \neq 0$  fan configuration :** Two sublattices feature identical wavefunctions, therefore two of the three spin vectors coincide with each other, however, the third spin vector is of different length and its  $z$  component is of opposite sign. All spins point in the same direction in the  $xy$  plane, and there is a net magnetization along the  $z$  axis in favour of the two coinciding spins. Furthermore, even though the directors are no longer parallel to the  $z$  axis, they still remain in a common plane with it. Setting the spin vectors in the  $yz$  plane with a positive  $y$  component, we may conveniently characterize this phase using the wavefunctions

$$\begin{aligned} |\psi_1\rangle &= i \cos \eta_1 |x\rangle + \sin \eta_1 (-\cos \varphi_1 |y\rangle + \sin \varphi_1 |z\rangle) = |\psi_2\rangle, \\ |\psi_3\rangle &= i \cos \eta_2 |x\rangle + \sin \eta_2 (-\cos \varphi_2 |y\rangle + \sin \varphi_2 |z\rangle), \end{aligned} \quad (3.17)$$

where  $\pi/4 < \eta_{1,2} < \pi/2$ , furthermore  $0 < \varphi_1 < \pi/2$  and  $\pi/2 < \varphi_2 < \pi$ . The value of these parameters may be obtained numerically as a

function of  $\{\vartheta, D/J\}$ . We note that the replacement  $\varphi_i \rightarrow \pi - \varphi_i$  in a variational ground state with magnetization  $(0, m_y, m_z)$  leads to another one with magnetization  $(0, m_y, -m_z)$ .

$m_z = 0$  **fan configuration** : Two of the spin vectors are reflections of each other with respect to the  $xy$  plane, while the third one is of different length and its  $z$  component is zero. All spin vectors point in the same direction in the  $xy$  plane, and all directors remain in a common plane with the  $z$  axis. This phase may be characterized with the help of the wavefunctions

$$\begin{aligned} |\psi_1\rangle &= i \cos \eta_1 |x\rangle + \sin \eta_1 (\cos \varphi |y\rangle + \sin \varphi |z\rangle), \\ |\psi_2\rangle &= i \cos \eta_1 |x\rangle + \sin \eta_1 (-\cos \varphi |y\rangle + \sin \varphi |z\rangle), \\ |\psi_3\rangle &= i \cos \eta_2 |x\rangle + \sin \eta_2 |z\rangle, \end{aligned} \quad (3.18)$$

where  $\pi/4 < \eta_{1,2} < \pi/2$  and  $0 < \varphi < \pi/2$ . For sufficiently large  $\vartheta$ , lowering the anisotropy leads eventually to  $\eta_2 \rightarrow \pi/4$ , i. e. the spin in the  $xy$  plane becomes fully polarized (this happens along the dashed line in the inset of figure 3.3). A further decrease in  $D/J$  pins the director of this spin to the  $xy$  plane, hence it becomes perpendicular to the director of the other two spins. This region is easily accessed by the above wavefunctions if we modify the domain of the parameter  $\eta_2$  to  $0 < \eta_2 < \pi/4$ .

The boundary between the two phases with fan-like spin configurations corresponds to a first-order transition, and both phases have a first-order boundary with the quadrupolar umbrella phase that is eventually stabilized for a sufficiently low anisotropy field. It is interesting to note that the quadrupolar umbrella phase is actually locally stable up to the value  $D/J = 9 \sin(2\vartheta)/(\sin \vartheta - 2 \cos \vartheta)$ , as one may confirm with the help of the stability analysis described in appendix A. However, since the energies defined in equations (3.12) and (3.14) cross below this value of the anisotropy field, we may conclude that a first-order transition shall indeed occur in the region  $0 < D/J < 9 \sin(2\vartheta)/(\sin \vartheta - 2 \cos \vartheta)$ . The location of this transition can be determined numerically.

### 3.1.3 Easy-axis anisotropy field: $D < 0$

This subsection discusses the phase diagram of the model (3.1) with  $D < 0$ . In contrast to the case of easy-plane anisotropy, the  $|D|/J \rightarrow \infty$  limit does not feature a unique ground state: in fact, any state is a ground state in which none of the sites have a  $|0\rangle$  component, we thus have a macroscopic

degeneracy of  $2^L$ , where  $L$  is the total number of sites. Therefore, as far as the variational approach is concerned, the minimization of the energy is simplified for “sufficiently large” anisotropy: this threshold value  $|D^*|/J$  depends on  $\vartheta$ , and it can be determined either numerically or with the help of simple analytic arguments, by looking for the disappearance of the local  $|0\rangle$  components. In the region of the FM phase for instance, i. e. for  $\vartheta \in ]\pi/2, 5\pi/4[$ , even an infinitesimal anisotropy field suffices to lift the continuous degeneracy, and we find a two-fold degenerate ferromagnetic state with all spins completely polarized along the (positive or negative)  $z$  axis. However, we should point out that the maximum value of  $|D^*|/J$ , reached for  $\vartheta = \arctan 4 \approx 0.4\pi$ , is about 4.37, therefore the region of the complete phase diagram where the anisotropy can not be considered “sufficiently large” is quite considerable nonetheless.

Let us first investigate the case  $|D| > |D^*|$ . Since the  $|0\rangle$  components vanish on every site, the single-site wavefunctions characterizing a three-sublattice ordered state assume the form

$$|\psi_i\rangle = e^{-i\varphi_i/2} \cos \frac{\vartheta_i}{2} |1\rangle + e^{i\varphi_i/2} \sin \frac{\vartheta_i}{2} |\bar{1}\rangle, \quad (3.19)$$

where  $\vartheta_i \in [0, \pi]$  and  $\varphi_i \in [0, 2\pi[$ . As a consequence, the  $x$  and  $y$  components of the spin vectors vanish, and  $\langle S_i^z \rangle = \cos \vartheta_i$ . The interaction terms in the Hamiltonian are simplified as follows:

$$\begin{aligned} \langle \mathbf{S}_i \mathbf{S}_j \rangle &= \cos \vartheta_i \cos \vartheta_j, \\ \langle P_{ij} \rangle &= |\langle \psi_i | \psi_j \rangle|^2 = \left| e^{i(\varphi_i - \varphi_j)/2} \cos \frac{\vartheta_i}{2} \cos \frac{\vartheta_j}{2} + e^{-i(\varphi_i - \varphi_j)/2} \sin \frac{\vartheta_i}{2} \sin \frac{\vartheta_j}{2} \right|^2. \end{aligned} \quad (3.20)$$

Let us now define an  $S = 1/2$  wavefunction  $|\psi'_i\rangle$  by carrying out the replacements  $|1\rangle \rightarrow |\uparrow\rangle$  and  $|\bar{1}\rangle \rightarrow |\downarrow\rangle$  in the wavefunction  $|\psi_i\rangle$ : this way, we have defined a pseudo-spin that points in the  $\{\vartheta_i, \varphi_i\}$  direction, i. e.

$$\begin{aligned} \langle \sigma_i^x \rangle &= \frac{1}{2} \sin \vartheta_i \cos \varphi_i, \\ \langle \sigma_i^y \rangle &= \frac{1}{2} \sin \vartheta_i \sin \varphi_i, \\ \langle \sigma_i^z \rangle &= \frac{1}{2} \cos \vartheta_i. \end{aligned} \quad (3.21)$$

Note that the term “pseudo” originates from the fact that  $|\psi'_i\rangle$  does not actually describe an angular momentum. While one may define  $SU(2)$  algebra in an arbitrary two-dimensional Hilbert space with the help of the Pauli matrices, a real spin one-half would reverse its components under time reversal.

In fact, it can be easily deduced from the equality  $\langle S_i^z \rangle = 2\langle \sigma_i^z \rangle$  that the  $xy$  components of the pseudo-spin represent the quadrupolar character of the original spin-one wavefunction, and indeed, time reversal will only reverse the  $z$  component of the pseudo-spin. It is furthermore straightforward to show that

$$\begin{aligned}\langle \mathbf{S}_i \mathbf{S}_j \rangle &= 4\langle \sigma_i^z \sigma_j^z \rangle, \\ \langle P_{ij} \rangle &= \langle p_{ij} \rangle,\end{aligned}\tag{3.22}$$

where  $p_{ij} = 2\vec{\sigma}_i \vec{\sigma}_j + 1/2$  is the transposition operator for the pseudo-spins. Since the anisotropy term is already minimized in the absence of  $|0\rangle$  components, the total energy per site is given by

$$\varepsilon = \langle \psi'_\Delta | H'_\Delta | \psi'_\Delta \rangle + \frac{9}{2} \sin \vartheta - |D|,\tag{3.23}$$

where

$$\begin{aligned}H'_\Delta &= J2 \sin \vartheta [\sigma_1^x \sigma_2^x + \sigma_1^y \sigma_2^y + \sigma_2^x \sigma_3^x + \sigma_2^y \sigma_3^y + \sigma_3^x \sigma_1^x + \sigma_3^y \sigma_1^y] + \\ &+ J(4 \cos \vartheta - 2 \sin \vartheta) [\sigma_1^z \sigma_2^z + \sigma_2^z \sigma_3^z + \sigma_3^z \sigma_1^z]\end{aligned}\tag{3.24}$$

and

$$|\psi'_\Delta\rangle = |\psi'_1\rangle |\psi'_2\rangle |\psi'_3\rangle.\tag{3.25}$$

We may conclude that within the framework of the variational approach, the spin-one bilinear-biquadratic model with a sufficiently large easy-axis anisotropy presents an identical problem to that of the  $S = 1/2$  XXZ model. Moreover, one may notice that the variational treatment of this latter effectively leads us to solve the classical XXZ model, since, neglecting an overall phase factor, spin-one-half wavefunctions are in one-to-one correspondence with coherent spin states. Amusingly enough, the ground states of the classical XXZ model on the triangular lattice may be obtained via analytical means: for a complete solution, we refer the reader to appendix B, here we will restrict ourselves to interpreting the results. With respect to the original spin-one system, we find two pure quadrupolar phases featuring directors in the  $xy$  plane: the directors are parallel in the region  $5\pi/4 < \vartheta \leq \theta$ , while they form 120-degree order for  $\pi/4 < \vartheta < \arctan 4 \approx 0.4\pi$ . A ferromagnetic state is realized with fully developed spins (local  $|1\rangle$  or  $|\bar{1}\rangle$  wavefunctions) in the region  $\arctan 4 < \vartheta < 5\pi/4$ , while a non-trivial one-parameter continuous degeneracy is found in the ground-state manifold for  $\theta < \vartheta < 2\pi$  and  $0 < \vartheta < \pi/4$ . The point  $\vartheta = \arctan 4$  also features a peculiar degeneracy: with the help of a freely-varying continuous parameter, we may interpolate between a ferromagnetic configuration of coherent spin states and a quadrupolar state with a 120-degree ordering of the directors in the  $xy$  plane. At

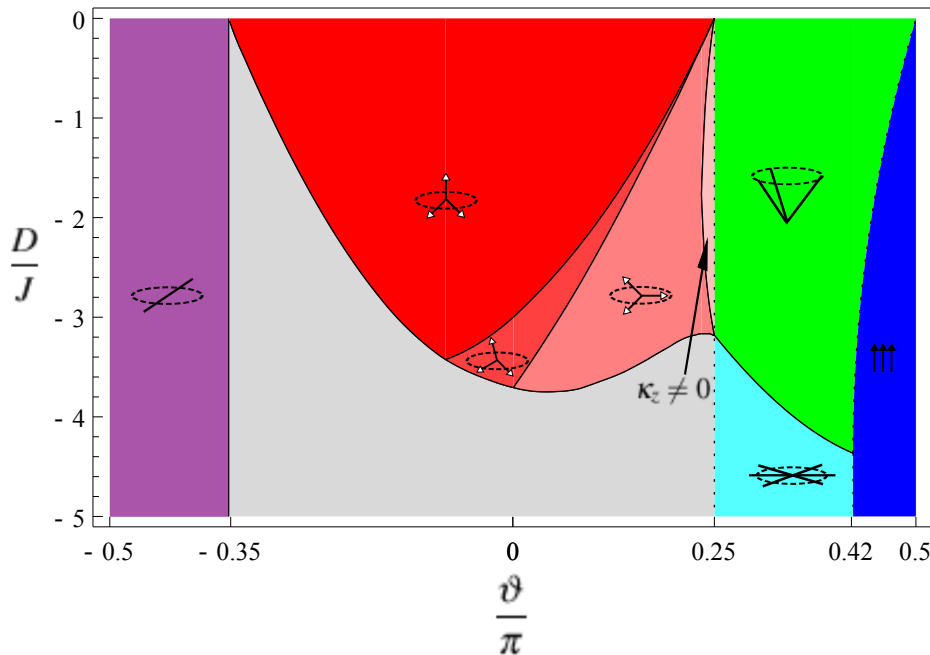


Figure 3.4: Variational phase diagram of the spin-one bilinear-biquadratic model with an easy-axis anisotropy field on the triangular lattice. Solid (dotted) lines denote second-order (first-order) phase boundaries. Filled (empty) arrows represent completely (partially) polarized magnetic moments. Solid black lines represent quadrupolar directors. The phase with a non-trivial degeneracy is shown in gray colour. Note the presence of a tiny antiferromagnetic phase where the common plane of the spins does not contain the easy axis.

the  $\vartheta = 0$  point, two sites of any given triangular plaquette will be fixed in a  $1\bar{1}$  configuration, however, the wavefunction of the third site is arbitrary, hence we encounter a macroscopic degeneracy in the ground-state manifold. Finally, for  $\vartheta = \pi/4$  ( $\vartheta = 5\pi/4$ ), the pseudo-spin model is isotropic<sup>5</sup>, therefore we find  $|\langle\psi_i|\psi_j\rangle| = 1/2$  ( $|\langle\psi_i|\psi_j\rangle| = 1$ ) for any pair of nearest-neighbour sites.

The preceding discussion might have lead us to expect a particularly rich phase diagram in the region  $\theta - 2\pi < \vartheta < \pi/4$ , and figure 3.4 confirms this notion indeed. However, let us first explore the case of an arbitrary anisotropy field in the region  $\pi/4 \leq \vartheta \leq \theta$ . It turns out that the threshold value  $|D^*|/J$  vanishes for  $\pi/2 \leq \vartheta \leq \theta$ , therefore the results presented in

<sup>5</sup>The remaining  $SU(2)$  symmetry that was uncovered in subsection 2.2.1 manifests itself at these points.

the previous paragraph are directly applicable to the complete range of  $D$  in this interval. On the other hand, simple considerations reveal that for  $\pi/4 < \theta < \pi/2$ , a quadrupolar umbrella configuration should be stabilized in the  $|D|/J \ll 1$  limit: this phase may be seen as a continuation of the one that we encountered in the case of easy-plane anisotropy, and an increasing easy-axis anisotropy field will have the same qualitative effect of opening up the umbrella, as a decreasing easy-plane anisotropy field had. If  $\vartheta \leq \arctan 4$ , the directors are eventually pinned to the  $xy$  plane at  $D/J = -9 \sin \vartheta/2$ , as one may check with the help of (3.12), however, the completion of this smooth process is prevented for  $\vartheta > \arctan 4$  by a first-order transition to the ferromagnetic phase: the corresponding boundary,  $D/J = -9 \sin \vartheta/2 + \sqrt{81 \sin \vartheta (\sin \vartheta - 4 \cos \vartheta)}/2$ , may be obtained by comparing the energy of the two phases. Finally, let us add that the quadrupolar umbrella configuration is admitted along the line  $\vartheta = \pi/4$ , where the general variational solution is a continuation of the one found in the case of easy-plane anisotropy.

A closer look at figure 3.4 reveals that there are four antiferromagnetic phases in the region  $|D| < |D^*|$ . As  $\vartheta$  is increased in the interval  $]\theta - 2\pi, \pi/4[$ , these phases emerge one-by-one via a series of second-order phase transitions, we will therefore find it convenient to describe them in order of their appearance. In these antiferromagnetic phases, the spin vectors are in general only partially polarized, furthermore the single-site wavefunctions representing three-sublattice order are rather complicated, therefore we will restrict our analysis to the arrangement of dipole moments. We should emphasize however that in our calculations, we have only encountered degeneracies that were associated with trivial symmetries of the model (3.1), such as the symmetry of rotation around the  $z$  axis, reflection symmetry with respect to the  $xy$  plane, or the symmetry of permutation with respect to the three sublattices. In other words, we have found a well-defined and essentially unique configuration of the spin vectors for an arbitrary set of parameters  $\{\vartheta, D/J\}$  in this domain of the phase diagram. In the first phase, two of the spin vectors are reflections of each other with respect to the  $z$  axis, while the third spin vector is of different length, its  $z$  component is of opposite sign, and it is parallel to the  $z$  axis. This configuration gives rise to a spontaneous magnetization component along the  $z$  axis. At the boundary of the second phase, the third spin tilts away from the  $z$  axis, and the first two spins cease to be mirror spins (their length also starts to differ), which leads to the appearance of a net magnetization component in the  $xy$  plane as well. We should point out however that the three spins remain in a common plane with the  $z$  axis. Entering the third phase, we find the same configuration as in the first phase, except that this time, the role of the  $z$  axis is played by an arbitrary axis in the  $xy$  plane. The  $z$  component of the total magnetization vanishes in

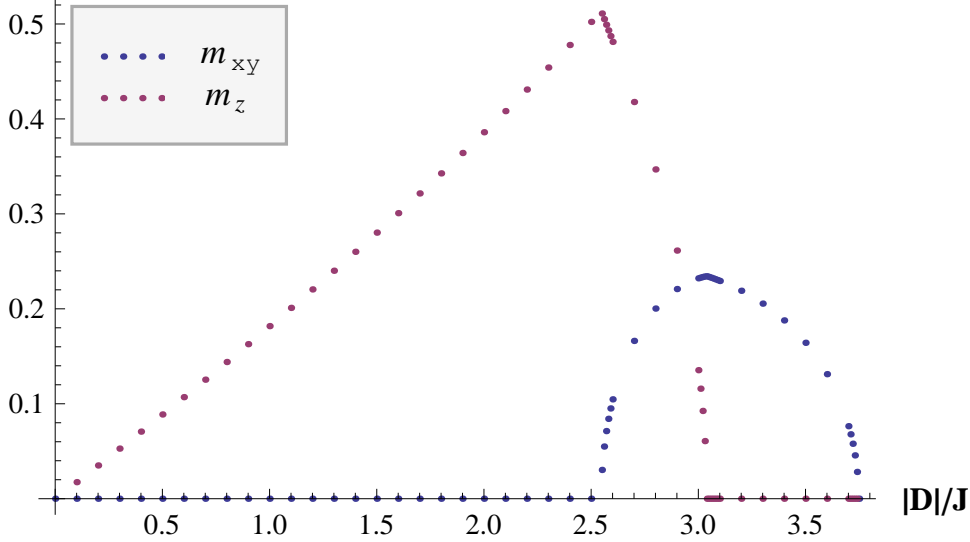


Figure 3.5: Magnetization components of a triangular plaquette for  $\vartheta = \pi/18$ . One may observe three second-order phase transitions driven by an increasing easy-axis anisotropy field. The final transition marks the beginning of the phase with a non-trivial degeneracy.

this phase, due to the fact that one of the spins is in the  $xy$  plane, while the other two spins are reflections of each other with respect to it. Finally, upon rotating this configuration around the spin vector that is pinned to the  $xy$  plane, we obtain the arrangement of dipole moments that is characteristic of the fourth antiferromagnetic phase. The three spin vectors remain in a common plane which no longer contains the  $z$  axis, and as a result, the spin chirality vector

$$\kappa = \frac{2}{3\sqrt{3}} (\mathbf{S}_1 \times \mathbf{S}_2 + \mathbf{S}_2 \times \mathbf{S}_3 + \mathbf{S}_3 \times \mathbf{S}_1) \quad (3.26)$$

will have a non-vanishing  $z$  component. In conclusion, if we take a triangular plaquette and calculate its magnetization components perpendicular and parallel to the easy axis, furthermore its chirality component parallel to the easy axis, we may consider the resulting quantities  $m_{xy}$ ,  $m_z$  and  $\kappa_z$  as the order parameters of the three phase transitions that occur in the  $\vartheta$ -interval  $]\theta - 2\pi, \pi/4[$  for  $|D| < |D^*|$ . A plot of these order parameters is shown as a function of the anisotropy field for two representative values of  $\vartheta$  in figures 3.5 and 3.6. It is particularly interesting to observe the reentrant behaviour that the phase transition between the third and the fourth antiferromagnetic phases exhibits along the lines of constant  $\vartheta$ .

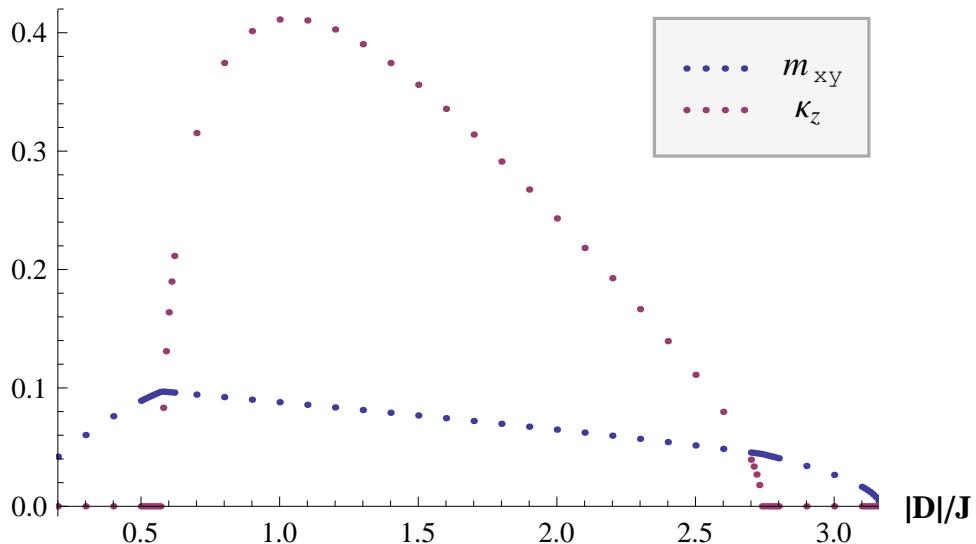


Figure 3.6: Magnetization and spin chirality of a triangular plaquette for  $\vartheta = 29\pi/120 \approx 0.24\pi$ . The magnetization (chirality) component shown is perpendicular (parallel) to the easy axis. Upon an increase of the anisotropy field, we find an intermediate phase with  $\kappa_z \neq 0$ .

### 3.2 Excitation spectrum of quadrupolar phases

We have previously mapped out the variational phase diagram of the spin-one bilinear-biquadratic model with a single-ion anisotropy field on the triangular lattice. In this section, we shall study the excitation spectrum of the quadrupolar phases that appear in the phase diagram, via the use of flavour-wave theory. This method relies on the SU(3)-bosonic representation of  $S = 1$  spins that was introduced in subsection 2.1.1: the local spin operators can be written as

$$\mathbf{S}_i = \begin{pmatrix} S_i^x \\ S_i^y \\ S_i^z \end{pmatrix} = \begin{pmatrix} i(a_z^\dagger a_y - a_y^\dagger a_z) \\ i(a_x^\dagger a_z - a_z^\dagger a_x) \\ i(a_y^\dagger a_x - a_x^\dagger a_y) \end{pmatrix}, \quad (3.27)$$

while the transposition operator becomes

$$P_{ij} = \sum_{\mu, \nu=x,y,z} a_\mu^\dagger a_\nu b_\nu^\dagger b_\mu. \quad (3.28)$$

The local bosonic operators  $\{a_x, a_y, a_z\}$  and  $\{b_x, b_y, b_z\}$  correspond to the time-reversal-invariant basis states

$$\begin{aligned} |x\rangle &= \frac{i}{\sqrt{2}} (|1\rangle - |\bar{1}\rangle), \\ |y\rangle &= \frac{1}{\sqrt{2}} (|1\rangle + |\bar{1}\rangle), \\ |z\rangle &= -i|0\rangle \end{aligned} \quad (3.29)$$

on sites  $i$  and  $j$ , respectively. The initial form of our Hamiltonian will be the following:

$$H = J \sum_{\langle i,j \rangle} \{(\cos \vartheta - \sin \vartheta) \mathbf{S}_i \mathbf{S}_j + \sin \vartheta (1 + P_{ij})\} + D \sum_i (S_i^z)^2. \quad (3.30)$$

### 3.2.1 Ferroquadrupolar phase

Let us first investigate the case of easy-plane anisotropy. We consider quantum fluctuations around the variational ground state by generalizing the local SU(3)-bosonic representation to an arbitrary “triangular” one, in which the total number of bosons is  $M$  on every site<sup>6</sup>. This local constraint may be eliminated [19]: for each site  $i$ , we carry out the replacements

$$a_z, a_z^\dagger \longrightarrow \sqrt{M - a_x^\dagger a_x - a_y^\dagger a_y}, \quad (3.31)$$

and thus we end up with two independent bosonic operators per site<sup>7</sup>. The classical (variational) limit corresponds to a condensation of the replaced bosons, and thus quantum fluctuations are taken into account via a  $1/M$ -expansion:

$$\sqrt{M - a_x^\dagger a_x - a_y^\dagger a_y} = \sqrt{M} - \frac{(a_x^\dagger a_x + a_y^\dagger a_y)}{2\sqrt{M}} + O\left(\frac{1}{\sqrt{M^3}}\right). \quad (3.32)$$

An expansion of order  $M$  of the interaction terms between site  $i$  and  $j$  leads to

$$\begin{aligned} \mathbf{S}_i \mathbf{S}_j &= M (a_x^\dagger b_x + a_x b_x^\dagger - a_x^\dagger b_x^\dagger - a_x b_x) + \\ &+ M (a_y^\dagger b_y + a_y b_y^\dagger - a_y^\dagger b_y^\dagger - a_y b_y) + O(1) \end{aligned} \quad (3.33)$$

<sup>6</sup>The original system may be recovered by setting  $M = 1$ .

<sup>7</sup>One may check that the replacements leave the local SU(3) commutation relations intact.

and

$$P_{ij} = M^2 - M (a_x^\dagger a_x + a_y^\dagger a_y + b_x^\dagger b_x + b_y^\dagger b_y) + \\ + M (a_x^\dagger b_x + a_y^\dagger b_y + a_x b_x^\dagger + a_y b_y^\dagger) + O(1). \quad (3.34)$$

As far as the anisotropy term is concerned, we might be tempted to simply take the expansion of  $S_i^z$  and multiply it by itself. However, since the expression of  $S_i^z$  does not contain the boson  $a_z$ , we end up with a quartic operator of order 1: neglecting this operator would correspond to neglecting the effect of anisotropy, while multiplying it by  $M$  for instance would force us to treat it using approximative methods. As a matter of fact, we would also encounter a difficulty if the  $a_x$  boson were condensed instead of  $a_z$ : in that case, we would find a quadratic term of order  $M$ , however, we would not recover the constant of order  $M^2$  that should appear in the classical energy. The situation can be remedied by noting that the SU(3)-bosonic representation makes it possible to express any on-site operator as a quadratic form. We first rewrite the anisotropy term using the definitions (2.8) that are valid for spins one:

$$(S_i^z)^2 = \frac{1}{3} \left( \sqrt{3} Q_i^{3z^2-r^2} + 2 \right). \quad (3.35)$$

The bosonic representation of  $Q_i^{3z^2-r^2}$  is given in (2.27):

$$Q_i^{3z^2-r^2} = \frac{1}{\sqrt{3}} (3a_x^\dagger a_x + 3a_y^\dagger a_y - 2), \quad (3.36)$$

and so we finally end up with

$$(S_i^z)^2 = a_x^\dagger a_x + a_y^\dagger a_y. \quad (3.37)$$

Note that the anisotropy term is an on-site term, therefore it has to be multiplied by  $M$  in the spirit of the flavour-wave expansion: as a result, it will have the same order of magnitude as the interaction terms that appear in the Hamiltonian (3.30). All in all, in order  $M^2$  we recover the classical interaction energy, and in order  $M$  we find a Hamiltonian that is quadratic in the bosonic operators. We may introduce propagating states over the whole lattice via a Fourier transformation of the form

$$a_{\mu i} = \sqrt{\frac{1}{L}} \sum_{\mathbf{k} \in BZ} e^{i\mathbf{k} \cdot \mathbf{R}_i} a_{\mu}(\mathbf{k}), \\ a_{\mu i}^\dagger = \sqrt{\frac{1}{L}} \sum_{\mathbf{k} \in BZ} e^{-i\mathbf{k} \cdot \mathbf{R}_i} a_{\mu}^\dagger(\mathbf{k}), \quad (3.38)$$

where  $L$  denotes the total number of sites of the triangular lattice, and the sum extends over all  $\mathbf{k}$  vectors in the Brillouin zone. Summing up all interaction terms leads to

$$\begin{aligned} & \sum_i (\mathbf{S}_{\mathbf{R}_i} \mathbf{S}_{\mathbf{R}_i - \mathbf{a}_1} + \mathbf{S}_{\mathbf{R}_i} \mathbf{S}_{\mathbf{R}_i - \mathbf{a}_2} + \mathbf{S}_{\mathbf{R}_i} \mathbf{S}_{\mathbf{R}_i + \mathbf{a}_1 + \mathbf{a}_2}) = \\ & = 3M \sum_{\mu=x,y} \sum_{\mathbf{k}} \{ (\gamma(\mathbf{k}) + \gamma(\mathbf{k})^*) a_{\mu}^{\dagger}(\mathbf{k}) a_{\mu}(\mathbf{k}) - \\ & \quad - \gamma(\mathbf{k}) a_{\mu}^{\dagger}(\mathbf{k}) a_{\mu}^{\dagger}(-\mathbf{k}) - \gamma(\mathbf{k})^* a_{\mu}(\mathbf{k}) a_{\mu}(-\mathbf{k}) \} \end{aligned} \quad (3.39)$$

and

$$\begin{aligned} & \sum_i (P_{\mathbf{R}_i \mathbf{R}_i - \mathbf{a}_1} + P_{\mathbf{R}_i \mathbf{R}_i - \mathbf{a}_2} + P_{\mathbf{R}_i \mathbf{R}_i + \mathbf{a}_1 + \mathbf{a}_2}) = \\ & = 3M \sum_{\mu=x,y} \sum_{\mathbf{k}} (\gamma(\mathbf{k}) + \gamma(\mathbf{k})^* - 2) a_{\mu}^{\dagger}(\mathbf{k}) a_{\mu}(\mathbf{k}), \end{aligned} \quad (3.40)$$

while the anisotropy term yields

$$\sum_i (S_i^z)^2 = \sum_{\mu=x,y} \sum_{\mathbf{k}} a_{\mu}^{\dagger}(\mathbf{k}) a_{\mu}(\mathbf{k}), \quad (3.41)$$

where  $\mathbf{a}_1 = a\mathbf{e}_x$  and  $\mathbf{a}_2 = -a\mathbf{e}_x/2 + a\mathbf{e}_y\sqrt{3}/2$  are elementary lattice vectors of the triangular lattice, furthermore  $\gamma(\mathbf{k}) = (e^{-i\mathbf{k}\cdot\mathbf{a}_1} + e^{-i\mathbf{k}\cdot\mathbf{a}_2} + e^{i\mathbf{k}\cdot(\mathbf{a}_1+\mathbf{a}_2)})/3$ . Denoting the Hamiltonian of order  $M$  by  $H^{(2)}$ , we may finally write

$$\begin{aligned} & \frac{H^{(2)}}{6JM} = \\ & = \sum_{\mu=x,y} \sum_{\mathbf{k}} \left\{ \left( \cos \vartheta \frac{\gamma(\mathbf{k}) + \gamma(\mathbf{k})^*}{2} - \sin \vartheta + \frac{D}{6J} \right) a_{\mu}^{\dagger}(\mathbf{k}) a_{\mu}(\mathbf{k}) - \right. \\ & \quad \left. - (\cos \vartheta - \sin \vartheta) \left( \frac{\gamma(\mathbf{k})}{2} a_{\mu}^{\dagger}(\mathbf{k}) a_{\mu}^{\dagger}(-\mathbf{k}) + \frac{\gamma(\mathbf{k})^*}{2} a_{\mu}(\mathbf{k}) a_{\mu}(-\mathbf{k}) \right) \right\}. \end{aligned} \quad (3.42)$$

The  $x$  and  $y$  bosons are decoupled from each other and they behave identically, which leads to a two-fold degeneracy of the spectrum of excitations. For sufficiently high  $D/J$ , the Hamiltonian  $H^{(2)}$  can be diagonalized via a Bogoliubov transformation:

$$\begin{aligned} \frac{H^{(2)}}{6JM} & = \sum_{\mu=x,y} \sum_{\mathbf{k}} \omega(\mathbf{k}) \alpha_{\mu}^{\dagger}(\mathbf{k}) \alpha_{\mu}(\mathbf{k}) + \\ & \quad + \frac{1}{2} \sum_{\mu=x,y} \sum_{\mathbf{k}} (\omega(\mathbf{k}) - (\cos \vartheta \gamma(\mathbf{k})' - \sin \vartheta + d)), \end{aligned} \quad (3.43)$$

where we have introduced the variables  $d = D/6J$  and  $\gamma(\mathbf{k})' = (\gamma(\mathbf{k}) + \gamma(\mathbf{k})^*)/2$ , and the dispersion is given by

$$\omega(\mathbf{k}) = \sqrt{(d + \cos \vartheta \gamma(\mathbf{k})' - \sin \vartheta)^2 - (\cos \vartheta - \sin \vartheta)^2 \gamma(\mathbf{k})'^2}. \quad (3.44)$$

Lowering the anisotropy field leads eventually to the closing of the gap, and one may show that for arbitrary  $\vartheta$ , this occurs either at  $\mathbf{k} = 0$  or at the corners of the Brillouin zone. A three-sublattice instability emerges at  $D/J = 6 \cos \vartheta + 3 \sin \vartheta$  for  $2\pi - \theta < \vartheta \leq \pi/4$ , furthermore at  $D/J = 9 \sin \vartheta$  for  $\pi/4 \leq \vartheta \leq \arctan 4$ , whereas the gap closes at  $\mathbf{k} = 0$  along the line  $D/J = 12(\sin \vartheta - \cos \vartheta)$  for  $\arctan 4 \leq \vartheta < 5\pi/4$ . On the other hand, no instability is found for a finite anisotropy field in the region  $5\pi/4 \leq \vartheta \leq \theta$ , and taking the  $d \rightarrow 0$  limit, we recover<sup>8</sup> the excitation spectrum that is characteristic of the isotropic model [5]. The phase boundaries indicated by the flavour-wave method are in perfect agreement with the variational calculus<sup>9</sup>. Figure 3.7 shows the closing of the gap for  $\vartheta = \arctan 4$ .

If the single-ion anisotropy field is of easy-axis type, ferroquadrupolar order is locally stable in the region  $5\pi/4 \leq \vartheta \leq \theta$  for an arbitrary  $D/J$ . While this phase is conceptually different from the gapped ferroquadrupolar phase discussed above, its excitation spectrum may be derived quite easily with the help of the results of the previous paragraph. Assuming that the directors are aligned parallel to the  $x$  axis, we may convince ourselves that a  $1/M$ -expansion of the interaction terms is obtained by replacing the index  $x$  with  $z$  in the expressions (3.33) and (3.34). However, the anisotropy term is more subtle: multiplying

$$(S_i^z)^2 = M - a_z^\dagger a_z \quad (3.45)$$

by  $M$ , we recover a classical on-site energy term of order  $M^2$ , and we may deduce furthermore that the dispersion of  $z$ -type bosons will acquire a gap.

<sup>8</sup>We should mention that the dispersion obtained in [5] actually corresponds to  $\omega(\mathbf{k})/2$ . We believe that this slight discrepancy is due to a misprint.

<sup>9</sup>This is essentially due to the fact that we may associate the corresponding second-order phase transitions with the closing of the gap, i. e. the appearance of zero modes in the spectrum. Whenever the flavour-wave expansion yields a zero mode for a wavevector, a “classical” flavour-wave expansion, in which the bosonic operators are replaced with complex numbers, will also feature a zero mode for the same wavevector. Finally, this latter method can not indicate a second-order instability on the triangular lattice that the stability analysis of appendix A would not detect.

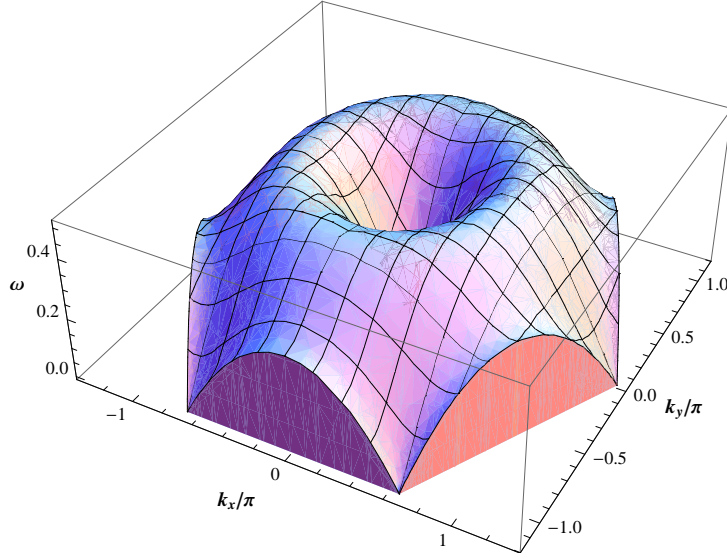


Figure 3.7: Closing of the gap of the ferroquadrupolar phase for  $\vartheta = \arctan 4 \approx 0.4\pi$ . The two-fold degenerate branch of excitations softens simultaneously at  $\mathbf{k} = 0$  and at the corners of the Brillouin zone. The lattice constant is chosen as unity.

The Hamiltonian of order  $M$  becomes

$$\begin{aligned}
\frac{H^{(2)}}{6JM} &= \\
&= \sum_{\mathbf{k}} \left\{ \left( \cos \vartheta \frac{\gamma(\mathbf{k}) + \gamma(\mathbf{k})^*}{2} - \sin \vartheta \right) a_y^\dagger(\mathbf{k}) a_y(\mathbf{k}) - \right. \\
&\quad \left. - (\cos \vartheta - \sin \vartheta) \left( \frac{\gamma(\mathbf{k})}{2} a_y^\dagger(\mathbf{k}) a_y^\dagger(-\mathbf{k}) + \frac{\gamma(\mathbf{k})^*}{2} a_y(\mathbf{k}) a_y(-\mathbf{k}) \right) \right\} + \\
&+ \sum_{\mathbf{k}} \left\{ \left( \cos \vartheta \frac{\gamma(\mathbf{k}) + \gamma(\mathbf{k})^*}{2} - \sin \vartheta - \frac{D}{6J} \right) a_z^\dagger(\mathbf{k}) a_z(\mathbf{k}) - \right. \\
&\quad \left. - (\cos \vartheta - \sin \vartheta) \left( \frac{\gamma(\mathbf{k})}{2} a_z^\dagger(\mathbf{k}) a_z^\dagger(-\mathbf{k}) + \frac{\gamma(\mathbf{k})^*}{2} a_z(\mathbf{k}) a_z(-\mathbf{k}) \right) \right\}, \tag{3.46}
\end{aligned}$$

and following a Bogoliubov transformation, we end up with

$$\begin{aligned}
\frac{H^{(2)}}{6JM} &= \sum_{\mathbf{k}} \{ \omega_y(\mathbf{k}) \alpha_y^\dagger(\mathbf{k}) \alpha_y(\mathbf{k}) + \omega_z(\mathbf{k}) \alpha_z^\dagger(\mathbf{k}) \alpha_z(\mathbf{k}) \} + \\
&+ \frac{1}{2} \sum_{\mathbf{k}} (\omega_y(\mathbf{k}) + \omega_z(\mathbf{k}) - 2(\cos \vartheta \gamma(\mathbf{k})' - \sin \vartheta) - |d|), \tag{3.47}
\end{aligned}$$

where  $d$  and  $\gamma(\mathbf{k})'$  are the familiar variables, and the dispersions are given by

$$\begin{aligned}\omega_y(\mathbf{k}) &= \sqrt{(\cos \vartheta \gamma(\mathbf{k})' - \sin \vartheta)^2 - (\cos \vartheta - \sin \vartheta)^2 \gamma(\mathbf{k})'^2}, \\ \omega_z(\mathbf{k}) &= \sqrt{(|d| + \cos \vartheta \gamma(\mathbf{k})' - \sin \vartheta)^2 - (\cos \vartheta - \sin \vartheta)^2 \gamma(\mathbf{k})'^2}.\end{aligned}\quad (3.48)$$

The  $\omega_y$  branch retains a gapless mode at  $\mathbf{k} = 0$ , which is the Goldstone-mode associated with the broken U(1) symmetry. Approaching  $\vartheta = \theta$ , a three-sublattice instability is indicated by a softening of the  $\omega_y$  dispersion at the corners of the Brillouin zone, in accordance with the variational results. We note that the zero-point energy vanishes for  $\vartheta = 5\pi/4$ , where the ferroquadrupolar state becomes an exact eigenstate of the Hamiltonian.

### 3.2.2 Quadrupolar umbrella phase

The umbrella phase is actually a helical phase: we may assume for instance that on site  $\mathbf{R}_i$  we have the wavefunction

$$|\psi_i\rangle = \cos \eta |z\rangle + \sin \eta (\cos \varphi_i |x\rangle + \sin \varphi_i |y\rangle), \quad (3.49)$$

and the distribution of the angles  $\varphi_i$  over the lattice satisfies  $\varphi_j - \varphi_i = 2\pi/3$  if  $\mathbf{R}_j - \mathbf{R}_i = \{-\mathbf{a}_1, -\mathbf{a}_2, \mathbf{a}_1 + \mathbf{a}_2\}$ . The angle  $\eta$  and the classical energy are given in (3.12), as a function of  $\vartheta$  and  $D/J$ . In order to derive a flavour-wave expansion around a classical ground state, we may introduce a local SU(3) rotation of the form

$$\begin{pmatrix} a_{1i} \\ a_{2i} \\ a_{3i} \end{pmatrix} = U_i^\dagger \begin{pmatrix} a_{xi} \\ a_{yi} \\ a_{zi} \end{pmatrix} \quad (3.50)$$

in such a way that the classical limit will correspond to a condensation of  $a_{1i}$ : in the present case, it is convenient to choose the rotation matrix as

$$U_i^\dagger = \begin{pmatrix} \sin \eta \cos \varphi_i & \sin \eta \sin \varphi_i & \cos \eta \\ \cos \eta \cos \varphi_i & \cos \eta \sin \varphi_i & -\sin \eta \\ -\sin \varphi_i & \cos \varphi_i & 0 \end{pmatrix}. \quad (3.51)$$

We may now express the local spin operators as

$$S^{\alpha i} = (a_{1i}^\dagger \quad a_{2i}^\dagger \quad a_{3i}^\dagger) s^{\alpha i} \begin{pmatrix} a_{1i} \\ a_{2i} \\ a_{3i} \end{pmatrix}, \quad \alpha = x, y, z, \quad (3.52)$$

with the help of the definition  $s^{\alpha i} = U_i^\dagger \lambda^\alpha U_i$ , where  $\lambda^x = \begin{pmatrix} 0 & 0 & 0 \\ 0 & 0 & -i \\ 0 & i & 0 \end{pmatrix}$ ,  $\lambda^y = \begin{pmatrix} 0 & 0 & i \\ 0 & 0 & 0 \\ -i & 0 & 0 \end{pmatrix}$  and  $\lambda^z = \begin{pmatrix} 0 & -i & 0 \\ i & 0 & 0 \\ 0 & 0 & 0 \end{pmatrix}$  are Gell-Mann matrices. Carrying out a  $1/M$ -expansion, we find

$$\begin{aligned} S^{\alpha i} &= M s_{11}^{\alpha i} + \sqrt{M} (s_{12}^{\alpha i} a_{2i} + s_{13}^{\alpha i} a_{3i} + s_{21}^{\alpha i} a_{2i}^\dagger + s_{31}^{\alpha i} a_{3i}^\dagger) + \\ &+ ((s_{22}^{\alpha i} - s_{11}^{\alpha i}) a_{2i}^\dagger a_{2i} + s_{23}^{\alpha i} a_{2i}^\dagger a_{3i} + s_{32}^{\alpha i} a_{3i}^\dagger a_{2i} + (s_{33}^{\alpha i} - s_{11}^{\alpha i}) a_{3i}^\dagger a_{3i}) + \\ &+ O\left(\frac{1}{\sqrt{M}}\right). \end{aligned} \quad (3.53)$$

Let us select a pair of nearest-neighbour sites  $i$  and  $j$  with bosons  $a_\mu$  and  $b_\mu$ , respectively: up to order  $M$ , the scalar product of the spin operators,  $\mathbf{S}_i \mathbf{S}_j = \sum_\alpha S^{\alpha i} S^{\alpha j}$ , assumes the form

$$\begin{aligned} \mathbf{S}_i \mathbf{S}_j &= M^2 \sum_\alpha s_{11}^{\alpha i} s_{11}^{\alpha j} + \\ &+ M \sqrt{M} \sum_\alpha \{ s_{11}^{\alpha i} (s_{12}^{\alpha j} b_2 + s_{13}^{\alpha j} b_3 + s_{21}^{\alpha j} b_2^\dagger + s_{31}^{\alpha j} b_3^\dagger) + \\ &\quad + s_{11}^{\alpha j} (s_{12}^{\alpha i} a_2 + s_{13}^{\alpha i} a_3 + s_{21}^{\alpha i} a_2^\dagger + s_{31}^{\alpha i} a_3^\dagger) \} + \\ &+ M \sum_\alpha \{ s_{11}^{\alpha i} ((s_{22}^{\alpha j} - s_{11}^{\alpha j}) b_2^\dagger b_2 + s_{23}^{\alpha j} b_2^\dagger b_3 + \\ &\quad + s_{32}^{\alpha j} b_3^\dagger b_2 + (s_{33}^{\alpha j} - s_{11}^{\alpha j}) b_3^\dagger b_3) + \\ &\quad + s_{11}^{\alpha j} ((s_{22}^{\alpha i} - s_{11}^{\alpha i}) a_2^\dagger a_2 + s_{23}^{\alpha i} a_2^\dagger a_3 + \\ &\quad + s_{32}^{\alpha i} a_3^\dagger a_2 + (s_{33}^{\alpha i} - s_{11}^{\alpha i}) a_3^\dagger a_3) + \\ &\quad + (s_{12}^{\alpha i} a_2 + s_{13}^{\alpha i} a_3 + s_{21}^{\alpha i} a_2^\dagger + s_{31}^{\alpha i} a_3^\dagger) \cdot \\ &\quad \cdot (s_{12}^{\alpha j} b_2 + s_{13}^{\alpha j} b_3 + s_{21}^{\alpha j} b_2^\dagger + s_{31}^{\alpha j} b_3^\dagger) \} + \\ &+ O(\sqrt{M}). \end{aligned} \quad (3.54)$$

Since  $S^{\alpha i}$  is a hermitian operator, the diagonal elements of  $s^{\alpha i}$  must be real: however, since the elements of the matrix  $U_i^\dagger$  are real while the matrix  $\lambda^\alpha$  is purely imaginary, we find that for any given site,

$$s_{mm}^\alpha = (s_{mm}^\alpha)^* = (U_{mk}^\dagger \lambda_{kl}^\alpha U_{lm})^* = U_{mk}^\dagger (-\lambda_{kl}^\alpha) U_{lm} = -s_{mm}^\alpha, \quad (3.55)$$

therefore  $s_{mm}^{\alpha i} = 0$ . It follows that (3.54) is greatly simplified, and the first non-vanishing term is of order  $M$ :

$$\begin{aligned} \mathbf{S}_i \mathbf{S}_j &= M \sum_{\alpha} \left\{ (s_{12}^{\alpha i} a_2 + s_{13}^{\alpha i} a_3 + s_{21}^{\alpha i} a_2^{\dagger} + s_{31}^{\alpha i} a_3^{\dagger}) \cdot \right. \\ &\quad \left. \cdot (s_{12}^{\alpha j} b_2 + s_{13}^{\alpha j} b_3 + s_{21}^{\alpha j} b_2^{\dagger} + s_{31}^{\alpha j} b_3^{\dagger}) \right\} + \\ &\quad + O(\sqrt{M}). \end{aligned} \quad (3.56)$$

Inserting the rotation matrix given in (3.51), we end up with

$$\begin{aligned} \mathbf{S}_i \mathbf{S}_j &= \\ &= M \left\{ (a_2 \ a_3) \begin{pmatrix} -\cos \delta & \cos \eta \sin \delta \\ -\cos \eta \sin \delta & -\cos^2 \eta \cos \delta - \sin^2 \eta \end{pmatrix} \begin{pmatrix} b_2 \\ b_3 \end{pmatrix} + \right. \\ &\quad + (a_2^{\dagger} \ a_3^{\dagger}) \begin{pmatrix} -\cos \delta & \cos \eta \sin \delta \\ -\cos \eta \sin \delta & -\cos^2 \eta \cos \delta - \sin^2 \eta \end{pmatrix} \begin{pmatrix} b_2^{\dagger} \\ b_3^{\dagger} \end{pmatrix} + \\ &\quad + (a_2^{\dagger} \ a_3^{\dagger}) \begin{pmatrix} \cos \delta & -\cos \eta \sin \delta \\ \cos \eta \sin \delta & \cos^2 \eta \cos \delta + \sin^2 \eta \end{pmatrix} \begin{pmatrix} b_2 \\ b_3 \end{pmatrix} + \\ &\quad \left. + (b_2^{\dagger} \ b_3^{\dagger}) \begin{pmatrix} \cos \delta & \cos \eta \sin \delta \\ -\cos \eta \sin \delta & \cos^2 \eta \cos \delta + \sin^2 \eta \end{pmatrix} \begin{pmatrix} a_2 \\ a_3 \end{pmatrix} \right\} + \\ &\quad + O(\sqrt{M}), \end{aligned} \quad (3.57)$$

where  $\delta = \varphi_j - \varphi_i$ .

In the absence of anisotropy, the only other term we need to take into account is the interaction  $P_{ij}$ , the  $1/M$ -expansion of which can be simplified using the fact that nearest-neighbour sites  $i$  and  $j$  have orthogonal wavefunctions for  $D/J = 0$ , i. e. the first rows of the matrices  $U_i^{\dagger}$  and  $U_j^{\dagger}$  are orthogonal vectors. In such cases, we may always find a third vector  $\{U_{31}, U_{32}, U_{33}\}$  so that

$$U^{\dagger} = \begin{pmatrix} U_{i,11}^{\dagger} & U_{i,12}^{\dagger} & U_{i,13}^{\dagger} \\ U_{j,11}^{\dagger} & U_{j,12}^{\dagger} & U_{j,13}^{\dagger} \\ U_{31} & U_{32} & U_{33} \end{pmatrix} \quad (3.58)$$

is an  $SU(3)$  rotation matrix, and define a common  $SU(3)$  rotation on both sites:

$$\begin{pmatrix} a'_1 \\ a'_2 \\ a'_3 \end{pmatrix} = U^{\dagger} \begin{pmatrix} a_x \\ a_y \\ a_z \end{pmatrix} \quad (3.59)$$

and

$$\begin{pmatrix} b'_1 \\ b'_2 \\ b'_3 \end{pmatrix} = U^{\dagger} \begin{pmatrix} b_x \\ b_y \\ b_z \end{pmatrix}, \quad (3.60)$$

where we have denoted the bosons on site  $i$  and  $j$  by  $a$  and  $b$ , respectively. Since  $P_{ij}$  is invariant with respect to  $SU(3)$  rotations,

$$P_{ij} = \sum_{\mu,\nu=x,y,z} a_\mu^\dagger a_\nu b_\nu^\dagger b_\mu = \sum_{\mu,\nu=1,2,3} a'_\mu{}^\dagger a'_\nu b'_\nu{}^\dagger b'_\mu, \quad (3.61)$$

we may easily carry out the  $1/M$ -expansion:

$$P_{ij} = M (a'_2{}^\dagger a'_2 + b'_1{}^\dagger b'_1 + a'_2{}^\dagger b'_1{}^\dagger + a'_2 b'_1) + O(1). \quad (3.62)$$

The operators  $a'_2$  and  $b'_1$  can be expressed using the locally rotated bosons:

$$\begin{aligned} a'_2 &= u'_{12} a_2 + u'_{13} a_3, \\ b'_1 &= u_{12} b_2 + u_{13} b_3, \end{aligned} \quad (3.63)$$

where  $u = U_i^\dagger U_j$  and  $u' = u^\dagger$ , and so we eventually find

$$\begin{aligned} P_{ij} &= M \left\{ (u_{21} a_2^\dagger + u_{31} a_3^\dagger + u_{12} b_2 + u_{13} b_3) \cdot \right. \\ &\quad \left. \cdot (u'_{21} b_2^\dagger + u'_{31} b_3^\dagger + u'_{12} a_2 + u'_{13} a_3) \right\} - \\ &\quad - M (u_{12} u'_{21} + u_{13} u'_{31}) + O(1). \end{aligned} \quad (3.64)$$

Note that the constant term at the end of (3.64) will vanish if the operators are written in normal-ordered form, furthermore, since  $u_{11} = u'_{11} = 0$  and  $uu' = U_i^\dagger U_j U_j^\dagger U_i = 1$ , the constant term is actually  $-M$ , hence it is independent of the actual parametrization. Inserting the rotation matrix given in (3.51) and setting  $\sin \eta = \sqrt{2/3}$ ,  $\cos \eta = \sqrt{1/3}$  and  $\varphi_j - \varphi_i = 2\pi/3$ , we end up with

$$\begin{aligned} P_{ij} &= M \frac{1}{2} \left\{ (a_2 \ a_3) \begin{pmatrix} 1 & 1 \\ -1 & -1 \end{pmatrix} \begin{pmatrix} b_2 \\ b_3 \end{pmatrix} + \right. \\ &\quad \left. + (a_2^\dagger \ a_3^\dagger) \begin{pmatrix} 1 & 1 \\ -1 & -1 \end{pmatrix} \begin{pmatrix} b_2^\dagger \\ b_3^\dagger \end{pmatrix} + \right. \\ &\quad \left. + (a_2^\dagger \ a_3^\dagger) \begin{pmatrix} 1 & -1 \\ -1 & 1 \end{pmatrix} \begin{pmatrix} a_2 \\ a_3 \end{pmatrix} + \right. \\ &\quad \left. + (b_2^\dagger \ b_3^\dagger) \begin{pmatrix} 1 & 1 \\ 1 & 1 \end{pmatrix} \begin{pmatrix} b_2 \\ b_3 \end{pmatrix} \right\} + \\ &\quad + O(1). \end{aligned} \quad (3.65)$$

Combining (3.65) and (3.57), and carrying out a Fourier transformation, we

find the bosonic Hamiltonian of order  $M$ :

$$\begin{aligned} \frac{H^{(2)}}{3JM} = \sum_{\mathbf{k}} \left\{ (a_2^\dagger(\mathbf{k}) \quad a_3^\dagger(\mathbf{k})) M_1(\mathbf{k}) \begin{pmatrix} a_2(\mathbf{k}) \\ a_3(\mathbf{k}) \end{pmatrix} + \right. \\ \left. + (a_2^\dagger(\mathbf{k}) \quad a_3^\dagger(\mathbf{k})) M_2(\mathbf{k}) \begin{pmatrix} a_2^\dagger(-\mathbf{k}) \\ a_3^\dagger(-\mathbf{k}) \end{pmatrix} + \right. \\ \left. + (a_2(\mathbf{k}) \quad a_3(\mathbf{k})) M_3(\mathbf{k}) \begin{pmatrix} a_2(-\mathbf{k}) \\ a_3(-\mathbf{k}) \end{pmatrix} \right\}, \end{aligned} \quad (3.66)$$

where

$$\begin{aligned} M_1(\mathbf{k}) &= \begin{pmatrix} \sin \vartheta - (\cos \vartheta - \sin \vartheta) \frac{\gamma + \gamma^*}{2} & (\cos \vartheta - \sin \vartheta) \frac{\gamma^* - \gamma}{2} \\ (\cos \vartheta - \sin \vartheta) \frac{\gamma - \gamma^*}{2} & \sin \vartheta + (\cos \vartheta - \sin \vartheta) \frac{\gamma + \gamma^*}{2} \end{pmatrix}, \\ M_2(\mathbf{k}) &= \begin{pmatrix} \cos \vartheta \frac{\gamma}{2} & \cos \vartheta \frac{\gamma}{2} \\ -\cos \vartheta \frac{\gamma}{2} & -\cos \vartheta \frac{\gamma}{2} \end{pmatrix}, \\ M_3(\mathbf{k}) &= M_2(\mathbf{k})^*. \end{aligned} \quad (3.67)$$

The Hamiltonian  $H^{(2)}$  can be diagonalized in the region  $\pi/4 < \vartheta < \pi/2$  via a Bogoliubov transformation:

$$\begin{aligned} \frac{H^{(2)}}{3JM} = \sum_{\mathbf{k}} \{ \omega_+(\mathbf{k}) \alpha_+^\dagger(\mathbf{k}) \alpha_+(\mathbf{k}) + \omega_-(\mathbf{k}) \alpha_-^\dagger(\mathbf{k}) \alpha_-(\mathbf{k}) \} + \\ + \frac{1}{2} \sum_{\mathbf{k}} (\omega_+(\mathbf{k}) + \omega_-(\mathbf{k}) - 2 \sin \vartheta), \end{aligned} \quad (3.68)$$

where the dispersions are given by

$$\omega_{\pm}(\mathbf{k}) = \sqrt{(\sin \vartheta \pm (\sin \vartheta - \cos \vartheta) |\gamma(\mathbf{k})|)^2 - \cos^2 \vartheta |\gamma(\mathbf{k})|^2}. \quad (3.69)$$

While  $\omega_+$  is gapped in the entire Brillouin zone,  $\omega_-$  vanishes for  $\mathbf{k} = 0$  and at the corners of the Brillouin zone, which reflects the breaking of the global  $SU(2)$  symmetry. In the  $\vartheta \rightarrow \pi/4$  limit, the two dispersions become degenerate. The zero-point energy disappears for  $\vartheta \rightarrow \pi/2$ , due to the fact that the quadrupolar umbrella configuration becomes an exact eigenstate of the original Hamiltonian. We note that we have found the same spectrum of excitations as the authors of [38], despite the fact that they use a different formulation to obtain a bosonic Hamiltonian.

Turning on an easy-plane anisotropy, one has to treat the  $(S_i^z)^2$  term in the Hamiltonian, furthermore, the wavefunctions on neighbouring sites cease to be orthogonal to each other, and as a consequence, the expansion of  $P_{ij}$

becomes more complicated than in the case  $D/J = 0$ . Let us deal with the anisotropy term first: it can be rewritten as

$$\begin{aligned} (S_i^z)^2 &= a_x^\dagger a_x + a_y^\dagger a_y = \\ &= (a_{1i}^\dagger \quad a_{2i}^\dagger \quad a_{3i}^\dagger) \begin{pmatrix} \sin^2 \eta & \sin \eta \cos \eta & 0 \\ \sin \eta \cos \eta & \cos^2 \eta & 0 \\ 0 & 0 & 1 \end{pmatrix} \begin{pmatrix} a_{1i} \\ a_{2i} \\ a_{3i} \end{pmatrix}, \end{aligned} \quad (3.70)$$

and therefore its flavour-wave expansion is simply

$$\begin{aligned} M (S_i^z)^2 &= M^2 \sin^2 \eta + M \sqrt{M} \sin \eta \cos \eta (a_{2i} + a_{2i}^\dagger) + \\ &+ M (\cos 2\eta a_{2i}^\dagger a_{2i} + \cos^2 \eta a_{3i}^\dagger a_{3i}) + O(\sqrt{M}). \end{aligned} \quad (3.71)$$

As far as  $P_{ij}$  is concerned, we may reexpress it using (2.91),

$$P_{ij} = \frac{1}{2} (\mathbf{S}_i \mathbf{S}_j + \mathbf{Q}_i \mathbf{Q}_j) + \frac{1}{3}, \quad (3.72)$$

and carry out a flavour-wave expansion of the  $\mathbf{Q}_i \mathbf{Q}_j$  term in a similar way as we did with the  $\mathbf{S}_i \mathbf{S}_j$  term<sup>10</sup>. We refrain from presenting calculatory details, and we quote the result that in order  $M^2$  one recovers the classical energy, while in order  $M\sqrt{M}$  the classical condition (3.12) leads to a cancellation of all one-boson terms. The quadratic Hamiltonian of order  $M$  assumes the same form as in (3.66), with the matrices

$$\begin{aligned} \frac{M_1(\mathbf{k})}{\sin \vartheta} &= \begin{pmatrix} 1 - (c - 1 - d + 2d^2) \frac{\gamma + \gamma^*}{2} & (c - 1 + d) \sqrt{1 + 2d} \frac{\gamma^* - \gamma}{2} \\ (c - 1 + d) \sqrt{1 + 2d} \frac{\gamma - \gamma^*}{2} & 1 + (c - 1 + d(1 - 2c)) \frac{\gamma + \gamma^*}{2} \end{pmatrix}, \\ \frac{M_2(\mathbf{k})}{\sin \vartheta} &= \begin{pmatrix} (c + d - 2d^2) \frac{\gamma}{2} & (c - d) \sqrt{1 + 2d} \frac{\gamma}{2} \\ (d - c) \sqrt{1 + 2d} \frac{\gamma}{2} & (-c + d(2c - 1)) \frac{\gamma}{2} \end{pmatrix}, \\ M_3(\mathbf{k}) &= M_2(\mathbf{k})^*, \end{aligned} \quad (3.73)$$

where we have introduced  $d = D/9J \sin \vartheta$  and  $c = \cot \vartheta$ . The Hamiltonian  $H^{(2)}$  can be diagonalized in the region  $\pi/4 < \vartheta \leq \arctan 4$  for  $0 < d < 1$  and in the region  $\arctan 4 \leq \vartheta < \pi/2$  for  $0 < d < 2c/(1 - 2c)$ , via a Bogoliubov transformation, and one finds the exact same form as in (3.68), including the expression for the zero-point energy. However, the dispersions are given this time as the two positive eigenvalues of the matrix

$$\begin{pmatrix} M_1(\mathbf{k})^* & M_2(\mathbf{k})^* + M_2(\mathbf{k})^T \\ -M_2(\mathbf{k})^* - M_2(\mathbf{k})^T & -M_1(\mathbf{k})^* \end{pmatrix}, \quad (3.74)$$

<sup>10</sup>Note that one has to simultaneously multiply the constant 1/3 by  $M^2$ .

and we may choose their labeling in agreement with the  $D/J = 0$  case. We find that  $\omega_+(\mathbf{k})$  remains gapped in the entire Brillouin zone, while  $\omega_-(\mathbf{k})$  retains a gapless  $\mathbf{k} = 0$  mode, which is the Goldstone mode of the broken U(1) rotation symmetry around the  $z$  axis. In the limits  $c \rightarrow 1$ ,  $d \rightarrow 0$ ,  $d \rightarrow 1$  and  $d \rightarrow 2c/(1 - 2c)$ , we find a softening of the dispersion  $\omega_-(\mathbf{k})$  at the corners of the Brillouin zone. The other branch of excitations,  $\omega_+(\mathbf{k})$ , loses its gap at  $\mathbf{k} = 0$  for  $c \rightarrow 1$  and  $d \rightarrow 1$ . It is interesting to note that flavour-wave theory fails to detect the first-order transition that occurs in the region  $\arctan 4 < \vartheta < \pi/2$ , and instead predicts the same boundary as the stability analysis of appendix A. This opens up the possibility of studying a  $1/M$ -renormalization of the boundary between the quadrupolar umbrella phase and the phases with fan-like spin configurations, via a calculation of the corresponding zero-point energies [49], however, such an analysis goes beyond the scope of the present work. Finally, we would like to emphasize that we have chosen  $D/J > 0$  mainly for a brevity of discussion: in fact, the calculations presented above are easily extended to the case of an easy-axis anisotropy field, and the dispersions are given by the same expressions as before. Again, we find a branch of excitations featuring a Goldstone mode, and a gapped dispersion that eventually softens at  $\mathbf{k} = 0$  when the directors open up to the  $xy$  plane. Similarly to the easy-plane case, the quadrupolar umbrella phase remains locally stable beyond the first-order phase boundary that is indicated by the variational calculus.

### 3.3 Perturbative analysis in the limit of large anisotropy

In this section we study the limits of large easy-plane and easy-axis anisotropy with the help of perturbation theory.

For  $D > 0$  and  $J = 0$ , the ground state of the system features the  $|0\rangle$  state on every site, while the first excited states will have it replaced with  $|1\rangle$  or  $|\bar{1}\rangle$  on exactly one site: the energy difference between the first excited states and the ground state is  $D$ . A small bilinear-biquadratic coupling will alter the ground-state energy and split the degeneracy of the first excited states: as a result, the gap of excitations is also modified. We will calculate perturbative corrections to the gap and draw a comparison with the result of flavour-wave theory. Note that the role of higher-lying excited states will be neglected in our treatment.

For  $D < 0$  and  $J = 0$ , the ground state is macroscopically degenerate, and a basis in this manifold is generated by setting the state on site  $i = 1 \dots L$

to be either  $|1\rangle$  or  $|\bar{1}\rangle$ , hence the dimensionality of the local Hilbert space is reduced to two. We will show that the effect of the perturbative terms that appear for  $J \neq 0$  may be described to lowest orders with the help of a relatively simple effective spin-one-half model, which is well-studied in literature. The quantum fluctuations that are induced by a finite  $J$  will lift the macroscopic degeneracy of the ground state and lead to the stabilization of a supersolid phase.

### 3.3.1 Easy-plane anisotropy: finite- $J$ corrections to the gap

We begin by dividing our Hamiltonian into an unperturbed part

$$H_0 = D \sum_i (S_i^z)^2 \quad (3.75)$$

and a perturbative term

$$H_1 = J \sum_{\langle i,j \rangle} \{(\cos \vartheta - \sin \vartheta) \mathbf{S}_i \mathbf{S}_j + \sin \vartheta (1 + P_{ij})\}. \quad (3.76)$$

The ground state of  $H_0$  is  $|0\rangle = |000\dots\rangle$ , and the ground-state energy is  $E_0 = 0$ . Let us denote the excited states of  $H_0$  as  $|n\rangle$ , and the corresponding energies as  $E_n$ , where  $n \neq 0$ : the first- and second-order corrections to the energy are given by

$$\varepsilon_1 = \langle 0 | H_1 | 0 \rangle \quad (3.77)$$

and

$$\varepsilon_2 = \langle 0 | H_1 \left( \sum_{n \neq 0} \frac{|n\rangle \langle n|}{E_0 - E_n} \right) H_1 | 0 \rangle. \quad (3.78)$$

Since

$$P_{ij} |0_i 0_j\rangle = |0_i 0_j\rangle \quad (3.79)$$

and

$$\mathbf{S}_i \mathbf{S}_j |0_i 0_j\rangle = |1_i \bar{1}_j\rangle + |\bar{1}_i 1_j\rangle, \quad (3.80)$$

the first-order correction is easily obtained:

$$\varepsilon_1 = 6LJ \sin \vartheta. \quad (3.81)$$

The second-order correction can be calculated as

$$\begin{aligned} \varepsilon_2 &= J(\cos \vartheta - \sin \vartheta) \sum_{\langle i,j \rangle} \langle 0 | H_1 \left( \sum_{n \neq 0} \frac{|n\rangle \langle n|}{E_0 - E_n} \right) \mathbf{S}_i \mathbf{S}_j | 0 \rangle = \\ &= \frac{J^2 (\cos \vartheta - \sin \vartheta)^2}{0 - 2D} \sum_{\langle i,j \rangle} \langle 0 | (\mathbf{S}_i \mathbf{S}_j)^2 | 0 \rangle, \end{aligned} \quad (3.82)$$

and since

$$(\mathbf{S}_i \mathbf{S}_j)^2 |0_i 0_j\rangle = 2|0_i \bar{0}_j\rangle - |1_i \bar{1}_j\rangle - |\bar{1}_i 1_j\rangle, \quad (3.83)$$

we find

$$\varepsilon_2 = \frac{J^2(\cos \vartheta - \sin \vartheta)^2}{0 - 2D} 3L2 = -6L \frac{J^2}{2D} (\cos \vartheta - \sin \vartheta)^2. \quad (3.84)$$

Note that the second-order correction vanishes if  $\cos \vartheta = \sin \vartheta$ : actually, since  $|0\rangle$  is an eigenstate of  $P_{ij}$ , all perturbative corrections disappear at the SU(3) points, except for the first-order shift in the energy  $\varepsilon_1$ . The total energy of the ground state can be written as

$$E_0 + \varepsilon_1 + \varepsilon_2 = 6LJ \sin \vartheta - 6L \frac{J^2}{2D} (\cos \vartheta - \sin \vartheta)^2, \quad (3.85)$$

up to corrections of order  $O(J^3/D^2)$ .

The first excited states of  $H_0$  can be labeled by a site index and a sign:

$$\begin{aligned} |i^+\rangle &= \frac{1}{\sqrt{2}} S_i^+ |0\rangle = |0 \dots 0 1_i 0 \dots\rangle, \\ |i^-\rangle &= \frac{1}{\sqrt{2}} S_i^- |0\rangle = |0 \dots 0 \bar{1}_i 0 \dots\rangle, \end{aligned} \quad (3.86)$$

and they all satisfy the equation

$$H_0 |i^\pm\rangle = D |i^\pm\rangle. \quad (3.87)$$

We will find it useful to introduce propagating states in this degenerate manifold:

$$|\mathbf{k}^\pm\rangle = \frac{1}{\sqrt{L}} \sum_i e^{i\mathbf{k}\cdot\mathbf{R}_i} |i^\pm\rangle, \quad (3.88)$$

and naturally,

$$H_0 |\mathbf{k}^\pm\rangle = D |\mathbf{k}^\pm\rangle. \quad (3.89)$$

Since the perturbative term  $H_1$  commutes with the total spin, we don't expect a mixing of states with different sign indices. Denoting the projector to the manifold of first excited states by  $P$ , i. e.

$$P = \sum_i (|i^+\rangle\langle i^+| + |i^-\rangle\langle i^-|) = \sum_{\mathbf{k}} (|\mathbf{k}^+\rangle\langle \mathbf{k}^+| + |\mathbf{k}^-\rangle\langle \mathbf{k}^-|), \quad (3.90)$$

we may write the first-order effective Hamiltonian as

$$H^{(1)} = P H_1 P. \quad (3.91)$$

The following equations are easy to verify:

$$\begin{aligned}
 \sum_{\langle l,m \rangle} P_{lm} |i^\pm\rangle &= (3L - 6) |i^\pm\rangle + \sum_{\vec{\delta}} |(i + \delta)^\pm\rangle, \\
 P \sum_{\langle l,m \rangle} \frac{1}{2} (S_l^+ S_m^- + S_l^- S_m^+) |i^\pm\rangle &= \sum_{\vec{\delta}} |(i + \delta)^\pm\rangle, \\
 \sum_{\langle l,m \rangle} S_l^z S_m^z |i^\pm\rangle &= 0,
 \end{aligned} \tag{3.92}$$

and thus we find

$$H^{(1)} |i^\pm\rangle = 6J(L - 1) \sin \vartheta |i^\pm\rangle + J \cos \vartheta \sum_{\vec{\delta}} |(i + \delta)^\pm\rangle, \tag{3.93}$$

where the  $\vec{\delta}$  vectors point towards all first neighbours of a site, and  $|(i + \delta)^\pm\rangle$  corresponds to the site  $\mathbf{R}_i + \vec{\delta}$ . The operator  $H^{(1)}$  is diagonal in the basis of propagating states:

$$\begin{aligned}
 H^{(1)} |\mathbf{k}^\pm\rangle &= 6J(L - 1) \sin \vartheta |\mathbf{k}^\pm\rangle + \\
 &+ J \cos \vartheta \frac{1}{\sqrt{L}} \sum_i e^{i\mathbf{k}\cdot\mathbf{R}_i} \sum_{\vec{\delta}} |(i + \delta)^\pm\rangle = \\
 &= 6J(L - 1) \sin \vartheta |\mathbf{k}^\pm\rangle + \\
 &+ J \cos \vartheta \sum_{\vec{\delta}} e^{-i\mathbf{k}\cdot\vec{\delta}} \frac{1}{\sqrt{L}} \sum_i e^{i\mathbf{k}\cdot(\mathbf{R}_i + \vec{\delta})} |(i + \delta)^\pm\rangle = \\
 &= \left( 6J(L - 1) \sin \vartheta + J \cos \vartheta \sum_{\vec{\delta}} e^{-i\mathbf{k}\cdot\vec{\delta}} \right) |\mathbf{k}^\pm\rangle,
 \end{aligned} \tag{3.94}$$

hence we indeed acquire dispersive modes. All in all, we may write

$$(H_0 + H^{(1)}) |\mathbf{k}^\pm\rangle = (D + \varepsilon_1 + \varepsilon_1(\mathbf{k})) |\mathbf{k}^\pm\rangle, \tag{3.95}$$

and the dispersion is given by

$$\varepsilon_1(\mathbf{k}) = 6J (\cos \vartheta \gamma(\mathbf{k})' - \sin \vartheta), \tag{3.96}$$

where we have used the quantity  $\gamma(\mathbf{k})' = \sum_{\vec{\delta}} e^{-i\mathbf{k}\cdot\vec{\delta}}/6$  that was already defined in the previous section. Let us now calculate the second-order effective Hamiltonian: it is given by

$$H^{(2)} = PH_1 \frac{Q}{a} H_1 P, \tag{3.97}$$

where the operator  $Q/a$  stands for

$$\frac{Q}{a} = \sum_{n, E_n \neq D} \frac{|n\rangle\langle n|}{D - E_n}. \quad (3.98)$$

It is immediately clear that

$$\begin{aligned} \frac{Q}{a} \sum_{\langle l, m \rangle} P_{lm} |i^\pm\rangle &= 0, \\ \frac{Q}{a} \sum_{\langle l, m \rangle} S_l^z S_m^z |i^\pm\rangle &= 0, \end{aligned} \quad (3.99)$$

furthermore

$$\frac{Q}{a} \sum_{\langle l, m \rangle} \frac{1}{2} (S_l^+ S_m^- + S_l^- S_m^+) |i^\pm\rangle = \frac{1}{D - 3D} \sum_{\substack{\langle l, m \rangle \\ l \neq i, m \neq i}} \frac{1}{2} (S_l^+ S_m^- + S_l^- S_m^+) |i^\pm\rangle, \quad (3.100)$$

therefore we find

$$\begin{aligned} \frac{Q}{a} H_1 |i^\pm\rangle &= -\frac{J(\cos \vartheta - \sin \vartheta)}{2D} \\ &\cdot \sum_{\substack{\langle l, m \rangle \\ l \neq i, m \neq i}} \{ |0 \dots 0 1_l \bar{1}_m 0 \dots 0 1_i 0 \dots\rangle + |0 \dots 0 \bar{1}_l 1_m 0 \dots 0 1_i 0 \dots\rangle \}. \end{aligned} \quad (3.101)$$

In order to calculate  $PH_1 \frac{Q}{a} H_1 |i^\pm\rangle$ , we must distinguish between different types of  $\langle l, m \rangle$  bonds in the above expression. There are  $3L - 30$  bonds that are connected neither to site  $i$  nor to any of its first-neighbour sites: these bonds will only contribute if a spin-flip term acts on them, and thus their total contribution is

$$-\frac{J^2(\cos \vartheta - \sin \vartheta)^2}{2D} (3L - 30) 2 |i^\pm\rangle. \quad (3.102)$$

There are 18 bonds that are connected to exactly one first neighbour of site  $i$ : these bonds will contribute both when a spin-flip term acts on them, and when a spin-flip term acts on the bond linking them to site  $i$ . Assuming that site  $i$  is in the state  $|1_i\rangle$  and site  $m$  is its first neighbour, we may write such processes in the concise form

$$|1_l \bar{1}_m 1_i\rangle + |\bar{1}_l 1_m 1_i\rangle \rightarrow 2|001\rangle + |100\rangle, \quad (3.103)$$

and we find that the total contribution of such terms is

$$-\frac{J^2(\cos\vartheta - \sin\vartheta)^2}{2D} 18 * 2|i^\pm\rangle - \frac{J^2(\cos\vartheta - \sin\vartheta)^2}{2D} \sum'_{\vec{\delta}, \vec{\delta}'} |(i + \delta + \delta')^\pm\rangle, \quad (3.104)$$

where  $\sum'$  denotes a sum in which we only take into account the 18 terms where  $\vec{\delta} + \vec{\delta}'$  neither vanishes nor points to a first neighbour. There are 6 bonds that are connected to exactly two first neighbours of site  $i$ : these bonds will contribute both when a spin-flip term acts on them, and when a spin-flip term acts on any of the two bonds that link them to site  $i$ . Assuming that site  $i$  is in the state  $|1_i\rangle$ , the corresponding processes can be written in the form

$$|1_l 1_i \bar{1}_m\rangle + |\bar{1}_l 1_i 1_m\rangle \rightarrow |100\rangle + 2|010\rangle + |001\rangle, \quad (3.105)$$

and therefore the total contribution of such terms is

$$-\frac{J^2(\cos\vartheta - \sin\vartheta)^2}{2D} 6 * 2|i^\pm\rangle - \frac{J^2(\cos\vartheta - \sin\vartheta)^2}{2D} 2 \sum_{\vec{\delta}} |(i + \delta)^\pm\rangle. \quad (3.106)$$

Summing up all the contributions, we find

$$\begin{aligned} H^{(2)}|i^\pm\rangle = & -\frac{J^2(\cos\vartheta - \sin\vartheta)^2}{2D} (6L - 12)|i^\pm\rangle - \\ & -\frac{J^2(\cos\vartheta - \sin\vartheta)^2}{2D} \sum'_{\substack{\vec{\delta}, \vec{\delta}' \\ \vec{\delta} + \vec{\delta}' \neq 0}} |(i + \delta + \delta')^\pm\rangle. \end{aligned} \quad (3.107)$$

Similarly to  $H^{(1)}$ , the second-order effective Hamiltonian  $H^{(2)}$  is diagonal in the basis of propagating states:

$$\begin{aligned} H^{(2)}|\mathbf{k}^\pm\rangle = & -\frac{J^2(\cos\vartheta - \sin\vartheta)^2}{2D} (6L - 18)|\mathbf{k}^\pm\rangle - \\ & -\frac{J^2(\cos\vartheta - \sin\vartheta)^2}{2D} \sum_{\vec{\delta}, \vec{\delta}'} e^{-i\mathbf{k}\cdot(\vec{\delta} + \vec{\delta}')} |\mathbf{k}^\pm\rangle, \end{aligned} \quad (3.108)$$

and thus we end up with

$$(H_0 + H^{(1)} + H^{(2)})|\mathbf{k}^\pm\rangle = (D + \varepsilon_1 + \varepsilon_2 + \varepsilon_1(\mathbf{k}) + \varepsilon_2(\mathbf{k}))|\mathbf{k}^\pm\rangle, \quad (3.109)$$

where

$$\varepsilon_2(\mathbf{k}) = -\frac{J^2(\cos\vartheta - \sin\vartheta)^2}{2D} (36\gamma(\mathbf{k})^2 - 18). \quad (3.110)$$

The energy gap as a function of  $\mathbf{k}$  is given by

$$\begin{aligned} \frac{D + \varepsilon_1(\mathbf{k}) + \varepsilon_2(\mathbf{k})}{D} &= 1 + \frac{6J}{D} (\cos \vartheta \gamma(\mathbf{k})' - \sin \vartheta) - \\ &\quad - \left( \frac{6J}{D} \right)^2 (\cos \vartheta - \sin \vartheta)^2 \left( \frac{1}{2} \gamma(\mathbf{k})'^2 - \frac{1}{4} \right) + \\ &\quad + O\left( \frac{J^3}{D^3} \right). \end{aligned} \quad (3.111)$$

One may compare this result to the expansion in powers of  $1/d = 6J/D$  of the excitation spectrum that was derived in the previous section using flavour-wave theory:

$$\begin{aligned} \frac{\omega(\mathbf{k})}{d} &= 1 + \frac{1}{d} (\cos \vartheta \gamma(\mathbf{k})' - \sin \vartheta) - \\ &\quad - \frac{1}{d^2} (\cos \vartheta - \sin \vartheta)^2 \frac{1}{2} \gamma(\mathbf{k})'^2 + \\ &\quad + O\left( \frac{1}{d^3} \right). \end{aligned} \quad (3.112)$$

We find that the perturbative and the semi-classical results coincide with each other in order  $\frac{J}{D}$ , however, in the next order, the earlier features a  $\mathbf{k}$ -independent term, while the latter does not. This discrepancy can most likely be attributed to the fact that the state  $|0\rangle$  is not an exact eigenstate of the Hamiltonian for a finite  $J$ .

### 3.3.2 Easy-axis anisotropy: emergence of supersolidity

It is convenient to use our earlier definitions of  $H_0$  and  $H_1$ , however, we have to keep in mind that  $D < 0$  in the present case. The ground-state manifold of  $H_0$  has a degeneracy of  $2^L$ , and the ground-state energy is given by  $E_0 = LD < 0$ . We may again denote excited states of  $H_0$  as  $|n\rangle$ : the  $l$ th excited level will feature exactly  $l$  sites with the state  $|0\rangle$ , and the energy shift is given by  $-lD > 0$ . Denoting the projector to the ground-state manifold by  $P$ , we may write the first-order effective Hamiltonian as

$$H^{(1)} = PH_1P = J \sum_{\langle i,j \rangle} Ph_{ij}P, \quad (3.113)$$

where

$$h_{ij} = (\cos \vartheta - \sin \vartheta) \mathbf{S}_i \mathbf{S}_j + \sin \vartheta (1 + P_{ij}). \quad (3.114)$$

It is simple to show that

$$\begin{aligned}
h_{ij}|\dots 1_i 1_j \dots\rangle &= (\cos \vartheta + \sin \vartheta)|\dots 1_i 1_j \dots\rangle, \\
h_{ij}|\dots 1_i \bar{1}_j \dots\rangle &= (\cos \vartheta - \sin \vartheta)|\dots 0_i 0_j \dots\rangle + \\
&\quad + (2 \sin \vartheta - \cos \vartheta)|\dots 1_i \bar{1}_j \dots\rangle + \\
&\quad + \sin \vartheta|\dots \bar{1}_i 1_j \dots\rangle, \\
h_{ij}|\dots \bar{1}_i 1_j \dots\rangle &= (\cos \vartheta - \sin \vartheta)|\dots 0_i 0_j \dots\rangle + \\
&\quad + (2 \sin \vartheta - \cos \vartheta)|\dots \bar{1}_i 1_j \dots\rangle + \\
&\quad + \sin \vartheta|\dots 1_i \bar{1}_j \dots\rangle, \\
h_{ij}|\dots \bar{1}_i \bar{1}_j \dots\rangle &= (\cos \vartheta + \sin \vartheta)|\dots \bar{1}_i \bar{1}_j \dots\rangle,
\end{aligned} \tag{3.115}$$

and introducing local effective spin-one-half states via the mappings  $|1\rangle \equiv |\uparrow\rangle$  and  $|\bar{1}\rangle \equiv |\downarrow\rangle$ , along with the corresponding SU(2) algebra<sup>11</sup>, we may furthermore write

$$\begin{aligned}
h_{ij}^{(1)}|\dots \uparrow_i \uparrow_j \dots\rangle &= (\cos \vartheta + \sin \vartheta)|\dots \uparrow_i \uparrow_j \dots\rangle, \\
h_{ij}^{(1)}|\dots \uparrow_i \downarrow_j \dots\rangle &= (2 \sin \vartheta - \cos \vartheta)|\dots \uparrow_i \downarrow_j \dots\rangle + \\
&\quad + \sin \vartheta|\dots \downarrow_i \uparrow_j \dots\rangle, \\
h_{ij}^{(1)}|\dots \downarrow_i \uparrow_j \dots\rangle &= (2 \sin \vartheta - \cos \vartheta)|\dots \downarrow_i \uparrow_j \dots\rangle + \\
&\quad + \sin \vartheta|\dots \uparrow_i \downarrow_j \dots\rangle, \\
h_{ij}^{(1)}|\dots \downarrow_i \downarrow_j \dots\rangle &= (\cos \vartheta + \sin \vartheta)|\dots \downarrow_i \downarrow_j \dots\rangle,
\end{aligned} \tag{3.116}$$

where  $h_{ij}^{(1)} = 4(\cos \vartheta - \sin \vartheta)\sigma_i^z \sigma_j^z + \sin \vartheta(1 + p_{ij})$ , and  $p_{ij} = 2\vec{\sigma}_i \vec{\sigma}_j + 1/2$  is the transposition operator for the effective spins one-half. A comparison of (3.115) and (3.116) reveals that

$$Ph_{ij}P = h_{ij}^{(1)}, \tag{3.117}$$

since the projection operator  $P$  suppresses the state  $|\dots 0_i 0_j \dots\rangle$  that does not belong to the ground-state manifold. All in all, we find

$$H^{(1)} = J \sum_{\langle i,j \rangle} \left\{ 2 \sin \vartheta (\sigma_i^x \sigma_j^x + \sigma_i^y \sigma_j^y) + (4 \cos \vartheta - 2 \sin \vartheta) \sigma_i^z \sigma_j^z + \frac{3}{2} \sin \vartheta \right\}, \tag{3.118}$$

in other words, the  $S = 1/2$  XXZ model introduced earlier is not only appropriate for a variational description of the original spin-one system for the

<sup>11</sup>It is trivial to show that the mapping between operators is the following:  $\sigma_i^+ \equiv S_i^+ S_i^+ / 2$ ,  $\sigma_i^- \equiv S_i^- S_i^- / 2$  and  $\sigma_i^z \equiv S_i^z / 2$ .

case of sufficiently high anisotropy, but it is also an effective model in the perturbative sense, at least to first order in  $J/D$ . As discussed in appendix B, the model (3.118) features a  $\sqrt{3} \times \sqrt{3}$  supersolid phase that breaks both the  $U(1)$  symmetry associated with rotations around the  $z$  axis, and the translational symmetry of the lattice. With respect to the original spin-one system, this corresponds to a simultaneous presence of long-range dipolar and quadrupolar ordering patterns in the parameter region  $-0.15\pi \lesssim \vartheta < \pi/4$ .

Let us push the perturbative expansion to second order: the effective Hamiltonian is given by

$$H^{(2)} = PH_1 \frac{Q}{a} H_1 P = J \sum_{\langle i,j \rangle} PH_1 \frac{Q}{a} h_{ij} P, \quad (3.119)$$

where the operator  $Q/a$  stands for

$$\frac{Q}{a} = \sum_{n, E_n \neq E_0} \frac{|n\rangle\langle n|}{E_0 - E_n}. \quad (3.120)$$

A glance at (3.115) reveals that

$$\begin{aligned} \frac{Q}{a} h_{ij} | \dots 1_i 1_j \dots \rangle &= 0, \\ \frac{Q}{a} h_{ij} | \dots 1_i \bar{1}_j \dots \rangle &= \frac{1}{2D} (\cos \vartheta - \sin \vartheta) | \dots 0_i 0_j \dots \rangle, \\ \frac{Q}{a} h_{ij} | \dots \bar{1}_i 1_j \dots \rangle &= \frac{1}{2D} (\cos \vartheta - \sin \vartheta) | \dots 0_i 0_j \dots \rangle, \\ \frac{Q}{a} h_{ij} | \dots \bar{1}_i \bar{1}_j \dots \rangle &= 0, \end{aligned} \quad (3.121)$$

and applying  $PH_1$  to the above equations, we may notice that only terms that act on the selected pair of sites  $(i, j)$  yield a non-vanishing result, i. e.

$$\begin{aligned} PH_1 \frac{Q}{a} h_{ij} | \dots 1_i \bar{1}_j \dots \rangle &= PH_1 \frac{Q}{a} h_{ij} | \dots \bar{1}_i 1_j \dots \rangle = \\ &= P \frac{J}{2D} (\cos \vartheta - \sin \vartheta) h_{ij} | \dots 0_i 0_j \dots \rangle = \\ &= \frac{J}{2D} (\cos \vartheta - \sin \vartheta)^2 (| \dots 1_i \bar{1}_j \dots \rangle + | \dots \bar{1}_i 1_j \dots \rangle). \end{aligned} \quad (3.122)$$

Defining

$$h_{ij}^{(2)} = \frac{J}{2D} (\cos \vartheta - \sin \vartheta)^2 (p_{ij} - 4\sigma_i^z \sigma_j^z), \quad (3.123)$$

we may deduce that

$$\begin{aligned}
h_{ij}^{(2)}|\dots\uparrow_i\uparrow_j\dots\rangle &= h_{ij}^{(2)}|\dots\downarrow_i\downarrow_j\dots\rangle = 0, \\
h_{ij}^{(2)}|\dots\uparrow_i\downarrow_j\dots\rangle &= h_{ij}^{(2)}|\dots\downarrow_i\uparrow_j\dots\rangle = \\
&= \frac{J}{2D}(\cos\vartheta - \sin\vartheta)^2(|\dots\uparrow_i\downarrow_j\dots\rangle + |\dots\downarrow_i\uparrow_j\dots\rangle),
\end{aligned} \tag{3.124}$$

and therefore

$$PH_1\frac{Q}{a}h_{ij}P = h_{ij}^{(2)}. \tag{3.125}$$

Finally, the second-order contribution to the effective Hamiltonian is given by

$$H^{(2)} = \frac{J^2}{2D}(\cos\vartheta - \sin\vartheta)^2 \sum_{\langle i,j \rangle} \left\{ 2(\sigma_i^x\sigma_j^x + \sigma_i^y\sigma_j^y - \sigma_i^z\sigma_j^z) + \frac{1}{2} \right\}. \tag{3.126}$$

We note that  $H^{(2)}$  vanishes at the  $SU(3)$  points, and so should all subsequent perturbative terms as well, since  $P_{ij}$  does not connect the ground-state manifold to excited states. Since further-neighbour interactions do not yet appear at this order, we may conclude that the only physical effect of  $H^{(2)}$  is a renormalization of the coefficients of  $H^{(1)}$ . As a result, the  $\vartheta \approx -0.15\pi$  boundary of the supersolid phase will be slightly shifted, however, the ordering patterns remain unharmed.

### 3.4 Conclusions

We have mapped out the complete phase diagram of the spin-one bilinear-biquadratic model with a single-ion anisotropy field on the triangular lattice, and have found that it exhibits a variety of unconventional phases, due to a competition between magnetic and quadrupolar degrees of freedom. It was shown in particular that a quadrupolar umbrella phase emerges when a positive biquadratic exchange overcomes the antiferromagnetic bilinear coupling, and the excitation spectrum of this phase features a Goldstone mode that is associated with the spontaneous breaking of the  $U(1)$  symmetry of rotations around the anisotropy field. Due to the remaining  $SU(2)$  symmetry of the model with identical bilinear and biquadratic coupling coefficients, the boundary between the quadrupolar umbrella phase and the neighbouring antiferromagnetic phase does not shift in the presence of anisotropy. In contrast to the umbrella-like arrangement of directors, ferroquadrupolar order is quite sensitive to the nature of the anisotropy field, as the common

director will turn perpendicular to an easy axis, and be pinned perpendicular to an easy plane. In the earlier case, a Goldstone mode is retained, while in the latter, a gap develops for an arbitrarily small field. We have calculated this gap both within the framework of a semi-classical approach and in the perturbative limit of a high anisotropy field, and have drawn a comparison between the two methods. It was also observed that an easy-plane anisotropy field will shift the boundary between the ferroquadrupolar phase and the antiferromagnetic phase, however, this effect only becomes appreciable if the anisotropy field is of the order of the exchange. Finally, we have shown that a sufficiently large easy-axis anisotropy leads to non-trivial degeneracies in the ground-state manifold in a considerable region of the phase diagram, and have argued on the grounds of perturbation theory that this degeneracy is lifted by the emergence of a supersolid phase.

Coming back to the discussion on  $\text{NiGa}_2\text{S}_4$ , we may conclude that quadrupolar order remains quite robust in the presence of single-ion anisotropy. Provided that a sufficiently large biquadratic exchange is present in the material, our results should help in identifying the nature of the low-temperature phase. In this respect, one should keep in mind that a coupling between quadrupolar degrees of freedom is inherently present for spin-one antiferromagnets, and even when it is weak, it will give rise to unconventional correlations in magnetically ordered phases, particularly in the presence of frustration. In future work, it will be highly desirable to explore the effect of impurities on quadrupolar phases, and to investigate microscopic electronic processes that may enhance an effective biquadratic exchange.

## Chapter 4

# Three-sublattice ordering on the square lattice for a spin-one antiferromagnet with biquadratic interactions

We have seen in the preceding chapter that antiferroquadrupolar order induced by a positive biquadratic exchange is unfrustrated on the triangular lattice in essentially the same manner as conventional antiferromagnetic order is on the square lattice. The mean-field analysis of the spin-one bilinear-biquadratic Hamiltonian

$$H = J \sum_{\langle i,j \rangle} [\cos \vartheta \mathbf{S}_i \mathbf{S}_j + \sin \vartheta (\mathbf{S}_i \mathbf{S}_j)^2] \quad (4.1)$$

has revealed a long-range ordered antiferroquadrupolar phase on the triangular lattice in the parameter region  $\pi/4 < \vartheta < \pi/2$ , and this phase has proved to remain robust in the presence of quantum fluctuations [38, 5]. The importance of geometrical frustration can be highlighted in this context by investigating the mean-field phase diagram of the model (4.1) on the square lattice. In fact, as explained in section 2.2.3, the variational energy of a bond is minimized for  $\pi/4 < \vartheta < \pi/2$  by any configuration in which one of the sites features a pure quadrupole, and the local wavefunctions of the two sites are orthogonal to each other. In the case of the triangular lattice, the three-sublattice structure of the lattice is ideal for three quadrupoles with mutually perpendicular directors to form a long-range ordered state: every bond is satisfied, and the state is uniquely determined up to global rotations. However, the connectivity of the square lattice is lower than that of the triangular lattice, so even if we restrict ourselves to pure quadrupolar wavefunctions,

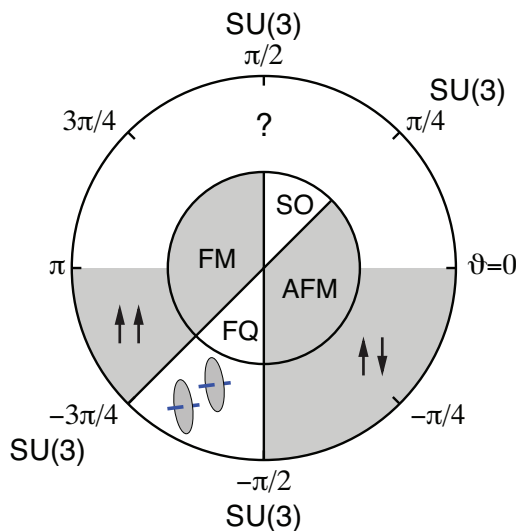


Figure 4.1: Phase diagram of the spin-one bilinear-biquadratic model on the square lattice. The inner circle shows the variational results: the ferromagnetic, ferroquadrupolar and antiferromagnetic phases are denoted by FM, FQ and AFM, respectively, while SO stands for “semi-ordered”. The outer circle shows the numerical results of [51], in the region where Quantum Monte Carlo simulations do not face a sign problem.

there are many configurations that satisfy all the bonds, similarly to the case of the three-state antiferromagnetic Potts-model on the square lattice [50]. Furthermore, nearest-neighbour sites of a quadrupolar site with director  $\mathbf{d}$  may also be magnetic, featuring a spin vector of arbitrary length parallel to  $\mathbf{d}$  (see figure 2.6). We may conclude therefore that on the square lattice, the variational approach leads to a highly degenerate ground-state manifold in the parameter region  $\pi/4 < \vartheta < \pi/2$ . Following Papanicolaou [19], we will call this phase “semi-ordered”.

The situation in the “semi-ordered” phase is reminiscent of frustrated antiferromagnetism, where the competition between exchange paths may give rise to an infinite number of classical ground states<sup>1</sup>. In that case, quantum or thermal fluctuations often restore long-range order by a selection mechanism that favours collinear or planar configurations and is known as the “order-by-disorder” mechanism [27], and one might wonder if a similar scenario might be realized for the present model. Figure 4.1 summarizes what is currently known about the phase diagram of the spin-one bilinear-biquadratic model on the square lattice. The variational approach reveals four phases that are

<sup>1</sup>We should emphasize however that no bond is frustrated in the “semi-ordered” phase.

separated from each other by the highly symmetric  $SU(3)$  points. Adjacent to the “semi-ordered” phase, we find two magnetic phases with fully developed spins: for  $-\pi/2 < \vartheta < \pi/4$ , a two-sublattice ordered Néel antiferromagnet is realized, while ferromagnetic order is stabilized in the region  $\pi/2 < \vartheta < 5\pi/4$ . Finally, a ferroquadrupolar phase emerges for  $5\pi/4 < \vartheta < 3\pi/2$ . Quantum Monte Carlo simulations by Harada and Kawashima have confirmed the variational phase diagram for the  $-\pi \leq \vartheta \leq 0$  case [51], however, much less is known about the  $0 < \vartheta < \pi$  region. While there can be little doubt that the ferromagnetic phase should persist in the interval  $\pi/2 < \vartheta < \pi$  (see the exact spectrum of a bond in figure 2.4), quantum effects remain truly unexplored in the case when the bilinear and the biquadratic exchange are both positive.

In the present chapter, we aim to eliminate the question mark in figure 4.1, via a combination of variational analysis, exact diagonalization calculations and flavour-wave theory. We will place particular emphasis on investigating the properties of the  $SU(3)$ -symmetric point  $\vartheta = \pi/4$ , which appears naturally as the low-energy effective model of the  $\rho = 1/3$  and  $2/3$  Mott insulators of repulsively interacting three-flavour fermions in an optical lattice. The exact diagonalization results that appear in the current chapter are all credited to Andreas M. Läuchli<sup>2</sup>.

## 4.1 Emergence of three-sublattice order in the “semi-ordered” phase

We will uncover the quantum phase diagram in the region  $\pi/4 < \vartheta < \pi/2$  in several steps. Firstly, we will show that the introduction of a magnetic field lifts the ground-state degeneracy in the “semi-ordered” phase and leads to the stabilization of an exotic  $1/2$ -magnetization plateau. We will complement this result by mapping out the full magnetic phase diagram of the model (4.1). Secondly, we will discuss the exact diagonalization calculations of A. M. Läuchli that confirm the presence of the plateau phase, but indicate the emergence of a three-sublattice ordered state in the low-field limit. We should emphasize that the latter finding is truly surprising, given the bipartite nature of the square lattice. Thirdly, we will demonstrate that quantum fluctuations give rise to a selection mechanism at the harmonic level which is in qualitative agreement with the implications of the numerical analysis. Finally, we will expand on the local stability of three-sublattice order on the square lattice.

---

<sup>2</sup>Max Planck Institut für Physik komplexer Systeme, D-01187 Dresden, Germany

### 4.1.1 Lift of degeneracy via a magnetic field

Owing to the fact that the variational bond configuration for  $\pi/4 < \vartheta < \pi/2$  admits a dipole moment on one of the sites, an infinitesimal magnetic field suffices to induce a first-order selection within the degenerate ground-state manifold of the “semi-ordered” phase. As a result, a two-sublattice ordered structure emerges, with an average magnetization of  $1/2$  per site: one of the sublattices retains ferroquadrupolar order with the common director parallel to the field, while the other sublattice is ferromagnetic, featuring fully developed spins aligned with the field. Assuming that the field points in the  $z$  direction, the configuration of every bond is given by  $|0\rangle \otimes |1\rangle$ . Since a magnetization process on the quadrupolar sublattice would require a tilting of the directors from the  $z$  axis, we expect a  $1/2$ -magnetization plateau to develop, analogously to the case of the  $2/3$ -magnetization plateau above the antiferroquadrupolar phase on the triangular lattice [5].

In figure 4.2, we mapped out the complete variational phase diagram of the model (4.1) in the presence of a magnetic field:

$$H = J \sum_{\langle i,j \rangle} [\cos \vartheta \mathbf{S}_i \mathbf{S}_j + \sin \vartheta (\mathbf{S}_i \mathbf{S}_j)^2] - h \sum_i S_i^z. \quad (4.2)$$

As suggested earlier, the  $1/2$ -magnetization plateau appears above the “semi-ordered” phase for an infinitesimal field, and it extends up to

$$\frac{h}{J} = 4 \left( \sqrt{\sin \vartheta (\sin \vartheta - \cos \vartheta)} - (\sin \vartheta - \cos \vartheta) \right), \quad (4.3)$$

where a second-order transition occurs: the director of the quadrupolar sublattice starts tilting away from the magnetic field so that a dipole moment with a non-vanishing  $z$  component may develop, however, due to the coupling between the two sublattices, the spin vector of the ferromagnetic sublattice will not be aligned with the field anymore. We enter a supersolid phase<sup>3</sup> characterized by two sublattices that feature partially polarized spins of different length, the  $xy$  components of which cancel each other out. Upon a further increase of the field, the supersolid phase evolves continuously into a canted Néel-like phase, where the two spin vectors become reflections of each other with respect to the  $z$  axis. Finally, the phase diagram is completed by two phases with  $\mathbf{k} = \mathbf{0}$  order: apart from the conventional ferromagnetic phase in which every site has a coherent spin state, we also obtain a peculiar ferromagnetic arrangement where the spins are only partially polarized.

<sup>3</sup>We use the word supersolid in the sense that one may simultaneously observe transverse order and a real-space modulation in the  $z$  component of the spin vectors.

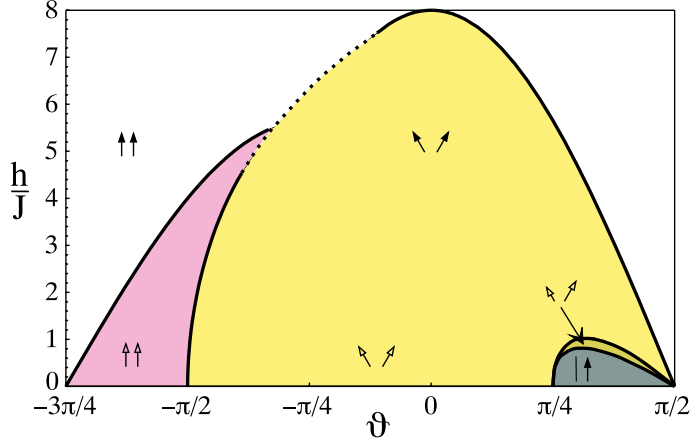


Figure 4.2: Variational phase diagram of the spin-one bilinear-biquadratic model in a magnetic field on the square lattice. Solid (dotted) lines denote second-order (first-order) phase boundaries. Filled (empty) arrows represent fully (partially) polarized magnetic moments, and the solid black line is a quadrupolar director. Note the presence of a phase with a magnetization plateau at  $1/2$  (shaded in gray), which is separated from the canted Néel phase by a tiny supersolid phase. In the Néel phase, coherent spin states are found only along the  $\vartheta = 0$  line.

In this latter phase, the single-site wavefunction is the same on every site: choosing the common director parallel to the  $y$  axis, we may write

$$|\psi_i\rangle = \cos(\pi/4 - \eta)|y\rangle - i \sin(\pi/4 - \eta)|x\rangle, \quad (4.4)$$

and a minimization with respect to  $\eta$  gives

$$\sin^2 \eta = \frac{2(\cos \vartheta - \sin \vartheta) - \frac{h}{2J}}{4(\cos \vartheta - \sin \vartheta)}. \quad (4.5)$$

At  $h/J = 4(\cos \vartheta - \sin \vartheta)$ , the spins become fully polarized, whereas in the  $h \rightarrow 0$  limit, we recover a ferroquadrupolar state. The transition between this phase and the Néel phase is generally continuous, with a boundary given by  $h/J = 2\sqrt{-16 \sin \vartheta \cos \vartheta}$ , however, if the magnetic field is of the order of  $5J$ , the two phases are separated from each other by a first-order boundary that runs above this line.

It is instructive to briefly investigate the stability of the ferromagnetic state against a single spin flip. Let us first rewrite our Hamiltonian as

$$H = \sum_{\langle i,j \rangle} [(J_1 - J_2) \mathbf{S}_i \mathbf{S}_j + J_2 (1 + P_{ij})] - h \sum_i S_i^z, \quad (4.6)$$

where we have introduced  $J_1 = J \cos \vartheta$  and  $J_2 = J \sin \vartheta$ . Noticing that

$$\mathbf{S}_i \mathbf{S}_j |1_i 1_j\rangle = P_{ij} |1_i 1_j\rangle = |1_i 1_j\rangle \quad (4.7)$$

and

$$\mathbf{S}_i \mathbf{S}_j |1_i 0_j\rangle = P_{ij} |1_i 0_j\rangle = |0_i 1_j\rangle, \quad (4.8)$$

we may deduce that the bilinear coupling and the transposition operator have an identical effect both on the ferromagnetic state and in the  $S^z = L - 1$  subspace of single spin flips ( $L$  is the number of lattice sites). Therefore, the form (4.6) makes it apparent that the  $J_2$  coefficient of the biquadratic exchange does not enter the expression of the gap that separates the ferromagnetic state from the single-magnon branch. Let us verify this by explicit calculation. The ferromagnetic state  $|111 \dots\rangle$  is an eigenstate of the Hamiltonian with energy  $E_0 = 2L(J_1 + J_2) - Lh$ , and in the subspace of single spin flips, propagating states of the form

$$|\mathbf{k}\rangle = \frac{1}{\sqrt{L}} \sum_i e^{i\mathbf{k}\cdot\mathbf{R}_i} \frac{1}{\sqrt{2}} S_i^- |111 \dots\rangle \quad (4.9)$$

will diagonalize the Hamiltonian:

$$(H - E_0)|\mathbf{k}\rangle = \varepsilon(\mathbf{k})|\mathbf{k}\rangle. \quad (4.10)$$

The single-magnon dispersion relation is given by

$$\varepsilon(\mathbf{k}) = h + 4J_1(\gamma(\mathbf{k}) - 1), \quad (4.11)$$

where  $\gamma(\mathbf{k}) = \sum_{\vec{\delta}} e^{-i\mathbf{k}\cdot\vec{\delta}}/4$ , and the sum extends over all first neighbours of a site. We may conclude that the gap is indeed independent of  $J_2$ , and if  $J_1 > 0$ , it will eventually close at the corners of the Brillouin zone, when the magnetic field is lowered to the value  $h = 8J_1$ . This boundary is in perfect agreement with the variational result in the  $J_2 \geq 0$  region, where we find a second-order transition to the canted Néel phase, however, if the coefficient of the biquadratic exchange is a sufficiently large negative number, figure 4.2 indicates either a first-order transition to the Néel phase, or a continuous instability towards a shortening of the spin vectors, and both of these events occur at a field  $h > 8J_1$ . Furthermore, the latter instability may also emerge for  $J_1 \leq 0$ , in which case the single-magnon gap would not close at a finite field. These features point towards the formation of bound-magnon states in the presence of a sufficiently large negative biquadratic exchange [18].

Let us also comment on the peculiar interplay between the magnetic field and the quadrupolar degrees of freedom in the Néel phase. We may

recall that in the zero-field phase, a coherent spin state was found on every site, even in the presence of a considerable biquadratic exchange, due to the unfrustrated nature of two-sublattice magnetic order<sup>4</sup>. However, once we turn on the field, the single-site wavefunctions acquire a quadrupolar character everywhere in the phase, aside from the  $\vartheta = 0$  line, and the sign of the biquadratic exchange becomes important. For  $\vartheta < 0$ , not surprisingly, the directors on the two sublattices coincide with each other, and they are pinned to the plane perpendicular to the magnetic field. On the other hand, if the coupling coefficient of the biquadratic term is positive, the directors are in a common plane with the spin vectors, and they too become reflections of each other with respect to the  $z$  axis. We may conclude that knowledge of the length and the  $z$  component of the spin vectors allows for a complete determination of the single-site wavefunctions everywhere in the Néel phase, and these two parameters may be obtained via a numerical minimization<sup>5</sup>. For the special case  $\vartheta = 0$ , the spins remain fully polarized for an arbitrary magnetic field, and their angle with respect to the  $z$  axis is given by  $\cos \eta = h/8J$ , thus the magnetization grows linearly with the field. In contrast to the Néel phase, the supersolid phase is a three-parameter phase. The reflection symmetry of the configuration with respect to the  $z$  axis is lost, however, the directors remain in a common plane with the spins, therefore the phase is characterized up to global rotations by the length of the spin vectors on the two sublattices, and the  $z$  component of the spin vectors on one of the sublattices<sup>6</sup>. The arrangement of dipole moments and quadrupolar directors is shown for the Néel phase and the supersolid phase in figure 4.3.

As a closing remark, we would like to emphasize that the excitation spectrum of the plateau phase may be obtained explicitly with the help of flavour-wave theory. A straightforward calculation yields four gapped dispersions in the reduced Brillouin zone of two-sublattice order, and one of the dispersions eventually softens at the  $\Gamma$ -point, as we approach the classical boundary of the plateau phase. This finding indicates a second-order transition into a two-sublattice ordered phase, in perfect agreement with the variational analysis that predicts the emergence of a supersolid phase. We may recall that while rotational symmetry around the  $z$  axis was preserved in the plateau phase, it is broken in the supersolid phase via the selection of a plane for the spin vectors.

---

<sup>4</sup>This behaviour is in sharp contrast with the one observed on the triangular lattice, where the single-site wavefunctions feature a director in the presence of an arbitrarily small biquadratic exchange.

<sup>5</sup>Note that the state breaks rotational symmetry around the  $z$  axis, so there is an extra degree of freedom associated with the selection of a common plane for the spin vectors.

<sup>6</sup>We may recall that there is no spontaneous magnetization in the  $xy$  plane.

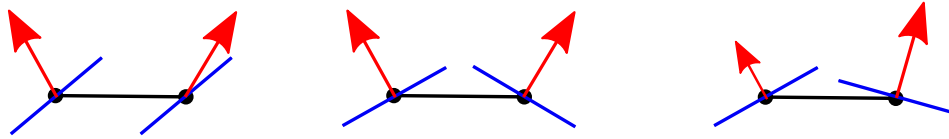


Figure 4.3: Spin vectors and quadrupolar directors on the two sublattices in the Néel phase for  $\vartheta < 0$  (left) and  $\vartheta > 0$  (middle), and in the supersolid phase (right). Dipole moments and directors are represented by red arrows and blue lines, respectively. Note that in the first picture, the directors are perpendicular to the plane of the spin vectors, whereas in the other pictures, they are in a common plane with them.

### 4.1.2 A numerical analysis of quantum effects

In order to check the scenario suggested by the mean-field calculations, A. M. Läuchli performed exact diagonalization studies of small clusters. In figure 4.4, we show magnetization curves for  $\vartheta = 3\pi/8$ . It appears that the plateau is indeed there, but starts only at a finite value of the field: below the plateau, there is another phase where the magnetization grows slowly from  $m = 0$ . We should emphasize that the magnetization process at  $\vartheta = 3\pi/8$  is representative of the entire “semi-ordered” region.

One may gain an insight into the nature of the zero-field phase by calculating the spin and quadrupole structure factors<sup>7</sup> via exact diagonalization for different momenta as a function of  $\vartheta$ : the results are shown in figure 4.5. For  $\vartheta = 0$ , the structure factor is the largest (and grows with the system size) at  $(\pi, \pi)$ , as we expect for a two-sublattice ordered Néel antiferromagnet. As we turn on a positive biquadratic exchange, the structure factor gradually decreases, and for  $\vartheta \approx 0.19\pi$ , a three-sublattice stripe order takes over with a structure factor that peaks at  $(2\pi/3, 2\pi/3)$ : spin-spin correlations prevail for  $\vartheta < \pi/4$ , while quadrupolar correlations become dominant in the region between the two  $SU(3)$  points. A three-sublattice ordering is also suggested by the peculiar dependence of the ground-state energy on the number of sites: we consistently get lower energies for clusters that are multiples of three. The low-energy spectrum of the 18-site cluster, shown for three different values of  $\vartheta$  in figure 4.6, provides further support for the above predictions: while the Anderson tower that is characteristic of two-sublattice Néel order is clearly recovered for sufficiently low values of  $\vartheta$ , it vanishes upon approaching the  $SU(3)$  point, and one eventually finds that for  $\vartheta > \pi/4$ , an Anderson tower emerges that corresponds to two copies of the Anderson tower of the three-

<sup>7</sup>The structure factor for a momentum  $\mathbf{k}$  is defined as  $\sum_j \exp(i\mathbf{k} \cdot \mathbf{R}_j) \langle C_0 C_j \rangle$ , where  $C_j$  stands for the spin or the quadrupolar operator at site  $j$ .

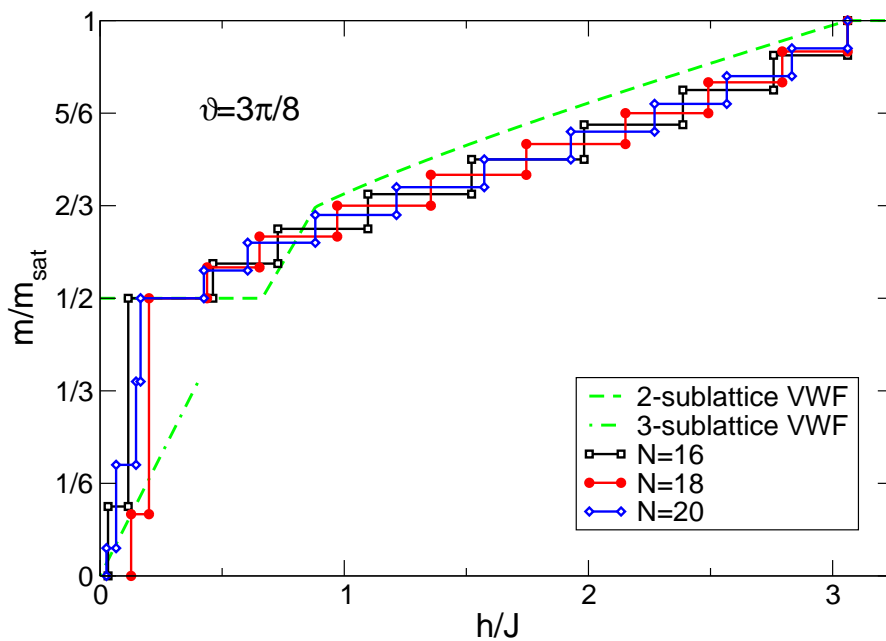


Figure 4.4: Magnetization curves of finite clusters for  $\vartheta = 3\pi/8$ . Variational magnetization curves are also shown for comparison: the dashed line is calculated with the help of the usual variational ansatz, while the dashed-dotted curve is the result of a restricted variational ansatz that assumes three-sublattice order. There is a clear indication of the presence of a 1/2-magnetization plateau.

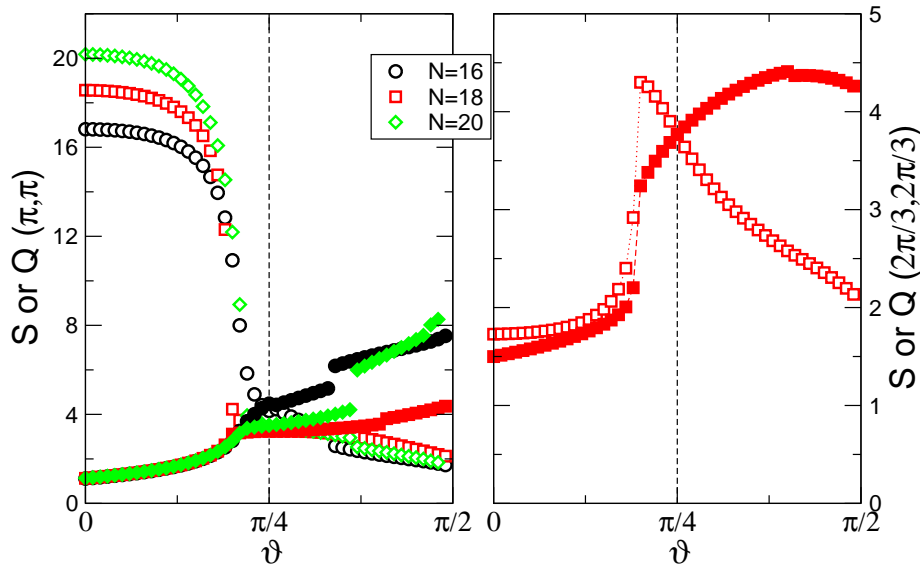


Figure 4.5: Structure factors for two different momenta, calculated by exact diagonalizations of small clusters. Empty (filled) symbols represent spin-spin (quadrupolar) correlations, while system sizes are labeled by the symbol type.

sublattice ordered antiferroquadrupolar state on the triangular lattice [18]. The two copies refer to the  $Z_2$  degeneracy of the state, i. e. to the orientation of the stripes. We should mention as a closing remark that while the stabilization of a three-sublattice ordered state on the square lattice is certainly an unexpected finding, it is not as difficult to accept as one may initially think. In fact, as we may recall from the discussion in subsection 2.2.2, the one-dimensional bilinear-biquadratic chain is in a critical phase between the  $SU(3)$  points  $\vartheta = \pi/4$  and  $\vartheta = \pi/2$ , and this phase features strong antiferroquadrupolar correlations with a period of three lattice spacings, therefore it does not seem unreasonable to assume that a long-range ordered state of similar character may emerge when quantum fluctuations become less pronounced due to an increase in dimensionality.

The strong tendency of quantum effects to drive the system towards three-sublattice ordering makes it tempting to see what the variational calculus yields, if we restrict it to three-sublattice ordered states. In figure 4.7, we sketch the spatial structure of single-site wavefunctions for a variational state that assumes either two- or three-sublattice order on the square lattice. In both cases, we may observe diagonal stripes, and there is an alternation between either two or three different stripes. However, a three-sublattice ordered state admits two inequivalent stripe orientations, which may be conveniently associated with the ordering wavevectors  $(2\pi/3, \pm 2\pi/3)$ . Upon

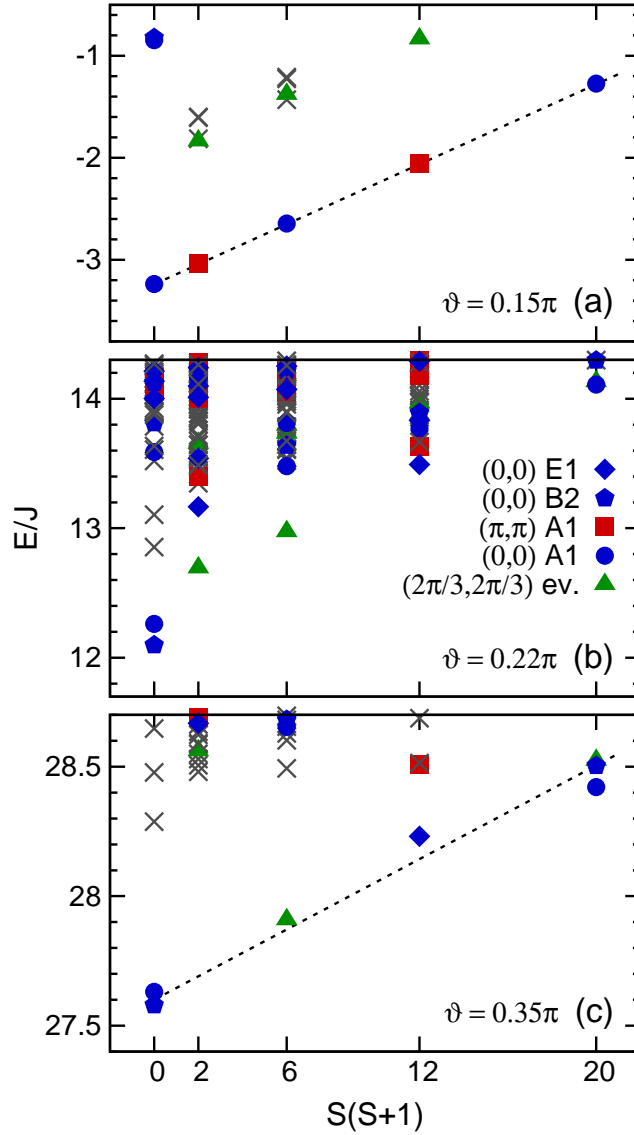


Figure 4.6: Energy spectrum of an 18-site cluster of the square lattice, calculated for three different values of  $\vartheta$ . In the vicinity of the Heisenberg point  $\vartheta = 0$ , the tower of states indicates two-sublattice Néel order (a), however, the structure obtained for  $\vartheta \lesssim \pi/4$  is difficult to interpret (b). The tower of states that is characteristic of the  $\vartheta > \pi/4$  region suggests the presence of a three-sublattice ordered antiferroquadrupolar phase (c).

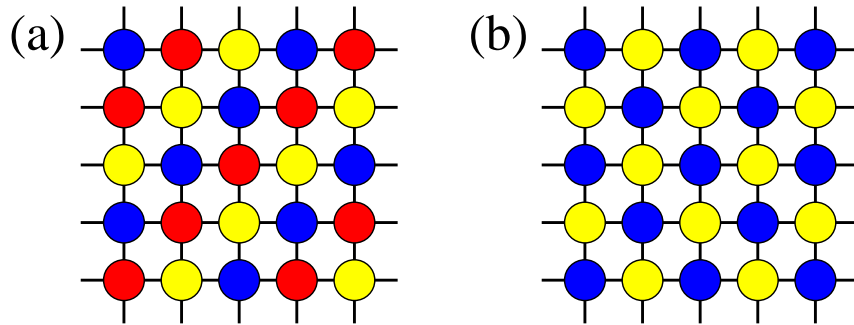


Figure 4.7: Pictorial representation of three-sublattice (a) and two-sublattice (b) order on the square lattice. For an ordered state of a given type, different colours correspond to different single-site wavefunctions in the variational ansatz.

taking a closer look at figure 4.7, it is easy to convince ourselves that minimizing the energy of a three-sublattice ordered variational wavefunction on the square lattice leads us back to solving the variational problem of a single triangle: indeed, the number of bonds connecting two given sublattices is  $2L/3$ , irrespective of which two sublattices we choose, and this gives rise to a frustration effect<sup>8</sup>. In zero magnetic field, we recover three quadrupolar states with mutually perpendicular directors for  $\pi/4 < \vartheta < \pi/2$ , which happens to be one of the many true variational ground-state configurations in the “semi-ordered” region, and as a result, a frustration relief occurs. However, once the magnetic field is finite, we may not expect to find the absolute variational energy-minimum using the restricted class of three-sublattice ordered states, since these may not account for the plateau phase, the supersolid phase or the canted Néel phase. According to [5], for sufficiently low fields, one of the sublattices retains a pure quadrupolar state with a director pinned parallel to the field, whereas the states on the other two sublattices develop a magnetic moment parallel to the field, however, the three directors remain mutually perpendicular in the process. We may characterize this phase with the help of the single-site wavefunctions

$$\begin{aligned}
 |\psi_1\rangle &= \cos(\pi/4 - \eta)|x\rangle + i \sin(\pi/4 - \eta)|y\rangle, \\
 |\psi_2\rangle &= \cos(\pi/4 - \eta)|y\rangle - i \sin(\pi/4 - \eta)|x\rangle, \\
 |\psi_3\rangle &= |z\rangle,
 \end{aligned}
 \tag{4.12}$$

<sup>8</sup>One should keep in mind that if the effective coupling constant on the triangle is taken to be  $J$ , the on-site magnetic field will have to be renormalized by a factor of  $1/2$ .

and a minimization with respect to  $\eta \in [0, \pi/4]$  gives

$$\sin^2 \eta = \frac{2 \cos \vartheta - \frac{h}{J}}{4 \cos \vartheta}. \quad (4.13)$$

When the magnetic field reaches the value  $h/J = 2 \cos \vartheta$ , which is above the boundary of the plateau phase, the magnetic sublattices become fully polarized, and the assumption of three-sublattice order will give rise to a distinct  $2/3$ -magnetization plateau. The magnetization curve, shown in figure 4.4 for  $\vartheta = 3\pi/8$ , is linear below this plateau. Let us emphasize once more that if a finite magnetic field is turned on in the region  $\pi/4 < \vartheta < \pi/2$ , the assumption of three-sublattice order leads to a variational energy that is higher than the one obtained with the help of the general variational ansatz. In fact, one may show by explicit calculation that the resulting mean-field state is unstable within the framework of linear wave theory.

### 4.1.3 “Order-by-disorder”

The fact that the variational picture is insufficient to account for the low-field numerical results is indicative of the presence of strong quantum fluctuations in the “semi-ordered” region. The large degeneracy of the variational solution for  $h = 0$  hints at an “order-by-disorder” effect: the spectrum of excitations and hence the zero-point energy will depend on the particular configuration, and this allows for a selection mechanism. In this subsection, we will use flavour-wave theory to calculate the zero-point energy associated with two-sublattice order and three-sublattice order in the region  $\pi/4 < \vartheta < \pi/2$ . The starting point of the upcoming analysis is essentially identical to that of the flavour-wave study of quadrupolar phases: see section 3.2 for details.

The three-sublattice ordered variational ground state corresponds to three quadrupolar states with perpendicular directors, we may therefore choose the single-site wavefunctions for sublattice  $A$ ,  $B$  and  $C$  as  $|z\rangle$ ,  $|x\rangle$  and  $|y\rangle$ , respectively, and induce quantum fluctuations via the familiar  $1/M$ -expansion. Carrying out the replacements

$$\begin{aligned} a_{zi}, a_{zi}^\dagger &\longrightarrow \sqrt{M - a_{xi}^\dagger a_{xi} - a_{yi}^\dagger a_{yi}}, \\ a_{xj}, a_{xj}^\dagger &\longrightarrow \sqrt{M - a_{yj}^\dagger a_{yj} - a_{zj}^\dagger a_{zj}}, \\ a_{yk}, a_{yk}^\dagger &\longrightarrow \sqrt{M - a_{zk}^\dagger a_{zk} - a_{xk}^\dagger a_{xk}}, \end{aligned} \quad (4.14)$$

for  $i \in A$ ,  $j \in B$  and  $k \in C$ , respectively, we end up with two independent bosonic operators per site, however, the lowest-order expansion of the interaction terms between site  $i$  of sublattice  $A$  and site  $j$  of sublattice  $B$  will

contain only two bosons of the possible four:

$$\mathbf{S}_i \mathbf{S}_j = -M (a_{xi}^\dagger a_{zj} + a_{xi} a_{zj}^\dagger - a_{xi}^\dagger a_{zj}^\dagger - a_{xi} a_{zj}) + O(\sqrt{M}) \quad (4.15)$$

and

$$P_{ij} = M (a_{xi}^\dagger a_{xi} + a_{zj}^\dagger a_{zj} + a_{xi}^\dagger a_{zj}^\dagger + a_{xi} a_{zj}) + O(\sqrt{M}). \quad (4.16)$$

We may introduce propagating states on each sublattice via a Fourier transformation of the form

$$\begin{aligned} a_{\mu i} &= \sqrt{\frac{3}{L}} \sum_{\mathbf{k} \in RBZ} e^{i\mathbf{k} \cdot \mathbf{R}_i} a_{\mu}(\mathbf{k}), \\ a_{\mu i}^\dagger &= \sqrt{\frac{3}{L}} \sum_{\mathbf{k} \in RBZ} e^{-i\mathbf{k} \cdot \mathbf{R}_i} a_{\mu}^\dagger(\mathbf{k}), \end{aligned} \quad (4.17)$$

where  $L$  denotes the total number of sites of the square lattice, and the sum extends over all  $\mathbf{k}$  vectors in the reduced Brillouin zone of three-sublattice order. Summing up all interaction terms between sublattices  $A$  and  $B$  leads to

$$\begin{aligned} &\sum_{i \in A} (\mathbf{S}_{\mathbf{R}_i} \mathbf{S}_{\mathbf{R}_i + \mathbf{a}_1} + \mathbf{S}_{\mathbf{R}_i} \mathbf{S}_{\mathbf{R}_i - \mathbf{a}_2}) = \\ &= -2M \sum_{\mathbf{k}} \{ \gamma(\mathbf{k}) a_x^\dagger(\mathbf{k}) a_z(\mathbf{k}) + \gamma(\mathbf{k})^* a_x(\mathbf{k}) a_z^\dagger(\mathbf{k}) - \\ &\quad - \gamma(\mathbf{k}) a_x^\dagger(\mathbf{k}) a_z^\dagger(-\mathbf{k}) - \gamma(\mathbf{k})^* a_x(\mathbf{k}) a_z(-\mathbf{k}) \} \end{aligned} \quad (4.18)$$

and

$$\begin{aligned} &\sum_{i \in A} (P_{\mathbf{R}_i \mathbf{R}_i + \mathbf{a}_1} + P_{\mathbf{R}_i \mathbf{R}_i - \mathbf{a}_2}) = \\ &= 2M \sum_{\mathbf{k}} \{ a_x^\dagger(\mathbf{k}) a_x(\mathbf{k}) + a_z^\dagger(\mathbf{k}) a_z(\mathbf{k}) + \\ &\quad + \gamma(\mathbf{k}) a_x^\dagger(\mathbf{k}) a_z^\dagger(-\mathbf{k}) + \gamma(\mathbf{k})^* a_x(\mathbf{k}) a_z(-\mathbf{k}) \}, \end{aligned} \quad (4.19)$$

where  $\mathbf{a}_1 = a\mathbf{e}_x$  and  $\mathbf{a}_2 = a\mathbf{e}_y$  are elementary lattice vectors of the square lattice, and  $\gamma(\mathbf{k}) = (e^{i\mathbf{k} \cdot \mathbf{a}_1} + e^{-i\mathbf{k} \cdot \mathbf{a}_2})/2$ . Note that we have omitted the sublattice indices, since  $a_x$  ( $a_z$ ) bosons come from the  $A$  ( $B$ ) sublattice, and the sublattices are chosen in such a way that they are spanned by the lattice vectors  $3\mathbf{a}_1$  and  $\mathbf{a}_1 + \mathbf{a}_2$ , furthermore the vectors  $\mathbf{a}_1$  and  $-\mathbf{a}_2$  connect

each site of sublattice  $A$  to its nearest neighbours from sublattice  $B$ . One may easily associate this configuration with a pictorial representation upon a straightforward introduction of the directions  $\mathbf{e}_x$  and  $\mathbf{e}_y$  in figure 4.7(a). Taking all the remaining interaction terms into account, we find that up to order  $M$ , the complete Hamiltonian may be written in the form

$$\frac{H}{J} = 2M^2L \sin \vartheta + 2M [h(a_{xA}, a_{zB}) + h(a_{yB}, a_{xC}) + h(a_{zC}, a_{yA})], \quad (4.20)$$

where

$$\begin{aligned} h(a, b) &= \\ &= (\sin \vartheta - \cos \vartheta) \sum_{\mathbf{k}} \{ \gamma(\mathbf{k}) a^\dagger(\mathbf{k}) b(\mathbf{k}) + \gamma(\mathbf{k})^* a(\mathbf{k}) b^\dagger(\mathbf{k}) - \\ &\quad - \gamma(\mathbf{k}) a^\dagger(\mathbf{k}) b^\dagger(-\mathbf{k}) - \gamma(\mathbf{k})^* a(\mathbf{k}) b(-\mathbf{k}) \} + \\ &+ \sin \vartheta \sum_{\mathbf{k}} \{ a^\dagger(\mathbf{k}) a(\mathbf{k}) + b^\dagger(\mathbf{k}) b(\mathbf{k}) + \\ &\quad + \gamma(\mathbf{k}) a^\dagger(\mathbf{k}) b^\dagger(-\mathbf{k}) + \gamma(\mathbf{k})^* a(\mathbf{k}) b(-\mathbf{k}) \}. \end{aligned} \quad (4.21)$$

Every boson enters the Hamiltonian (4.20), and the three terms  $h(a_{xA}, a_{zB})$ ,  $h(a_{yB}, a_{xC})$  and  $h(a_{zC}, a_{yA})$  may be diagonalized independently from each other<sup>9</sup>. We should emphasize that in the  $\vartheta \rightarrow \pi/4$  limit, one may associate the indices  $x$ ,  $y$  and  $z$  with an arbitrary basis in the Hilbert space of a spin one, i. e. the bosonic spectrum and the zero-point energy will be the same for any three-sublattice ordered state. The case of the other SU(3)-symmetric point is also special: the bond equation

$$(P_{12} - \mathbf{S}_1 \mathbf{S}_2) |x\rangle |y\rangle = 0 \quad (4.22)$$

implies that the variational state becomes an exact eigenstate of the initial Hamiltonian in the  $\vartheta \rightarrow \pi/2$  limit, and this results in an absence of quantum fluctuations. We will define the zero-point energy  $\varepsilon_{\text{ZP}}$  of a three-sublattice ordered state as the ground-state energy of the Hamiltonian (4.20) in the case  $M = 1$ , divided by the number of sites<sup>10</sup>: we obtain

$$\frac{\varepsilon_{\text{ZP}}}{J} = \frac{3}{L} \sum_{\mathbf{k}} \{ \omega_+(\mathbf{k}) + \omega_-(\mathbf{k}) \}, \quad (4.23)$$

<sup>9</sup>It is straightforward to extend our results to the triangular lattice, where the variational ground state in the  $\pi/4 < \vartheta < \pi/2$  region is also a three-sublattice ordered antiferroquadrupolar state.

<sup>10</sup>Note that in section 3.2, we used a slightly different definition and referred to the ground-state energy of the bosonic part of the flavour-wave Hamiltonian as “zero-point energy”.

where each of the dispersions

$$\omega_{\pm}(\mathbf{k}) = \sqrt{(\sin \vartheta \pm (\sin \vartheta - \cos \vartheta)|\gamma(\mathbf{k})|)^2 - (\cos \vartheta |\gamma(\mathbf{k})|)^2} \quad (4.24)$$

is three-fold degenerate. While  $\omega_+(\mathbf{k})$  is gapped all throughout the reduced Brillouin zone, the other branch features a line of zero modes: it can be shown that

$$\omega_-(\mathbf{k}) = 0 \Leftrightarrow |\gamma(\mathbf{k})| = 1 \Leftrightarrow k_y = -k_x \quad (4.25)$$

for an arbitrary value of  $\vartheta$ . This particular softening of the excitation spectrum may be seen as a sign of classical degeneracy: we may easily convince ourselves that a simultaneous rotation of the directors of two neighbouring diagonals in their common plane does not cost energy, as long as they remain perpendicular to each other, and such a wave-like excitation is essentially one-dimensional. This interpretation of the gapless modes is given further support, if we extend our calculus to the triangular lattice: indeed, we recover the same dispersions as the authors of [38], and the line of zero modes is absent, demonstrating a lift of this peculiar classical degeneracy<sup>11</sup>. Let us add as a closing remark that in the  $\vartheta \rightarrow \pi/4$  limit, the  $\omega_+$  branch also softens along the  $k_y = -k_x$  line, as it becomes degenerate with the  $\omega_-$  branch.

The two-sublattice ordered variational ground state corresponds to a pure quadrupolar state with a director  $\mathbf{d}$  and either another quadrupole with its director orthogonal to  $\mathbf{d}$ , or a spin vector of arbitrary length pointing along  $\mathbf{d}$ . We will choose the single-site wavefunctions for sublattice  $A$  and  $B$  as  $|z\rangle$  and  $\cos \eta|x\rangle + i \sin \eta|y\rangle$ , respectively, where  $\eta \in [0, \pi/4]$  is a freely varying parameter that is associated with the magnetization of the state<sup>12</sup>. Let us carry out a global rotation of the  $a_x$  and  $a_y$  operators:

$$\begin{aligned} a_{\uparrow}^{\dagger} &= \cos \eta a_x^{\dagger} + i \sin \eta a_y^{\dagger}, \\ a_{\uparrow} &= \cos \eta a_x - i \sin \eta a_y, \\ a_{\downarrow}^{\dagger} &= \sin \eta a_x^{\dagger} - i \cos \eta a_y^{\dagger}, \\ a_{\downarrow} &= \sin \eta a_x + i \cos \eta a_y, \end{aligned} \quad (4.26)$$

<sup>11</sup>A triangular lattice can be constructed by introducing cross-couplings perpendicular to the diagonals in figure 4.7(a). If we now rotate a neighbouring blue and red diagonal, there will be an increase in energy, unless we simultaneously rotate every other blue and red diagonal of the lattice.

<sup>12</sup>Note that the director of the magnetic sublattice may be rotated around the director of the ferroquadrupolar sublattice without an energy cost.

and use the inverse relations

$$\begin{aligned}
 a_x^\dagger &= \cos \eta a_\uparrow^\dagger + \sin \eta a_\downarrow^\dagger, \\
 a_x &= \cos \eta a_\uparrow + \sin \eta a_\downarrow, \\
 a_y^\dagger &= -i \sin \eta a_\uparrow^\dagger + i \cos \eta a_\downarrow^\dagger, \\
 a_y &= i \sin \eta a_\uparrow - i \cos \eta a_\downarrow
 \end{aligned} \tag{4.27}$$

to express all terms in the Hamiltonian. Condensing the  $a_z$  boson on sublattice  $A$  and the  $a_\uparrow$  boson on sublattice  $B$ , one finds the following interaction terms in the leading order of the  $1/M$ -expansion:

$$\begin{aligned}
 \mathbf{S}_i \mathbf{S}_j &= \\
 &= -M \left\{ \cos \xi (a_{\uparrow i}^\dagger a_{zj} + a_{\uparrow i} a_{zj}^\dagger) + \sin \xi (a_{\downarrow i}^\dagger a_{zj} + a_{\downarrow i} a_{zj}^\dagger) - \right. \\
 &\quad - (a_{\uparrow i}^\dagger a_{zj}^\dagger + a_{\uparrow i} a_{zj}) - \sin^2 \xi (a_{\uparrow i}^\dagger a_{\uparrow i} - a_{\downarrow i}^\dagger a_{\downarrow i}) + \\
 &\quad \left. + \sin \xi \cos \xi (a_{\uparrow i}^\dagger a_{\downarrow i} + a_{\downarrow i}^\dagger a_{\uparrow i}) \right\}
 \end{aligned} \tag{4.28}$$

and

$$P_{ij} = M (a_{\uparrow i}^\dagger a_{\uparrow i} + a_{zj}^\dagger a_{zj} + a_{\uparrow i}^\dagger a_{zj}^\dagger + a_{\uparrow i} a_{zj}), \tag{4.29}$$

where site  $i$  ( $j$ ) belongs to sublattice  $A$  ( $B$ ), furthermore  $\xi = 2\eta \in [0, \pi/2]$ . One may notice that the bilinear interaction does not involve the  $a_\downarrow$  boson of the  $B$  sublattice, while the transposition operator leaves out the  $a_\downarrow$  boson of the  $A$  sublattice as well. We introduce propagating states on each sublattice via a Fourier transformation of the form

$$\begin{aligned}
 a_{\mu i} &= \sqrt{\frac{2}{L}} \sum_{\mathbf{k} \in RBZ} e^{i\mathbf{k} \cdot \mathbf{R}_i} a_\mu(\mathbf{k}), \\
 a_{\mu i}^\dagger &= \sqrt{\frac{2}{L}} \sum_{\mathbf{k} \in RBZ} e^{-i\mathbf{k} \cdot \mathbf{R}_i} a_\mu^\dagger(\mathbf{k}),
 \end{aligned} \tag{4.30}$$

where  $L$  denotes the total number of sites of the square lattice and the sum extends over all  $\mathbf{k}$  vectors in the reduced Brillouin zone of two-sublattice

order. Summing up all interaction terms leads to

$$\begin{aligned}
& \sum_{i \in A} \sum_{\boldsymbol{\delta}} \mathbf{S}_{\mathbf{R}_i} \mathbf{S}_{\mathbf{R}_i + \boldsymbol{\delta}} = \\
& = -4M \sum_{\mathbf{k}} \left\{ \cos \xi \gamma(\mathbf{k}) (a_{\uparrow}^{\dagger}(\mathbf{k}) a_z(\mathbf{k}) + a_{\uparrow}(\mathbf{k}) a_z^{\dagger}(\mathbf{k})) + \right. \\
& \quad + \sin \xi \gamma(\mathbf{k}) (a_{\downarrow}^{\dagger}(\mathbf{k}) a_z(\mathbf{k}) + a_{\downarrow}(\mathbf{k}) a_z^{\dagger}(\mathbf{k})) - \\
& \quad - \gamma(\mathbf{k}) (a_{\uparrow}^{\dagger}(\mathbf{k}) a_z^{\dagger}(-\mathbf{k}) + a_{\uparrow}(\mathbf{k}) a_z(-\mathbf{k})) - \\
& \quad - \sin^2 \xi (a_{\uparrow}^{\dagger}(\mathbf{k}) a_{\uparrow}(\mathbf{k}) - a_{\downarrow}^{\dagger}(\mathbf{k}) a_{\downarrow}(\mathbf{k})) + \\
& \quad \left. + \sin \xi \cos \xi (a_{\uparrow}^{\dagger}(\mathbf{k}) a_{\downarrow}(\mathbf{k}) + a_{\downarrow}^{\dagger}(\mathbf{k}) a_{\uparrow}(\mathbf{k})) \right\} \tag{4.31}
\end{aligned}$$

and

$$\begin{aligned}
& \sum_{i \in A} \sum_{\boldsymbol{\delta}} P_{\mathbf{R}_i \mathbf{R}_i + \boldsymbol{\delta}} = \\
& = 4M \sum_{\mathbf{k}} \left\{ a_{\uparrow}^{\dagger}(\mathbf{k}) a_{\uparrow}(\mathbf{k}) + a_z^{\dagger}(\mathbf{k}) a_z(\mathbf{k}) + \right. \\
& \quad \left. + \gamma(\mathbf{k}) (a_{\uparrow}^{\dagger}(\mathbf{k}) a_z^{\dagger}(-\mathbf{k}) + a_{\uparrow}(\mathbf{k}) a_z(-\mathbf{k})) \right\}, \tag{4.32}
\end{aligned}$$

where we have omitted the sublattice indices: every ‘‘up’’ and ‘‘down’’ boson comes from sublattice  $A$ , while the  $a_z$  bosons belong to sublattice  $B$ . The  $\boldsymbol{\delta}$  vectors point towards the four nearest neighbours of a site, and  $\gamma(\mathbf{k}) = (\cos(\mathbf{k} \cdot \mathbf{a}_1) + \cos(\mathbf{k} \cdot \mathbf{a}_2))/2$ , where  $\mathbf{a}_1 = a\mathbf{e}_x$  and  $\mathbf{a}_2 = a\mathbf{e}_y$  are elementary lattice vectors of the square lattice. Up to order  $M$ , the Hamiltonian assumes the form

$$\frac{H}{J} = 2M^2 L \sin \vartheta + 4Mh(a_{\uparrow A}, a_{zB}, a_{\downarrow A}), \tag{4.33}$$

where

$$\begin{aligned}
 h(a, b, c) &= \\
 &= (\sin \vartheta - \cos \vartheta) \sum_{\mathbf{k}} \left\{ \cos \xi \gamma(\mathbf{k}) (a^\dagger(\mathbf{k})b(\mathbf{k}) + a(\mathbf{k})b^\dagger(\mathbf{k})) + \right. \\
 &\quad + \sin \xi \gamma(\mathbf{k}) (c^\dagger(\mathbf{k})b(\mathbf{k}) + c(\mathbf{k})b^\dagger(\mathbf{k})) - \\
 &\quad - \gamma(\mathbf{k}) (a^\dagger(\mathbf{k})b^\dagger(-\mathbf{k}) + a(\mathbf{k})b(-\mathbf{k})) - \\
 &\quad - \sin^2 \xi (a^\dagger(\mathbf{k})a(\mathbf{k}) - c^\dagger(\mathbf{k})c(\mathbf{k})) + \\
 &\quad \left. + \sin \xi \cos \xi (a^\dagger(\mathbf{k})c(\mathbf{k}) + a(\mathbf{k})c^\dagger(\mathbf{k})) \right\} + \\
 &+ \sin \vartheta \sum_{\mathbf{k}} \left\{ a^\dagger(\mathbf{k})a(\mathbf{k}) + b^\dagger(\mathbf{k})b(\mathbf{k}) + \right. \\
 &\quad \left. + \gamma(\mathbf{k}) (a^\dagger(\mathbf{k})b^\dagger(-\mathbf{k}) + a(\mathbf{k})b(-\mathbf{k})) \right\}.
 \end{aligned} \tag{4.34}$$

The “down” bosons from sublattice  $B$  do not enter the Hamiltonian (4.33), and therefore they form a completely flat band in the reduced Brillouin zone. This is indicative of the fact that the variational solution allows for a local rotation on any set of sites of sublattice  $B$ , provided that ferroquadrupolar order is preserved on sublattice  $A$ . In the  $\vartheta \rightarrow \pi/4$  limit, local rotations are allowed on both sublattices, which results in another flat band that is associated with the “down” bosons of sublattice  $A$ , furthermore, the remaining two bosons may actually correspond to any two orthogonal spin-one states. At the other  $SU(3)$ -symmetric point, the variational state becomes an exact eigenstate of the initial Hamiltonian, therefore the zero-point energy will coincide with the variational energy when  $\vartheta \rightarrow \pi/2$ . Rewriting the bosonic part of the Hamiltonian (4.33) as

$$\begin{aligned}
 h(a, b, c) &= \sum_{\mathbf{k}} \left\{ (a^\dagger(\mathbf{k}) \quad b^\dagger(\mathbf{k}) \quad c^\dagger(\mathbf{k})) M_1(\mathbf{k}) \begin{pmatrix} a(\mathbf{k}) \\ b(\mathbf{k}) \\ c(\mathbf{k}) \end{pmatrix} + \right. \\
 &\quad + (a^\dagger(\mathbf{k}) \quad b^\dagger(\mathbf{k}) \quad c^\dagger(\mathbf{k})) M_2(\mathbf{k}) \begin{pmatrix} a^\dagger(-\mathbf{k}) \\ b^\dagger(-\mathbf{k}) \\ c^\dagger(-\mathbf{k}) \end{pmatrix} + \\
 &\quad \left. + (a(\mathbf{k}) \quad b(\mathbf{k}) \quad c(\mathbf{k})) M_2(\mathbf{k}) \begin{pmatrix} a(-\mathbf{k}) \\ b(-\mathbf{k}) \\ c(-\mathbf{k}) \end{pmatrix} \right\},
 \end{aligned} \tag{4.35}$$

where

$$\begin{aligned} \frac{M_1(\mathbf{k})}{\sin \vartheta} &= \\ &= \begin{pmatrix} (\cot \vartheta - 1) \sin^2 \xi + 1 & (1 - \cot \vartheta) \cos \xi \gamma(\mathbf{k}) & (1 - \cot \vartheta) \sin \xi \cos \xi \\ (1 - \cot \vartheta) \cos \xi \gamma(\mathbf{k}) & 1 & (1 - \cot \vartheta) \sin \xi \gamma(\mathbf{k}) \\ (1 - \cot \vartheta) \sin \xi \cos \xi & (1 - \cot \vartheta) \sin \xi \gamma(\mathbf{k}) & (1 - \cot \vartheta) \sin^2 \xi \end{pmatrix}, \\ \frac{M_2(\mathbf{k})}{\sin \vartheta} &= \begin{pmatrix} 0 & \cot \vartheta \gamma(\mathbf{k}) & 0 \\ 0 & 0 & 0 \\ 0 & 0 & 0 \end{pmatrix}, \end{aligned} \quad (4.36)$$

we may obtain a convenient form for a Bogoliubov transformation. The zero-point energy, defined in analogy with the case of three-sublattice order, becomes

$$\frac{\varepsilon_{\text{ZP}}}{J} = \frac{2}{L} \sum_{\mathbf{k}} \{\omega_1(\mathbf{k}) + \omega_2(\mathbf{k}) + \omega_3(\mathbf{k})\}, \quad (4.37)$$

where the three dispersions are given as the positive eigenvalues of the matrix

$$\begin{pmatrix} M_1(\mathbf{k}) & M_2(\mathbf{k}) + M_2(\mathbf{k})^T \\ -M_2(\mathbf{k}) - M_2(\mathbf{k})^T & -M_1(\mathbf{k}) \end{pmatrix}. \quad (4.38)$$

If the magnetization is non-vanishing, i. e.  $0 < \xi \leq \pi/2$ , two of the branches are gapped, while the third one features a soft mode at  $\mathbf{k} = 0$ . However, if both sublattices are ferroquadrupolar ( $\xi = 0$ ), the “down” bosons of sublattice  $A$  do not enter the Hamiltonian, which leads to a completely flat band in the spectrum<sup>13</sup>. Among the remaining two branches, one is gapped, while the other one softens at the  $\Gamma$ -point.

In figure 4.8(a), we compare the zero-point energies of the two-sublattice ordered antiferroquadrupolar state, the 1/2-magnetization plateau, and the three-sublattice ordered antiferroquadrupolar state in the region  $\pi/4 \leq \vartheta \leq \pi/2$ . We find that three-sublattice order prevails in a convincing manner all throughout the region, and this conclusion remains valid even if one takes into account two-sublattice ordered configurations with an arbitrary magnetization value  $0 < m < 1/2$ , since their zero-point energy can be shown to increase with a decreasing  $m$ . In other words, even though quantum fluctuations favour the 1/2-magnetization plateau among all states with two-sublattice order, it is still not plausible for small magnetic fields. An estimate can be given of the extent of the three-sublattice ordered phase in the magnetic phase diagram between the two SU(3) points by comparing the

<sup>13</sup>In this case, local rotations are allowed on both sublattices.

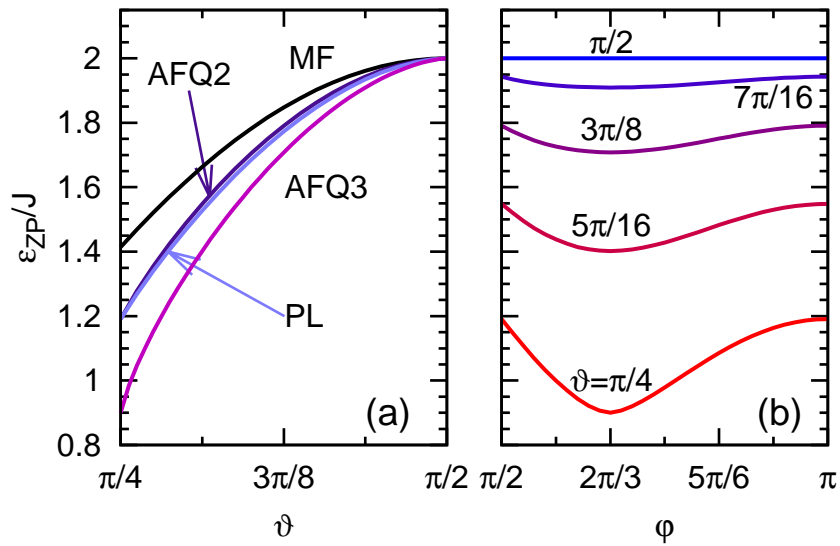


Figure 4.8: (a) Zero-point energy of the two-sublattice ordered antiferro-quadrupolar state “AFQ2”, the 1/2-magnetization plateau “PL”, and the three-sublattice ordered antiferroquadrupolar state “AFQ3”, as a function of  $\vartheta$ . The variational energy “MF” is also shown for comparison. (b) Zero-point energy of the helical states as a function of  $\varphi$ , for different values of  $\vartheta$ . All  $\pi/4 \leq \vartheta < \pi/2$  curves feature a minimum at  $\varphi = 2\pi/3$ , while the  $\vartheta = \pi/2$  curve is completely flat.

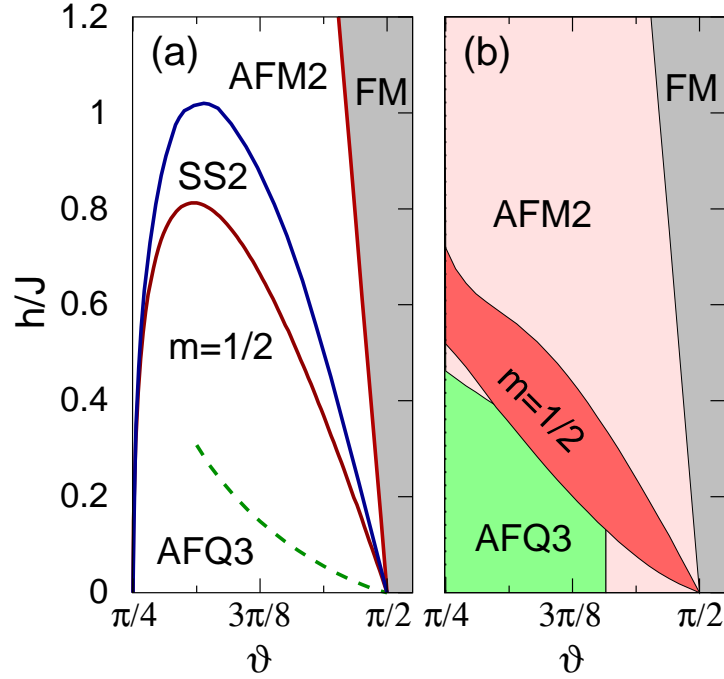


Figure 4.9: (a) Variational phase diagram of the “semi-ordered” region in the presence of a magnetic field. AFM2 and SS2 denote two-sublattice ordered Néel and supersolid phases, respectively, while FM stands for ferromagnet. Flavour-wave theory suggests that a three-sublattice ordered phase (AFQ3) is stabilized by quantum fluctuations: the dashed line represents an estimate of the corresponding phase boundary. (b) The ground states of the 18-site cluster, calculated via exact diagonalizations.

zero-point energy at  $h = 0$  to the Zeeman-energy of different states. Based on the discussion at the end of the previous subsection, one may deduce that the variational energy per site of the three-sublattice ordered state is  $\varepsilon_3 = \varepsilon_{\text{SO}} - h^2/6J_1$ , where  $J_1 = J \cos \vartheta$ , and it decreases slower in the field than the energy of the  $1/2$ -magnetization plateau given by  $\varepsilon_2 = \varepsilon_{\text{SO}} - h/2$ . Therefore, assuming that the change in the zero-point energy difference may be principally attributed to the classical magnetic energy terms, the extent of the three-sublattice ordered phase will eventually be limited by the linear Zeeman-energy of the plateau state: we show a sketch of the phase boundary in figure 4.9. In agreement with the numerical results, flavour-wave theory predicts that a considerable fraction of the variationally conjectured plateau phase is replaced by a three-sublattice ordered phase in the presence of quantum fluctuations.

#### 4.1.4 The role of helical states

In the previous subsection, we have demonstrated that quantum fluctuations on top of the three-sublattice ordered classical ground state induce a line of zero-energy excitations in the Brillouin zone<sup>14</sup> for  $\pi/4 < \vartheta < \pi/2$ . On the one hand this line of soft modes defined by  $k_x + k_y = 0$  reduces considerably the zero-point energy of the state, but on the other it can be shown to yield a divergent correction to the classical order parameter and thereby render linear wave theory inconsistent. On the classical level, one may interpret the presence of this line as an indicator of degeneracy, similarly to the  $(0, 0)$  and  $(\pi, \pi)$  Goldstone modes of the Néel state of a conventional spin-one-half antiferromagnet on the square lattice<sup>15</sup>. In the present case, we may select a  $\mathbf{k}$  vector of arbitrary length along the line, which implies that one may construct helical states of one continuous parameter in the classical ground-state manifold. Quantum fluctuations will lift the degeneracy of these helices, however, three-sublattice order may only prevail if its zero-point energy remains the lowest. In this subsection, we shall investigate the stability of three-sublattice order with respect to helical states.

Let us write the single-site wavefunction of a general helical state in the form

$$|\psi_{\mathbf{R}}\rangle = U^{R_x - R_y} |\psi_0\rangle, \quad (4.39)$$

where  $U$  is an  $SU(3)$  matrix, the vectors  $\mathbf{R} = R_x a \mathbf{e}_x + R_y a \mathbf{e}_y$  are lattice vectors of the square lattice, and  $a$  is the lattice constant. Our choice corresponds to a helix with  $k_x + k_y = 0$ , as the single-site wavefunction does not change along the diagonals where  $R_x - R_y$  is kept fixed. If we allow for a magnetic diagonal, it follows that the neighbouring diagonals will have to feature identical quadrupolar states, and we eventually end up with a two-sublattice ordered state of alternating quadrupolar and magnetic diagonals over the whole lattice. Such states may be discarded immediately, since their energy is higher than that of the three-sublattice ordered antiferroquadrupolar state in the presence of quantum fluctuations. However, if we restrict ourselves to pure quadrupolar states,  $U$  may be associated with a fixed-angle rotation of the directors around a given axis, and as a result, we obtain a

<sup>14</sup>Even though the dispersion with a line of soft modes is defined in the reduced Brillouin zone of three-sublattice order, it is three-fold degenerate, thus in total we may define one dispersion with a line of soft modes over the complete Brillouin zone of the square lattice.

<sup>15</sup>Both of these modes arise due to the breaking of spin-rotational symmetry. One may create the corresponding classical helices  $|\psi_{(0,0)}\rangle = \prod_{\mathbf{R}} U |\uparrow_{\mathbf{R}}\rangle$  and  $|\psi_{(\pi,\pi)}\rangle = \prod_{\mathbf{R}} U'^{R_x + R_y} |\uparrow_{\mathbf{R}}\rangle$ , where  $U$  and  $U'$  are  $SU(2)$  matrices,  $U'^2 = 1$ , and  $|\uparrow_{\mathbf{R}}\rangle$  is either  $|\uparrow\rangle$  or  $|\downarrow\rangle$ , depending on whether  $\mathbf{R} = R_x a \mathbf{e}_x + R_y a \mathbf{e}_y$  belongs to sublattice  $A$  or  $B$ . One may parametrize the matrices  $U$  and  $U'$  and minimize the classical energy with respect to the resulting parameters. In both cases, we end up with the conventional Néel state.

quadrupolar umbrella configuration. Let the  $z$  axis be the axis of the rotation, let us choose the state of the site  $R_x = R_y = 0$  as  $\cos \eta |z\rangle - \sin \eta |y\rangle$ , where  $\eta \in [0, \pi/2]$ , and let  $\varphi \in [0, \pi]$  denote the angle of the rotation with a corresponding direction defined according to the right-hand rule, as  $R_x - R_y$  is increased<sup>16</sup>: the resulting configuration may be described by the single-site wavefunctions

$$|\psi_{\mathbf{R}}\rangle = \cos \eta |z\rangle + \sin \eta [\sin((R_x - R_y)\varphi) |x\rangle - \cos((R_x - R_y)\varphi) |y\rangle]. \quad (4.40)$$

In the “semi-ordered” phase, neighbouring sites have to feature orthogonal wavefunctions, which leads to the condition

$$\cos^2 \eta + \sin^2 \eta \cos \varphi = 0. \quad (4.41)$$

The condition (4.41) may only be satisfied for  $\varphi \in [\pi/2, \pi]$ , and the parameter  $\eta$  is given by

$$\sin^2 \eta = \frac{1}{1 - \cos \varphi}. \quad (4.42)$$

We may conclude that the three-sublattice ordered ( $\varphi = 2\pi/3$ ) and the two-sublattice ordered ( $\varphi = \pi/2$  or  $\varphi = \pi$ ) antiferroquadrupolar states are in fact adiabatically connected to each other via a class of helical states. We should emphasize that while the stabilization of two-sublattice order may be excluded on the basis of our earlier results, there is no a priori reason to rule out the emergence of a helical phase with  $\varphi \neq 2\pi/3$  in the “semi-ordered” region, and it is important to keep in mind in this respect that a helical state with an incommensurate wavevector close to  $(2\pi/3, \pm 2\pi/3)$  can not be detected by exact diagonalization methods. Nonetheless, the effect of quantum fluctuations can be studied at the harmonic level via the use of flavour-wave theory. Since the calculation of the excitation spectrum of the helical states is similar to the one shown in subsection 3.2.2, we prefer to omit technical details and we discuss the results straightaway instead. We obtain two dispersive branches for an arbitrary value of the helical parameter in the region  $\pi/2 < \varphi < \pi$ : one of the dispersions is gapped all throughout the Brillouin zone, while the other one retains the  $k_x + k_y = 0$  line of zero modes, i. e. the qualitative behaviour of the excitation spectrum is independent of the helical parameter. A plot of the zero-point energy is shown as a function of  $\varphi$ , for different values of  $\pi/4 \leq \vartheta \leq \pi/2$ , in figure 4.8(b). We find that apart from the  $\vartheta = \pi/2$  point, where all helical states are eigenstates of the Hamiltonian, quantum fluctuations favour three-sublattice order for an arbitrary value of  $\vartheta$ .

<sup>16</sup>In this case, a choice of  $\pi \leq \varphi \leq 2\pi$  could be interpreted as a rotation of angle  $2\pi - \varphi$  in the inverse direction.

## 4.2 Three-sublattice ordering of the SU(3) Heisenberg model

This section will be devoted to the investigation of the properties of the SU(3) Heisenberg model on the square lattice, which can be seen both as a special high-symmetry point of the SU(2) spin-one bilinear-biquadratic model, when the two couplings are equal, and as an effective model of strongly interacting three-flavour fermions in an optical lattice. For the sake of simplicity, we will define the model as

$$H = J \sum_{\langle i,j \rangle} P_{ij}, \quad (4.43)$$

where  $J > 0$  sets an energy scale and  $P_{ij}$  is the familiar transposition operator that exchanges the states of sites  $i$  and  $j$ . We aim to present an overview of the results of the previous section that are relevant to the model (4.43) and provide further arguments in favour of the stabilization of three-sublattice order by extending both the semi-classical and the numerical analysis. We will also study the “order-by-disorder” phenomenon in the presence of thermal fluctuations and discuss the role of dimensionality.

### 4.2.1 Semi-classical approach

In subsection 4.1.4, we have demonstrated the existence of one-parameter helical states that connect the two-sublattice ordered state to the three-sublattice ordered one. In the “semi-ordered” region, these states corresponded to a quadrupolar umbrella configuration, however, as we have already suggested in subsection 4.1.3, this need not be the case for the SU(3)-symmetric model. In fact, based on (4.40), we may now characterize a general helical state with the help of the single-site wavefunctions

$$|\psi_{\mathbf{R}}\rangle = \cos \eta |z'\rangle + \sin \eta [\sin((R_x + R_y)\varphi) |x'\rangle - \cos((R_x + R_y)\varphi) |y'\rangle], \quad (4.44)$$

where  $\varphi \in [\pi/2, \pi]$ ,  $\eta \in [0, \pi/2]$  is given by (4.42), and the set of states  $|x'\rangle$ ,  $|y'\rangle$  and  $|z'\rangle$  forms an arbitrary basis in the local Hilbert space of a site<sup>17</sup>. Thinking of a spin-one system, we are not restricted to time-reversal-invariant single-site wavefunctions in the presence of SU(3) symmetry: for instance, if we choose  $|x'\rangle = i|x\rangle$ ,  $|y'\rangle = i|y\rangle$  and  $|z'\rangle = |z\rangle$ , where  $|x\rangle$ ,  $|y\rangle$  and  $|z\rangle$  are the familiar quadrupolar states, we obtain a magnetic helix for any value  $\varphi \neq \pi/2$ . In these helices, neighbouring spin vectors subtend an angle  $\varphi$  with each

<sup>17</sup>Note that in contrast to (4.40), we have now chosen a helix with  $k_y = k_x$ , as this choice will facilitate the extension of our results to higher dimensions.

other, and the spin length is given by  $\sin(2\eta)$ . The case  $\varphi = \pi$  corresponds to the conventional Néel state with fully polarized spin vectors, while the helix  $\varphi = \pi/2$  describes two-sublattice antiferroquadrupolar order: the two configurations have the same classical energy for the SU(3)-symmetric model (4.43).

In order to derive the excitation spectrum of the helical states, we may rely on the formalism of subsection 3.2.2. Using the rotation matrix

$$U_i^\dagger = \begin{pmatrix} \sin \eta \sin \varphi_i & -\sin \eta \cos \varphi_i & \cos \eta \\ -\cos \eta \sin \varphi_i & \cos \eta \cos \varphi_i & \sin \eta \\ \cos \varphi_i & \sin \varphi_i & 0 \end{pmatrix}, \quad (4.45)$$

where  $\varphi_i = (R_x^i + R_y^i)\varphi$ , we may introduce a local rotation of the form

$$\begin{pmatrix} a_{1i} \\ a_{2i} \\ a_{3i} \end{pmatrix} = U_i^\dagger \begin{pmatrix} a_{x'i} \\ a_{y'i} \\ a_{z'i} \end{pmatrix} \quad (4.46)$$

and express the transposition operator with the help of the new bosons in accordance with (3.64). For a pair of nearest-neighbour sites that satisfy  $\varphi_j - \varphi_i = \varphi$ , we obtain

$$\begin{aligned} P_{ij} &= \\ &= M \left\{ (a_2^\dagger \ a_3^\dagger) \begin{pmatrix} -\cos \varphi & \sqrt{-\cos \varphi \sqrt{1 + \cos \varphi}} \\ \sqrt{-\cos \varphi \sqrt{1 + \cos \varphi}} & 1 + \cos \varphi \end{pmatrix} \begin{pmatrix} a_2 \\ a_3 \end{pmatrix} + \right. \\ &\quad + (b_2^\dagger \ b_3^\dagger) \begin{pmatrix} -\cos \varphi & -\sqrt{-\cos \varphi \sqrt{1 + \cos \varphi}} \\ -\sqrt{-\cos \varphi \sqrt{1 + \cos \varphi}} & 1 + \cos \varphi \end{pmatrix} \begin{pmatrix} b_2 \\ b_3 \end{pmatrix} + \\ &\quad + (a_2^\dagger \ a_3^\dagger) \begin{pmatrix} -\cos \varphi & -\sqrt{-\cos \varphi \sqrt{1 + \cos \varphi}} \\ \sqrt{-\cos \varphi \sqrt{1 + \cos \varphi}} & -(1 + \cos \varphi) \end{pmatrix} \begin{pmatrix} b_2^\dagger \\ b_3^\dagger \end{pmatrix} + \\ &\quad \left. + (a_2 \ a_3) \begin{pmatrix} -\cos \varphi & -\sqrt{-\cos \varphi \sqrt{1 + \cos \varphi}} \\ \sqrt{-\cos \varphi \sqrt{1 + \cos \varphi}} & -(1 + \cos \varphi) \end{pmatrix} \begin{pmatrix} b_2 \\ b_3 \end{pmatrix} \right\} + \\ &\quad + O(1), \end{aligned} \quad (4.47)$$

where we have denoted the bosons on site  $i$  and  $j$  by  $a$  and  $b$ , respectively. We would like to emphasize that the matrices in the expression (4.47) are independent of our original choice of the basis states  $|x'\rangle$ ,  $|y'\rangle$  and  $|z'\rangle$ , which demonstrates explicitly that harmonic quantum fluctuations will only distinguish between helices with a different helical parameter<sup>18</sup>. A Fourier transformation over the whole lattice, followed by a Bogoliubov transformation,

<sup>18</sup>The conclusion remains valid in the presence of anharmonic terms as well, due to the SU(3) symmetry of the model (4.43).

## 4.2. Three-sublattice ordering of the SU(3) Heisenberg model 111

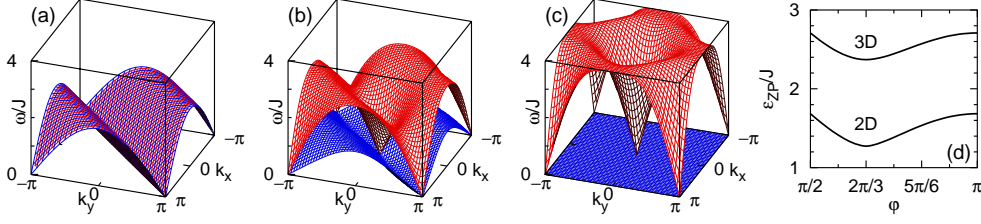


Figure 4.10: Flavour-wave dispersions of (a) the three-sublattice ordered state, (b) a helical state with  $\varphi = 0.75\pi$ , and (c) the two-sublattice ordered state. (d) Zero-point energy per site, as a function of the helical parameter. The minimum is located at  $\varphi = 2\pi/3$  in both two and three dimensions.

yields the ground-state energy of the flavour-wave Hamiltonian at the level of harmonic fluctuations:

$$\frac{\varepsilon_{\text{ZP}}}{J} = \frac{1}{2L} \sum_{\mathbf{k}} \{\omega_1(\mathbf{k}) + \omega_2(\mathbf{k})\}, \quad (4.48)$$

where we have omitted a constant term  $-2$  on the right-hand side<sup>19</sup>. The dispersions are given by the equation

$$\omega^4 - 4 [2(1 - \gamma\gamma^*) + (2 - \gamma^2 - (\gamma^*)^2)(1 + 2\cos\varphi)] \omega^2 + 256(\cos\varphi + \cos^2\varphi)^2(1 - \gamma\gamma^*)^2 = 0, \quad (4.49)$$

where  $\gamma = \gamma(\mathbf{k}) = (e^{ik_x} + e^{ik_y})/2$  (the lattice constant is chosen as unity). For the three-sublattice ordered state, the branches are degenerate,

$$\omega_1(\mathbf{k}) = \omega_2(\mathbf{k}) = 2\sqrt{1 - |\gamma(\mathbf{k})|^2}, \quad (4.50)$$

while in the case of two-sublattice order, i. e.  $\varphi = \pi/2$  and  $\varphi = \pi$ , one finds the dispersions

$$\begin{aligned} \omega_1(\mathbf{k}) &= 0, \\ \omega_2(\mathbf{k}) &= 2\sqrt{4 - (\gamma(\mathbf{k}) + \gamma^*(\mathbf{k}))^2}. \end{aligned} \quad (4.51)$$

The corresponding spectra are shown in figures 4.10(a) and 4.10(c). All helical states give rise to a line of zero modes, as we demonstrate by an example in figure 4.10(b). A comparison of the zero-point energies is shown in figure 4.10(d): in accordance with the results of subsection 4.1.4 (see figure

<sup>19</sup>In fact, the energy of the state is lowered in the presence of quantum fluctuations. We may recall that the classical energy value is zero.

4.8(b)), we find that among all helical states, the three-sublattice ordered one is favoured by quantum fluctuations. We have also compared the zero-point energy of the three-sublattice ordered state with that of random ground states on finite clusters, as well as with that of stripe states featuring three different stripes with a higher period, with the conclusion that it is always lower. In summary, the three-sublattice ordered state appears to be quite robust within the framework of flavour-wave theory.

### 4.2.2 Numerical approach

The numerical study of the spin-one bilinear-biquadratic model that we presented in subsection 4.1.2 mainly focused on the magnetization process, the behaviour of the correlation functions as a function of  $\vartheta$ , and the structure of the low-energy spectrum in the “semi-ordered” region, however, it nonetheless provided a strong indication that three-sublattice order may be stabilized at the SU(3)-symmetric point  $\vartheta = \pi/4$ . Let us now address directly the properties of the Hamiltonian (4.43) via exact diagonalization calculations for finite clusters. The results presented in this subsection are credited to A. M. Läuchli.

The energy per site for square samples of up to 20 sites is shown in figure 4.11(a): as it was suggested in subsection 4.1.2, the energy is significantly lower for the samples whose number of sites is a multiple of 3 (9 and 18), providing evidence in favour of a three-sublattice symmetry breaking. In order to check if the continuous SU(3) symmetry is also broken, we have plotted in figure 4.11(b) the energy levels as a function of the quadratic Casimir operator  $C_2$  of SU(3), keeping track of the irreducible representations (IRs) of the space group symmetry. Should a symmetry breaking occur, one expects the low-energy part of the spectrum to align linearly as a function of  $C_2$ , giving rise to a tower of states [52]. This is clearly the case in figure 4.11(b), as highlighted by the dashed line. This tower of states can be thought of as a combination of two towers corresponding to the two possible propagation directions, which results in the finite-size splitting of some levels (e.g.  $\Gamma A1$  and  $\Gamma B2$ ), as well as the increased degeneracy of some IRs (e.g.  $W$ ). Note also that the tower is not as well-separated from the rest of the spectrum as in other systems [52], which is a consequence of the “order-by-disorder” selection mechanism that leads to low-lying excitations associated with other mean-field solutions. The structure of the energy spectrum further indicates that the state with an equal population of the SU(3) basis states is stable with respect to the occurrence of spontaneous population imbalance or phase separation. Finally, based on an inspection of the real-space correlation functions of the 18-site sample, one may roughly estimate the ordered moment to

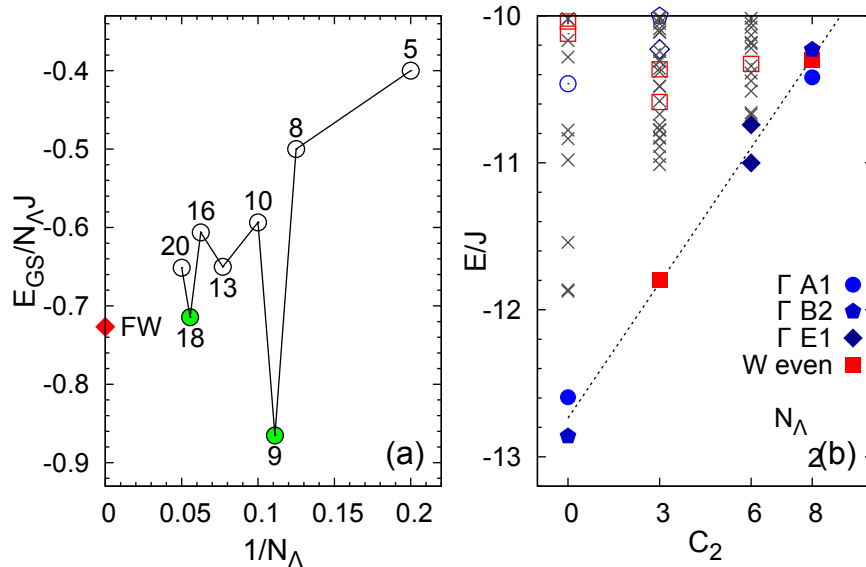


Figure 4.11: (a) Energy per site from exact diagonalizations of various finite-size square clusters, compared to the flavour-wave (FW) result. (b) Tower of states for 18 sites.  $\Gamma$  denotes points in the centre of the Brillouin zone, with A1 and B2 one-dimensional and E1 two-dimensional IRs, while W is a four-dimensional IR with wavevectors  $(\pm 2\pi/3, \pm 2\pi/3)$ .

be about 60-70% of the saturation value. Long-wavelength fluctuations on larger systems might further reduce this moment, but with such a large value on 18 sites, we expect the order to survive in the thermodynamic limit<sup>20</sup>. Altogether, we may conclude that exact diagonalization calculations provide very clear evidence in favour of the three-sublattice ordered flavour-wave state.

### 4.2.3 Thermal fluctuations and dimensionality

We should emphasize that the selection of the three-sublattice ordered state is quite surprising from the point of view of “order-by-disorder”. Indeed, the two-sublattice ordered state has by far the largest number of zero modes<sup>21</sup>, and according to common wisdom, it should be selected. However, this need not be the case for quantum fluctuations: if the non-zero modes have sufficiently large energy, they may compensate for the vanishing contribution

<sup>20</sup>We note that the ordered moment may not be estimated within linear flavour-wave theory, due to the line of zero modes.

<sup>21</sup>We may recall that a completely flat band is found in the excitation spectrum, due to the fact that a local rotation is allowed on any site.

of the zero modes. This is what happens here for the two-sublattice ordered structure, the upper branch of which is larger than twice the degenerate branch of the three-sublattice ordered structure, for all wavevectors. By contrast, for thermal fluctuations, the stabilization of the configuration with the largest number of zero modes is systematic, since the low-temperature free energy reads [53]

$$F = E_0 - \frac{N_{ZM}}{4} T \ln T - \frac{N_M - N_{ZM}}{2} T \ln T, \quad (4.52)$$

where  $N_M$  is the total number of modes and  $N_{ZM}$  is the number of zero modes. The classical spectrum is found for the helical states by replacing the creation and the annihilation operators in (4.47) by complex numbers<sup>22</sup>: its four branches are given by the equation

$$\lambda^2 - 2 [2 \pm (1 + 2 \cos \varphi)(\gamma + \gamma^*)] \lambda + 16(-\cos \varphi - \cos^2 \varphi) (1 - \gamma\gamma^*) = 0. \quad (4.53)$$

Similarly to the SU(2) case, the classical and the quantum spectrum are different, but they are related to each other: in particular, one may show that if the classical spectrum softens for a wavevector  $\mathbf{k}$ , the quantum spectrum will also soften at the same wavevector  $\mathbf{k}$ , and vice versa. Therefore, this analysis predicts that thermal fluctuations stabilize the two-sublattice ordered state, in agreement with classical Monte Carlo simulations [54].

Let us now briefly discuss the model (4.43) on the cubic lattice. The quantum spectrum of the helical states is easily generalized for the case of a lattice of dimension  $D$ : one only needs to replace equation (4.49) by

$$\omega^4 - D^2 [2(1 - \gamma\gamma^*) + (2 - \gamma^2 - (\gamma^*)^2)(1 + 2 \cos \varphi)^2] \omega^2 + 16D^4(\cos \varphi + \cos^2 \varphi)^2(1 - \gamma\gamma^*)^2 = 0, \quad (4.54)$$

and redefine  $\gamma$  as  $\gamma = \gamma(\mathbf{k}) = (e^{ik_x} + e^{ik_y} + \dots)/D$ . The zero-point energy of the helical states is shown in figure 4.10(d) for the cubic lattice: we find that the three-sublattice ordered helical structure is again favoured by quantum fluctuations. Equation (4.53) is generalized as

$$\lambda^2 - D [2 \pm (1 + 2 \cos \varphi)(\gamma + \gamma^*)] \lambda + 4D^2(-\cos \varphi - \cos^2 \varphi) (1 - \gamma\gamma^*) = 0, \quad (4.55)$$

and we may convince ourselves that the two-sublattice ordered state possesses the largest number of zero modes for  $D = 3$ , as well as for  $D = 2$ , therefore, as far as entropic selection is concerned, we reach the same conclusion in both cases.

---

<sup>22</sup>We note that in the literature, the term ‘‘classical spectrum’’ may often refer to the quantum spectrum obtained in linear wave theory.

The above results enable us to make predictions both for the square and the cubic lattice, and we may expect that the competition between quantum and thermal “order-by-disorder” leads to a rather rich physics. In both 2D and 3D, the system should first develop two-sublattice ordering tendencies, as it is cooled below the exchange scale. In two dimensions, we expect the system to undergo a finite-temperature transition at lower temperatures into a directionally ordered state (selection between the two independent spiral propagation directions), and to reach a three-sublattice ordered state at zero temperature. In three dimensions however, a finite-temperature transition into a two-sublattice ordered state is possible in principle, therefore we may think of two different scenarios. Upon lowering the temperature, the system might first undergo a transition into a two-sublattice ordered state, which is followed by a second transition into the three-sublattice ordered state selected by quantum fluctuations. Alternatively, it could undergo a direct first-order transition from the paramagnetic into the three-sublattice ordered state. A high-temperature series expansion of the SU(N) case on the 3D cubic lattice seems to favour the second possibility [55].

### 4.3 Instability of the Néel state below the antiferro SU(3) point

In the region  $0 \leq \vartheta < \pi/4$ , the variational ground state is unambiguous: it is a two-sublattice ordered Néel state with fully polarized spins. However, the considerable zero-point energy difference between the two-sublattice ordered and the three-sublattice ordered helical states at the SU(3) point makes it clear that quantum fluctuations will suppress this state in a finite window of  $\vartheta$  below the antiferro SU(3) point. This prediction of flavour-wave theory is in qualitative agreement with the numerical results of subsection 4.1.2: the structure factors in figure 4.5 indicate that three-sublattice stripe order emerges with dominant spin-spin correlations for  $\vartheta \approx 0.19\pi$ , and an instability of the two-sublattice ordered Néel state above this value of  $\vartheta$  is further suggested by the absence of the corresponding tower of states in the low-energy spectrum of finite-size clusters (see figure 4.6). We should emphasize however that the true nature of the ordering in the intermediate phase remains an elusive issue: first of all, the structure of the low-lying states is quite difficult to interpret in the region  $\vartheta \lesssim \pi/4$ , and secondly, we must bear in mind the deficiency of finite-size cluster methods in probing small shifts in the ordering wavevector. In this section, we will discuss the implications of flavour-wave theory concerning the region below the antiferro SU(3) point.

We will begin our analysis by investigating the excitation spectrum and the zero-point energy of the two-sublattice ordered Néel state in the region  $0 \leq \vartheta < \pi/4$ . We choose the single-site wavefunctions for sublattice  $A$  and  $B$  as  $(|x\rangle + i|y\rangle)/\sqrt{2}$  and  $(|x\rangle - i|y\rangle)/\sqrt{2}$ , respectively. Let us carry out a global rotation of the  $a_x$  and  $a_y$  operators:

$$\begin{aligned} a_{\uparrow}^{\dagger} &= \frac{1}{\sqrt{2}}(a_x^{\dagger} + ia_y^{\dagger}), \\ a_{\uparrow} &= \frac{1}{\sqrt{2}}(a_x - ia_y), \\ a_{\downarrow}^{\dagger} &= \frac{1}{\sqrt{2}}(a_x^{\dagger} - ia_y^{\dagger}), \\ a_{\downarrow} &= \frac{1}{\sqrt{2}}(a_x + ia_y), \end{aligned} \tag{4.56}$$

and use the inverse relations

$$\begin{aligned} a_x^{\dagger} &= \frac{1}{\sqrt{2}}(a_{\uparrow}^{\dagger} + a_{\downarrow}^{\dagger}), \\ a_x &= \frac{1}{\sqrt{2}}(a_{\uparrow} + a_{\downarrow}), \\ a_y^{\dagger} &= \frac{-i}{\sqrt{2}}(a_{\uparrow}^{\dagger} - a_{\downarrow}^{\dagger}), \\ a_y &= \frac{i}{\sqrt{2}}(a_{\uparrow} - a_{\downarrow}) \end{aligned} \tag{4.57}$$

to express all terms in the Hamiltonian. Condensing the  $a_{\uparrow}$  boson on sublattice  $A$  and the  $a_{\downarrow}$  boson on sublattice  $B$ , one finds the following interaction terms in the leading orders of the  $1/M$ -expansion:

$$\begin{aligned} \mathbf{S}_i \mathbf{S}_j &= -M^2 + \\ &+ M \{ 2a_{\downarrow i}^{\dagger} a_{\downarrow i} + 2a_{\uparrow j}^{\dagger} a_{\uparrow j} + a_{z i}^{\dagger} a_{z i} + a_{z j}^{\dagger} a_{z j} - \\ &- (a_{z i}^{\dagger} a_{z j}^{\dagger} + a_{z i} a_{z j}) \} \end{aligned} \tag{4.58}$$

and

$$P_{ij} = M (a_{\downarrow i}^{\dagger} a_{\downarrow i} + a_{\uparrow j}^{\dagger} a_{\uparrow j} + a_{\downarrow i}^{\dagger} a_{\uparrow j}^{\dagger} + a_{\downarrow i} a_{\uparrow j}), \tag{4.59}$$

where site  $i$  ( $j$ ) belongs to sublattice  $A$  ( $B$ ). One may notice that the spin-spin interaction involves all of the bosons, while the transposition operator leaves out the  $a_z$  bosons of both sublattices. We introduce propagating states

on each sublattice via a Fourier transformation of the form

$$\begin{aligned} a_{\mu i} &= \sqrt{\frac{2}{L}} \sum_{\mathbf{k} \in RBZ} e^{i\mathbf{k} \cdot \mathbf{R}_i} a_{\mu}(\mathbf{k}), \\ a_{\mu i}^{\dagger} &= \sqrt{\frac{2}{L}} \sum_{\mathbf{k} \in RBZ} e^{-i\mathbf{k} \cdot \mathbf{R}_i} a_{\mu}^{\dagger}(\mathbf{k}), \end{aligned} \quad (4.60)$$

where  $L$  denotes the total number of sites of the square lattice and the sum extends over all  $\mathbf{k}$  vectors in the reduced Brillouin zone of two-sublattice order. Summing up all interaction terms leads to

$$\begin{aligned} \sum_{i \in A} \sum_{\delta} \mathbf{S}_{\mathbf{R}_i} \mathbf{S}_{\mathbf{R}_i + \delta} &= -2LM^2 + \\ &+ 4M \sum_{\mathbf{k}} \{ 2 (a_{\downarrow}^{\dagger}(\mathbf{k}) a_{\downarrow}(\mathbf{k}) + a_{\uparrow}^{\dagger}(\mathbf{k}) a_{\uparrow}(\mathbf{k})) + \\ &\quad + a_{zA}^{\dagger}(\mathbf{k}) a_{zA}(\mathbf{k}) + a_{zB}^{\dagger}(\mathbf{k}) a_{zB}(\mathbf{k}) - \\ &\quad - \gamma(\mathbf{k}) (a_{zA}^{\dagger}(\mathbf{k}) a_{zB}^{\dagger}(-\mathbf{k}) + a_{zA}(\mathbf{k}) a_{zB}(-\mathbf{k})) \} \end{aligned} \quad (4.61)$$

and

$$\begin{aligned} \sum_{i \in A} \sum_{\delta} P_{\mathbf{R}_i \mathbf{R}_i + \delta} &= 4M \sum_{\mathbf{k}} \{ a_{\downarrow}^{\dagger}(\mathbf{k}) a_{\downarrow}(\mathbf{k}) + a_{\uparrow}^{\dagger}(\mathbf{k}) a_{\uparrow}(\mathbf{k}) + \\ &\quad + \gamma(\mathbf{k}) (a_{\downarrow}^{\dagger}(\mathbf{k}) a_{\uparrow}^{\dagger}(-\mathbf{k}) + a_{\downarrow}(\mathbf{k}) a_{\uparrow}(-\mathbf{k})) \}, \end{aligned} \quad (4.62)$$

where we have omitted the sublattice indices for the “down” and the “up” bosons, as they all come from sublattices  $A$  and  $B$ , respectively. The  $\delta$  vectors point towards the four nearest neighbours of a site, and  $\gamma(\mathbf{k}) = (\cos(\mathbf{k} \cdot \mathbf{a}_1) + \cos(\mathbf{k} \cdot \mathbf{a}_2))/2$ , where  $\mathbf{a}_1 = a\mathbf{e}_x$  and  $\mathbf{a}_2 = a\mathbf{e}_y$  are elementary lattice vectors of the square lattice. Up to order  $M$ , the Hamiltonian assumes the form

$$\frac{H}{J} = 2M^2L \sin \vartheta - 2M^2L (\cos \vartheta - \sin \vartheta) + 4M (h_1(a_{\downarrow A}, a_{\uparrow B}) + h_2(a_{zA}, a_{zB})), \quad (4.63)$$

where

$$h_1(a, b) = (2 \cos \vartheta - \sin \vartheta) \sum_{\mathbf{k}} \left\{ a^\dagger(\mathbf{k})a(\mathbf{k}) + b^\dagger(\mathbf{k})b(\mathbf{k}) + \frac{\tan \vartheta}{2 - \tan \vartheta} \gamma(\mathbf{k}) (a^\dagger(\mathbf{k})b^\dagger(-\mathbf{k}) + a(\mathbf{k})b(-\mathbf{k})) \right\} \quad (4.64)$$

and

$$h_2(c, d) = (\cos \vartheta - \sin \vartheta) \sum_{\mathbf{k}} \left\{ c^\dagger(\mathbf{k})c(\mathbf{k}) + d^\dagger(\mathbf{k})d(\mathbf{k}) - \gamma(\mathbf{k}) (c^\dagger(\mathbf{k})d^\dagger(-\mathbf{k}) + c(\mathbf{k})d(-\mathbf{k})) \right\} \quad (4.65)$$

are independent terms that can be diagonalized separately. A Bogoliubov transformation yields

$$h_1 = \sum_{\mathbf{k}} \omega_1(\mathbf{k}) (\alpha_1^\dagger(\mathbf{k})\alpha_1(\mathbf{k}) + \beta_1^\dagger(\mathbf{k})\beta_1(\mathbf{k})) + \sum_{\mathbf{k}} (\omega_1(\mathbf{k}) - (2 \cos \vartheta - \sin \vartheta)) \quad (4.66)$$

and

$$h_2 = \sum_{\mathbf{k}} \omega_2(\mathbf{k}) (\alpha_2^\dagger(\mathbf{k})\alpha_2(\mathbf{k}) + \beta_2^\dagger(\mathbf{k})\beta_2(\mathbf{k})) + \sum_{\mathbf{k}} (\omega_2(\mathbf{k}) - (\cos \vartheta - \sin \vartheta)), \quad (4.67)$$

where the dispersion relations are given as

$$\omega_1(\mathbf{k}) = (2 \cos \vartheta - \sin \vartheta) \sqrt{1 - \left( \frac{\tan \vartheta}{2 - \tan \vartheta} \gamma(\mathbf{k}) \right)^2} \quad (4.68)$$

and

$$\omega_2(\mathbf{k}) = (\cos \vartheta - \sin \vartheta) \sqrt{1 - \gamma^2(\mathbf{k})}, \quad (4.69)$$

furthermore both branches are two-fold degenerate in the reduced Brillouin zone of two-sublattice order. Setting  $\vartheta = \pi/4$ , we recover the dispersion relations that are characteristic of the SU(3) point: it is interesting to note that apart from the presence of a completely flat band, which can be attributed to the extra degree of freedom in local rotations, the flavour-wave expansion

of an SU(3) antiferromagnet gives the same spectrum of excitations as the spin-wave expansion of an SU(2) antiferromagnet, under the assumption of two-sublattice order. A closer look at the case  $\vartheta = 0$  reveals that while flavour-wave theory reproduces the conventional spin-wave branches for an SU(2) antiferromagnet, it also gives rise to a non-dispersive mode which is separated from the ground state by an energy gap of  $8J$ : while these high-lying excitations may be safely neglected in the treatment of conventional SU(2) antiferromagnets, they start to play a role once the biquadratic coupling is sufficiently strong. We will define the zero-point energy of the Néel state as the energy of the complete Hamiltonian (4.63) for  $M = 1$ , in accordance with the definition used in subsection 4.1.3.

Based on the discussion at the end of subsection 4.1.2, and on the results of subsection 3.1.1, we may deduce that within the framework of the variational picture, three-sublattice order in the region  $0 < \vartheta < \pi/4$  corresponds to a 120-degree ordering of partially developed spin vectors in a common plane. The single-site wavefunctions are given by the expressions (3.8) and (3.9), however, the energy per site needs to be rescaled by a factor of  $2/3$ , due to the reduced connectivity of the square lattice:

$$\frac{\varepsilon}{J} = \frac{2}{3} \left( 6 \sin \vartheta - \frac{(3 \sin \vartheta + 6 \cos \vartheta)^2}{3 \sin \vartheta + 24 \cos \vartheta} \right). \quad (4.70)$$

In contrast to the two-sublattice ordered Néel state, the three-sublattice ordered spiral state does not minimize the energy of every bond<sup>23</sup>, and one may explicitly show that linear flavour-wave theory breaks down for this state. However, we may nonetheless estimate its energy in the presence of quantum fluctuations by using an argument similar to the one presented at the end of subsection 4.1.3: we will assume that the change in the zero-point energy of the state may be approximated by the change in its classical energy, at least in the neighbourhood of the SU(3) point. In figure 4.12, we show a comparison of the zero-point energies of the two-sublattice ordered Néel state and the three-sublattice ordered spiral state: a naive assumption of a first-order transition yields an estimated phase boundary of  $\vartheta \approx (0.17 - 0.18)\pi$ , which is a slightly lower value than the one predicted by exact diagonalization calculations.

We should emphasize that the situation becomes more subtle once we consider the helical states that are adiabatically connected to the three-sublattice ordered state. The discussion presented at the beginning of subsection 4.2.1 suggests that upon an SU(3) rotation of the quadrupolar helices, we may ob-

---

<sup>23</sup>We may recall that the situation was drastically different in the “semi-ordered” region.

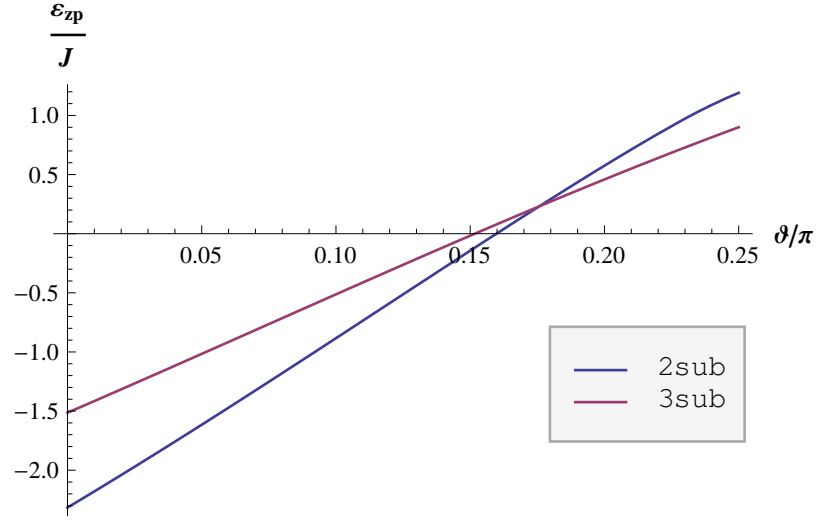


Figure 4.12: Zero-point energy per site of the two-sublattice ordered Néel state and the three-sublattice ordered spiral state, below the SU(3) point. While the earlier curve was calculated exactly in the framework of linear wave theory, the latter one relies on an approximation (see text for details). The boundary between the two phases is slightly below the one suggested by the numerical analysis of finite-size clusters.

tain magnetic helices that are characterized by the single-site wavefunctions

$$|\psi_{\mathbf{R}}\rangle = \cos \eta |z\rangle + i \sin \eta [\sin((R_x + R_y)\varphi)|x\rangle - \cos((R_x + R_y)\varphi)|y\rangle], \quad (4.71)$$

where  $\varphi \in [\pi/2, \pi]$  and  $\eta \in [0, \pi/2]$ . These helical states interpolate between the three-sublattice ordered spiral state ( $\varphi = 2\pi/3$ ) and the two-sublattice ordered Néel state ( $\varphi = \pi$ ). Upon minimizing the variational energy of these states in the region  $0 < \vartheta < \pi/4$ , we find

$$\sin^2 \eta = \frac{\sin \vartheta(1 + \cos \varphi) - 2 \cos \vartheta \cos \varphi}{\sin \vartheta(1 + \cos \varphi)^2 - 4 \cos \vartheta \cos \varphi} \quad (4.72)$$

and

$$\frac{\varepsilon}{J} = 2 \sin \vartheta + 2 \left( \sin \vartheta - \frac{(\sin \vartheta(1 + \cos \varphi) - 2 \cos \vartheta \cos \varphi)^2}{\sin \vartheta(1 + \cos \varphi)^2 - 4 \cos \vartheta \cos \varphi} \right). \quad (4.73)$$

Setting  $\vartheta = \pi/4$  recovers the condition (4.41), while setting  $\varphi = 2\pi/3$  reproduces (4.70). For an arbitrary value of  $\vartheta$ , the energy curve (4.73) features a minimum at  $\varphi = \pi$ , furthermore, one may show that  $\frac{dE}{d\varphi} < 0$  in general and

$\frac{dE}{d\varphi} = 0$  if and only if  $\varphi = \pi/2$ . Introducing the deviation  $\delta = 1/2 + \cos \varphi$  from the three-sublattice ordered state, we find that the variational energy of the helical states is a linear function of  $\delta$  around  $\varphi = 2\pi/3$ , and since the  $\vartheta = \pi/4$  curve in figure 4.8(b) seems to show quadratic behaviour around the minimum, one may argue on the basis of the approximation used in the previous paragraph that the helical parameter will immediately shift from the value  $\varphi = 2\pi/3$  once we move away from the SU(3) point. Actually, a more thorough investigation of the zero-point energy curve for  $\vartheta = \pi/4$  reveals a non-analytic behaviour around the minimum:

$$\frac{\varepsilon_{\text{ZP}}}{J} = \frac{2\sqrt{2}}{\pi} + \frac{2\sqrt{2}}{\pi}\delta^2 \left( \ln \frac{4}{|\delta|} - 1 \right) + \dots, \quad (4.74)$$

where we neglected terms that are of higher order in  $\delta$ , however, the non-analyticity is not strong enough to pin the three-sublattice ordering for  $\vartheta < \pi/4$ .

In conclusion, linear wave theory presents us with two possible alternatives with respect to the nature of the ordering in the intermediate phase between the two-sublattice ordered Néel phase and the SU(3) point. Both of these proposals rely on an approximation of the zero-point energy for  $\vartheta < \pi/4$ , since linear wave theory breaks down for the helical states with  $\varphi \neq \pi$  in this region. We should emphasize that while neither the semiclassical approach nor the numerical study seems to be able to settle the question whether a three-sublattice ordered stripe state or a continuously evolving helical state, if any of the two, is a more likely candidate to be realized, they nonetheless provide strong arguments in favour of the destabilization of the Néel phase in a finite window below the antiferro SU(3) point.

## 4.4 Conclusions

In this chapter, we have explored the quantum phase diagram of the spin-one bilinear-biquadratic model on the square lattice: a summary of our results is shown in figure 4.13. We have demonstrated that the introduction of a magnetic field lifts the degeneracy in the “semi-ordered” phase and leads to the stabilization of a remarkable 1/2-magnetization plateau of mixed magnetic and quadrupolar character. Exact diagonalization calculations by A. M. Läuchli confirmed the presence of the plateau phase, however, they suggested that it emerges via a first-order transition from a state with finite spin susceptibility that governs the low-field limit. We have studied the zero-field case with the help of flavour-wave theory and have shown that

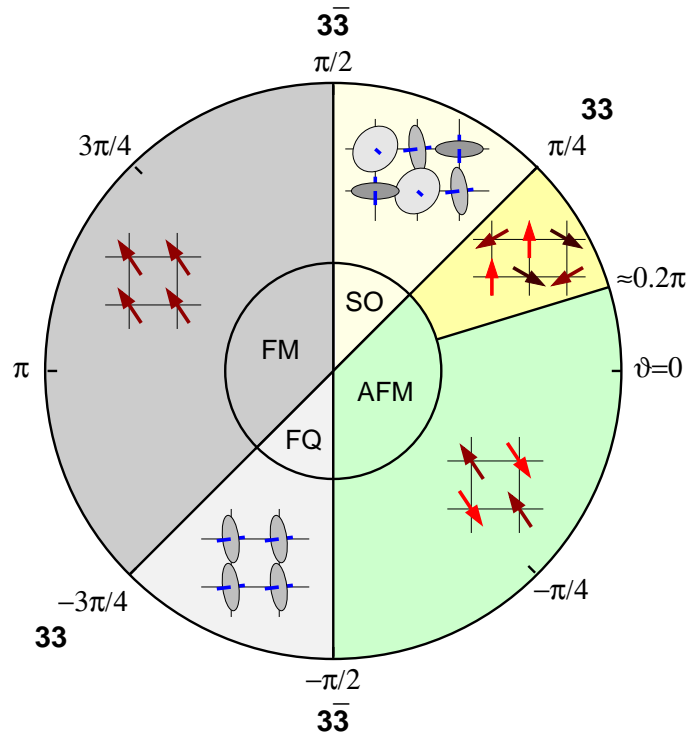


Figure 4.13: Schematic phase diagram of the spin-one bilinear-biquadratic model on the square lattice. The inner circle shows the variational results: the ferromagnetic, ferroquadrupolar and antiferromagnetic phases are denoted by FM, FQ and AFM, respectively, while SO stands for “semi-ordered”. The outer circle represents the numerical results. Quantum fluctuations give rise to a three-sublattice ordered antiferroquadrupolar phase in the region  $\pi/4 < \vartheta < \pi/2$ , and they destabilize the classical Néel state between  $\vartheta \approx 0.2\pi$  and  $\vartheta = \pi/4$ .

“order-by-disorder” mechanism gives rise to a three-sublattice ordered antiferroquadrupolar state in the entire “semi-ordered” region, which is a rather exotic finding for a bipartite lattice. We have thoroughly investigated the nature of the ordering at the antiferro SU(3) point as well, where we have uncovered a subtle competition between quantum and thermal fluctuations. We presented strong numerical and analytical arguments in support of the suppression of two-sublattice Néel order below the antiferro SU(3) point, and put forward alternative proposals for the intermediate phase. Finally, we have discussed the shortcomings of linear wave theory and finite-size studies in clarifying the role of helical states, and suggested that a more sophisticated analysis will be required to explore the properties of the intermediate phase.

Let us briefly discuss the experimental implications of our results. While we do not know of a spin-one antiferromagnet with sufficiently large bi-quadratic interactions to destabilize the Néel phase, ultracold atomic systems might provide a means of observing a three-sublattice ordered stripe state on the square lattice. Recent experimental advances using multi-flavour atomic gases [56, 57, 58, 59] have paved the way to the investigation of Mott-insulating states with more than two flavours in optical lattices [60, 61, 62, 63, 64], and since the exchange integral of the SU( $N$ ) case is equal to  $2t^2/U$ , independently of  $N$ , it is realistic to expect that the exchange scale can be reached for SU( $N$ ) fermions as soon as it is reached for SU(2) ones. In this respect, it will be important in experiments to carefully choose the optimal coupling strength  $U/t$ , which should be large enough to put the system into the Mott-insulating phase described by the SU(3) Heisenberg model, but not too large to lead to accessible values of the energy scale set by the exchange integral. The detection of three-sublattice order might be attempted using noise correlations [65], since the structure factor is expected to have a peak at the ordering wavevector, and a recent report of single atom resolution experiments [66, 67] suggests that direct imaging might also be possible, provided that some contrast can be achieved between different atomic species.



# Appendix A

## Stability analysis in the variational approach

In this appendix, we will discuss an analytic way to treat second-order instabilities in the framework of the variational approach. Let us assume that a numerical or analytical minimization of (3.5) in a parameter range  $R$  of the Hamiltonian (3.1) indicates the presence of a phase that is characterized by

$$|\psi_0\rangle = |\psi_1\rangle|\psi_2\rangle|\psi_3\rangle, \quad (\text{A.1})$$

where  $|\psi_1\rangle$ ,  $|\psi_2\rangle$  and  $|\psi_3\rangle$  may depend continuously and in a well-defined manner on the parameters of the Hamiltonian (3.1). Our goal is to investigate the question whether the phase reveals an instability of second order beyond the parameter region  $R$ , and if it does, to discuss the nature and the exact location of the corresponding second-order phase transition. We would like to emphasize that the method we present here might fail to capture a first-order transition that occurs before we reach the proposed point of instability, therefore its predictions will have to be verified numerically in general.

Let us allow for a continuous deviation of the wavefunction from (A.1) in the following form:

$$|\psi\rangle = \prod_{i=1}^3 \left( \sqrt{1 - \delta^2 (d_{i1}^* d_{i1} + d_{i2}^* d_{i2})} |\psi_i\rangle + \delta d_{i1} |\psi_{i1}\rangle + \delta d_{i2} |\psi_{i2}\rangle \right), \quad (\text{A.2})$$

where  $\mathbf{d} = (d_{11}, d_{12}, d_{21}, d_{22}, d_{31}, d_{32})$  is a complex vector of norm one, i. e.  $\mathbf{d}^* \cdot \mathbf{d} = 1$ ,  $\delta$  is a small non-negative parameter, i. e.  $0 \leq \delta \ll 1$ , furthermore, the normalized spin-one wavefunctions  $|\psi_{i1}\rangle$  and  $|\psi_{i2}\rangle$  are chosen such that together with  $|\psi_i\rangle$ , they form a basis in the Hilbert space of the local spin  $i$ . We assume that the quantity

$$\Delta\varepsilon = \langle \psi | H_\Delta | \psi \rangle - \langle \psi_0 | H_\Delta | \psi_0 \rangle \quad (\text{A.3})$$

has a series expansion with respect to  $\delta$  in the parameter region  $R$  of the Hamiltonian (3.1), and expanding it to second order leads to a non-vanishing result. A straightforward calculation shows that

$$\begin{aligned} \Delta\varepsilon = & \delta (\mathbf{d}^* \cdot \mathbf{v} + \mathbf{d} \cdot \mathbf{v}^*) + \\ & + \delta^2 \left( \frac{1}{2} \mathbf{d} \cdot H_1 \mathbf{d} + \frac{1}{2} \mathbf{d}^* \cdot H_1^+ \mathbf{d}^* + \mathbf{d}^* \cdot (H_2 - \varepsilon_0 I) \mathbf{d} \right) + \\ & + O(\delta^3), \end{aligned} \quad (\text{A.4})$$

where  $\varepsilon_0 = \langle \psi_0 | H_\Delta | \psi_0 \rangle$ ,

$$\mathbf{v} = \begin{pmatrix} \langle \psi_{11} | \langle \psi_2 | \langle \psi_3 | H_\Delta | \psi_0 \rangle \\ \langle \psi_{12} | \langle \psi_2 | \langle \psi_3 | H_\Delta | \psi_0 \rangle \\ \langle \psi_{13} | \langle \psi_2 | \langle \psi_3 | H_\Delta | \psi_0 \rangle \\ \vdots \\ \langle \psi_{14} | \langle \psi_2 | \langle \psi_3 | H_\Delta | \psi_0 \rangle \end{pmatrix}, \quad (\text{A.5})$$

and finally  $H_1$  ( $H_2$ ) is a symmetric (hermitian)  $6 \times 6$  matrix, whose explicit form is easy to derive but shall nonetheless be omitted here for brevity. Introducing the decomposition  $\mathbf{d} = \mathbf{d}_1 + i\mathbf{d}_2$ , where  $\mathbf{d}_1$  and  $\mathbf{d}_2$  are real vectors, the normalized vector  $\mathbf{D} = \begin{pmatrix} \mathbf{d}_1 \\ \mathbf{d}_2 \end{pmatrix}$ , the vector  $\mathbf{V} = \begin{pmatrix} \mathbf{v} + \mathbf{v}^* \\ i\mathbf{v}^* - i\mathbf{v} \end{pmatrix}$ , as well as the matrix

$$\Omega = \begin{pmatrix} H_2 - \varepsilon_0 I + \frac{1}{2}(H_1 + H_1^+) & iH_2 - i\varepsilon_0 I + \frac{i}{2}(H_1 - H_1^+) \\ -iH_2 + i\varepsilon_0 I + \frac{i}{2}(H_1 - H_1^+) & H_2 - \varepsilon_0 I - \frac{1}{2}(H_1 + H_1^+) \end{pmatrix}, \quad (\text{A.6})$$

we may rewrite  $\Delta\varepsilon$  in a concise manner:

$$\Delta\varepsilon = \delta \mathbf{D} \cdot \mathbf{V} + \delta^2 \mathbf{D} \cdot \Omega \mathbf{D} + O(\delta^3). \quad (\text{A.7})$$

The hermiticity of  $\Omega$  ensures the realness of the quadratic term, and the decomposition into real and imaginary parts,  $\Omega = \Re\Omega + i\Im\Omega$ , leads finally to

$$\Delta\varepsilon = \delta \mathbf{D} \cdot \mathbf{V} + \delta^2 \mathbf{D} \cdot \Re\Omega \mathbf{D} + O(\delta^3). \quad (\text{A.8})$$

The stability of the phase (A.1) in the parameter region  $R$  of the Hamiltonian (3.1) requires  $\mathbf{V} = 0$ , as well as that the symmetric matrix  $\Re\Omega$  be positive semidefinite<sup>1</sup>. Assuming that the above expansion can be extended in a continuous manner beyond the parameter region  $R$  with the linear term

<sup>1</sup>If the phase breaks a continuous symmetry of the Hamiltonian, the eigenvectors of  $\Re\Omega$  that can be associated with symmetry operations of the Hamiltonian will automatically belong to the eigenvalue zero.

still vanishing, one may look for a boundary across which one or more of the eigenvalues of  $\Re\Omega$  change sign. Let us suppose that we have only one such eigenvalue, we may then inject the corresponding eigenvector  $\mathbf{D}_1$  into the expression (A.3) and push the expansion to the first non-vanishing order at the boundary: if the resulting term contains an even power of  $\delta$  with a positive coefficient, we may talk about an instability of second order with respect to deformations along the vector  $\mathbf{D}_1$ , and conclude that we have found a second-order phase boundary<sup>2</sup>. If the eigenvalue that changes sign across the boundary is  $p$ -fold degenerate, we may find a set of orthonormal eigenvectors belonging to this eigenvalue,  $\{\mathbf{D}_i, i = 1 \dots p\}$ , and inject an arbitrary normalized real linear combination of the form  $\sum_{i=1}^p \alpha_i \mathbf{D}_i$  into the expression (A.3): the coefficients of a subsequent series expansion with respect to  $\delta$  at the boundary will then depend on  $\alpha_i$  and instability issues therefore become more complicated. We will only mention a simple case where the first non-vanishing term is of fourth order in  $\delta$  and has a positive coefficient: if the minimization of this coefficient with respect to  $\alpha_i$  yields a unique result, the corresponding vector  $\sum_{i=1}^p \alpha_i \mathbf{D}_i$  can be associated with the dominant instability.

Let us briefly demonstrate the practical use of the stability analysis outlined above by considering the isotropic model ( $D = 0$ ). The discussion at the end of subsection 2.2.3 suggested that spins on a triangular lattice would retain ferroquadrupolar order in a finite window above  $\vartheta = 3\pi/2$ , however, it did not reveal the true extent of the phase. Assuming that all directors are parallel to the  $z$  axis, we have  $|\psi_0\rangle = |z\rangle|z\rangle|z\rangle$ , and it is convenient to choose  $|\psi_{i1}\rangle = |x\rangle$  and  $|\psi_{i2}\rangle = |y\rangle$  for all  $i$ . Diagonalizing the matrix  $\Re\Omega$  for  $\vartheta = 3\pi/2$ , we find that the eigenvalue zero is two-fold degenerate, and the vectors

$$\begin{aligned} \mathbf{D}_1 &= \left( 0, \frac{1}{\sqrt{3}}, 0, \frac{1}{\sqrt{3}}, 0, \frac{1}{\sqrt{3}}, 0, 0, 0, 0, 0, 0 \right), \\ \mathbf{D}_2 &= \left( \frac{1}{\sqrt{3}}, 0, \frac{1}{\sqrt{3}}, 0, \frac{1}{\sqrt{3}}, 0, 0, 0, 0, 0, 0, 0 \right) \end{aligned} \quad (\text{A.9})$$

define a basis in the corresponding eigenspace. An arbitrary (normalized and real) linear combination of these vectors corresponds to a simultaneous rotation of the director axis on every site, and this deformation obviously costs no energy. In other words, the zero eigenvalue that we found may simply be attributed to the symmetry-breaking nature of the ferroquadrupolar

---

<sup>2</sup>We remind the reader again that we may not exclude on the basis of the present method that a first-order phase transition occurs before we reach the proposed second-order phase boundary.

phase, and the corresponding eigenspace is two-dimensional since the common director may tilt in two independent directions. All other eigenvalues of  $\Re\Omega$  are strictly positive for  $\vartheta = 3\pi/2$ , however, increasing the parameter  $\vartheta$ , we find that a four-fold degenerate eigenvalue eventually changes sign at  $\vartheta = 2\pi - \arctan 2 \approx 1.65\pi$ . The first six components of the corresponding eigenvectors vanish, which means that dipole moments start developing in the  $xy$  plane that is perpendicular to the directors. Injecting an arbitrary eigenvector  $\mathbf{D}$  into (A.3) and carrying out an expansion in  $\delta$  at the proposed phase boundary, we find that the first non-vanishing term is of order  $\delta^4$  and its coefficient is positive, hence the transition is expected to be continuous. Furthermore, it turns out that this coefficient is minimized only by eigenvectors that correspond to a 120-degree ordering of the dipole moments, such as the vector

$$\mathbf{D} = \frac{1}{\sqrt{3}} \left( 0, 0, 0, 0, 0, 0, 0, -1, \frac{\sqrt{3}}{2}, \frac{1}{2}, -\frac{\sqrt{3}}{2}, \frac{1}{2} \right). \quad (\text{A.10})$$

A numerical minimization of (3.5) confirms all of these predictions.

# Appendix B

## Ground-state configurations of the classical XXZ model on the triangular lattice

In this appendix, we derive analytically the ground-state configurations of the model

$$H = J \sum_{\langle i,j \rangle} \{ (\sigma_i^x \sigma_j^x + \sigma_i^y \sigma_j^y) + A \sigma_i^z \sigma_j^z \}, \quad (\text{B.1})$$

where  $J$  sets the energy scale, as well as the sign of the in-plane coupling,  $A \in [-\infty, +\infty]$  is the anisotropy parameter, and the spins  $\vec{\sigma}_i$  are classical vectors of length  $|\vec{\sigma}_i| = 1/2$  defined on the sites of a triangular lattice. In spite of the fact that this model has been studied extensively, we feel that a complete and detailed analysis of all ground-state configurations is still missing in the literature, and therefore we aim to present one in this appendix. Naturally, our discussion will rely on earlier works [68, 69, 70, 71].

We may convince ourselves, using arguments similar to those presented at the beginning of section 3.1, that it is a priori sufficient to consider the minimization problem on a triangular plaquette, however, as a second step, one has to examine whether setting the state on one triangular plaquette leads to a unique ground state over the whole lattice. The energy of a three-sublattice ordered configuration is given by

$$\begin{aligned} \frac{4E}{JL} &= \sin \vartheta_1 \sin \vartheta_2 \cos(\varphi_1 - \varphi_2) + \\ &+ \sin \vartheta_2 \sin \vartheta_3 \cos(\varphi_2 - \varphi_3) + \\ &+ \sin \vartheta_3 \sin \vartheta_1 \cos(\varphi_3 - \varphi_1) + \\ &+ A (\cos \vartheta_1 \cos \vartheta_2 + \cos \vartheta_2 \cos \vartheta_3 + \cos \vartheta_3 \cos \vartheta_1), \end{aligned} \quad (\text{B.2})$$

where  $\vartheta_i \in [0, \pi]$ ,  $\varphi_i \in [0, 2\pi[$  and  $\sin \vartheta_i = \sqrt{1 - \cos^2 \vartheta_i} \geq 0$ . Note that from the point of view of the physical interpretation of the configurations, it poses no problem whatsoever to leave the variables  $\{\vartheta_i, \varphi_i\}$  completely unconstrained: this enables us to treat the energy (B.2) as a smooth periodic function in all variables, which might only feature a minimum at stationary points. Obviously, due to periodicity, it is then sufficient to solve the stationary equations in a domain  $\{\vartheta_i, \varphi_i\} \in [-\pi, \pi[$ . In the following, we will use the notations  $s_i = \sin \vartheta_i$  and  $c_i = \cos \vartheta_i$  for brevity.

We begin our analysis by considering the case  $|A| \rightarrow \infty$ , where the in-plane couplings can be neglected. Dividing the energy (B.2) by  $A$ , we have

$$\frac{4E}{JAL} = c_1 c_2 + c_2 c_3 + c_3 c_1, \quad (\text{B.3})$$

i. e. the dependence on the  $\varphi_i$  variables is suppressed. It is then straightforward to consider  $\vartheta_i$  as freely running variables and look for stationary points of the energy by solving the system of equations  $\frac{\partial}{\partial \vartheta_i} \frac{4E}{JAL} = 0$ , which can be explicitly written as

$$\begin{aligned} s_1(c_2 + c_3) &= 0, \\ s_2(c_3 + c_1) &= 0, \\ s_3(c_1 + c_2) &= 0. \end{aligned} \quad (\text{B.4})$$

Taking into account the symmetry of reflection with respect to the  $xy$  plane, as well as the fact that one may freely permute the three spins, we find the following types of solutions:

$s_1 = s_2 = s_3 = 0$ : The spins are parallel to the  $z$  axis, ferromagnetic configurations such as  $\uparrow\uparrow\uparrow$  have energy  $4E/JL = 3A$ , while other configurations such as  $\uparrow\uparrow\downarrow$  have energy  $-A$ .

$c_2 + c_3 = s_2 = s_3 = 0$ : Two antiparallel spins are fixed along the  $z$  axis, while the third spin is arbitrary. The energy of this configuration is  $-A$ .

$c_2 + c_3 = c_3 + c_1 = s_3 = 0$ : These are configurations along the  $z$  axis of the type  $\uparrow\uparrow\downarrow$  with energy  $-A$ .

$c_2 + c_3 = c_3 + c_1 = c_1 + c_2 = 0$ : All spins are in the  $xy$  plane and the energy is zero.

We conclude that in the ferromagnetic case, i. e.  $JA < 0$ , all spins point in the (positive or negative)  $z$  direction, while in the antiferromagnetic case  $JA > 0$ ,

two of the spins are fixed along the  $z$  axis in an antiparallel way, and the third spin remains arbitrary. In this latter case, setting the spin configuration on one triangular plaquette does not determine the configuration over the whole lattice: in fact, similarly to the case of the Ising model, we are faced with a macroscopic classical degeneracy and a non-vanishing entropy at zero temperature.

Let us also give a brief reminder of the case of an isotropic exchange coupling. Setting  $A = 1$  enables us to rewrite the energy as

$$\frac{4E}{JL} = 4(\vec{\sigma}_1\vec{\sigma}_2 + \vec{\sigma}_2\vec{\sigma}_3 + \vec{\sigma}_3\vec{\sigma}_1) = 2(\vec{\sigma}_1 + \vec{\sigma}_2 + \vec{\sigma}_3)^2 - \frac{3}{2}, \quad (\text{B.5})$$

and therefore we may easily deduce that in the ferromagnetic case ( $J < 0$ ), all three spins point in the same direction and the energy of the configuration is 3, while for  $J > 0$ , the three spins are in a common plane subtending an angle of 120 degrees with each other and the energy is  $-3/2$ .

In the following sections, we will consider an arbitrary anisotropy parameter  $A \in ]-\infty, +\infty[$  (however, we will assume  $A \neq 1$ ) and derive all stationary configurations that are possible candidates for minimizing the energy. The discussion will naturally break into two parts, one where we treat the general case of so-called “non-planar” configurations, and one where we investigate “planar” configurations that feature all three spins in a common plane with the  $z$  axis. At the end of this rather technical analysis, we will present the phase diagram of the classical XXZ model. Finally, we will conclude the appendix by discussing some peculiar features of the XXZ model in the case of quantum spins.

## B.1 Stationary “non-planar” configurations

Returning to the expression (B.2), we may note that the energy is invariant under a simultaneous rotation of all three spins around the  $z$  axis, therefore we may choose  $\varphi_1 = 0$  without loss of generality. It will again prove useful to consider all other angles as freely running variables: this way, one may look for the energy minima simply by comparing the energy of all stationary points. Taking the derivatives with respect to  $\varphi_2$  and  $\varphi_3$ , we find the equations

$$\left. \begin{aligned} s_1 s_2 \sin \varphi_2 &= -s_2 s_3 \sin(\varphi_2 - \varphi_3) \\ s_3 s_1 \sin \varphi_3 &= s_2 s_3 \sin(\varphi_2 - \varphi_3) \end{aligned} \right\} \Rightarrow s_1 s_2 \sin \varphi_2 = -s_3 s_1 \sin \varphi_3,$$

while the derivatives with respect to  $\vartheta_i$  lead to the equations

$$\begin{aligned} c_1 (s_2 \cos \varphi_2 + s_3 \cos \varphi_3) &= A s_1 (c_2 + c_3), \\ c_2 (s_1 \cos \varphi_2 + s_3 \cos (\varphi_2 - \varphi_3)) &= A s_2 (c_3 + c_1), \\ c_3 (s_2 \cos (\varphi_2 - \varphi_3) + s_1 \cos \varphi_3) &= A s_3 (c_1 + c_2). \end{aligned} \quad (\text{B.6})$$

If we assume  $s_1 = 0$ , it follows that

$$0 = s_2 s_3 \sin (\varphi_2 - \varphi_3) = 4 (\sigma_2^y \sigma_3^x - \sigma_2^x \sigma_3^y) = -4 (\vec{\sigma}_2 \times \vec{\sigma}_3)^z, \quad (\text{B.7})$$

in other words, all three spins lie in a common plane with the  $z$  axis. Since the cases  $s_2 = 0$  and  $s_3 = 0$  yield similar results, and since we intend to treat such “planar” configurations separately, we have to assume  $s_1 s_2 s_3 \neq 0$ , which allows us to rewrite the system of equations as

$$\begin{aligned} s_1 \sin \varphi_2 &= -s_3 \sin (\varphi_2 - \varphi_3), \\ s_1 \sin \varphi_3 &= s_2 \sin (\varphi_2 - \varphi_3), \\ s_2 \sin \varphi_2 &= -s_3 \sin \varphi_3, \\ c_1 \frac{s_2 \cos \varphi_2 + s_3 \cos \varphi_3 + s_1}{s_1} - c_1 &= A (c_2 + c_3), \\ c_2 \frac{s_1 \cos \varphi_2 + s_3 \cos (\varphi_2 - \varphi_3) + s_2}{s_2} - c_2 &= A (c_3 + c_1), \\ c_3 \frac{s_2 \cos (\varphi_2 - \varphi_3) + s_1 \cos \varphi_3 + s_3}{s_3} - c_3 &= A (c_1 + c_2). \end{aligned} \quad (\text{B.8})$$

If we now assume  $\sin \varphi_2 \sin \varphi_3 \sin (\varphi_2 - \varphi_3) = 0$ , we find  $\sin \varphi_2 = \sin \varphi_3 = \sin (\varphi_2 - \varphi_3) = 0$  and we end up with “planar” configurations again. Therefore, let us write  $\sin \varphi_2 \sin \varphi_3 \sin (\varphi_2 - \varphi_3) \neq 0$  instead, which leads to a simplification in the last three equations: for instance, the fourth equation features the expression

$$\begin{aligned} \frac{s_2}{s_1} \cos \varphi_2 + \frac{s_3}{s_1} \cos \varphi_3 + 1 &= \frac{\sin \varphi_3 \cos \varphi_2 - \sin \varphi_2 \cos \varphi_3 + \sin (\varphi_2 - \varphi_3)}{\sin (\varphi_2 - \varphi_3)} = \\ &= 0. \end{aligned} \quad (\text{B.9})$$

We find that the  $c_i$  variables are solutions of the equation

$$\begin{pmatrix} 1 & A & A \\ A & 1 & A \\ A & A & 1 \end{pmatrix} \begin{pmatrix} c_1 \\ c_2 \\ c_3 \end{pmatrix} = 0, \quad (\text{B.10})$$

and the  $\varphi_i$  angles can be derived with the help of the following identities:

$$\begin{aligned} \frac{s_1^2 - s_2^2 - s_3^2}{2s_2s_3} &= \cos(\varphi_2 - \varphi_3), \\ \frac{s_3^2 - s_2^2 - s_1^2}{2s_1s_2} &= \cos \varphi_2, \\ \frac{s_2^2 - s_3^2 - s_1^2}{2s_1s_3} &= \cos \varphi_3. \end{aligned} \tag{B.11}$$

A trivial solution is given by  $c_1 = c_2 = c_3 = 0$ : in this case, all three spins are in the  $xy$  plane and, since  $s_i s_j \cos(\varphi_i - \varphi_j) = -1/2$ , they show 120-degree order with an energy value of  $-3/2$ . Noting that

$$\det \begin{pmatrix} 1 & A & A \\ A & 1 & A \\ A & A & 1 \end{pmatrix} = (1 - A)^2(1 + 2A), \tag{B.12}$$

we may deduce that another type of solution exists for  $A = -1/2$ : in this case,  $c_1 = c_2 = c_3 = \alpha$  is an arbitrary number in the interval  $] -1, 1[$ , furthermore  $s_i s_j \cos(\varphi_i - \varphi_j) = -1/2(1 - \alpha^2)$ , hence the spins form an umbrella around the  $z$  axis and they show 120-degree order in the  $xy$  plane. The energy of this configuration is given by

$$\frac{4E}{JL} = -\frac{3}{2}(1 - \alpha^2) - \frac{3}{2}\alpha^2 = -\frac{3}{2}, \tag{B.13}$$

and the case  $\alpha = 0$  reproduces the solution found earlier for an arbitrary  $A$ .

## B.2 Stationary “planar” configurations

Let us turn our attention now to configurations where all three spins lie in a common plane with the  $z$  axis. Without loss of generality, we may set  $\varphi_1 = \varphi_2 = \varphi_3 = 0$  if we extend the interval of the variables  $\vartheta_i$  to  $[-\pi, \pi[$ . The energy can then be written as

$$\frac{4E}{JL} = s_1s_2 + s_2s_3 + s_3s_1 + A(c_1c_2 + c_2c_3 + c_3c_1). \tag{B.14}$$

We may easily find the minimum in the special case  $A = 0$ : indeed, let us consider  $\vartheta_i$  as freely running variables and introduce the variables  $\vartheta_i^* = \pi/2 - \vartheta_i$ , then the energy assumes the simple form

$$\frac{4E}{JL} = c_1^*c_2^* + c_2^*c_3^* + c_3^*c_1^*, \tag{B.15}$$

which is identical to the one we encountered for  $|A| \rightarrow \infty$ . All in all, we find that in the ferromagnetic case, all spins point in the (positive or negative)  $x$  direction, while in the antiferromagnetic case, two of the spins are fixed along the  $x$  axis in an antiparallel way and the third spin remains arbitrary. However, one may note that the energy of this latter configuration is higher than that of the “non-planar” configuration featuring a 120-degree ordering of the spins in the  $xy$  plane. We conclude that for  $A = 0$ , all three spins are in the  $xy$  plane, and they show either ferromagnetic order ( $J < 0$  case) or 120-degree order ( $J > 0$  case).

Let us now consider the general case  $A \neq 0, 1$ . Leaving the variables  $\vartheta_i$  unconstrained, we find the following equations for the stationary points:

$$\begin{aligned} c_1 (s_2 + s_3) &= A s_1 (c_2 + c_3), \\ c_2 (s_3 + s_1) &= A s_2 (c_3 + c_1), \\ c_3 (s_1 + s_2) &= A s_3 (c_1 + c_2). \end{aligned} \tag{B.16}$$

It would be sufficient to solve this system of equations in the interval  $\vartheta_i \in [-\pi, \pi[$ , however, this is a non-trivial task due to the fact that the three  $\vartheta_i$  variables appear both through sine and cosine functions, i. e. one effectively has to treat six variables with three constraints of the type  $s_i^2 + c_i^2 = 1$  between them. We may introduce the function  $\tan(\vartheta_i/2)$  and use the formulae

$$\begin{aligned} \sin \vartheta_i &= \frac{2 \tan \frac{\vartheta_i}{2}}{1 + \tan^2 \frac{\vartheta_i}{2}}, \\ \cos \vartheta_i &= \frac{1 - \tan^2 \frac{\vartheta_i}{2}}{1 + \tan^2 \frac{\vartheta_i}{2}} \end{aligned} \tag{B.17}$$

in order to satisfy the constraints automatically, however, we have to keep in mind that the case where any of the  $\vartheta_i$  variables becomes  $-\pi$  can not be treated this way. Let us employ the notation  $t_i = \tan(\vartheta_i/2)$  for brevity, then we may rewrite the stationary equations as

$$\begin{aligned} (1 + t_2 t_3) ((1 - t_1^2)(t_2 + t_3) - 2A t_1 (1 - t_2 t_3)) &= 0, \\ (1 + t_3 t_1) ((1 - t_2^2)(t_3 + t_1) - 2A t_2 (1 - t_3 t_1)) &= 0, \\ (1 + t_1 t_2) ((1 - t_3^2)(t_1 + t_2) - 2A t_3 (1 - t_1 t_2)) &= 0. \end{aligned} \tag{B.18}$$

We can easily convince ourselves that demanding that the first term disappear in all three equations yields complex solutions, let us first assume therefore that the second term vanishes in the first equation, while the first term vanishes in the other two equations: in that case we find  $t_3 = t_2 = -1/t_1$ , furthermore  $(t_1^2 - 1)(1 - A) = 0$ . We conclude that for an arbitrary  $A$  there exist

stationary configurations with energy  $-1$ , where the spins are fixed along the  $x$  axis in an  $\uparrow\uparrow\downarrow$  arrangement. On the other hand, if we assume that the first term vanishes in the first equation, while the second term vanishes in the other two, we find the equations

$$\begin{aligned} t_2 t_3 &= -1, \\ (-1)t_3(1 - t_3^2 - 2A) &= t_1(1 - t_3^2 + 2At_3^2), \\ t_1 t_3(1 - t_3^2 - 2A) &= 1 - t_3^2 + 2At_3^2, \end{aligned} \quad (\text{B.19})$$

which can be shown to possess only complex solutions. Finally, we are left with the case where the second term disappears in all three equations<sup>1</sup>. We find the following stationary configurations:

$t_1 = t_2 = t_3 = 0$ : Ferromagnetic alignment along the  $z$  axis. The energy of this configuration is given by  $4E/JL = 3A$ .

$t_1 = t_2 = t_3 = \pm 1$ : Ferromagnetic alignment along the  $x$  axis. This configuration has an energy value of 3.

$t_1 = 0, t_2 = -t_3 = \pm\sqrt{1+2A}$ , for  $A > -1/2$ : This configuration has energy

$$\frac{4E}{JL} = -\frac{1+A+A^2}{1+A}, \quad (\text{B.20})$$

and it may describe for instance a continuous transition between a 120-degree ordering of the spins with one spin pointing in the  $z$  direction ( $A \rightarrow 1^+$ ), and an  $\uparrow\downarrow\downarrow$  configuration along the  $z$  axis ( $A \rightarrow \infty$ ).

$t_1 = \pm 1$ , and the other two variables are given by  $t_1(-1 - A \pm \sqrt{2A + A^2})$ , for  $A < -2$  and  $A \geq 0$ : The energy of this configuration is given by (B.20). This arrangement of spins is suitable for a continuous interpolation between states where one spin is pointing in the  $x$  direction and the other two spins are either adjusted to form 120-degree order ( $A \rightarrow 1^+$ ), or they have closed up onto the  $z$  axis in an antiparallel way. Another physically interesting domain of anisotropy is  $A \in ]-2, -\infty[$ , where we find a transition between a ferromagnetic configuration along the  $x$  axis ( $A \rightarrow -2^-$ ) and a configuration where one of the spins is unchanged, but the other two form an  $\uparrow\downarrow$  pair along the  $z$  axis ( $A \rightarrow -\infty$ ).

---

<sup>1</sup>While a complete analytical solution exists for this case, it is cumbersome to derive. We employed the Reduce function of Mathematica 7.0 for this purpose.

**one-parameter degeneracy** : As long as  $t_1 \neq 0, \pm 1$ , furthermore  $t_1^2(1 + 2A) \neq 1$ , and the expressions

$$\frac{-2At_1(1 + A) \pm \sqrt{p(t_1)}}{t_1^2(1 + 2A) - 1} \quad (\text{B.21})$$

with

$$p(t_1) = 1 + 2A + t_1^2(4A^4 + 8A^3 - 4A - 2) + t_1^4(1 + 2A) \quad (\text{B.22})$$

remain real, the parameter  $t_1$  may be arbitrarily chosen. The other two variables are given by (B.21), and the energy of each resulting configuration is (B.20). An analysis of the polynomial  $p(t_1)$  in the square root reveals that the degenerate solution exists for  $A < -2$  and  $A > -1/2$ . It is particularly interesting to note that for  $A < -2$ , one may choose  $t_1^2$  from the domain  $[t_-^2, t_+^2]$ , where

$$t_{\mp}^2 = \frac{1 + 2A - 4A^3 - 2A^4 \pm 2\sqrt{(A + A^2)^3(A + A^2 - 2)}}{1 + 2A}, \quad (\text{B.23})$$

and choosing either of the two extreme values corresponds to a transition between a ferromagnetic configuration along the  $x$  axis ( $A \rightarrow -2^-$ ) and a configuration where the three spins feature an  $\uparrow\uparrow\downarrow$  or an  $\uparrow\downarrow\downarrow$  arrangement along the  $z$  axis ( $A \rightarrow -\infty$ ). In fact,  $p(t_1)$  vanishes in both cases, which implies that  $t_2 = t_3$ , and choosing furthermore  $t_{\mp} > 0$ , one may easily verify that

$$t_+t_- = t_2(t_1 = t_+)t_2(t_1 = t_-) = t_3(t_1 = t_+)t_3(t_1 = t_-) = 1, \quad (\text{B.24})$$

i. e. the two configurations are related to each other via reflection with respect to the  $xy$  plane.

We conclude our discussion on “planar” states by solving the set of equations (B.16) in the case where one of the variables, say  $\vartheta_1$ , is set to  $-\pi$ . The equations are simplified as follows:

$$\begin{aligned} s_2 + s_3 &= 0, \\ c_2s_3 &= As_2(c_3 - 1), \\ c_3s_2 &= As_3(c_2 - 1). \end{aligned} \quad (\text{B.25})$$

A set of solutions is given by  $s_2 = s_3 = 0$ , which corresponds to an arrangement where all three spins are fixed along the  $z$  axis: ferromagnetic

configurations such as  $\downarrow\downarrow\downarrow$  have energy  $3A$ , while other configurations such as  $\downarrow\downarrow\uparrow$  have energy  $-A$ . On the other hand, assuming  $s_2s_3 \neq 0$  and switching to the variables  $t_2 = \tan(\vartheta_2/2)$  and  $t_3 = \tan(\vartheta_3/2)$ , we may rewrite our system of equations and find a stable configuration for  $A > -1/2$  with  $t_2 = -t_3 = \pm 1/\sqrt{1+2A}$ . Note however that this latter configuration has already occurred in our calculations, as reflecting it with respect to the  $xy$  plane corresponds to a  $\vartheta_i \rightarrow \pi - \vartheta_i$  transformation, therefore we may easily recover the solution  $\{t_1 = 0, t_2 = -t_3 = \pm 1/\sqrt{1+2A}\}$  found earlier.

### B.3 Ground-state configurations

A comparison of the energies of all stationary configurations gives the ground-state phase diagram of the model (B.1). In order to facilitate the use of these results in the main text, let us redefine the coupling constants:

$$H = J' \sum_{\langle i,j \rangle} \{2 \sin \vartheta' (\sigma_i^x \sigma_j^x + \sigma_i^y \sigma_j^y) + (4 \cos \vartheta' - 2 \sin \vartheta') \sigma_i^z \sigma_j^z\}, \quad (\text{B.26})$$

where  $J' > 0$  and  $\vartheta' \in [0, 2\pi]$ . The ground-state energy is plotted as a function of  $\vartheta'$  in figure B.1. We find the following ground-state configurations<sup>2</sup>:

$\vartheta' = 0$ : For each triangle, two of the spins are fixed along the  $z$  axis in an antiparallel way, while the third spin is arbitrary. There is a macroscopic degeneracy in the ground-state manifold.

$0 < \vartheta' < \pi/4$ : In addition to the symmetry of rotations around the  $z$  axis, there is a continuous one-parameter degeneracy present. In a three-sublattice ordered state, one of the sublattices may feature a completely arbitrary spin, while the spins on the other two sublattices are adjusted so that all spins lie in a common plane with the  $z$  axis<sup>3</sup>. This degeneracy is referred to as “non-trivial”, because it does not correspond to symmetry operations of the XXZ model<sup>4</sup>. In figure B.2, we show

<sup>2</sup>We will use the notation  $\theta = 2\pi - \arctan 2 \approx 1.65\pi$  that was introduced in the main text.

<sup>3</sup>In fact, this parameter region of  $\vartheta'$  corresponds to  $A > 1$ , i. e. all coefficients of the polynomial (B.22) are strictly positive and  $t_1$  may be chosen arbitrarily. One may check that the limits  $t_1 \rightarrow 0, t_1 \rightarrow \pm 1, t_1 \rightarrow \pm 1/\sqrt{1+2A}$  and  $t_1 \rightarrow \pm\infty$  of the expression (B.21) make sense and reproduce expected solutions.

<sup>4</sup>The classical  $J_1$ - $J_2$  Heisenberg model on the square lattice also features a non-trivial degeneracy in the ground-state manifold for  $J_2/J_1 \geq 1/2$ .

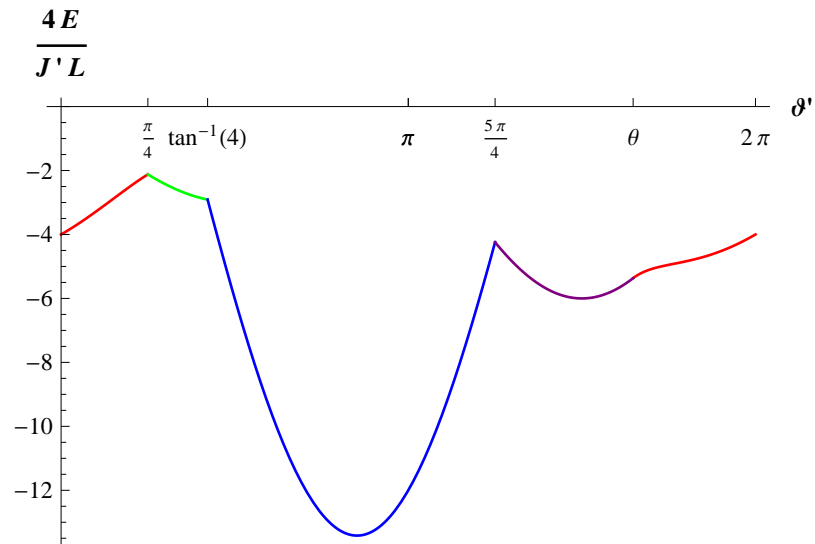


Figure B.1: Ground-state energy of the classical XXZ model on the triangular lattice. Ferromagnetic configurations along the  $z$  axis and in the  $xy$  plane are represented by blue and purple curves, respectively, while the green curve corresponds to a 120-degree ordering of the spins in the  $xy$  plane. The energy curve of phases featuring a non-trivial continuous degeneracy has red colour. The ground state is ferromagnetic between the points  $\arctan 4 \approx 0.4\pi$  and  $\theta \approx 1.65\pi$ .

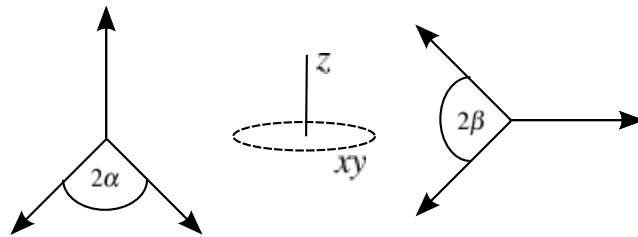


Figure B.2: Symmetric “planar” configurations for  $0 < \vartheta' < \pi/4$ . The angle  $\alpha$  ( $\beta$ ) decreases (increases) as we move away from the  $\vartheta' = \pi/4$  point.

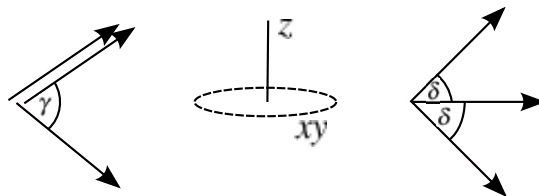


Figure B.3: “Planar” configurations for  $\theta < \vartheta' < 2\pi$ . The angles  $\gamma$  and  $\delta$  increase as we move away from the  $\vartheta' = \theta$  point.

symmetric “planar” configurations where one of the spins is kept fixed either along the  $z$  axis or in the  $xy$  plane, while the other two spins are reflections of each other with respect to the first spin.

$\vartheta' = \pi/4$ : The spins form 120-degree order in an arbitrary plane.

$\pi/4 < \vartheta' < \arctan 4 \approx 0.4\pi$ : The spins form 120-degree order in the  $xy$  plane.

$\vartheta' = \arctan 4$ : We find a continuous degeneracy associated with an umbrella configuration around the  $z$  axis that interpolates between a 120-degree ordering of spins in the  $xy$  plane and a ferromagnetic alignment along the  $z$  axis.

$\arctan 4 < \vartheta' < 5\pi/4$ : Ferromagnetic configuration along the  $z$  axis.

$\vartheta' = 5\pi/4$ : Ferromagnetic configuration along an arbitrary axis.

$5\pi/4 < \vartheta' \leq \theta$ : Ferromagnetic alignment in the  $xy$  plane.

$\theta < \vartheta' < 2\pi$ : A non-trivial one-parameter degeneracy allows for, among other states, a particular “planar” configuration where two of the spins coincide. We find furthermore a symmetric “planar” configuration where one of the spins is kept fixed in the  $xy$  plane, while the other two are reflections of each other with respect to it. See figure B.3.

## B.4 Quantum effects in the XXZ model

We conclude this appendix with a discussion on the way quantum effects restore the discrete degeneracy of the XXZ Hamiltonian. Linear spin wave theory reveals that quantum fluctuations lift the non-trivial continuous degeneracy that the model (B.1) exhibits in the ( $J > 0, A > 1$ ) region, via an “order-by-disorder” mechanism [71, 72]: the selected configurations are the symmetric ones with one of the spins pointing along the  $z$  axis (see figure B.2). This fluctuation effect can be conveniently modeled [71] by introducing a phenomenological biquadratic exchange of the form

$$H' = -16\kappa \sum_{\langle i,j \rangle} (\vec{\sigma}_i \vec{\sigma}_j)^2, \quad (\text{B.27})$$

which gives rise to an energy term

$$\frac{E'}{\kappa L} = -(s_1 s_2 + c_1 c_2)^2 - (s_2 s_3 + c_2 c_3)^2 - (s_3 s_1 + c_3 c_1)^2. \quad (\text{B.28})$$

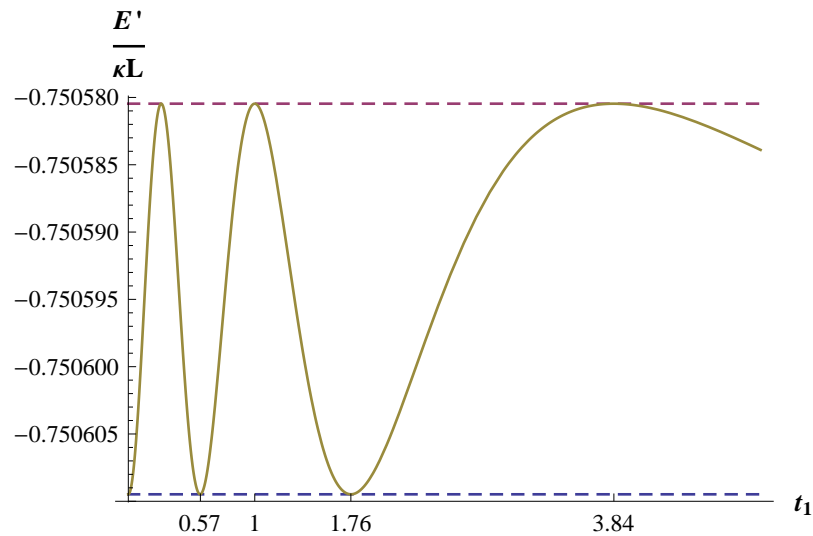


Figure B.4: Energy of the biquadratic exchange as a function of the parameter  $t_1$  for  $A = 1.05$ . The minima (maxima) correspond to symmetric spin configurations where one of the spins points along the  $z$  axis (is kept fixed in the  $xy$  plane).

One may express this energy with the help of the familiar variables  $t_i = \tan(\vartheta_i/2)$  and eliminate  $t_2$  and  $t_3$  using (B.21). For a given anisotropy parameter  $A > 1$ , the resulting expression will depend on  $t_1^2$ , which leads to a lift of the one-parameter degeneracy. We find that all extrema correspond to symmetric configurations, and for  $\kappa > 0$  the minima (maxima) will feature a spin pointing along the  $z$  axis (kept fixed in the  $xy$  plane). More precisely, for  $t_1 \geq 0$ , the minima are attained at  $t_1 = 0$ ,  $t_1 = 1/\sqrt{1+2A}$ ,  $t_1 = \sqrt{1+2A}$  and in the  $t_1 \rightarrow \infty$  limit, the maxima are located at  $t_1 = 1 + A - \sqrt{2A + A^2}$ ,  $t_1 = 1$  and  $t_1 = 1 + A + \sqrt{2A + A^2}$ , and the width of the energy curve is  $2(A-1)^3/(A+1)^3$ . In figure B.4, we show the dependence of the energy on the parameter  $t_1$  for  $A = 1.05$ . Interestingly enough, thermal selection takes place beyond the order of harmonic excitations, and it favours a different subset of the ground-state manifold [71], namely the symmetric configurations with one of the spins kept fixed in the  $xy$  plane (see figure B.2).

A semi-classical treatment is appropriate to account for small fluctuations around classical ground states, however, the extreme quantum case of the model (B.1), where the on-site objects  $\vec{\sigma}_i$  are spins one-half, is also well-studied in the literature. In particular, a hard-core boson representation of the local spins is often employed: the spin operators are expressed as  $\sigma_i^+ = a_i^\dagger$ ,  $\sigma_i^- = a_i$  and  $\sigma_i^z = n_i - 1/2$ , and the XXZ Hamiltonian (B.1) is

rewritten as

$$H = \sum_{\langle i,j \rangle} \{ -t (a_i^\dagger a_j + a_j^\dagger a_i) + V (n_i - 1/2) (n_j - 1/2) \}, \quad (\text{B.29})$$

where  $t = -J/2$  and  $V = JA$ . Ordering of the  $z$  component of the spins at a non-zero wavevector translates into solid order (diagonal long-range order) in the bosonic language, while spin order in the  $xy$  plane corresponds to superfluidity (off-diagonal long-range order). Since we are mainly interested in the parameter regions where the classical model features a non-trivial degeneracy, we may restrict ourselves to a repulsive bosonic interaction ( $V > 0$ ), however, we allow both for a non-frustrated ( $t > 0$ ) and a frustrated ( $t < 0$ ) hopping term. For the latter case, Quantum Monte Carlo simulations are faced with the infamous sign problem, but other sophisticated techniques [73, 74, 75] have revealed the presence of a robust  $\sqrt{3} \times \sqrt{3}$  supersolid phase in the region  $-1 < 2t/V < 0$ . Crystal order is of the type  $(2m_z + \delta, -m_z, -m_z)$ , i. e. there is a small spontaneous magnetization along the  $z$  axis in the spin model, while the structure of superfluid order is  $(0, m_\perp, -m_\perp)$ . Both  $\delta$  and  $m_z$  become more pronounced when the interaction strength  $V$  is increased, superfluid order on the other hand, while it can be shown to persist in the  $V \rightarrow \infty$  limit, becomes gradually suppressed. It is interesting to note that the semi-classical picture we discussed earlier is actually consistent with a number of these features. When the hopping term is unfrustrated, Quantum Monte Carlo methods are available, and several studies [76, 77, 78, 79] have shown that a distinct  $\sqrt{3} \times \sqrt{3}$  supersolid emerges from the large- $t$  superfluid phase when the hopping amplitude is sufficiently low,  $t/V \approx 0.1$ , and it persists down to arbitrarily small values of  $t/V$ . While crystal order is the same as in the frustrated case, and there is again a small density deviation from half-filling, superfluid order is of the type  $(m_\perp, m'_\perp, m'_\perp)$ . We note that the fact that two of the three sublattices behave identically is reminiscent of the classical “planar” configuration in the left-hand side of figure B.3.



# Bibliography

- [1] A. Messiah, *Quantum Mechanics* (Dover, New York, 1999)
- [2] S. Chaturvedi and N. Mukunda, *J. Math. Phys.* **43**, 5262-5277 (2002)
- [3] J. M. Radcliffe, *J. Phys. A: Gen. Phys.* **4**, 313-323 (1971)
- [4] B. A. Ivanov and A. K. Kolezhuk, *Phys. Rev. B* **68**, 052401 (2003)
- [5] A. Läuchli, F. Mila, and K. Penc, *Phys. Rev. Lett.* **97**, 087205 (2006)
- [6] T. Moriya, *Phys. Rev.* **120**, 91 (1960)
- [7] M. Elhajal, B. Canals, and C. Lacroix, *Phys. Rev. B* **66**, 014422 (2002)
- [8] P. Fazekas, *Lecture Notes on Electron Correlation and Magnetism* (World Scientific, Singapore, 1999)
- [9] J. Romhányi, *private communication*
- [10] H. Georgi, *Lie Algebras in Particle Physics* (Westview Press, 1999)
- [11] I. Affleck et al, *Phys. Rev. Lett.* **59**, 799 (1987)
- [12] G. Fáth and J. Sólyom, *Phys. Rev. B* **51**, 3620 (1995)
- [13] A. Klümper, *Europhys. Lett.* **9**, 815 (1989)
- [14] C. D. Batista, G. Ortiz, and J. E. Gubernatis, *Phys. Rev. B* **65**, 180402(R) (2002)
- [15] C. K. Lai, *J. Math. Phys.* **15**, 1675 (1974)
- [16] B. Sutherland, *Phys. Rev. B* **12**, 3795 (1975)
- [17] G. Fáth and J. Sólyom, *Phys. Rev. B* **44**, 11836 (1991)

- 
- [18] K. Penc and A. M. Läuchli, in *Introduction to Frustrated Magnetism*, Eds. C. Lacroix, P. Mendels, and F. Mila, Springer (2010)
- [19] N. Papanicolaou, *Nuclear Physics B* **305**, 367-395 (1988)
- [20] A. Virosztek, *J. Phys. C: Solid State Phys.* **18**, 4735 (1985)
- [21] C. Kittel, *Phys. Rev.* **120**, 335 (1960)
- [22] O. Tchernyshyov and G. -W. Chern, in *Introduction to Frustrated Magnetism*, Eds. C. Lacroix, P. Mendels, and F. Mila, Springer (2010)
- [23] O. Tchernyshyov, R. Moessner, and S. L. Sondhi, *Phys. Rev. B* **66**, 064403 (2002)
- [24] K. Penc, N. Shannon, and H. Shiba, *Phys. Rev. Lett.* **93**, 197203 (2004)
- [25] D. L. Bergman et al, *Phys. Rev. B* **74**, 134409 (2006)
- [26] C. L. Henley, *J. Appl. Phys.* **61**, 3962 (1987)
- [27] C. L. Henley, *Phys. Rev. Lett.* **62**, 2056 (1989)
- [28] A. V. Chubukov and D. V. Golosov, *J. Phys.: Condens. Matter* **3**, 69 (1991)
- [29] Q. Sheng and C. L. Henley, *J. Phys.: Condens. Matter* **4**, 2937 (1992)
- [30] J. Villain et al, *J. Phys. France* **41**, 1263 (1980)
- [31] E. A. Harris and J. Owen, *Phys. Rev. Lett.* **11**, 9 (1963)
- [32] D. S. Rodbell et al, *Phys. Rev. Lett.* **11**, 10 (1963)
- [33] F. Michaud, *private communication*
- [34] F. Mila and F. C. Zhang, *Eur. Phys. J. B* **16**, 7 (2000)
- [35] R. N. Bhatt and K. Yang, *J. Appl. Phys.* **83**, 7231 (1998)
- [36] P. Millet et al, *Phys. Rev. Lett.* **83**, 4176 (1999)
- [37] S. Nakatsuji et al., *Science* **309**, 1697 (2005)
- [38] H. Tsunetsugu and M. Arikawa, *J. Phys. Soc. Jpn.* **75**, 083701 (2006)
- [39] S. Bhattacharjee, V. B. Shenoy, and T. Senthil, *Phys. Rev. B* **74**, 092406 (2006)

- 
- [40] A. F. Andreev and I. A. Grishchuk, *Zh. Eksp. Teor. Fiz.* **87**, 467 (1984)
- [41] V. Barzykin and L. P. Gor'kov, *Phys. Rev. Lett.* **70**, 2479 (1993)
- [42] H. Tsunetsugu and M. Arikawa, *J. Phys.: Condens. Matter* **19**, 145248 (2007)
- [43] H. Kawamura and A. Yamamoto, *J. Phys. Soc. Jpn.* **76**, 073704 (2007)
- [44] S. Fujimoto, *Phys. Rev. B* **73**, 184401 (2006)
- [45] E. M. Stoudenmire, S. Trebst, and L. Balents, *Phys. Rev. B* **79**, 214436 (2009)
- [46] P. W. Anderson, *Phys. Rev.* **86**, 694 (1952)
- [47] B. Bernu, C. Lhuillier, and L. Pierre, *Phys. Rev. Lett.* **69**, 2590 (1992)
- [48] C. Lhuillier, *Frustrated Quantum Magnets*, arxiv:cond-mat/0502464 (2005)
- [49] T. Coletta, *private communication*
- [50] S. J. Ferreira and A. D. Sokal, *J. Stat. Phys.* **96**, 461 (1999)
- [51] K. Harada and N. Kawashima, *Phys. Rev. B* **65**, 052403 (2002)
- [52] K. Penc et al, *Phys. Rev. B* **68**, 012408 (2003)
- [53] J. T. Chalker, P. C. W. Holdsworth, and E. F. Shender, *Phys. Rev. Lett.* **68**, 855 (1992)
- [54] B. Chakrabarti, D. Charrier, and A.M. Läuchli (unpublished)
- [55] N. Fukushima, arxiv:cond-mat/0502484 (unpublished)
- [56] T. B. Ottenstein et al, *Phys. Rev. Lett.* **101**, 203202 (2008)
- [57] J. H. Huckans et al, *Phys. Rev. Lett.* **102**, 165302 (2009)
- [58] S. Stellmer et al, *Phys. Rev. Lett.* **103**, 200401 (2009)
- [59] Y. N. Martinez de Escobar et al, *Phys. Rev. Lett.* **103**, 200402 (2009)
- [60] C. Honerkamp and W. Hofstetter, *Phys. Rev. Lett.* **92**, 170403 (2004)
- [61] C. Wu, *Mod. Phys. Lett. B* **20**, 1707 (2006)

- 
- [62] M. Hermele, V. Gurarie, and A. M. Rey, *Phys. Rev. Lett.* **103**, 135301 (2009)
- [63] M. A. Cazalilla, A. F. Ho, and M. Ueda, *New Journal of Physics* **11**, 103033 (2009)
- [64] A. V. Gorshkov et al, *Nature Physics* **6**, 289 (2010)
- [65] E. Altman, E. Demler, M. D. Lukin, *Phys. Rev. A* **70**, 013603 (2004)
- [66] J. F. Sherson et al, *Nature* **467**, 68 (2010)
- [67] W. S. Bakr et al, *Science* **329**, 547 (2010)
- [68] S. Miyashita and H. Kawamura, *J. Phys. Soc. Jpn.* **54**, 3385 (1985)
- [69] S. Miyashita, *J. Phys. Soc. Jpn.* **55**, 3605 (1986)
- [70] S. Miyashita, *Prog. Theor. Phys. Suppl.* **87**, 112 (1986)
- [71] Q. Sheng and C. L. Henley, *J. Phys.: Condens. Matter* **4**, 2937 (1992)
- [72] B. Kleine et al, *Z. Phys. B* **87**, 103 (1992)
- [73] F. Wang, F. Pollmann, and A. Vishwanath, *Phys. Rev. Lett.* **102**, 017203 (2009)
- [74] H. C. Jiang et al, *Phys. Rev. B* **79**, 020409(R) (2009)
- [75] D. Heidarian and A. Paramekanti, *Phys. Rev. Lett.* **104**, 015301 (2010)
- [76] S. Wessel and M. Troyer, *Phys. Rev. Lett.* **95**, 127205 (2005)
- [77] D. Heidarian and K. Damle, *Phys. Rev. Lett.* **95**, 127206 (2005)
- [78] R. G. Melko et al, *Phys. Rev. Lett.* **95**, 127207 (2005)
- [79] M. Boninsegni and N. Prokof'ev, *Phys. Rev. Lett.* **95**, 237204 (2005)

# Curriculum Vitae

- **Name:** TÓTH, Tamás András
  - **Date of Birth:** 11<sup>th</sup> December, 1982
  - **Citizenship:** Hungarian
  - **Home address:** Kapitány utca 1., 1123 Budapest, Hungary
  - **E-mail addresses :** [tamas.toth@epfl.ch](mailto:tamas.toth@epfl.ch), [tmasplace@gmail.com](mailto:tmasplace@gmail.com)
- 

## Education:

- 2006-2011: Ecole Polytechnique Fédérale de Lausanne, Institute of Theoretical Physics, *Ph. D. in Theoretical physics*  
*Ph. D. thesis:* Quadrupolar ordering in two-dimensional spin-one systems  
supervisors: Prof. Frédéric Mila and Dr. Karlo Penc
  - 2001-2006: Budapest University of Technology and Economics, Faculty of Natural Sciences, *M. Sc. in Engineering physics*  
*M. Sc. thesis:* Quasi-particle excitations in fermionic systems  
supervisor: Prof. Attila Viroztek
  - 1995-2001: ELTE Apáczai Csere János Secondary School, Budapest
- 

## Teaching activity at EPF Lausanne:

- assistant for the General Physics course by Prof. Henrik Ronnow, autumn 2009
- expert at the exams of the Classical Electrodynamics course by Prof. Mikhail Shaposhnikov, spring 2009
- assistant for and expert at the exams of the Quantum Physics course by Prof. Frédéric Mila, spring 2009
- tutor at masters level (“travaux pratiques 4”) under the direction of Prof. Frédéric Mila, autumn 2008
- assistant for the Solid State Physics course by Prof. Frédéric Mila, autumn 2008

- assistant for and expert at the exams of the Classical Electrodynamics course by Prof. Mikhail Shaposhnikov, spring semesters of 2007 and 2008
- 

#### **Oral presentations:**

- invited seminar talk at the Technische Universität Dortmund, 20 october 2010, Dortmund (Germany)
  - contributed talk at the Workshop on Emergence of New States of Matter in Magnetic Systems and Beyond, 5-9 july 2010, Trieste (Italy)
  - contributed talk at the Romand meeting on Correlated Systems, 17 june 2010, Fribourg (Switzerland)
  - short presentation at the International Workshop on Perspectives in Highly Frustrated Magnetism, 19-23 april 2010, Max Planck Institute for the Physics of Complex Systems, Dresden (Germany)
  - short presentation at the Swiss Workshop on Materials with Novel Electronic Properties, 26-28 august 2009, Les Diablerets (Switzerland)
- 

#### **Poster presentations:**

- International Workshop on Perspectives in Highly Frustrated Magnetism, 19-23 april 2010, Max Planck Institute for the Physics of Complex Systems, Dresden (Germany)
- Swiss Workshop on Materials with Novel Electronic Properties, 26-28 august 2009, Les Diablerets (Switzerland)
- Joint European Japanese Conference: Frustration in Condensed Matter, 12-15 may 2009, Ecole Normale Supérieure de Lyon (France)
- International Conference on Highly Frustrated Magnetism, 7-12 september 2008, Braunschweig (Germany)
- Workshop organized by the ESF Program Highly Frustrated Magnetism: Entanglement in Spin & Orbital Systems, 18-22 june 2008, Cracow (Poland)
- Annual meeting of the Swiss Physical Society, section MaNEP, 26-27 march 2008, Geneva (Switzerland)

## Publications:

- T. A. Tóth, A. M. Läuchli, F. Mila, and K. Penc:  
*Three-Sublattice Ordering of the  $SU(3)$  Heisenberg Model of Three-Flavor Fermions on the Square and Cubic Lattices*  
Phys. Rev. Lett. **105**, 265301 (2010)
- T. A. Tóth, A. M. Läuchli, F. Mila, and K. Penc:  
*Competition Between Two- and Three-Sublattice Ordering for Spins One on the Square Lattice*  
draft in preparation
- T. A. Tóth, K. Penc, and F. Mila:  
*Quadrupolar Phases of the Triangular Lattice  $S=1$  Bilinear-Biquadratic Heisenberg Model with Single-Ion Anisotropy*  
draft in preparation